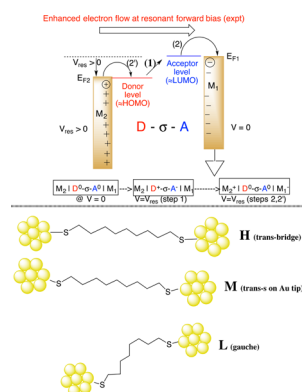


## Unimolecular Electronics

Robert M. Metzger\*

Laboratory for Molecular Electronics, Department of Chemistry, The University of Alabama, Box 870336, Tuscaloosa, Alabama 35487-0336, United States



### CONTENTS

1. Introduction	5056
2. Summary of Significant Results	5057
3. Contacts from Molecule to Metal and Energy Level Shifts	5058
4. Marcus Theory of Electron Transfer within a Molecule	5062
5. Electrical Conductivity, Classical and Quantized: Ohm's Law and Tunneling	5063
6. WKBJ or Quasi-classical Method	5066
7. Fowler–Nordheim equation	5066
8. Simmons Equation	5067
9. Newns–Anderson Equation and Eigenvalue Staircase	5068
10. Other Tunneling Regimes	5068
11. Landauer Equation	5069
12. Two-Probe Conductivity Measurement Techniques	5070
13. Thermopower	5070
14. Coulomb Blockade, Coulomb Staircase, and Coulomb Diamonds	5082
15. Negative Differential Resistance and Potential Power Gain with Two-Probe Methods	5083
16. Gating in Field-Effect Transistors and in Molecular Conductance	5083
17. Spintronics	5084
18. Conductivity of Molecular Wires	5085
19. Transition Voltage Spectroscopy	5089
20. Asymmetries in <i>I/V</i> Curves: Rectification	5089
21. Rectifier or Diode: What Is in a Name?	5090
22. Three Mechanisms for Rectification by Molecules	5094
23. Unimolecular Rectification by One Level: Schottky Barrier Rectifiers (S)	5095
24. Unimolecular Rectification (U by One or Two Levels)	5095
25. Rectification in Macroscopic Films and Langmuir–Blodgett Multilayers	5096

26. A and S Rectification by Resonance with Only One Molecular Energy Level	5096
27. Monolayer Photodiode and Electrochemical Rectification	5097
28. Rectification To Help Artificial Photosynthesis	5097
29. Inelastic Electron Tunneling Spectroscopy Orbital-Mediated Tunneling and STM	5097
30. Unimolecular Amplifier	5100
31. DNA Conductivity, Complementarity, And Origami	5100
32. Conclusion	5100
Author Information	5100
Corresponding Author	5100
Notes	5100
Biography	5100
Acknowledgments	5101
References	5101

### 1. INTRODUCTION

Unimolecular electronics (UME) narrowly defined (*sensu stricto*),<sup>1</sup> or molecular-scale electronics,<sup>2</sup> is the study of electrical processes measured or controlled on a molecular scale.<sup>1</sup> UME also includes the study of monolayers, when single molecules conduct independently of their neighbors. In contrast, molecular electronics loosely defined (*sensu lato*),<sup>1</sup> or molecule-based electronics (MBE) or organic electronics,<sup>2</sup> encompasses electrical processes in molecular assemblies of any scale, including crystals and conducting polymers. MBE grew from the study of organic metals and superconductors,<sup>3</sup> as well as of conducting polymers,<sup>4,5</sup> and is “maturing” in organic light-emitting devices (OLEDs)<sup>6–8</sup> and “emerging” in organic photovoltaics.<sup>9</sup> The status of UME was reviewed by this author in 2003<sup>10</sup> and also in 2012,<sup>11</sup> but recent progress has prompted the present update.

UME holds promise in that electronic components at the 2 nm scale would present potential technological solutions for denser and faster circuitry and computing. UME was first discussed in the United States Defense Department as a potentially promising subject in the late 1950s; it was presaged, albeit indirectly, by Richard P. Feynman's visionary comments (“there is plenty of room at the bottom”).<sup>12</sup> UME started in earnest in 1974, when Ari Aviram and Mark A. Ratner (AR) proposed electrical rectification, or diode behavior, by a single molecule with suitable electronic asymmetry.<sup>13</sup> Unimolecular rectification has now been confirmed experimentally, and new insights have been made into the interface between metal electrodes and molecules. UME was popularized by several conferences chaired by the late Forrest L.

Received: August 22, 2014

Published: May 7, 2015

Carter in 1981, 1982, and 1985<sup>14–16</sup> that gathered seminal ideas but also some exaggerated hype, as well as by conferences organized by Aviram<sup>17–20</sup> or inspired by him.<sup>21</sup>

Researchers in intramolecular electron transfer and in artificial photosynthetic systems had been studying electron transfer within large molecules. In the 1950s and 1960s, Henry Taube proved that electron transfer across an organic bridge between two dissimilar metal ions occurs more slowly across aliphatic bridges than across conjugated aromatic bridges.<sup>22</sup> Intramolecular electron transfer (adiabatic or nonadiabatic, by direct exchange or by superexchange) has been put under the theoretical microscope, because of the pioneering work by Willard F. Libby,<sup>23</sup> Rudolph A. Marcus,<sup>24</sup> Noel S. Hush,<sup>25</sup> Harden M. McConnell,<sup>26</sup> and others.<sup>27</sup>

Since the mid-1990s, UME was rekindled by many direct measurements of the electronic behavior of single molecules, of Langmuir–Blodgett (LB) monolayers of molecules,<sup>28,29</sup> or of self-assembled monolayers (SAMs)<sup>30–32</sup> (typically, thiols on gold). Finally, we can “touch” molecules and measure their individual electrical behavior! We can touch a single molecule by a scanning tunneling microscopy (STM) tip or by a conducting-tip atomic force microscopy (C-AFM) tip, between two Au tips, or a monolayer by making electrical contacts to sandwiches of organic monolayers placed between superthin inorganic metal pads (with areas from 1  $\mu\text{m}^2$  to 1  $\text{cm}^2$ ). We can measure the current versus voltage (*IV*) characteristics either of a single molecule, of a monolayer of molecules, or of many layers, either locally, by scanning tunneling spectroscopy (STS), or as a macroscopic average, over a pad.

UME could become an alternate vehicle for technologically useful active electronic devices. There are concerns about how much smaller silicon-based integrated circuits can be shrunk to make electronic components closer and, therefore, the speed of computing faster. Gordon E. Moore found in 1965 that the computing power doubled every two years:<sup>33</sup> this empirical rule of thumb, driven by commercial interests and technological innovation, held unabated until about 2008. Indeed, as the “design rules” (DR) for integrated circuits (i.e., the smallest distance between adjacent components) get smaller and smaller, the circuit clock cycles (CC) can become shorter and shorter.<sup>34</sup> Intel Corp. is now building a 28-nm DR (14-nm half-pitch) fabrication laboratory in Arizona at a cost of \$5B. This shrinkage cannot go on forever. Quantum tunneling and heat (phonon release in Si) have become serious problems; at present CC is limited commercially to 3 GHz. Electronic excited states in Si can only decay by phonons; in contrast, molecules can also decay from excited states by photon emission and may present a realistic advantage. Breakthrough advances in silicon-based electronics may become a moving target for UME. However, it is fun to try to be both successful and maybe useful.

Several monographs with “molecular electronics” in their title have appeared,<sup>35–42</sup> and symposia and topical issues of journals have been dedicated to the subject. Many review articles have appeared.<sup>43–79</sup>

UME may seem to be a perennial adolescent, trying to grow up! A recent summary agrees with this “adolescence” viewpoint;<sup>80</sup> several suggestions have been made for future progress.<sup>71,72,80</sup> We should always remember Yogi Berra’s dictum, “It is very difficult to make predictions, especially about the future.”

This review summarizes experiments and theories from several convergent research fields that bear upon the molecule/metal interface, discusses the present status and future prospect of one-

molecule electronic devices, and connects several constituencies interested in closely related problems: (i) the photoelectron spectroscopy community, (ii) the scanned probe, (iii) the mechanical break junction community, (iv) some theoretical chemists who seem insulated from the richness of physical phenomena being unraveled, (v) some physicists who seem unaware of certain profound insights of physical organic chemistry, (vi) aficionados of spintronics, and (vii) some semiconductor engineers who still remain skeptical of UME.

Incidentally, chemists tend to use the term “electron transfer”, while physicists prefer “electron transport”. The former may refer to coherent unistep hopping, while the latter may refer to incoherent multistep hopping;<sup>54</sup> in the present discussion, this distinction will not be made.

## 2. SUMMARY OF SIGNIFICANT RESULTS

Here is a brief, subjective list of significant advances in UME:

(1) Experiments with the scanning tunneling spectroscopy (STS) mode of the scanning tunneling microscope (STM) by Paul S. Weiss and co-workers showed that the electrical currents across alkanethiols and aromatic thiols bonded to a Au(111) surface are larger when the molecules are aromatic chains than if they are aliphatic,<sup>81,82</sup> confirming directly an earlier result by Taube.<sup>22</sup>

(2) Two-electrode mechanical break junctions (MBJs) (pioneered by Moreland and Ekin<sup>83</sup> and then by Jan van Ruitenbeek and co-workers<sup>84</sup>) were used by Mark A. Reed and co-workers to probe the conductance of a single 1,4-benzenedithiol molecule covalently bound to two Au electrodes.<sup>85</sup>

(3) The two-electrode electromigration break junction (EBJ) was developed by Paul L. McEuen, Daniel C. Ralph, Hector D. Abruña, and students<sup>86</sup> to interrogate a bithiol-terminated Co(II)hexapyridine complex between two Au electrodes at 0.1 K. This was labeled a single-atom transistor (an analogue to the single-electron transistor (SET))<sup>87</sup> but is in reality an addressable Coulomb blockade (CB) device with zero power gain, called an SET because a single electron can affect the conductance.<sup>88</sup>

(4) The STM and C-AFM were used in a two-electrode scanning break junction (SBJ) mode pioneered by Nongjian Tao and student<sup>89</sup> to study the conductivity of single dithiols and diamines just before the metal–molecule bond is broken.

(5) Field-effect transistor (FET) behavior was observed by Cees Dekker and co-workers by STM for a single-walled carbon nanotube (SWCNT) curled over parallel Au lines, with the STM acting as a gate electrode; the power gain was only 0.33.<sup>90</sup> FET behavior had been seen earlier in LB multilayers of conducting polymers<sup>91</sup> and in thin-film organic semiconductors, such as sexithiophene.<sup>92,93</sup> Any thin semiconductor can be the “active” material in an FET!

(6) Electrical bistability was observed by James Heath and Sir Fraser Stoddart et al. in an LB monolayer of a [3]catenane closed-loop molecule, with a naphthalene group as one “station” and tetrathiafulvalene as the second station, and a tetracationic catenane hexafluorophosphate salt traveling on the catenane, like a “train” on a closed track. The current–voltage plot is asymmetric as a function of bias (which moves the train on the track), and a succession of read–write cycles shows that the resistance changes stepwise as the train(s) move from the lower-conductivity station(s) to the higher-conductivity station(s).<sup>94</sup> However, its practical implementations in crossbar memory gave disappointing results.<sup>95</sup>

(7) The electronic bistability found by Reed et al. in SAMs of certain substituted terphenylenes at low temperature led to negative differential resistance (NDR) and negative resistance.<sup>96</sup> This effect, already known in Esaki tunnel diodes,<sup>97,98</sup> could provide power gain in two-electrode diode logic, so that devices, operating in NDR mode, would not need third electrodes! However, practical implementations for these NDRs failed.

(8) Following the 1974 AR proposal,<sup>13</sup> unimolecular rectification across an LB monolayer of hexadecylquinolinium tricyanoquinodimethanide was detected between Mg and Pt electrodes by John Roy Sambles, Geoffrey J. Ashwell, and co-workers,<sup>99,100</sup> and confirmed by Metzger and co-workers between Al electrodes<sup>101–103</sup> as well as between oxide-free Au electrodes;<sup>104,105</sup> however, the direction of rectification differs<sup>11</sup> from the AR Ansatz.<sup>13</sup>

(9) The discovery of graphene by the group of Konstantin Novoselov, André Geim, and co-workers.<sup>106</sup>

### 3. CONTACTS FROM MOLECULE TO METAL AND ENERGY LEVEL SHIFTS

How should we make electrical contact with molecules? With metal electrodes connected to measuring instruments. But should we really “touch” molecules with inorganic metals? If so, which metal is best? Most recent work has used Au electrodes, Au nanoelectrodes, template-stripped Au electrodes (Au<sup>TS</sup>),<sup>107,108</sup> or atomically sharp Au tips (Au NT), drops of Hg, and drops of a Ga–In eutectic, graphite, or doped highly degenerate Si.

Au is very malleable, and under bias, Au<sup>109</sup> and even Pt<sup>110</sup> atoms will move during electrical measurements by electromigration, causing either electrical short circuits or the appearance of stalactites or stalagmites of metal atoms within the monolayer (which drastically increase the conductivity without shorting); this retraces metal “whiskers” research of the 1960s. Compared to Au, Pt and Pd are more expensive and difficult to work with.<sup>111–114</sup>

Ti is not suitable, because it interpenetrates aliphatic monolayers.<sup>115</sup> Al has a defect-prone Al<sub>2</sub>O<sub>3</sub> covering, which will reduce the overall current. Mg<sup>99,100,116–119</sup> is very reactive to moisture and must be protected by a noble metal layer like Ag. Is it better to use carbon nanotubes, graphene, graphitic pyrolyzed photoresist,<sup>121</sup> a derivatized Si surface, Hg (liquid) with its thin oxide HgO?<sup>120</sup> or GaIn eutectic liquid (with its own thin oxide Ga<sub>2</sub>O<sub>3</sub>), rebaptized as “EGaIn”?<sup>122–125</sup> Each metal electrode has advantages and drawbacks.

Furthermore, if many molecules must be interrogated electrically in parallel, then the flatness of the electrode surface becomes an issue. Graphite and a single layer of it (“graphene”)<sup>106</sup> are atomically flat, as is the layered mineral MoS<sub>2</sub>; CdI<sub>2</sub> is another layered mineral, with only van der Waals forces between layers. Electropolishing is a very successful commercial process of the semiconductor industry, whereby a Si wafer to be flattened is bombarded by a patented slurry of abrasives plus acids and ionic solutes under an applied electric field: thus, on a 4-in. or 6-in. diameter Si wafer, one can achieve 0.05 nm flatness. One can use such superflat degenerate n-level or p-level Si wafers as substrates, but there will be an oxide covering (which can be displaced if derivatized trichlorosilanes are chemisorbed onto the surface). As mentioned earlier, the relative flatness of Si can be replicated on Au or Ag by depositing a 100-nm thick Au (or Ag) film on top of a flat Si wafer; the outer Au (or Ag) surface is bonded to a second Si wafer by an epoxide resin. Finally, the Au or Ag film is lifted off the flat Si surface, is bonded by epoxy to the second substrate, and exhibits the 0.05-nm flatness of template-

stripped Au<sup>TS</sup> or Ag<sup>TS</sup>.<sup>107,108</sup> Sapphire, a gemstone version of corundum,  $\alpha$ -Al<sub>2</sub>O<sub>3</sub> with trace metal contaminants, can also be super-polished to a flatness of <0.05 nm.<sup>126</sup>

To discuss the metal–organic interface, one must worry about the work function  $\Phi_B$  of the metal, defined as the energy required to pull an electron out of the metal and move it in vacuum to an infinite distance away: the latter is the vacuum level. The  $\Phi_B$  values for inorganic metals do depend (by 0.1–0.2 eV) on the Miller indices of the exposed crystal face.

In a bulk inorganic metal the Fermi level  $E_F$ (metal) (or  $E_{Fermi}$ (metal)) is placed at the topmost filled (at 0 K) or half-filled (at finite  $T$ ) energy level within the metal conduction band. The energy difference between the vacuum level at infinity (VL(m,∞)) and  $E_F$ (metal) is the work function  $\Phi_B$ . At 0 K the Fermi level is called the Fermi energy  $E_F$ . Inside a bulk semiconductor the Fermi level  $E_F$ (semiconductor) is really a statistical concept;<sup>127</sup> it is traditionally placed halfway between the top of the (filled) valence band (VB) and the bottom of the (unfilled) conduction band (CB).

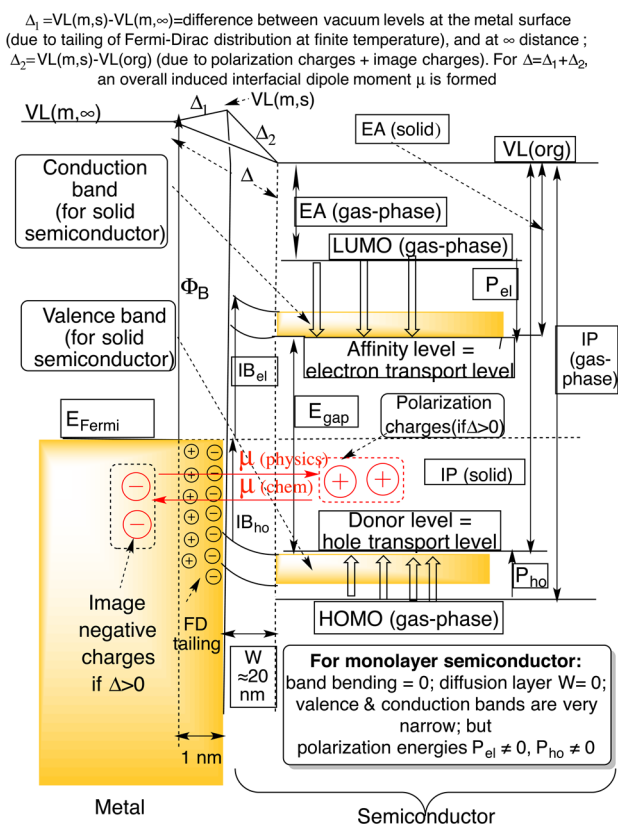
A molecule has, inter alia, a highest occupied molecular orbital (HOMO) and a lowest unoccupied molecular orbital (LUMO); when it is accosted to another molecule or to a metal, it is best to refer to the shifted HOMO as the donor level (DL) and to the shifted LUMO as the affinity level (AL).<sup>66</sup> If there are enough molecules present (how many?), then HOMOs are very closely spaced and merge into a VB; similarly, LUMOs are also closely spaced and merge into a CB. The energy difference between the bottom of the conduction band and the top of the valence band is defined as the band gap  $E_G$ .

At finite temperature the high-energy tail of the Fermi–Dirac distribution accumulates electrons at the inner surface (Faraday’s law) and gegenions (holes) probably about 1 nm within the metal. This creates a relatively small positive energy barrier  $\Delta_1$  and a static electric dipole moment  $\mu_1$ ; both  $\Delta_1$  and  $\mu_1$  will depend strongly on absolute temperature  $T$  but only weakly on which metal it is. Typically,  $\Delta_1$  is of the order of fractions of an eV and vanishes at 0 K.

The donor level and the affinity level are also broadened by approximately Gaussian envelopes associated with the vibronic sublevels of the HOMO and LUMO. For “floppy” molecules these envelopes are broader; for very rigid molecules (e.g., tetrapyrroles, phthalocyanines, fullerenes, or polyacenes), the envelopes are much narrower (e.g., Soret bands). When we accost a single molecule, an organic monolayer, or a bulk organic semiconductor to an inorganic metal (some organic metals do exist),<sup>3</sup> then two possible levels of interaction exist: zero interaction and significant interaction (Figure 1).

For zero interaction, the Schottky–Mott rule-of-thumb<sup>128</sup> (named after Walter Schottky<sup>129,130</sup> and Sir Nevill F. Mott) states that, if there is zero or negligible interaction between the metal and the molecule(s), then a vacuum level alignment occurs: the vacuum level remains constant over both molecule(s) and metal (this zero interaction case is not shown in Figure 1).

When, instead, there are significant metal–molecule interactions, then a fairly large vacuum level shift will form (also called dipolar stabilization energy)  $\Delta_2$  (e.g., VL(m,∞) versus VL(org) in Figure 1), which is negative, and with it, a second static electric dipole  $\mu_2$  will form within a diffusion region  $W$  (ca. 20 nm wide); all this is known as the Schottky barrier.<sup>131</sup>  $\Delta_2$  is typically of the order of 1–2 eV. At thermodynamic equilibrium,  $E_F$ (semiconductor) must move to match  $E_F$ (metal): the chemical potential or partial molar Gibbs free energy becomes equal across the interface (dotted line in Figure 1). For an



**Figure 1.** Depiction of a junction formed between (left) a metal and (right) a molecule, a monolayer, or a bulk organic semiconductor.

organic or inorganic semiconductor, this equalization can be achieved by band bending with space-charge formation,<sup>132</sup> i.e., local imbalance of electrical charge inside the bulk semiconductor, matched by more image charges formed within the metal. In this equalization, all the semiconductor energy bands move uniformly upward (see the arcs inclined upward in the diffusion region  $W$  of Figure 1). Experiments are usually discussed in terms of a single overall  $\Delta \equiv \Delta_1 + \Delta_2$  and a single overall  $\mu \equiv \mu_1 + \mu_2$ ,<sup>133–135</sup> and in terms of a decrease  $\Delta$  in the work function measured at the outer surface of an organic adlayer ( $\Phi_{\text{B}} - \Delta$ ); in some cases  $\Delta$  is negative.

Both alkylthiolates and partially fluorinated alkylthiolates on Au(111) are tilted ca. 30° from the normal to the surface.<sup>136</sup> The Au–S bond is calculated to be nearly apolar (despite the “polar?” entry in Table 2);<sup>137</sup> the experiment agrees with a low polarity for the Au–S bond.<sup>138</sup>

Experimental results for the shift (decrease)  $\Delta$  in work function due to a SAM adlayer are  $\Delta = 1.01$  ( $n = 2$ ) to 1.35 eV ( $n = 15$ ) for alkanethiolates  $\text{CH}_3(\text{CH}_2)_n\text{SH}$  of different chain lengths  $n$  on Au(111)<sup>136</sup> (the work function decreases), but  $\Delta = 0.12$  ( $n = 13$ ,  $m = 0$ ) to  $-0.46$  eV ( $n = 15$ ,  $m = 9$ ) for partially fluorinated alkylthiolates  $\text{CF}_3(\text{CF}_2)_m(\text{CH}_2)_{n-m}\text{SH}$  on Au(111); the effective work function increases with fluorinated adlayers.<sup>136</sup> Similarly, measured shifts are  $\Delta = 0.8$  eV for Au hexadecanethiolate<sup>139</sup> but  $\Delta = -0.6$  for Au 1H,1H,2H,2H-perfluorodecanethiolate.<sup>139</sup> They are  $\Delta = 1.2$  and 1.3 eV for Au dodecylamine and for Au hexadecylamine, respectively.<sup>140</sup>

Theoretical results are  $\mu_{\perp}$  (along normal axis) = 2.1 to 2.3 D for alkylthiolates on Au(111), with the moment in the direction shown in Figure 1 (positive end in the hydrocarbon, negative end in Au)<sup>136</sup> but  $\mu_{\perp} = -0.7$  to  $-1.8$  D (opposite polarity) for

partially fluorinated alkylthiolates on Au(111).<sup>136</sup> Calculated shifts are  $\Delta = 1.44$  ( $n = 0$ ) and 1.32 eV ( $n = 1$ ) for alkanethiolates  $\text{CH}_3(\text{CH}_2)_n\text{SH}$  on Au(111),<sup>137</sup>  $-0.72$  ( $n = 0$ ,  $m = 0$ ) and  $-1.02$  eV ( $n = 1$ ,  $m = 0$ ) for partially fluorinated alkylthiolates on Au(111),<sup>137</sup>  $\Delta = 1.44$  eV for Au methylthiolate and 1.32 eV for Au ethylthiolate, but (note the change in sign)  $-0.72$  for Au trifluoromethylthiolate and  $-1.02$  for Au 1,1,1-trifluoroethylthiolate.<sup>141</sup>

For an organic semiconductor with large intramolecular energies and small intermolecular energies, the discussion thus shifts to polarization energies (due to polarizable molecules), which work in two mutually opposite directions.<sup>142</sup> Indeed, polarization will raise the energy from the HOMO (with vertical ionization energy  $I_{\text{D}}(\text{gas-phase})$ ) to the donor level (or hole transport level) by a polarization energy for holes  $P_{\text{ho}}$ , so that the top of the VB is at an energy  $\text{IP}(\text{solid}) = \text{IP}(\text{gas-phase}) - P_{\text{ho}}$  below the vacuum level.

In contrast, polarization will lower the energy from the LUMO (with vertical electron affinity  $A_{\text{A}}(\text{gas-phase})$ ) to the affinity level (or electron transport level) by a polarization energy for electrons  $P_{\text{el}}$ , so that the affinity level is at an energy  $A_{\text{A}}(\text{solid}) = A_{\text{A}}(\text{gas-phase}) - P_{\text{el}}$  below the vacuum level: thus, polarization acts in opposite directions for the VB and the CB of an organic semiconductor.

As a special case, a single molecule does not have the energy bands of a bulk semiconductor. Therefore, no band bending can occur for a single molecule;<sup>143–145</sup> rather, two effects exist for that molecule. First, the Schottky barrier will form, shifting the donor level and the affinity level uniformly upward (or downward) in energy to match the  $E_{\text{F}}(\text{metal})$  and will also distort the molecular orbital amplitudes in the immediate proximity of the metal surface to accommodate the formation of the interface dipole  $\mu_2$ . Second, the molecule-to-molecule polarizability will shift the donor level and affinity levels toward each other.<sup>133</sup>

Other contributions to  $\Delta_2$  are (i) formal electron transfer between the metal and the organic layer; (ii) the reorientation of any permanent dipoles that may already exist within the organic layer; and (iii) the compression of the tail of the metallic electron density reaching outside the metal surface (push-back or pillow effect: the adsorbate wave functions are mixed with the metal wave functions).<sup>146,147</sup>

If the polarization becomes very large, then a “compression” of the donor level and the affinity level toward each other occurs.<sup>121</sup> If the polarization becomes even larger, then the donor level (or the affinity level) also becomes pinned to the Fermi energy of the relevant electrode.<sup>148</sup> This can be verified when chemical modifications of the molecule, which will shift the molecular HOMO or LUMO energies considerably, do not affect the electron transport across the barrier: the donor or affinity levels are as if glued (pinned) to the Fermi level of the metal electrode.<sup>148,149</sup>

Figure 1 also shows, in red, the direction of the induced dipole moment vector  $\mu$  formed by the polarization charges within the molecule and the corresponding image charges in the metal. Alas, the vector  $\mu$  can be oriented in two opposite ways: physicists orient  $\mu$  from negative to positive charges, while the chemists, following Linus Pauling, orient  $\mu$  with the arrow tail starting from the positive charges and the arrowhead toward the negative charges.

The left part of Table 1 provides experimentally estimated polarization energies for holes  $P_{\text{ho}}$  and for electrons  $P_{\text{el}}$  (they are between 1 and 2 eV) for electron donor (D) molecules 1–11 and

Table 1. Vertical Gas-Phase Ionization Potentials  $I_D$  and Electron Affinities  $A_A$ , Measured by Direct and Inverse Photoelectron Spectroscopy, Respectively<sup>a,b,c,150</sup>

molecule	crystal	$I_D(g)$	$I_D(c)$	$P_{ho}$	$A_A(g)$	$A_A(c)$	$P_{el}$	$\Phi_B$	$E_{1/2,ox}$	$E_{1/2,red}$
benzene (1)	self	9.24 <sup>d</sup>	7.58 <sup>e</sup>	1.6 <sup>e</sup>		−1.15 <sup>g</sup> −0.72 <sup>j</sup>	0.4 <sup>h</sup>	1.5		2.30 <sup>i</sup> −3.42 <sup>j</sup>
naphthalene (2)	self	8.12 <sup>e</sup>	6.4 <sup>e</sup>	1.7 <sup>e</sup>	0.15 <sup>j</sup>					−2.51 <sup>j</sup>
anthracene (3)	self	7.42 <sup>f</sup>	5.77 <sup>f</sup>	1.65 <sup>f</sup>	0.58 <sup>f</sup>				1.09 <sup>cd</sup>	−1.96 <sup>j</sup>
pentacene (4)	self	6.64 <sup>f</sup>	5.01 <sup>f</sup>	1.63 <sup>f</sup>		1.35 <sup>j</sup>				−1.30 <sup>j</sup>
pyrene (5)	Au	6.58 <sup>e</sup>	5.1 <sup>k</sup>	1.5 <sup>k</sup>	1.37 <sup>f</sup>	2.8 <sup>k</sup>				
	self	7.37 <sup>e</sup> 7.41 <sup>l</sup>	5.8 <sup>e</sup>	1.6 <sup>e</sup>	0.56 <sup>j</sup> 0.39 <sup>m</sup> 0.406 <sup>o</sup>				1.16 <sup>l</sup> 0.58 <sup>n</sup>	−2.10 <sup>j</sup>
perylene (6)	self	6.90 <sup>e</sup>	5.2 <sup>e</sup>	1.7 <sup>e</sup>	0.97 <sup>j</sup>					−1.67 <sup>j</sup>
	Au				0.973 <sup>p</sup> 0.993 <sup>q</sup>					
Pc (7)	self	6.41 <sup>r</sup>	5.20 <sup>s</sup>	1.21						−0.66 <sup>t</sup>
CuPc (8a)	self	6.38 <sup>r</sup>	5.00 <sup>t</sup>	1.38	3.4 <sup>k</sup>					−0.54 <sup>t</sup>
	C flat	6.38 <sup>r</sup>	5.15 <sup>u</sup> 4.82 <sup>w</sup>	1.23	4.3 <sup>v</sup>	2.65 <sup>v</sup>	−1.65			
	Au/up		4.75 <sup>u</sup>							−0.54 <sup>t</sup>
ZnPc (8b)	self	7.37 <sup>k</sup>	5.28 <sup>x</sup>	2.09		3.34 <sup>x</sup>				−0.89 <sup>t</sup>
MgPc (8c)	self		4.96 <sup>s</sup>							−0.91 <sup>t</sup>
Cu–F <sub>16</sub> Pc (8d)	C flat		5.65 <sup>u</sup>							
	Au/up		6.50 <sup>u</sup> 6.3 <sup>k</sup>			4.5 <sup>k</sup>				
TMPD (9)	self	6.2 <sup>y</sup>							0.10 <sup>z</sup>	
	self	6.84 <sup>aa</sup>								
TTF (10)	self	6.83 <sup>ab</sup>	5.0 <sup>e</sup>	1.8					0.35 <sup>ac</sup>	
	self	6.4 <sup>e</sup>	5.0 <sup>e</sup>	1.4 <sup>e</sup>						
BEDT-TTF (11)	self	6.7 <sup>ab</sup>							0.54 <sup>ac</sup>	
1,4-benzoquinone	self	9.99 <sup>ad</sup>			1.91 <sup>ae</sup>					−0.48 <sup>af</sup>
9,10-anthraquinone	self	9.34 <sup>ag</sup>	7.00 <sup>ah</sup>	2.34	1.59 <sup>ad</sup>	2.77 <sup>ah</sup>	1.2		1.21 <sup>ai</sup>	−0.98 <sup>aj</sup>
chloranil (12)	self	9.74 <sup>e</sup>	8.1 <sup>e</sup>	1.6 <sup>e</sup>						0.01 <sup>ak</sup>
TCNQ (13a)	self	9.5 <sup>e</sup>	7.4 <sup>e</sup>	2.1 <sup>e</sup>						0.127 <sup>al</sup>
	Pt	9.6 <sup>am</sup>	7.8 <sup>k</sup>	1.8		3.3 <sup>an</sup>	(3.9) <sup>ao</sup>	−0.6		
TCNQF <sub>4</sub> (13b)	self		8.34 <sup>x</sup>							0.53 <sup>ap</sup>
	Cu				(3.72) <sup>aq</sup>	5.24 <sup>x</sup>	−1.5			
PBI (14)	self							1.06 <sup>ar</sup>		−1.36 <sup>as</sup>
Alq <sub>3</sub> (15)	Au	7.25 <sup>at</sup>	5.80 <sup>k</sup>	1.45		1.0 <sup>bh</sup>	2.2 <sup>k</sup>	−1.2		0.35 <sup>av</sup> −2.68 <sup>av</sup>
	Au	7.25 <sup>at</sup>	5.70	1.55	3.25 <sup>au</sup>					
C <sub>60</sub> (16)	Au	7.58 <sup>ax</sup>	6.2 <sup>ay</sup>	1.4	2.65 <sup>aq</sup>	4.5 <sup>aw</sup>	−1.9			−0.18 <sup>az</sup>
SWCNT (17)	graphite		4.44 <sup>bb</sup>			4.44 <sup>bb</sup>		4.8 <sup>ba</sup> 4.44 <sup>bb</sup>		
	graphene	self	4.62 <sup>bc</sup>		4.62 <sup>bc</sup>			4.62 <sup>bc</sup>		
	Au(polyxt)							5.22 <sup>bd</sup>		
	Au(111)							5.26 <sup>bd</sup>		
	Au(110)							5.20 <sup>bd</sup>		
	Ag(polyxt)							4.3 <sup>bd</sup>		
	Ag(111)							4.46 <sup>bd</sup>		
	Ag(110)							4.14 <sup>be</sup>		
	Ag(100)							4.22 <sup>be</sup>		
	Al							4.06–4.26		
	Cu							4.46 <sup>bf</sup>		
	Zn							4.33 <sup>bg</sup>		

<sup>a</sup>Gas-phase (“g”) values for single molecules and their condensed-phase (“c”) values estimated for films either on the specified solid metal surface or for the pure crystalline solids when “self” is listed. The superscript % means that  $A_A$  was estimated from electrochemical data.<sup>151</sup> “Au/” means Au(111) topped by a SAM of C<sub>8</sub>H<sub>17</sub>SH. The chemical structures of compounds 1–17 are given in Figure 2. The polarization energy for holes is  $P_{ho} \equiv I_D(g) - I_D(c)$ ; the polarization energy for electrons is  $P_{el} \equiv A_A(g) - A_A(c)$ . Also listed are metal work functions  $\Phi_B$  as well as the solution half-wave oxidation ( $E_{1/2,o}$ ) and reduction ( $E_{1/2,r}$ ) potentials, relative to the standard calomel electrode (SCE) (or converted to this standard if so indicated). <sup>b</sup>The solution  $E_{1/2,ox}$  and  $E_{1/2,red}$  electrochemical values listed in Table 1 can be converted, approximately, to gas-phase  $I_D$  or  $A_A$  by adding to them two quantities: (1) the difference in solvation free energies of the neutral molecule and the anion (or cation), which is about −2 eV;<sup>151</sup> (2) the difference between a datum referenced to vacuum and the datum referenced to a solution reference electrode (RE), i.e., (2a) either 4.44 (±0.02

Table 1. continued

V)<sup>152</sup> or between 4.50 to 4.75 V<sup>127</sup> if the RE was the standard hydrogen electrode; (2b) 4.68 V<sup>152</sup> or 4.71 V<sup>153</sup> if the RE was the saturated calomel electrode (SCE); (2c) 5.24 V<sup>152</sup> if the RE was the Ag/Ag<sup>+</sup> electrode; and (2d) 5.21 V<sup>154</sup> if the RE was the ferrocene/ferricinium electrode. <sup>156–159</sup>The older literature values for the work function of Au, affected by Hg vapor on diffusion pumps,<sup>155</sup> quote  $\Phi_B(\text{Au})$  between 4.3 and 4.83 eV. More recent results are  $\sim 5.1$  eV;<sup>160,161</sup> 5.3<sup>141</sup> to 5.26 eV<sup>162</sup> for Au(111); 5.20 eV<sup>162</sup> for Au(100); and for polycrystalline Au 5.22<sup>155</sup> or 5.1 eV.<sup>140</sup> <sup>a</sup>Ref 163. <sup>b</sup>Ref 164. <sup>c</sup>Ref 165. <sup>d</sup>Ref 166. <sup>e</sup>Ref 167. <sup>f</sup>Ref 168. <sup>g</sup>Ref 151. <sup>h</sup>Ref 147. <sup>i</sup>Ref 169. <sup>j</sup>Ref 170. <sup>k</sup>Ref 171. <sup>l</sup>Ref 172. <sup>m</sup>Ref 173. <sup>n</sup>Ref 174. <sup>o</sup>Ref 175. <sup>p</sup>Ref 176. <sup>q</sup>Ref 177. <sup>r</sup>Ref 178. <sup>s</sup>Ref 179. <sup>t</sup>Ref 180. <sup>u</sup>Ref 181. <sup>v</sup>Ref 182. <sup>w</sup>Ref 183. <sup>x</sup>Ref 184. <sup>y</sup>Ref 185. <sup>z</sup>Ref 186. <sup>aa</sup>Ref 187. <sup>ab</sup>Ref 188. <sup>ac</sup>Ref 189. <sup>ad</sup>Ref 190. <sup>ae</sup>Ref 191. <sup>af</sup>Ref 192. <sup>ag</sup>Ref 193. <sup>ah</sup>Ref 194. <sup>ai</sup>Ref 195. <sup>aj</sup>Ref 196. <sup>ak</sup>Ref 197. <sup>al</sup>Ref 198. <sup>am</sup>Ref 199. <sup>an</sup>Ref 200. <sup>ao</sup>Ref 201; after subtracting 0.38 V<sup>202</sup> from the listed value<sup>201</sup> vs Fc/Fc<sup>+</sup> in MeCN. <sup>ap</sup>Ref 203. <sup>aq</sup>Ref 204. <sup>ar</sup>Ref 205; after subtracting 0.38 V<sup>202</sup> from listed values<sup>205</sup> vs Fc/Fc<sup>+</sup> in MeCN. <sup>as</sup>Ref 206. <sup>at</sup>Ref 207. <sup>au</sup>Ref 208. <sup>av</sup>Ref 209. <sup>aw</sup>Ref 210. <sup>ax</sup>Ref 152. <sup>ay</sup>Ref 211. <sup>az</sup>Ref 162. <sup>ba</sup>Ref 212. <sup>bb</sup>Ref 213. <sup>bc</sup>Ref 214. <sup>bd</sup>Ref 215.

electron acceptor (A) molecules 12–17 (see Figure 1). The reduction in the energy gap between the affinity level and the donor level, due to nonzero  $P_{\text{ho}} + P_{\text{el}}$ , has also been called gap renormalization.<sup>135</sup> The third-last column of Table 1 lists the work functions  $\Phi_B$  for inorganic metals.

The last two columns of Table 1 list relevant electrochemical half-wave potentials in solution for oxidation to the monocation ( $E_{1/2,\text{o}}$ ) and for reduction to the monoanion ( $E_{1/2,\text{r}}$ ), for molecules of interest (updating a previous list),<sup>150</sup> in particular for strong electron donors and acceptors: such data are more readily measured than gas-phase  $I_D$  or  $A_A$ .

Table 1 shows that the polarization energies are of the order of  $\pm 1$  to  $\pm 2$  eV. The polarization shifts  $P_{\text{ho}} \equiv I_D(\text{gp}) - I_D(\text{on m})$  and  $P_{\text{el}} \equiv A_A(\text{gp}) - A_A(\text{on m})$  affect indirectly the break junction experiments described below. Large  $\Delta$  values probably increase the coupling energy between metal and molecule and hence increase the molecular conductance: these  $\Delta$  can be estimated by calculations of the molecule plus the metal (see below). How should the molecules be connected to the electrode? Physisorbed Langmuir–Blodgett (LB) (vertical transfer)<sup>28,29</sup> or Langmuir–Shafer (LS) (horizontal transfer)<sup>216</sup> monolayers are kinetically ordered during transfer but may rearrange while seeking thermodynamic equilibrium or when a voltage is applied. Both LB and LS films are obtained after transfer to a solid substrate of a Langmuir film, which was defined precisely by George L. Gaines, Jr. (1930–1995) as an insoluble film at the gas–water interface. The present author baptizes these films at the air–water interface Pockels–Langmuir films, to honor both Agnes Pockels (1862–1935) and Irving Langmuir (1881–1957), as well as to differentiate them from the LB or LS films formed after transfer onto solid supports.

Chemisorbed monolayers (also known as self-assembled monolayers, SAMs; see Table 2) or chemisorbed single molecules are sturdily attached by covalent bond(s) to the metal electrode(s) (most often organic thiols on Au) and will budge less, but SAMs have less long-range order than LB or LS monolayers. The chemisorbed SAMs displace any adventitious impurities that may have physisorbed previously on the electrode, while LB and LS films merely cover them. Remember that the Au surface is hydrophilic when freshly made but develops a carbonaceous surface coating within 15 min of exposure to air and becomes hydrophobic.<sup>57,104,105,217</sup> Molecules can be connected to an atomically sharp tip or to a planar surface either by physisorption (small enthalpy of attachment, typically  $< 40$  kJ/mol = 0.41 eV/molecule, due to van der Waals forces) or by chemisorption (larger enthalpy of attachment, 40–500 kJ/mol = 0.41–5 eV/molecule) due to the formation of a covalent bond or a strong ionic bond.

Physisorption from the vapor phase normally produces an orientationally disordered adsorbate, and there is no control over which end of an electroactive molecule is closer to an electrode.

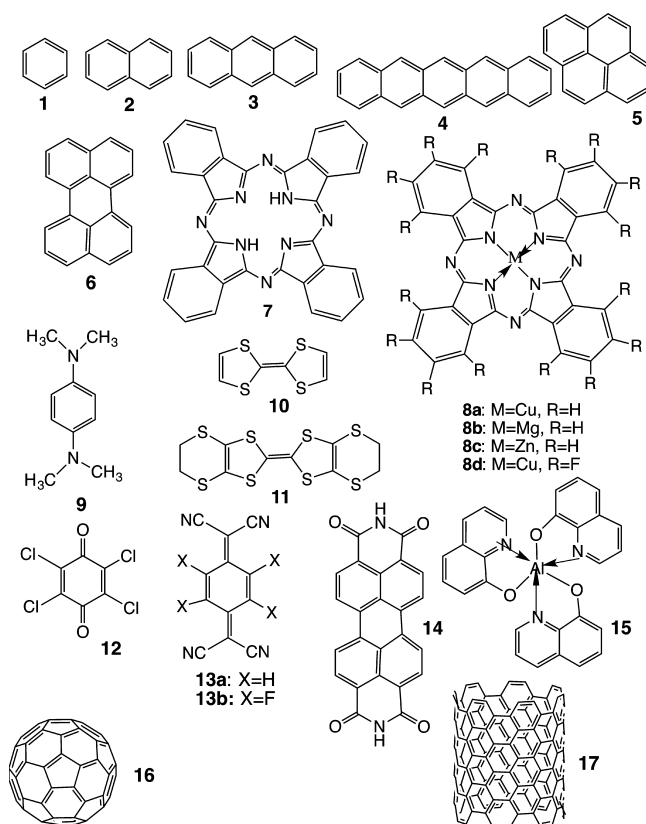


Figure 2. Electron donors and acceptors.

Ordered physisorption, either by the LB<sup>28,29</sup> or the LS<sup>216</sup> methods, achieves a monolayer that is relatively defect-free, not single-domain, but weakly bound.

Orientation of the molecule, relative to a planar metal substrate, affects strongly the coupling of the molecular orbitals of the molecule to the conduction band of the metal: for instance, for a film of the almost planar CuPc molecule, the ionization potential for the standing-up thin film is 0.40 eV greater than the ionization potential for the lying-down film, while for the terminally fluorinated F<sub>16</sub>CuPc  $I_D = 6.50$  is 0.85 eV higher than for the lying-down film, because of the opposite polarities of the C–H and C–F bonds.<sup>218</sup>

The most studied SAMs have been reviewed recently.<sup>219</sup> When thiols (R–SH) are chemisorbed onto Au, a homolytic cleavage of the S–H bond occurs, with loss of one hydrogen atom per thiol (presumably two H atoms then escape as a H<sub>2</sub> molecule); the R–S• radical then forms a bond to Au that is partly covalent, forming R–S–Au, and partly ionic, forming R–S<sup>−</sup> Au<sup>+</sup> (estimates of 50%–50% exist). When dithiols (R–S–S–R) or thioesters are bonded, the same R–S• radical forms. Thus, for chemists the R–S–Au bond may be polar (but see below);

**Table 2. Partial List of Molecules R–X That Either Chemisorb or Physisorb onto Planar Substrates<sup>58,219</sup> (ITO = Indium-Doped Tin Oxide; RLR = Representative Literature Reference)**

molecule R–X	substrate	bound species	RLR
R–CN	Ag, Au	physisorbed (polar)	220
R–COO <sup>−</sup> /R–COOH	Al <sub>2</sub> O <sub>3</sub> , Fe <sub>2</sub> O <sub>3</sub> , Ni, ITO	physisorbed (polar)	221, 222
R–COO–OOC–R	Si(111):H, Si(100):H	physisorbed (polar)	223
R–CH=CH <sub>2</sub>	Si	R–	224
R–C≡CH	Si(111):H	R–C≡C–	225
R–C <sub>3</sub> H <sub>5</sub> N	Au	physisorbed	89
R–NH <sub>2</sub>	FeS <sub>2</sub>	physisorbed	226
	Au	physisorbed	227
R–NC	Pt	physisorbed (polar)	228
R–N≡N <sup>+</sup> X <sup>−</sup>	pyrolytic graphite	R–	229
R–N≡N <sup>+</sup> BF <sub>4</sub> <sup>−</sup>	Pt, GaAs(100), Si(111):H	R–	230
R–OH	Fe <sub>2</sub> O <sub>3</sub> , Si–H	R–O–	231, 232
	Si	R–O–	224
R <sub>3</sub> –P	FeS <sub>2</sub>	R <sub>2</sub> P–	226
R–PO <sub>3</sub> <sup>−2</sup> , R–P(O)(OH) <sub>2</sub>	Al, Al–OH, GaAs, GaN,	physisorbed (polar)	233
	mica	physisorbed (polar)	234
	TiO <sub>2</sub>	physisorbed (polar)	235, 236
	ZrO <sub>2</sub>	physisorbed (polar)	236, 237
R–PO <sub>4</sub> <sup>−3</sup>	Al <sub>2</sub> O <sub>3</sub> , Nb <sub>2</sub> O <sub>5</sub>	physisorbed (polar)	238
	Ti <sub>2</sub> O <sub>3</sub> , TiO <sub>2</sub>	physisorbed (polar)	239
R–SH	Au, Ag, Cu	R–S– (polar ?)	240
	Hg	R–S– (polar ?)	241
	Ni	R–S– (polar?)	242
R–S–Ac	Ag, Au	R–S– (polar?)	243, 244
R–S–R′	Au	R–S– (polar?)	245
R–SeH	Ag, Au	R–Se– (polar?)	246, 247
R–SiX <sub>3</sub> (X = H, Cl, OC <sub>2</sub> H <sub>5</sub> )	ITO, HfO <sub>2</sub> , PtO, Si–O	R–Si–	248, 249
R–Hg–O– <i>p</i> -S(O)–C <sub>6</sub> H <sub>4</sub> –CH <sub>3</sub>	Au	R–	250
R <sub>3</sub> –SnX (X = O–C(O)CF <sub>3</sub> , O– <i>p</i> -S(O)–C <sub>6</sub> H <sub>4</sub> CH <sub>3</sub> , O–S(O)–CF <sub>3</sub> )	Au	R <sub>3</sub> –Sn–	251
R–Sn–(CH <sub>3</sub> ) <sub>3</sub>	Au	R– (or maybe R–Sn–)	252

for physicists, the resulting local dipole moment is associated with a Schottky barrier. Furthermore, a thiol binds to the Au surface by lifting one Au atom significantly above the plane of the other Au atoms.<sup>253</sup> SAMs are sturdily anchored at the right distance from the metal substrate; however, perfect monolayer coverage, easily achieved kinetically for LB films, is very difficult to obtain in SAMs.

The chemical stability of thiol SAMs has been reviewed.<sup>65</sup> Three conclusions therein are emphasized here: (i) All-trans-alkanethiols tilt by  $\sim 30^\circ$  from the normal to the surface because van der Waals forces stabilize the adsorbate when the adsorption sites would not be commensurate to close-packed alkanes<sup>254</sup> (similar tilting occurs in LB films and even in alkane crystals). (ii)

The preferential bonding of thiols on Au is an instance of “hard” versus “soft” acid–base chemistry;<sup>32</sup> upon exposure to ozone, or even air, or UV radiation over time (several weeks), the thiolate adsorbates can become sulfonates<sup>255</sup> or sulfinate, particularly at defect sites. (iii) Displacement reactions are possible.<sup>65</sup>

The enthalpy of bond formation for chemisorbed species is not measurable directly: the heats involved are too small. The bond energy for Au–S is estimated as 1.74 eV,<sup>43,63</sup> while the net energy for adsorption of alkanethiols on Au was computed to be  $-0.22$  eV (exothermic).<sup>43</sup> The bond energy for the Au–N bond is much smaller, 0.35 eV.<sup>63,256</sup> Estimates for the enthalpy of bond formation of chemisorbed species are now available from temperature-programmed desorption and helium scattering: a desorption enthalpy of  $1.31 \pm 0.02$  eV/molecule for a thiol on Au(111) was obtained, independent of alkyl chain length.<sup>257</sup> Similar measurements for packed monolayers of long-chain alkanes on Au show a desorption enthalpy of 0.063 eV/CH<sub>2</sub> group (and, therefore, 1.01 eV/hexadecane molecule);<sup>258</sup> this value is large because of intermolecular attractions within the monolayer, which are absent for a single molecule. For 2-phenylethanolamine chemisorbed onto powdered SiO<sub>2</sub>, silica sites of different acidities yield desorption energies between 0.46 and 0.98 eV/molecule.<sup>259</sup>

The HOMO and LUMO energies of highly conjugated oligomers decrease gradually with the molecular size and ultimately converge into a single value at the work function of grapheme, which can be thought of as an infinite, two-dimensional, planar, aromatic molecule. In summary, the gas-phase ionization energies and electron affinities decrease by 0.5–2 eV, as the molecule or monolayer comes into contact with a metal; this effect, attributable either to polarization or to image charges, decreases the energy difference between the donor level and the affinity level, i.e., decreases the energy gap.

To reduce the electrical bias  $V$  needed to achieve resonant electron flow to (or from) metal electrodes and donor levels (or affinity levels), Table 1 suggests that the donor (affinity) levels become as small (as large) as possible, respectively. However, this design principle may have to be modified to accommodate what both Marcus theory and experimental results teach us about intermolecular electron transfer rates, as is explained later.

#### 4. MARCUS THEORY OF ELECTRON TRANSFER WITHIN A MOLECULE

The speed (and/or efficiency) of electron transfer (or transport) across a single molecule or monolayer of molecules has not been measured electrically, but it is estimated spectroscopically. Relatively efficient and fast electron transfer (as well as reduced back-transfer) have been vital goals in artificial photosynthesis; the design criteria for molecular wires and devices should be aware of the implications of Marcus theory.

Within a molecule, an intramolecular coupling energy  $\Gamma_{\text{intramol}}$  (lowering of potential energy barrier) must be considered: if there is resonance between a molecular energy level and the Fermi level of at least one metal electrode, then the elastic regime of electron transfer must be considered (with large currents). Here  $\Gamma_{\text{intramol}}$  is large and the currents should be relatively larger, by  $\sim 2$  orders of magnitude.

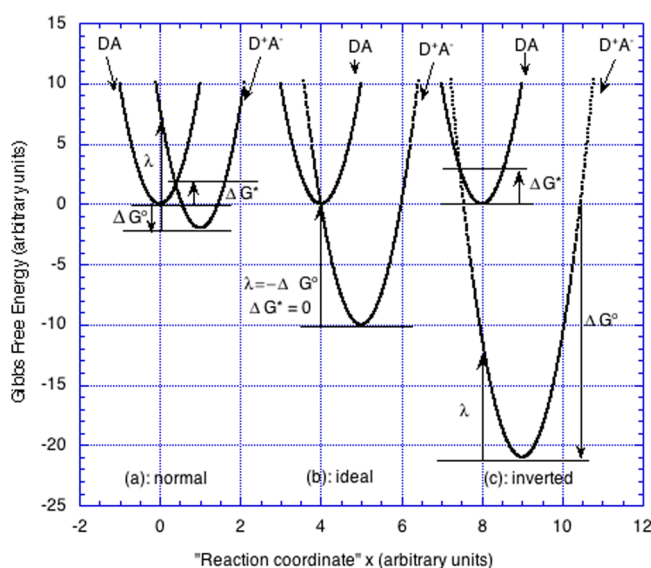
Semiclassical intramolecular electron transfer is best treated within Marcus theory;<sup>24,260</sup> the electron transfer rate  $k_{\text{ET}}$  is given by

$$k_{\text{ET}} = (2\pi/\hbar)|T_{\text{DA}}|^2 F_{\text{DA}} \quad (1)$$

where  $\hbar$  is Planck's constant  $h$  divided by  $2\pi$ ,  $T_{\text{DA}}$  is the electronic coupling energy between the electron donor moiety D and the electron acceptor moiety A, and  $F_{\text{DA}}$  is the thermally averaged (i.e., density-of-states weighted) Franck–Condon rearrangement factor, or vibrational overlap integral, between an electron donor region D and an electron acceptor region A connected by a rigid group  $\sigma$  in a molecule  $D-\sigma-A$ .<sup>24,260</sup> In the classical limit  $F_{\text{DA}}$  becomes

$$F_{\text{DA}} = (4\pi\lambda k_{\text{B}}T)^{-1/2} \exp[-(\Delta G^\circ + \lambda)^2/4\lambda k_{\text{B}}T] \quad (2)$$

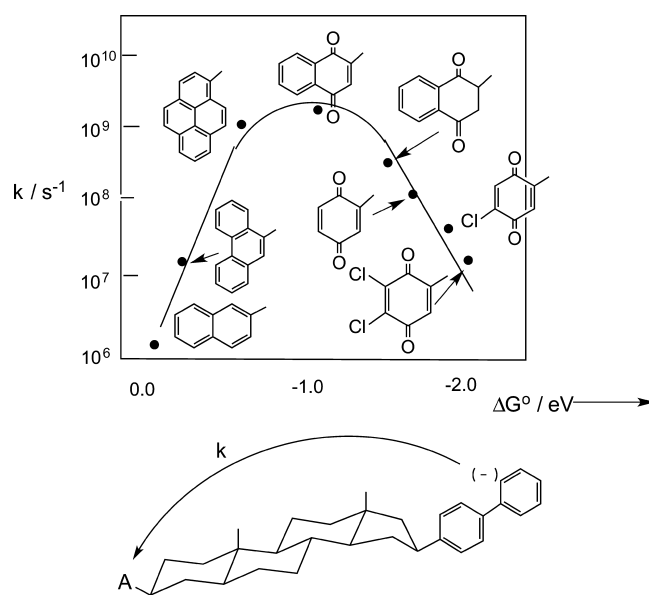
where, in turn,  $\lambda$  is the nuclear (molecular geometry) reorganization energy and  $\Delta G^\circ$  is the standard free energy of reaction ( $\Delta G^\circ < 0$  for exergonic reactions). There are three cases: normal, ideal, and inverted, shown in Figure 3. The free energy



**Figure 3.** Simplified representation of three cases for Marcus electron transfer theory. The relevant Gibbs free energy surfaces are represented as a parabola centered around the equilibrium coordinate(s) of the reagent (DA) and as a displaced parabola for the product ( $D^+A^-$ ) after the transfer of one electron. In all 3 cases the Gibbs free energy of reaction  $\Delta G^\circ$  is assumed to be negative (exergonic process). (a) Normal case: the free energy of activation  $\Delta G^*$  is positive, and the reorganization free energy  $\lambda$  is larger in absolute value than  $\Delta G^\circ$ :  $\lambda > -\Delta G^\circ$ . (b) Ideal case:  $\Delta G^* = 0$  and  $\lambda = -\Delta G^\circ$ . (c) Inverted case:  $\lambda < -\Delta G^\circ$ . For (a) and (c),  $\Delta G^* = (1/4)(\lambda + \Delta G^\circ)^2\lambda^{-1}$ . Reprinted by permission from ref 58. Copyright 2008 Royal Society of Chemistry.

difference  $\Delta G^\circ$  contains inter alia the difference ( $I_{\text{D}} - A_{\text{A}}$ ). As ( $I_{\text{D}} - A_{\text{A}}$ ) increases from zero,  $F_{\text{DA}}$  initially remains close to 1, so the reaction speeds up as  $|\Delta G^\circ|$  increases; if  $I_{\text{D}} - A_{\text{A}}$  becomes too large,  $F_{\text{DA}}$  becomes small (big Franck–Condon effect), so the rate slows down by several orders of magnitude. Figure 4 shows the experimental evidence for the inverted case.<sup>261,262</sup> The important messages are (i) the difference ( $I_{\text{D}} - A_{\text{A}}$ ) should be minimized; (ii) in a device, and under bias, ( $I_{\text{D}} - A_{\text{A}}$ ) becomes smaller than in the gas phase; (iii) if ( $I_{\text{D}} - A_{\text{A}}$ ) is too large, then the rate of electron transfer may become unacceptably slow because of the Franck–Condon factor. It is a waste of time to make unimolecular devices that are supersmall but superslow.

In the early days of molecular electronics, inspired by the pioneering paper of Aviram and Ratner,<sup>13</sup> a goal was to increase the chance for resonant electron transfer from metal to molecule to metal by using components with the smallest possible  $I_{\text{D}}(\text{gp})$  and the largest possible  $A_{\text{A}}(\text{gp})$  (see Table 1). Obviously, using



**Figure 4.** Intramolecular electron transfer rate constants  $k$  ( $\text{s}^{-1}$ ) as a function of the free energy difference for the reaction biphenyl(–) androstane-A  $\rightarrow$  biphenyl androstane-A(–), estimated from the electrochemical reduction potentials in 2-methyltetrahydrofuran; the inverted region for electron transfer rates is prominent. Redrawn by permission from refs 262 (copyright 1984 American Chemical Society) and 58 (copyright 2008 Royal Society of Chemistry).

graphite or graphene for which  $I_{\text{D}}(\text{gp}) = A_{\text{A}}(\text{gp}) \approx 4.5$  eV would not work: this would confer no directionality to the organic device. The important lesson from Figure 3 is that, for very small  $I_{\text{D}}(\text{gp})$  or for very large  $A_{\text{A}}(\text{gp})$ , the electron transfer rate would undergo an unwanted decrease because of large reorganization energies.

Thus, there is some wisdom in using either medium  $I_{\text{D}}(\text{gp})$  or  $A_{\text{A}}(\text{gp})$  (with small reorganization energies), e.g., PBI (**14**), or very rigid molecular geometries, e.g.,  $C_{60}$  (**16**), which narrows the vibrational spectrum and reduces the molecular reorganization energy. For the excellent strong electron acceptors TCNQ (**13a**) or TCNQF<sub>4</sub> (**13b**), the Franck–Condon factor  $F_{\text{DA}}$  becomes very small (the considerable change in geometry between neutral and quinonoid TCNQ and the benzenoid TCNQ<sup>–</sup> monoanion is tracked very well in respective crystal structures). As will be discussed again later, one view is that the Franck–Condon factor  $F_{\text{DA}}$  is NOT involved in the conduction from metal to molecule to metal.<sup>46</sup>

## 5. ELECTRICAL CONDUCTIVITY, CLASSICAL AND QUANTIZED: OHM'S LAW AND TUNNELING

If one puts either a single molecule or a monolayer of molecules between two identical metal electrodes (typically Au, but also Pt, Pd, or Al), a metal 1|molecule|metal 2 sandwich ensues. Many people use the term “junction”, but with two junctions on two sides of a molecule or monolayer the term “sandwich” may be palatable<sup>11</sup> (with apologies to John Montagu, the fourth Earl of Sandwich (1718–1792)!). If the second electrode has the same macroscopic dimensions as the first one, as well as the same crystallinity (same average crystal face), then the electrodes are considered symmetrical. If the second electrode is an STM tip, and the first electrode is a metal plane, then there are corona effects: a nanotip (NT) concentrates the electric field, as discussed earlier. If both electrodes are atomically sharp tips, as in



a break junction, the electric field at the tips can be very intense, of the order of  $\text{GV m}^{-1}$ .

The most appropriate theoretical language, which will describe adequately the dynamical situation when the current is flowing through the molecule, is still evolving. Many theories deal with electron transport across monolayers or other thin films (“electron transfer” is the term preferred by chemists). Discussing some concepts may be helpful: mechanisms, characteristic lengths, and times for each process, compared to the working length  $d$  of a single molecule (say  $d = 2 \text{ nm}$ ).

In vacuum, or in thin films over very short distances (e.g.,  $< d$ ), quantum-mechanical tunneling is a crucial concept and can be the dominant process. Tunneling events are very fast; remember that, for a photon in vacuum the speed is  $3.0 \times 10^{17} \text{ nm s}^{-1}$ , so in vacuum  $2 \text{ nm}$  are traveled in  $6.7 \text{ as}$ ; however, a detailed estimate for the characteristic time  $t_{\text{tun}}$  for a tunneling event is of the order of  $1 \text{ fs}$ ,<sup>46</sup> i.e., faster than the time for a molecular vibration.

Tunneling implies an energy barrier  $\Phi_{\text{B}}$  (eV) and a width  $d$  (nm), within which a quantum-mechanical wave function has finite amplitude (which approaches zero asymptotically as  $d \rightarrow \infty$ ). The wave function can be conceived as a wave coming from the left, partially reflected back to the left, and partially transmitted to the right through the barrier with probability amplitude  $\psi$  and probability  $P = |\psi|^2$ .

Elastic (or ballistic) transport happens if the electron in a material medium does “feel” the dielectric constant it travels in but does not interact with either phonons (acoustic or optical) or excitons; this ballistic electron has a transmission probability  $P = 1$ . For an electron in Cu metal, the instantaneous speed is  $1.6 \times 10^{15} \text{ nm s}^{-1}$  (0.53% of the speed of light).

If the electron does interact with phonons or excitons, then scattering occurs, the transfer slows down, and the transport becomes inelastic. The elastic mean free path  $l$  is defined as the length between successive scattering events.

Coherent transport occurs if the phase of the wave is conserved: the phase-coherence length  $L_{\varphi}$  is not so important in the present discussion. The coupling of nanoscopic objects to measuring electrodes can be weak, intermediate, or strong; alas, this classification is somewhat imprecise.

When scattering is the dominant mechanism limiting conduction, then temperature-dependent phase-incoherent hopping between energy levels occurs, the electron spends some time localized in each intermediate state, the current decreases in a complicated way with distance, and Ohm’s law applies,<sup>263</sup>

$$G = 1/R = I/V \quad (3)$$

where  $G$  is the conductance (siemens  $\equiv 1/\text{ohms}$ ),  $R$  is the resistance (ohms),  $I$  is the current (ampères), and  $V$  is the voltage (volts).

Maxwell found<sup>264</sup> that, for a sample of contact radius  $r$ , cross-sectional area  $\pi r^2$ , and volume conductivity  $\sigma$  (Siemens/m), the conductance  $G$  is given by

$$G = 2r\sigma = 2r/\rho \quad (4)$$

where  $\rho$  is the volume resistivity (ohm/m), provided that contact radius  $r$  is greater than the mean-free-path  $l$ .<sup>40</sup>

Using Fermi–Dirac statistics for electrons in metals, and in particular the Fermi wavevector  $k_{\text{F}}$  for a metal, eq 4 can be rewritten,<sup>40,265</sup> using  $e$  as the electronic charge and  $h$  as Planck’s constant of action, as

$$G = (2e^2/h)(k_{\text{F}}r/2)^2 \equiv G_0(k_{\text{F}}r/2)^2 \quad (5)$$

where

$$G_0 \equiv (2e^2/h) = 77480.9 \text{ nanoSiemens} \quad (6)$$

$G_0$  is the Landauer quantum of conductance,<sup>266–269</sup> discussed further later.

The temperature dependence of resistivity  $\rho$  in ordinary metals is well-described experimentally in terms of a finite temperature-independent term  $\rho_0$  plus a linear temperature dependence above a certain temperature  $T_0$ :

$$\rho(T) = \rho_0 + a(T - T_0) \quad (7)$$

Theoretical expressions for  $\rho(T)$  have a more complicated power-series dependence on  $T$ .

There are three effects that should be discussed:

(1) Superconductivity: for several metals (and even many cuprates and ferrates), below a critical temperature  $T_{\text{C}}$  and a critical applied magnetic field  $H_{\text{C}}$ , electrons with equal but opposite momenta close to the Fermi level form Cooper pairs, which creates a collective lower-energy superconducting state with zero resistivity ( $\rho_0 = 0$  in eq 7) and diamagnetic susceptibility (flux exclusion, or Meissner effect). Superconductivity has not yet been reported in unimolecular electronics.

(2) Kondo effect: in nonmagnetic metals with a small added paramagnetic impurity (e.g., with spin  $S = 1/2$ ), at a finite, low temperature now called the Kondo temperature  $T_{\text{K}}$ , the resistivity has a broad minimum (the conductance has a broad maximum). This was explained by Jun Kondo as a many-body effect that produces a logarithmic singularity in the resistivity:<sup>270</sup> around  $T_{\text{K}}$ , the impurity spin-couples with an itinerant spin to form a local  $S = 0$  state, which removes that itinerant spin from scattering processes. Later theorists showed that the conductance  $G$  reached not infinity but the Landauer limit  $G_0$ , eq 6.<sup>271</sup> Kondo-like effects have been seen in semiconducting GaAs quantum dots,<sup>272,273</sup> and Kondo physics became a popular area of study. The term “quantum dot” was coined by Mark Reed.<sup>274</sup>

(3) CB<sup>275</sup> can occur in semiconducting quantum dots, single-walled metallic carbon nanotubes (SWCNTs), or metallic islands while measuring current  $I$  as a function of applied voltage  $V$ ; for some voltage ranges no current is seen, i.e., the electron has trouble getting on or off the dot. This CB is seen if, and only if,

$$k_{\text{B}}T < E_{\text{C}} \quad (8)$$

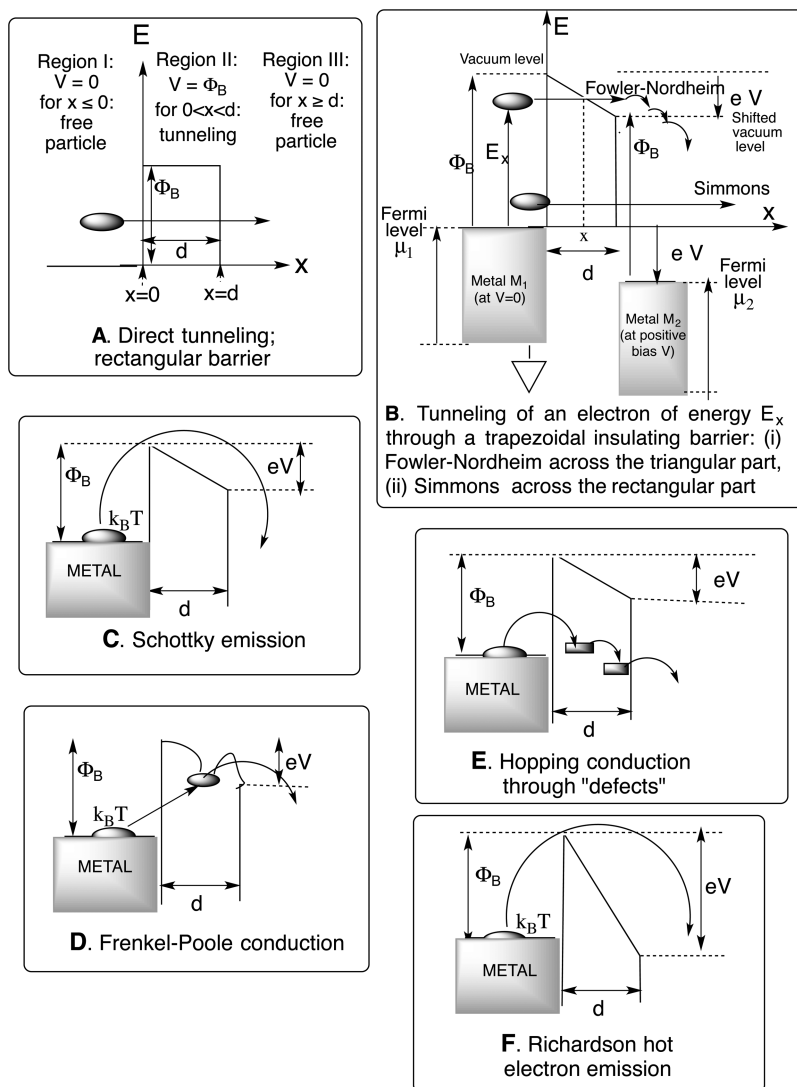
where  $E_{\text{C}}$  is the charging energy, or energy required to put one more electron onto a quantum dot:

$$E_{\text{C}} = e^2/2C \quad (9)$$

The CB can also be seen in the single-electron transistors (SETs)<sup>87,275–277</sup> discussed later.

During measurements, because of high electric fields (a potential of  $2 \text{ V}$  across a  $2\text{-nm}$  thick monolayer is a field of  $1 \text{ GV/m}$ ), electromigration of Au can occur, either causing short circuits or else forming Au whiskers, which then dominate the device conductance.<sup>109,110</sup>

One can also discuss the different relevant time scales for electron travel from metal to molecule to metal.<sup>64,66</sup> Using the Heisenberg uncertainty principle and  $\hbar \equiv 6.583 \times 10^{-16} \text{ eV s}$ , we can define, for elastic tunneling, a Landauer–Büttiker time<sup>66</sup>  $T_{\text{LB}} \equiv \hbar/\Delta E$ , where  $\Delta E$  is the energy gap between the Fermi level of the electrode and the molecular donor level or affinity level; for  $\Delta E = 2 \text{ eV}$ , the formula yields  $T_{\text{LB}} = 0.33 \text{ fs}$ .<sup>66</sup> If the itinerant electron interacts with (gets trapped by) a molecular vibrational



**Figure 5.** One-dimensional tunneling: (A) direct tunneling across a rectangular barrier (no metal present). (B) Fowler–Nordheim (cold emission) tunneling across the triangular top part of a trapezoidal insulating barrier between two metallic electrodes, and Simmons tunneling through the lower rectangular part. (C) Schottky emission. (D) Frenkel–Poole conduction. (E) Hopping conduction through defects (slow) or virtual states (superechange, fast). (F) Richardson thermoionic hot electron emission.

level ( $\Delta E \approx 2000 \text{ cm}^{-1} \approx 0.25 \text{ eV}$ ) then a vibrational residence time becomes  $T_{\text{vib}} \approx 2.6 \text{ fs}$ . If the itinerant electron interacts with a surface plasmon polariton, then the times increase further. Finally, if the electron (or hole) gets trapped in a molecular energy level, then very long residence times ( $\mu\text{s}$  to  $\text{s}$ ) become possible.

Image charges in the metal electrodes are dealt with by classical electrostatics. Polaron theory discusses new states in the gap between HOMO and LUMO (or donor level and acceptor level) due to (partial) charge formation within a molecule (usually in a polymer or in an assembly of identical molecules), which is balanced by induced counter-charges (gegen ions) within the metal. When molecules interact with metal nanoparticles, then surface plasmon-polaritons (also called surface plasmons) can be excited in the nanoparticle.

While solutions of the time-independent Schrödinger equation rely on the comforting reassurance provided by the Ritz variational theorem,<sup>278</sup> quantum-mechanical treatments of time-dependent electron transport do not benefit from similar reassurances. Let us first consider the rectangular barrier (Figure

5A) for which the Schrödinger equation can be solved analytically. First of all, for any energy barrier of height  $\Phi_B$ , if the electron has energy  $E > \Phi_B$ , then the barrier is ineffective and the eigenfunction of the free particle is

$$\psi(x) = A \exp(ikx) + B \exp(-ikx) \quad (10)$$

where  $k$  is the wavevector. If the electron energy  $E < \Phi_B$ , then tunneling becomes possible. As shown in Figure 5A, an electron of mass  $m_e$  and energy  $E$  in vacuum can tunnel through a rectangular barrier of width  $d$  and height  $\Phi_B$  ( $E < \Phi_B$ ) with a probability  $P$  that can be calculated by elementary quantum mechanics:<sup>289</sup>

$$P \approx 16 \exp(-2\alpha d)(\alpha k)^2 / (k^2 + \alpha^2)^2 \quad (11)$$

where

$$k \equiv (2m_e E)^{1/2} \hbar^{-1} \quad (12)$$

$$\alpha \equiv [2m_e(\Phi_B - E)]^{1/2} \hbar^{-1} \quad (13)$$

The resultant conductance  $G$  is

$$G = G_0 P = (2e^2/h)P \quad (14)$$

where  $G_0$  is the Landauer quantum of conductance.<sup>266–269</sup> The current  $I$  across the barrier is

$$I = GV \quad (15)$$

If  $E < \Phi_B$  and  $d = 1$  nm, then  $P$  is small. For instance, if  $E = 1$  eV =  $1.602 \times 10^{-19}$  J,  $\Phi_B = 2$  eV,  $m_e = 9.109 \times 10^{-31}$  kg, and  $d = 1$  nm, then one gets  $\alpha = k = 5.134 \times 10^9$  and  $P = 1.389 \times 10^{-4}$ , whence  $G = G_0 P = 10.76$  nanoSiemens. Further, if  $V = (E - \Phi_B)/e = 1$  V, then  $I = GV = 1.076 \times 10^{-8}$  A =  $6.7217 \times 10^{10}$  electrons  $s^{-1}$ . To fit results in actual materials, an effective mass  $m^*$  is often used as an adjustable parameter instead of  $m_e$ : this  $m^*$  can be up to 2 orders of magnitude larger (or smaller) than  $m_e$ . Finally, combining eqs 11, 14, and 15 with  $V = (E - \Phi_B)/e$ , one gets that the current  $I$ , if dominated by tunneling, is

$$I = \{(32e^2 h^{-1})[(\alpha k)^2/(k^2 + \alpha^2)^2]\}V \exp[-(2m_e V)^{1/2} d \hbar^{-1}] \quad (16)$$

which is linear in  $V$  at low bias.

## 6. WKBJ OR QUASI-CLASSICAL METHOD

If the electron source is a metallic electrode, then approximate quantum-mechanical formulas are used. One starts from the 1-dimensional time-independent Schrödinger equation,

$$(\hbar^2/2m_e)(d^2\psi(x)/dx^2) + [E - U(x)]\psi(x) = 0 \quad (17)$$

where  $E$  is the energy and  $U(x)$  is the potential energy. Exact analytical solutions exist for eq 17 for only a limited menu of potentials  $U(x)$ , so often approximate numerical methods become necessary. The approximate Wentzel–Kramers–Brillouin–Jeffreys or WKBJ method (also called the quasi-classical method)<sup>290</sup> first considers the electron momentum  $p(x)$ ,

$$p(x) = \pm [2m_e(E - U(x))]^{1/2} \quad (18)$$

and proposes the formally simple trial solution,

$$\psi(x) \equiv \exp[i\hbar^{-1}s(x)] \quad (19)$$

which yields the WKBJ differential equation,

$$(1/2m_e)(ds(x)/dx)^2 - (i\hbar/2m_e)(d^2s(x)/dx^2) = E - U(x) \quad (20)$$

which is simpler than the Schrödinger equation. Next,  $s(x)$  is expanded in powers of  $(\hbar/i)$ :

$$s(x) = s_0(x) + (\hbar/i)s_1(x) + (\hbar/i)^2s_2(x) + (\hbar/i)^3s_3(x) + \dots \quad (21)$$

In this asymptotic expansion, one often ignores all terms involving powers of  $\hbar$  and also neglects the second term on the left-hand side of eq 21; the result is the first-order differential equation

$$(1/2m_e)(ds_0(x)/dx)^2 = E - U(x) \quad (22)$$

which can be integrated formally and simply,

$$s_0(x) = \pm \int_{x=a}^{x=b} [2m_e(E - U(x))]^{1/2} dx = \pm \int_{x=a}^{x=b} p(x) dx \quad (23)$$

where the limits  $a$  and  $b$  are the carefully chosen classical turning points ( $a < b$ ) at which the momentum  $p(x)$  in eq 18 goes to zero. The non-oscillatory approximate eigenfunction of eq 19 becomes

$$\psi(x) \approx \exp\left\{-\frac{i}{\hbar} \int_{x=a}^{x=b} [2m_e(E - U(x))]^{1/2} dx\right\} \quad (24)$$

For the tunneling case ( $E < U(x)$ ), the momentum is imaginary and  $\psi(x)$  decays exponentially as  $x$  increases. The WKBJ method is valid if and only if  $|(d/dx)[\hbar/(ds(x)/dx)]| \ll 1$ . Using the definition of the de Broglie wavelength  $\lambda \equiv 2\pi\hbar p^{-1}$ , this condition becomes  $|(d/dx)(\lambda/2\pi)| \ll 1$ ; the WKBJ approximation is valid if the de Broglie wavelength of the particle varies only slightly over the particle's extent. The WKBJ result fails dramatically at the classical turning points of the motion, where  $[2m_e(E - U(x))]^{1/2}$  becomes zero before changing sign, as the particle reverses its motion. At these classical turning points  $a$  and  $b$ , the de Broglie wavelength  $\lambda$  becomes infinite, and the classical mechanics limit is reached.

For the free-particle case,  $E > U(x)$ , eq 24 becomes real, and the WKBJ quasi-eigenfunction is complex and oscillatory. Close to  $E = U(x)$ , and also for the exact solution of eq 17 for a trapezoidal barrier,<sup>291</sup> the eigenfunctions consist of Airy functions, which for practical values of the relevant parameters resemble sine or cosine functions.<sup>291</sup>

We now evaluate the probability  $P(E_x)$  for the tunneling case ( $E < U(x)$ ) in the absence of metals:

$$P(E_x) = \psi^*(x)\psi(x)/\psi^*(0)\psi(0) = \exp\left[(-2/\hbar) \int_{x=a}^{x=b} [2m_e(E - U(x))]^{1/2} dx\right] \quad (25)$$

If the tunneling barrier has width  $d$ , then

$$\psi(d) = \psi(0) \exp\left\{-\int_{x=0}^{x=d} [2m_e(U(x) - E)/\hbar] dx\right\} \quad (26)$$

whence the tunneling probability  $P(d)$  becomes

$$P(d) \equiv \psi(d)^*\psi(d)/\psi^*(0)\psi(0) = \exp\left\{-2 \int_{x=0}^{x=d} [2m_e(U(x) - E)]^{1/2} \hbar^{-1} dx\right\} \quad (27)$$

For different shapes of the tunneling barrier, the integrand in eq 23 is handled in different ways.

## 7. FOWLER–NORDHEIM EQUATION

When a single metallic electrode is covered by an insulator, then the current density  $J$  exiting the insulator in the  $x$ -direction can be evaluated from

$$J = e \int_{E_x=-E_x}^{E_x=\infty} N(E_x)P(E_x) dE_x \quad (28)$$

where  $N(E_x)$  is the electron supply function and  $P(E_x)$  is the electron transmission coefficient or transmission probability.<sup>292</sup> The supply function  $N(E_x)$  is obtained from the Fermi–Dirac distribution function  $\varphi(E) = \{1 + \exp[(E - \mu)/k_B T]\}^{-1}$ , where  $\mu$  is the Fermi level of the metal relative to the bottom of the Fermi–Dirac distribution,  $k_B$  is Boltzmann’s constant, and  $T$  is the absolute temperature; the integration over  $dE_{yz}$  is simple (and is carried out only in the two directions transverse to  $x$ ), by changing variables from energies to momenta and integrating the distribution function in the  $y$  and  $z$  directions in plane polar coordinates:

$$N(E_x) = 2h^{-3} \int_{p_y=-\infty}^{p_y=\infty} \int_{p_z=-\infty}^{p_z=\infty} [1 + \exp\{(U(x) + E_x + p_y^2 + p_z^2 - \mu)/k_B T\}]^{-1} dp_y dp_z \quad (29)$$

The result is

$$N(E_x) = (4\pi m_e k_B T/h^3) \ln_e \{1 + \exp[-(U(x) + E_x - \mu)/k_B T]\} \quad (30)$$

We now derive the equation for Fowler–Nordheim tunneling (Figure 5B(i)),<sup>281</sup> since this equation is not well explained in sources familiar to chemists. When two metallic electrodes are involved in a metal 1|insulator|metal 2 sandwich, the Fermi functions of metal 1 and metal 2,  $\varphi_1(E)$  and  $\varphi_2(E)$ , respectively, both must be included in the discussion, so, by 5 successive approximations,  $J$  is calculated, starting from the Tsu–Esaki formula:<sup>292–299</sup>

$$J = (4\pi m_e/h^3) \int_{E=0}^{E=\infty} dE_{yz} [\varphi_1(E) - \varphi_2(E)] \int_{E_{\min}}^{E_{\max}} P(E_x) dE_x \quad (31)$$

Approximation 1: at  $T = 0$ , the integral over  $dE_{yz}$  simplifies to

$$\int_{E=0}^{E=\infty} dE_{yz} [\varphi_1(E) - \varphi_2(E)] = \mu_1 - \mu_2 \quad (\text{if } T = 0 \text{ and } E_x \leq \mu_2) \quad (32)$$

$$= \mu_1 - E_x \quad (\text{if } T = 0 \text{ and } \mu_2 \leq E_x \leq \mu_1) \quad (33)$$

$$= 0 \quad (\text{if } T = 0 \text{ and } E_x \geq \mu_1) \quad (34)$$

This becomes two integrals:

$$J = (4\pi m_e/h^3) \left\{ \int_{E_x=-\infty}^{E_x=\mu_2} (\mu_1 - \mu_2) P(E_x) dE_x + \int_{E_x=\mu_2}^{E_x=\mu_1} (\mu_1 - E_x) P(E_x) dE_x \right\} \quad (35)$$

Approximation 2: the first integral of eq 35 is neglected, leaving

$$J = (4\pi m_e/h^3) \int_{E_x=\mu_2}^{E_x=\mu_1} (\mu_1 - E_x) P(E_x) dE_x \quad (36)$$

Approximation 3: assume the same metal for metal 1 and metal 2. The Fowler–Nordheim equation describes cold emission from a metal; to derive it, assume a triangular barrier (i.e., the triangular upper part of a trapezoidal barrier, Figure 5B above) with the left electrode grounded and a positive bias  $V$  (volts) applied to the right-hand electrode. The transmission coefficient  $P(E_x)$  in eq 36 now becomes

$$P(E_x) = \exp \left\{ - (2/\hbar) \int_{x=0}^{x=d(\mu_1+\Phi_B-E_x)/V} [2m_e(\mu_1 + \Phi_B - Vx/d - E_x)]^{1/2} dx \right\} \quad (37)$$

A formal integration then yields

$$P(E_x) = \exp \left\{ - (2/\hbar)(2m_e)^{1/2} (-2d/3V) [(\mu_1 + \Phi_B - Vx/d - E_x)^{3/2}]_{x=0}^{x=d(\mu_1+\Phi_B-E_x)/V} \right\} \quad (38)$$

$$P(E_x) = \exp \left\{ - (4d/3\hbar V)(2m_e)^{1/2} [\mu_1 + \Phi_B - E_x]^{3/2} \right\} \quad (39)$$

Then the remaining integral of eq 36 becomes

$$J = (4\pi m_e/h^3) \int_{E_x=\mu_2}^{E_x=\mu_1} (\mu_1 - E_x) \exp \left\{ - (4d/3\hbar V)(2m_e)^{1/2} [\mu_1 + \Phi_B - E_x]^{3/2} dE_x \right\} \quad (40)$$

Approximation 4: Equation 40 cannot be solved analytically, so we expand  $[\mu_1 + \Phi_B - E_x]^{3/2}$  in a Taylor expansion around  $\Phi_B$ :

$$[\mu_1 + \Phi_B - E_x]^{3/2} \approx \Phi_B^{3/2} + (3/2)(E_x - \mu)\Phi_B^{1/2} \quad (41)$$

Inserting eq 41 into eq 40 and defining  $\varepsilon \equiv E_x - \Phi_B$  and  $\lambda \equiv (2d/\hbar V)(2m_e)^{1/2}\Phi_B^{1/2}$  yields

$$J = (4\pi m_e/h^3) \exp \left\{ - (4d/3\hbar V)(2m_e)^{1/2} \Phi_B^{3/2} \right\} \int_{\varepsilon=\mu_2-\mu_1}^{\varepsilon=0} \exp \{ \lambda \varepsilon \} \varepsilon d\varepsilon \quad (42)$$

$$J = (4\pi m_e/h^3 \lambda^2) \exp \left\{ - (4d/3\hbar V)(2m_e)^{1/2} \Phi_B^{3/2} \right\} \exp [\lambda(\mu_2 - \mu_1)] [\lambda(\mu_2 - \mu_1)]^{-1} \quad (43)$$

Approximation 5: If  $\mu_2 \gg \mu_1$ , then eq 43 finally reduces to the Fowler–Nordheim equation for cold-electron emission (temperature-independent coherent tunneling):<sup>281</sup>

$$J = (e^3/8\pi\hbar)(V^2/\Phi_B d^2) \exp \left[ - (8\pi d/3e\hbar V)(2m_e)^{1/2} \Phi_B^{3/2} \right] \quad (44)$$

If in eq 44  $d$  is in Å,  $V$  is in volts, and  $\Phi_B$  is in eV, then the Fowler–Nordheim exponent  $-(8\pi d/3e\hbar V)(2m_e)^{1/2}\Phi_B^{3/2}$  becomes  $-0.002278dV^{-1}\Phi_B^{3/2}$ .

## 8. SIMMONS EQUATION

Simmons also used the WKB method and barrier (for a generalized, arbitrarily shaped barrier, but with the tunneling electrons feeling the applied voltage  $6V$  throughout the whole rectangular thickness of the barrier, rather than only the upper triangular part of it, as in Fowler–Nordheim theory) and smaller voltages  $V$  than in Fowler–Nordheim theory. Figure 5B shows both Fowler–Nordheim and Simmons tunneling. Because Simmons explained his derivations very well, we simply quote his equation for the current density:<sup>280,282,300</sup>

$$J = (e/4\pi^2\hbar d^2) \{ (\Phi_B - eV/2) \exp \left[ - (2d/\hbar)(2m_e)^{1/2} (\Phi_B - eV/2)^{1/2} \right] + (\Phi_B + eV/2) \exp \left[ - (2d/\hbar)(2m_e)^{1/2} (\Phi_B + eV/2)^{1/2} \right] \} \quad (45)$$

Equation 45 covers electron flows from metal 1 to metal 2 (first term inside the braces) and also from metal 2 to metal 1 (second term inside the braces).

At small bias ( $0 \approx V \ll \Phi_B$ ), the Simmons equation becomes approximately<sup>50,280,301</sup>

$$J \propto (e^2/h^2 d^2)(2m_e \Phi_B)^{1/2} V \exp[-(2d/\hbar)(2m_e \Phi_B)^{1/2}] \quad (46)$$

So, except for the exponential factor, the sandwich becomes ohmic.<sup>280,282</sup>

At large bias the first term in eq 45 becomes dominant:<sup>50</sup>

$$J = (e/2\pi\hbar d^2)(\Phi_B - eV/2) \exp[-(2d/\hbar)(2m_e)^{1/2}(\Phi_B - eV/2)^{1/2}] \quad (47)$$

When the bias  $V$  is even higher, then the Simmons equation reduces to the Fowler–Nordheim equation, eq 44.<sup>282,301</sup> The inclusion of image forces softens the edges of the energy barrier.<sup>282</sup> The Stratton equation for direct tunneling is much simpler:<sup>296,302</sup>

$$I = A \sinh(2^{-1/2} \hbar^{-1} eV d m_e^{1/2} \Phi_B^{-1/2}) \quad (48)$$

## 9. NEWNS–ANDERSON EQUATION AND EIGENVALUE STAIRCASE

The inverse-tangent equation was derived for other applications as the Newns–Anderson equation<sup>303,304</sup> but has been discussed for conductivity within molecules by several groups,<sup>305–308</sup>

$$I = A \{ \tan^{-1}[2(|\epsilon_{\text{HOMO}} - \mu| + eV/2)/B] - \tan^{-1}[2(|\epsilon_{\text{HOMO}} - \mu| - eV/2)/B] \} \quad (49)$$

where  $A$  and  $B$  are constants,  $\mu$  is the chemical potential or Fermi level of the metal electrode, and  $\epsilon_{\text{HOMO}}$  is the donor level of the monolayer ( $\approx$  highest occupied molecular orbital of the single molecule). The constants  $A$  and  $B$  in eq 49 have been defined as  $A \equiv 4N\Gamma_1\Gamma_2e/\hbar(\Gamma_1 + \Gamma_2)$  and  $B \equiv (\Gamma_1 + \Gamma_2)$ , where  $\Gamma_1$  ( $\Gamma_2$ ) is the molecular energy level broadening at the first (second) electrode–molecule interface.<sup>305</sup>

In eq 49 the zero of energy is placed in the middle of the gap. If the most significant molecular orbital coefficients of the  $\epsilon_{\text{HOMO}}$  are approximately centered at a fractional distance  $p$  from, say, the right electrode,<sup>305,306</sup> then the arguments of the two inverse tangent functions become  $(2|\epsilon_{\text{HOMO}} - \mu| + peV)$  and  $(2|\epsilon_{\text{HOMO}} - \mu| + (1 - p)eV)$ , respectively,

$$I = A \{ \tan^{-1}[2(|\epsilon_{\text{HOMO}} - \mu| + peV)/B] - \tan^{-1}[2(|\epsilon_{\text{HOMO}} - \mu| + (1 - p)eV)/B] \} \quad (50)$$

assuming that a lever rule is applicable;<sup>308</sup> if  $p$  is far from 0.5, then mildly asymmetric  $IV$  curves should ensue even for molecular wires.<sup>305,306</sup>

When a molecular device with only one accessible electronic energy level  $E_0$  for the electroactive moiety (electron donor or acceptor) situated at a fractional position  $p$  ( $0 \leq p \leq 1$ ) within a gap between two metal electrodes is addressed by an applied voltage  $V$ , then the current  $I$  is described by<sup>306</sup>

$$I = e^2 D^3 \hbar^{-1} \{ \tan^{-1}[(E_0 + epV)/D] - \tan^{-1}[(E_0 - epV)/D] \} \quad (51)$$

where  $D$  is a normalization constant. Equation 51 can be derived from eq 45.<sup>40</sup> If  $(\Gamma_1 + \Gamma_2)/2 \ll |\epsilon_{\text{HOMO}} - \mu|$ , then eq 49 simplifies to a Lorentzian line shape,

$$I = (2NeV\Gamma_1\Gamma_2/h)[(|\epsilon_{\text{HOMO}} - \mu| + \gamma eV)^2 - (\gamma eV/2)^2]^{-1} \quad (52)$$

where the parameter  $\gamma$  ( $-1/2 \leq \gamma \leq 1/2$ ) estimates where within the insulator layer (molecule or monolayer) the HOMO is localized.

The function  $\tan^{-1}V$  in eqs 49, 50, and 51 predicts a plateauing of the current at higher  $V$ <sup>306</sup> and, when several eigenvalues are sequentially accessible, an eigenvalue staircase.<sup>307,308</sup> This eigenvalue staircase (not to be confused with the Coulomb staircase discussed later) is intellectually appealing, but for unimolecular rectifiers a plateau has been seen only rarely (e.g., Figure 13 of ref 105), presumably because dielectric breakdown occurs before the plateau is reached; eigenvalue staircases have not been observed.

## 10. OTHER TUNNELING REGIMES

Other tunneling regimes shown in Figure 5 and listed in Table 3 are (i) Richardson thermoionic or hot emission tunneling;<sup>283,284</sup>

**Table 3. Behavior of the Current Density  $J$  for Various Conduction Mechanisms:  $\Phi_B$  Is the Energy Barrier<sup>a</sup>**

conduction mechanism	behavior	scheme	refs
direct tunneling (low $V$ )	$J \propto V \exp[-(2d/\hbar)(2m_e\Phi_B)^{1/2}]$	A	280
Fowler–Nordheim tunneling (cold field emission)	$J \propto (V/d)^2 \exp[-(4d/3e\hbar V)(2m)^{1/2}\Phi_B^{3/2}]$	B	281
Simmons	$J \propto (\Phi_B - eV/2)d^{-2} \exp[-(2d/\hbar)(2m)^{1/2}(\Phi_B - eV/2)^{1/2}]$	B	282
Schottky emission	$J = A_R T^2 \exp[-\Phi_B + (eV/4\pi\epsilon_{\text{ins}}d)^{1/2}]/k_B T$	C	283–285
Frenkel–Poole conduction	$J \propto (V/d)^2 \exp[-\Phi_B + (eV/\pi\epsilon_{\text{ins}}d)^{1/2}]/k_B T$	D	286, 287
hopping conduction via defects or superexchange	$J \propto V \exp[-\Delta E/k_B T] \propto \exp(-\beta d)$	E	26
Richardson hot thermoionic emission	$J \propto T^2 \exp[-\Delta E/k_B T]$	F	283, 284
Mott–Gurney space-charge-limited conduction (SCLC)	$J = 9\epsilon_0 \epsilon_{\text{ins}} \mu V^2 / 8 d^3$		132
SCLC with exponential distribution of traps	$J = [(2l + 1)/(1 + 1)^{1/2} \mu N_t q^{-1}  \epsilon_0 \epsilon_{\text{ins}} / (l + 1) N_t]^{1/2} [V^{l+1} / d^{2l+1}]$ for $l > 1$		288
activated ohmic conduction	$J \propto (V/d) \exp[-\Delta E/k_B T]$		
ionic conduction	$J \propto (V/dT) \exp[-\Delta E/k_B T]$		

<sup>a</sup> $V$  is the applied voltage,  $d$  is the thickness of the insulating barrier,  $\epsilon_{\text{ins}}$  is the dynamic dielectric permittivity ( $\approx$  relative dielectric constant) of the insulator,  $\mu$  is the electron mobility,  $m_e$  and  $e$  are the electronic mass (effective if desired) and charge, respectively,  $\hbar$  is Planck's constant divided by  $2\pi$ ,  $k_B$  is Boltzmann's constant,  $T$  is the absolute temperature,  $\Delta E$  is the relevant Arrhenius activation energy,  $A_R$  is the effective Richardson constant ( $A_R = em_e k_B^2 / 2\pi^2 \hbar^3$ ), and  $\beta$  is the superexchange decay constant. Schemes A–F are shown in Figure 5. In jest, “there are nearly as many models as there are publications.”<sup>279</sup>

(ii) Schottky emission;<sup>285</sup> (iii) Frenkel–Poole conduction;<sup>286,287</sup> (iv) ionic conduction; and (v) hopping conduction through either defect states or virtual states linked by quantum-mechanical superexchange.<sup>26</sup> For hopping conduction, if  $\Gamma_{\text{intramol}}$  is small, then nonresonant phase-coherent temperature-independent superexchange-modulated tunneling dominates,<sup>26</sup>

with an exponential decay of the current  $I$  with a distance  $d$  within the molecule,

$$I = I_0 \exp(-\beta d) \quad (53)$$

(Figure 5C). When  $d$  is given in Å, then typically  $\beta \approx 0.6\text{--}1.4 \text{ \AA}^{-1}$ , but  $\beta = 0.2\text{--}0.6 \text{ \AA}^{-1}$  for highly conjugated bridges.<sup>46</sup> In contrast, in a vacuum, for a barrier  $\Phi_B = 5 \text{ eV}$ ,  $\beta = 2.4 \text{ \AA}^{-1}$ .<sup>46</sup>

This superexchange model is used routinely for length-dependent incoherent tunneling in biological systems. The McConnell superexchange<sup>26</sup> mechanism is distinct from the magnetic spin superexchange theory of Kramers,<sup>309</sup> Anderson,<sup>310</sup> Goodenough,<sup>311,312</sup> and Kanamori,<sup>313</sup> which concentrates on spin exchange (rather than charge exchange); both originate in the exchange Coulomb repulsion integrals in Hartree–Fock theory. The McConnell mechanism allows electrons to tunnel across a succession of virtual states in very short times.

If  $\Gamma_{\text{intramol}}$  is large and an available energy level is available within the molecule, then resonant phase-coherent temperature-independent tunneling occurs. The current is typically at least 2 orders of magnitude larger than those for comparable molecules where superexchange dominates.

If phase-incoherent temperature-dependent hopping between stationary states occurs, then superexchange is no longer invoked, but experimentally

$$I \propto A \exp(-\Phi_B/k_B T) \quad (54)$$

where  $A$  is some constant; this hopping leads to Ohm's law. Experimentalists often compare eqs 53 and 54 to describe their results, even though they imply different mechanisms. The kinetics derived from superexchange in DNA have been linked theoretically<sup>314</sup> to Ohm's law.<sup>263</sup>

## 11. LANDAUER EQUATION

Quantum theoretical calculations of tunneling have also prospered. As discussed in eq 24, the elastic conductance through a nanoscopic system in one dimension can be conceived as a transmission problem,<sup>40,266,267,315</sup>

$$I = VG = (2e/h) \int_{-\infty}^{\infty} [f_L(E) - f_R(E)]P(E) dE \quad (55)$$

where  $f_L(E)$  and  $f_R(E)$  are the Fermi–Dirac distribution functions of the electron reservoir of the left and right electrodes, respectively,

$$f_L(E) \equiv \{1 + \exp[(E - \mu_L)/k_B T]\}^{-1} \equiv f_0(E - \mu_L) \quad (56)$$

$$f_R(E) \equiv \{1 + \exp[(E - \mu_R)/k_B T]\}^{-1} \equiv f_0(E - \mu_R) \quad (57)$$

where  $\mu_L$  and  $\mu_R$  are the Fermi levels and  $P(E)$  is the transmission probability discussed earlier. At 0 K and an applied voltage  $V$ , the Fermi levels become Fermi energies, and  $f_L(E) = f_R(E) = 1$  below  $\mu_L + eV/2$  (or below  $\mu_R + eV/2$ ), but  $f_L(E) = f_R(E) = 0$  above them.

In the tunneling regime, when the coupling between the (now 3-dimensional) electrodes and the nanoscopic channel (molecule, thin film, nanotube, etc.) is large, then the current  $I$  is given by the Landauer–Imry–Büttiker–Keldysh formula (simply, the Landauer formula, based on Fermi's golden rule):<sup>266–269</sup> the total current  $I$  from the left metal electrode L to the right metal electrode R, due to the presence of either one or many molecules (or strings of metal atoms) in the gap, is given by

$$I = (2e/h) \int_{-\infty}^{\infty} [f_L(E) - f_R(E)] \text{Tr}\{G^A(E)\Gamma^R(E)G^I(E)\Gamma^L(E)\} dE \quad (58)$$

where  $G^A(E)$  and  $G^I(E)$  are the advanced and retarded Green's functions for the molecule, respectively,  $\Gamma^R(E)$  and  $\Gamma^L(E)$  are matrices that describe the coupling between the molecule and the right and left metal electrodes, respectively, and  $\text{Tr}\{\}$  is the trace operator. The use of nonequilibrium Green's functions is due to Keldysh;<sup>269</sup> the best explanation of eq 58 is due to Imry.<sup>268</sup> The Landauer formula assumes elastic scattering of the electrons across the molecule or other nanoscopic object.<sup>66</sup> The computations implementing eq 58 have been discussed.<sup>40</sup>

As presented already in eq 14, the Landauer quantum of conductance,

$$G_0 \equiv 2e^2/h = 77481 \text{ nS} = 1/12.9064 \text{ k}\Omega \quad (59)$$

is the maximum conductance allowed for a two-probe measuring geometry (the factor of 2 is due to the two spin states). The quantum of resistance,  $R_0$ , the reciprocal of  $G_0$ , is also known as the von Klitzing constant.<sup>316</sup> If four-probe measurements on a single molecule were ever to become possible, then the intrinsic conductance of the molecule, independent of the electrodes, could vastly exceed  $G_0$ .

For simple cases the transition probability  $P(E)$  in eq 55 becomes a Lorentzian or Breit–Wigner function,

$$P(E) = 4\Gamma_L\Gamma_R / [(E - eV)^2 + (\Gamma_L + \Gamma_R)^2] \quad (60)$$

where  $\Gamma_L$  ( $\Gamma_R$ ) is the coupling energy from the left (right) electrode to the gap. Equation 60 ignores the energy levels of the molecule or molecular wire within the gap.<sup>40,315</sup> The tunneling rates into (out of) the left (right) gap are  $\Gamma_L/\hbar$  ( $\Gamma_R/\hbar$ ).

We next try to include details about the molecule in the gap. Marcus theory, eq 1, can be applied to the rate constant  $k_{DA}$  for intramolecular electron transfer within a D–B–A (donor–bridge–acceptor) molecule, by writing<sup>46</sup>

$$k_{DA} = (2\pi/\hbar) |\Gamma_{LD}\Gamma_{AR}|^2 |G_{DA}(E)|^2 F_{DA} \quad (61)$$

where  $\Gamma_{LD}$  and  $\Gamma_{AR}$  are the coupling energies between the left electrode and the donor (D) end of the D–B–A molecule and between the acceptor (A) end of the molecule and the right electrode, respectively.  $\Gamma_{LD}$  and  $\Gamma_{AR}$  in eq 61 are more specific coupling energies than  $\Gamma_D$  and  $\Gamma_R$  in eq 60.  $G_{DA}(E)$  is the Green's function for the molecule D–B–A,

$$G_{DA}(E) = [E - \langle ij \rangle - H(E)]^{-1} \quad (62)$$

where  $\langle ij \rangle$  is the overlap integral between relevant molecular orbitals  $i$  and  $j$  and  $H(E)$  is the Hamiltonian operator for the molecule.<sup>46</sup> In eq 61  $F_{DA}$  is again the Franck–Condon factor. One can connect eq 61 with a vast simplification of eq 58; to wit,<sup>46,315</sup> the conductance from left electrode L to the molecule D–B–A to the right electrode R is now given by

$$G_{L\text{--}DBA\text{--}R} \approx (8e^2/\pi^2 \Gamma_{LD}\Gamma_{AR}) k_{DA} \quad (63)$$

This formally introduces coupling energies  $\Gamma_{LD}$  and  $\Gamma_{AR}$  between electrodes and molecule and also includes the Franck–Condon factor  $F_{DA}$ . In contrast, it was stated<sup>46</sup> that the factor  $F_{DA}$  should be omitted from eq 61 “because the reorganization energy ... does not affect the conduction through the molecule”.<sup>46</sup> If only McConnell superexchange<sup>26</sup> is operative within D–B–A, eq 63 should definitely be divided by  $F_{DA}$ . However, if resonant tunneling occurs through the molecule,

then  $F_{\text{DA}}$  must be involved. This nontrivial difference of opinion may affect future molecular design.

The coupling energies  $\Gamma_{\text{LD}}$  and  $\Gamma_{\text{AR}}$  (in general,  $\Gamma$ ) between metal electrodes and molecule are the lowering of the energy barrier to electron transfer between metal and molecule. One must also consider the barrier to intramolecular electron transfer  $U$ , which is the HOMO–LUMO gap, or, better yet, the energy difference between the affinity and the donor levels of Figure 1. There are three regimes, depending on the size of the ratio  $\Gamma/U$ :<sup>77</sup>

(1) If  $\Gamma \gg U$ , if a strong covalent bond couples a single molecule to an electrode (or if the molecule lies down directly onto the plane of the electrode and its molecular orbitals acquire a partial metallic character)<sup>317</sup> and also if the molecular orbitals are accessible from the Fermi levels of the metal electrodes, then  $\Gamma$  is considered large (compared to the HOMO–LUMO energy gap,  $k_{\text{B}}T$ , and  $e/2C$ ); the Landauer–Imry–Büttiker–Keldysh approach described later will best estimate the elastic through-molecule currents.

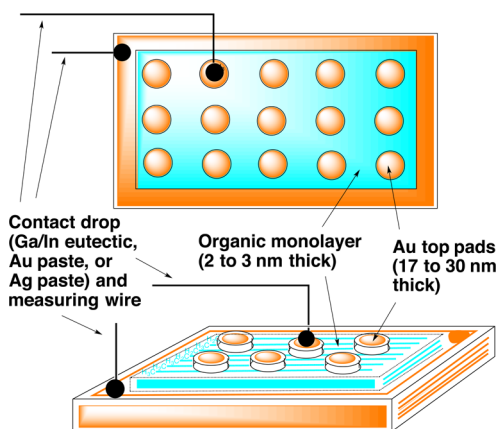
(2) If  $\Gamma$  is intermediate ( $\Gamma \approx U$ ), then at low enough temperature an unpaired spin (e.g., a trapped magnetic impurity or a localized spin on a molecule) may generate a Kondo conductance maximum;<sup>270</sup> in this (typically many-body) effect, a local spin-pairing with that spin decreases the number of conduction electrons available for scattering and resistance.<sup>86,270,271,318</sup>

(3) If  $\Gamma$  is small ( $\Gamma \ll U$ ), then for a certain bias window CB may occur; sometimes the CB can coexist in the same system with a Kondo-type conductance maximum.<sup>272,273</sup>

## 12. TWO-PROBE CONDUCTIVITY MEASUREMENT TECHNIQUES

Macroscopic measurements of the electrical conductivity of macroscopic crystals and bulk polymers can be done by either two-probe or four-probe methods. The conductivities obtained by two probes always include the resistance of the probes and the probe–crystal interfaces. The four-probe method can eliminate the resistance due to probes or contacts.

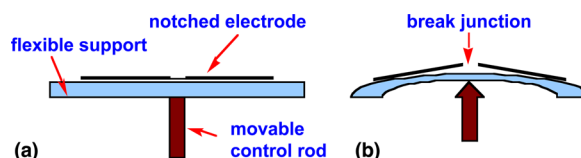
A two-probe macroscopic measurement of the electrical conductivity of a monolayer (of nanoscopic thickness) is shown in Figure 6: typically,  $10^{11}$ – $10^{12}$  molecules are probed beneath each pad. Smaller areas (typically  $5 \times 10^3$  molecules chemisorbed



**Figure 6.** Macroscopic two-probe setup for measuring the conductivity of an organic monolayer (typically 2–3 nm thick). Each top pad contact area is typically 1–100 mm<sup>2</sup>. Reprinted by permission from ref 11. Copyright 2012 Springer Verlag.

in parallel) were probed by the nanopore method introduced by Mark Reed.<sup>50,319–321</sup>

A crossed-wire technique allowed the measurement of  $\sim 10^3$  molecules trapped between two cylindrical Au wires of 10  $\mu\text{m}$  diameter placed normal to each other and brought together in soft contact.<sup>301,322,323</sup> The conductance of single molecules placed between two electrodes, at least one of which is of nanoscopic dimensions, has evolved from (i) the STS mode of STM,<sup>81</sup> to (ii) the mechanical break junction (MBJ) (Figure 7),<sup>84,85</sup> to (iii) the electromigration break junction (EMBJ),<sup>86</sup> and finally to (iv) the scanning break junction (SBJ).<sup>89</sup>



**Figure 7.** Depiction of the mechanical break junction (MBJ) (a) before the break and (b) after the control rod has caused the break. A piezoelectrically driven piston (movable control rod) can bend a sample of Kapton polymer that is rigidly clamped between two rigid supports (not shown). The thin, notched Au electrode predeposited atop the Kapton is forced to break at the notch, creating a 0.1–1 nm gap, whose size is controlled by the piston. A solution of a dithiol chemisorbs and bridges the Au gap. Reprinted by permission from ref 11. Copyright 2012 Springer Verlag.

The MBJ (Figure 7) has become a veritable cottage industry, particularly for physicists (who love to measure at 4.2 K). In more recent work, the Kapton polymer of Figure 7 was replaced by Si(111), and Au nanogaps were achieved by electroplating Au into an initially large Au metal gap.<sup>324</sup>

Earlier, 1000 painfully repeated conducting-tip AFM measurements had been performed on individual 1,8-octanedithiol (**19d**) molecules topped by Au nanoparticles.<sup>325</sup> (Chemical structures **18**–**147** are depicted in Table 4 of section 18.) Two years later, Nongjian Tao and student developed the SBJ: using an Au substrate and either a conducting-tip AFM or an STM, a solvent, and bonding terminal diamines or bithiols to both electrodes, they measured the current repeatedly across the chemisorbed molecule at several potentials (–1 V to +1 V) until the tip-to-molecule junction was broken and found a broad minimum in the conductance  $G$  at low potentials (of the order of 0.01–0.05 V) (Figure 8).<sup>89</sup> The solvent presumably helped the molecules “stand up” to be measured. Thousands of repeated measurements ensured good statistics.

## 13. THERMOPOWER

The thermoelectric effect in SBJ was first studied by Ludolph and van Ruitenbeek,<sup>326</sup> then developed,<sup>327</sup> and measured for several molecules, by keeping the STM Au tip at room temperature, while placing a Peltier-effect heater below the bottom STM Au substrate and heating it from room temperature to 60 °C.<sup>328</sup> The measured current  $I$  has two contributions:  $I = G\Delta V + GS\Delta T$ , where  $G$  is the electrical conductance and  $S$  is the thermopower. Measuring (at zero  $\Delta V$ ) the current  $I$  through the molecule due to the temperature gradient  $\Delta T$  (held at 14 K)<sup>328</sup> yields the thermopower (or Seebeck coefficient)  $S$ .  $S > 0$  for hole conduction and  $S < 0$  for electron conduction;  $S$  is usually measured in microvolts per degree Kelvin. From the Landauer formalism for the transmission probability  $P = P(E)$  evaluated

Table 4. Method<sup>a</sup>, Molecular Structure, Conductance  $G$  (nS), and Other Data for Unimolecular Wires 18–147 in Electrode|Electrode Sandwiches, at a Stated Voltage  $V$  (volts), Either at Room Temperature or at a Stated Temperature  $T$ ; Most SBJs Were Studied in a Solvent<sup>b</sup>

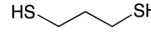
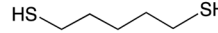
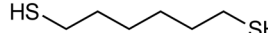
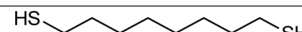
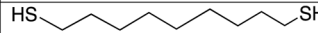

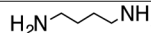
Method	Str.#	Structure	Results ( $G$ -, $\Phi_B$ -, $\beta$ -, $S$ -, $RF$ -) [Ref]
S	--	Au nanowire	$G=7.7 \times 10^4$ [89]
M	--	Pt-Pt-Pt-Pt nanowire	$G=3.0 \times 10^5 > G_0$ [112]
M	18	H-H	$G=7.36 \times 10^4$ @ 0.05 V & 4.2 K [353]
S	19a		[(CH <sub>2</sub> ) <sub>3</sub> ]: $G=5 \times 10^2$ @ 0.05 V & ca. 4 K & IETS [354]
S	19b		[(CH <sub>2</sub> ) <sub>5</sub> ]: $G=64 \pm 5^{MC}$ & $1.9 \pm 0.05^{LC}$ @ 0.1 V in TMB [67], [355]; $G=4.5$ @ 0.1 V & 293 K; T-dep. [356]
S	19c		[(CH <sub>2</sub> ) <sub>6</sub> ]: $G=95$ @ 0.013 V in TMB [89]; $G=95 \pm 10^{HC}$ & $20 \pm 2^{MC}$ & $2.45 \pm 0.06^{LC}$ @ 0.1 V in TMB [67], [355]; $G=2.7$ @ 0.1 V & 293 K; T-dep. [356]; $G=1.2 \times 10^2$ @ 0.025 V in TCB [357]; $G=30$ @ 0.100 V (+AC) in TMB [358]; $G=93^{HC}$ & $17^{LC}$ @ low V in $\phi\text{CH}_3$ [114]; $G=93$ & $\beta=1.0$ @ 0.3 V in $\phi\text{CH}_3$ [359]; $G=80^{HC}$ & $31^{MC}$ & $\beta=0.81$ @ low V in $\phi\text{CH}_3$ [360]
N	19d		[(CH <sub>2</sub> ) <sub>8</sub> ]: $J=93,000$ A cm <sup>-2</sup> & $\Phi_B=1.20$ eV in Eq.(45), $\alpha=0.59$ & $\beta=0.66$ Å <sup>-1</sup> in Eq. (53) [320]
P	19d		[(CH <sub>2</sub> ) <sub>8</sub> ]: $I=1$ nA @ 0.5 V in C <sub>8</sub> H <sub>17</sub> SH + $\phi\text{CH}_3$ [325]
S	19d		[(CH <sub>2</sub> ) <sub>8</sub> ]: $G=21 \pm 2^{HC}$ & $4.4 \pm 0.4^{MC}$ & $0.89 \pm 0.08^{LC}$ @ 0.1 V in TMB [67]; $G=19$ @ 0.013 V in $\phi\text{CH}_3$ [89]; $G=20^{HC}$ & $5^{LC}$ @ low V in $\phi\text{CH}_3$ [114]; $G=13 \pm 4^{HC}$ & $3.25 \pm 1^{MC}$ @ 0.1 to 0.4 V in $\phi\text{CH}_3$ [352]; $G=1.0$ @ 0.1 V & 293 K; T-dep. [356]; $G=4$ @ 0.100 V (+AC) in TMB [358]; $G=19$ & $\beta=1.0$ @ 0.3 V in $\phi\text{CH}_3$ [359]; $G=4^{HC}$ & $5^{MC}$ @ low V in H <sub>2</sub> O [360]; $G=20$ @ 0.100 V & $RF=1.6$ & $\Delta E_{rupt}=0.66$ eV (like Au-Au bond rupture force!) in $\phi\text{CH}_3$ [361]; $G=19$ @ 0.100 V (+AC) in $\phi\text{CH}_3$ [362]; $G=19^{HC}$ & $4^{MC}$ & $\beta=0.85$ @ 0.1 V in $\phi\text{CH}_3$ [363]; $G=4.8^{MC}$ @ low V & 4 K to 300 K; IETS [364]; $G=19$ & $\beta=0.84$ @ low V in $\phi\text{CH}_3$ [365]; $G=4^{LC}$ @ low V in $\phi\text{CH}_3$ (Au-Au bond breaks in stretching) [366]
S	19e		[(CH <sub>2</sub> ) <sub>9</sub> ]: $G=9.9 \pm 0.9^{HC}$ , $2.0 \pm 0.2^{MC}$ & $0.47 \pm 0.03^{LC}$ @ 0.1 V in TMB [67], [355]; $G=0.52$ @ 0.1 V & 293 K; T-dependence [356]
S	19f		[(CH <sub>2</sub> ) <sub>10</sub> ]: $G=1.68 \pm 0.03^{HC}$ , $0.45 \pm 0.04^{MC}$ & $0.22 \pm 0.02^{LC}$ @ 0.1 V in TMB [67]; $G=1.6$ @ 0.013 V in $\phi\text{CH}_3$ [89]; $G=1.7^{HC}$ & $0.33^{LC}$ @ low V in $\phi\text{CH}_3$ [114]; $G=1.68^{HC}$ & $0.45^{MC}$ & $0.22^{LC}$ @ 0.010-0.200 V in TMB [355]; $G=1$ @ 0.100 V (+AC) in TMB [358]; $G=1.5$ & $\beta=1.0$ @ 0.3 V (but $G=2.3$ @ 0.5 V; $G=3.5$ @ 0.7 V; $G=5.4$ @ 0.9 V) in $\phi\text{CH}_3$ [359]; $G=2.3^{HC}$ & $0.5^{MC}$ & $\beta=0.81$ @ low V in $\phi\text{CH}_3$ [360]
S	20a		[(CH <sub>2</sub> ) <sub>4</sub> ]: $G=112^{HC}$ & $1.5^{MC}$ & $\beta=0.65$ @ low V in H <sub>2</sub> O [360]; $G=7.0 \times 10^2$ & $RF=0.84$ @ 0.025 V [367]



Table 4. continued

Method	Str.#	Structure	Results ( $G$ -, $\Phi_B$ -, $\beta$ -, $S$ -, $RF$ -) [Ref]
S	20b		[(CH <sub>2</sub> ) <sub>6</sub> ]: $G=112^{HC}$ & $1.5^{MC}$ & $\beta=0.65$ @ low V in H <sub>2</sub> O [360]; $G=8.5$ & $RF=0.62$ @ 0.075 V [367]
S	20		[(CH <sub>2</sub> ) <sub>2n</sub> ]: [ $n=1,1.5,2,2.5,3,3.5,4$ measured] for $n \rightarrow 0$ $G=2.7 \times 10^3$ & $\beta=0.79$ @ 0.025 V in TCB [227], [368]; [ $n=2,3,4,5$ measured] for $n \rightarrow 0$ $G=2.9 \times 10^3$ & $\beta=0.65$ @ low V [360]
S	21		[(CH <sub>2</sub> ) <sub>2n</sub> ]: [ $n=1,2,3,4$ measured] for $n \rightarrow 0$ $G=7.7 \times 10^3$ @ 0.025 V in TCB [368]
S	22		[(CH <sub>2</sub> ) <sub>n</sub> ]: [ $n=2,4,6,8$ measured] for $n \rightarrow 0$ $G=3.7 \times 10^3$ & $\beta=0.75$ @ 0.025 V in TCB [368]
S	23a		[(CH <sub>2</sub> ) <sub>4</sub> ]: $G=147^{HC}$ & $15^{MC}$ @ low V in $\phi$ CH <sub>3</sub> [114]
S	23b		[(CH <sub>2</sub> ) <sub>6</sub> ]: $G=15^{HC}$ & $1.5^{MC}$ @ low V in $\phi$ CH <sub>3</sub> [114]
S	23c		[(CH <sub>2</sub> ) <sub>7</sub> ]: $G=2.6^{HC}$ & $0.33^{MC}$ @ low V in $\phi$ CH <sub>3</sub> [114]
S	24		[(CH <sub>2</sub> ) <sub>2n</sub> ]: [ $n=2,4,5,6$ measured] for $n \rightarrow 0$ : $G=5 \times 10^3$ & $\beta=0.82$ @ low V in TCB [252]; [ $n=3$ : (CH <sub>2</sub> ) <sub>6</sub> ]: $G=1.04 \times 10^3$ & $S=5.0$ @ low V [328]; [ $n=4$ : (CH <sub>2</sub> ) <sub>8</sub> ]: $G=1.5 \times 10^2$ & $S=5.6$ @ low V [328]; [ $n=5$ : (CH <sub>2</sub> ) <sub>10</sub> ]: $G=22$ & $S=5.6$ @ low V [328]
S	25		[(CH <sub>2</sub> ) <sub>4</sub> ]: $G=21$ @ low V in H <sub>2</sub> O [369]
S	25a		[(CH <sub>2</sub> ) <sub>n</sub> ]: [ $n=2,3,4,5$ measured] for $n \rightarrow 0$ $G=5.50 \times 10^2$ HC & $2.50 \times 10^2$ LC & $\beta=0.61^{HC}$ & $\beta=0.70^{LC}$ @ low V [360]
S	26		[(CH <sub>2</sub> ) <sub>n</sub> ]: [ $n=1,2,3,4$ measured] for $n \rightarrow 0$ $G=1.7 \times 10^3$ & $\beta=0.76$ @ 0.45 V in C <sub>14</sub> H <sub>30</sub> [370]
S	27a		[ $n=2$ : (CH <sub>2</sub> ) <sub>6</sub> ]: $G=77$ & $RF=0.7$ @ low V in TCB [371]
N	27b		[ $n=3$ : (CH <sub>2</sub> ) <sub>8</sub> ]: $J=3.1 \times 10^4$ A cm <sup>-2</sup> , $\Phi_B=1.83$ eV, $\alpha=0.37$ , $\beta=0.85$ [320], [321]
N	27c		[ $n=5$ : (CH <sub>2</sub> ) <sub>12</sub> ]: $J=1.5 \times 10^3$ , $\Phi_B=1.42$ eV, $\alpha=0.65$ , $\beta=0.79$ [320],[321]
N	27d		[ $n=7$ : (CH <sub>2</sub> ) <sub>16</sub> ]: $J=23$ , $\Phi_B=1.40$ eV, $\alpha=0.82$ , $\beta=0.82$ [320],[321]
X	27d		[ $n=7$ : (CH <sub>2</sub> ) <sub>16</sub> ]: $R_{SAM}=0.73$ $\Omega$ cm <sup>2</sup> & $C_{SAM}=2.44$ $\mu$ F cm <sup>-2</sup> [372]
X	27e		[ $n=9$ : (CH <sub>2</sub> ) <sub>20</sub> ]: $R_{SAM}=5.8$ $\Omega$ cm <sup>2</sup> & $C_{SAM}=2.06$ $\mu$ F cm <sup>-2</sup> [372]
X	27f		[ $n=11$ : (CH <sub>2</sub> ) <sub>24</sub> ]: $R_{SAM}=51$ $\Omega$ cm <sup>2</sup> & $C_{SAM}=1.76$ $\mu$ F cm <sup>-2</sup> [372]
X	27g		[ $n=13$ : (CH <sub>2</sub> ) <sub>28</sub> ]: $R_{SAM}=339$ $\Omega$ cm <sup>2</sup> & $C_{SAM}=1.47$ $\mu$ F cm <sup>-2</sup> [372]
S	28a		$G=19$ @ pH 2 in H <sub>2</sub> O; $G=15$ @ pH 7; $G=9$ @ pH 13; $\beta=0.87$ ; all @ 0.1 V in H <sub>2</sub> O [373]
S	28b		$G=0.37$ @ pH 2; $G=0.31$ @ pH 13; $\beta=0.87$ ; all @ 0.1 V in H <sub>2</sub> O [373]
S	28c		$G=0.61$ @ pH 2; $G=0.40$ @ pH 13; $\beta=0.87$ ; all @ 0.1 V in H <sub>2</sub> O [373]

Table 4. continued

Method	Str.#	Structure	Results ( $G$ -, $\Phi_B$ -, $\beta$ -, $S$ -, $RF$ -) [Ref]
S	29a		$G=65\pm 26^{HC}$ & $7\pm 1^{MC}$ & $2.5^{HC}$ @ low V in $\phi CH_3$ [374]
S	29b		$G=3^{HC}$ , $0.3^{MC}$ & $0.08^{LC}$ @ low V in $\phi CH_3$ [374]
S	29c		$G=0.077^{HC}$ @ low V in $\phi CH_3$ [374]
M	30a		$G=1.0\times 10^3$ @ 1 V [85]; $G=49$ @ low V in ethanol [375]; SERS peaks @ 1068, 1179 & $1368\text{ cm}^{-1}$ polariz.    to gap [376]; $G=8.0\times 10^2(LC)$ & $G=8.0\times 10^3(HC)$ @ 1 V [377]
E	30a		$G=1.0\times 10^2$ @ $<0.3$ V [378]
S	30a		$G=8.5\times 10^2$ @ 0.025 V in TCB & RT or 30 K [357]; $G=8.5\times 10^2$ @ 0.1 V in 0.1 M aq. $NaClO_4$ [379]; $G=6.39\times 10^2$ @ 0.05 V in TMB [380]
S	30b		$[\varphi=36.4^\circ]$ $G=13.3$ @ low V in TMB/THF [381]
S	30c		$G=8.5\times 10^2$ @ 0.025 V in TCB & RT or 30 K [357]; $G=8.3\times 10^2$ @ 0.1 V ( $G=8.5\times 10^2$ @ -0.2 V) in aq. $NaClO_4$ [379]; $G=6.39\times 10^2$ @ 0.05 V in $\phi CH_3$ [380]
M	31a		$G=5.1\times 10^2$ @ 0.2 V [382]; $G=31$ @ 0.05 V [383]
S	31a		$G=5.0\times 10^2$ @ 0.025 V in TCB [227],[384]; $G=4.8\times 10^2$ & $RF=0.53$ @ 0.025 V [367]; $\Delta H_{ads}=1.0$ eV [385];
S	31b		$G=90$ @ 0.025 V in TCB [386]
S	32		$[\varphi=48^\circ]$ $G=50$ @ 0.025 V in TCB [386]
S	33		$[\varphi=88^\circ]$ $G=5.9$ @ 0.025 V in TCB [386]
S	34		$[\varphi=52^\circ]$ $G=38$ @ 0.025 V in TCB [386]
S	35		$[\varphi=62^\circ]$ $G=29$ @ 0.025 V in TCB [386]
E	36		$G=40$ @ $<0.3$ V [378]
S	36		$G=50$ @ 0.1 V, $G=46$ @ -0.2 V in aq. $NaClO_4$ [379]; $G=56$ [331]; $G=1.1\times 10^2$ [332]; $G=7.7\times 10^2$ @ 0.45 V in $C_{14}H_{30}$ [370]
S	37		$G=27$ @ low V [387]
S	38		$G=1.0\times 10^2$ @ 0.45 V in $C_{14}H_{30}$ & in $H_2O$ @ pH 11 [370]
S	39		$[n=1]$ : $G=7.0\times 10^4$ @ low V in TCB [388]; $G=6.2\times 10^4$ & $S=2.4$ [328]; $[n=2]$ : $G=7.7\times 10^4$ , $G=6.2\times 10^4$ & $S=14.3$ [328]; $G=7.7\times 10^3$ @ low V in TCB [388];

Table 4. continued

Method	Str.#	Structure	Results ( $G$ -, $\Phi_B$ -, $\beta$ -, $S$ -, $RF$ -) [Ref]
			$[n=3]$ : $G=1.0 \times 10^3$ & $S=20.9$ [328]; $G=1.0 \times 10^3$ @ low V in TCB [388]; $[n=4]$ : $G=1.5 \times 10^2$ & $S=23.9$ [328]; $G=1.7 \times 10^2$ @ low V in TCB [388]
S	40a		$G=1.0 \times 10^4$ & $\beta=0.51$ @ 0.3 V [369]
S	40b		$G=2.5 \times 10^3$ & $\beta=0.51$ @ 0.3 V [369]
S	40c		$G=1.0 \times 10^3$ & $\beta=0.51$ @ 0.3 V [369]
M	41		$G=1.05 \times 10^3$ @ 0.2 V [382]
S	42		$[\varphi=1.1^\circ]$ $G=11.2$ @ low V in TMB+THF [381]
S	43		$[\varphi=16.8^\circ]$ $G=17.0$ @ low V in TMB+THF [381]
S	44		$[\varphi=44.7^\circ]$ $G=10.0$ @ low V in TMB+THF [381]
S	45		$[\varphi=57.8^\circ]$ $G=5.40$ @ low V in TMB+THF [381]
S	46		$[\varphi=71.5^\circ]$ $G=1.30$ @ low V in TMB+THF [381]
S	47		$G=6.3 \times 10^2$ @ 0.025 V in TCB [384]; $\Delta H_{ads}=1.2$ eV [385]
S	48		$G=5.4 \times 10^2$ @ 0.025 V in TCB [384]
S	49		$G=5.3 \times 10^2$ @ 0.025 V in TCB [384]
S	50		$G=5.0 \times 10^2$ @ 0.025 V in TCB [384]
S	51		$G=4.7 \times 10^2$ @ 0.025 V in TCB [384]
S	52		$G=4.7 \times 10^2$ @ 0.025 V in TCB [384]
S	53		$G=4.7 \times 10^2$ @ 0.025 V in TCB [384]; $\Delta H_{ads}=0.9$ eV [385]
S	54		$G=4.6 \times 10^2$ @ 0.025 V in TCB [384]
S	55		$G=4.5 \times 10^2$ @ 0.025 V in TCB [384]
S	56		$G=4.6 \times 10^2$ @ 0.025 V in TCB [384]
S	57		$G=4.3 \times 10^2$ @ 0.025 V in TCB [384], [385]
S	58		$G=1.2 \times 10^2$ @ 0.025 V in TCB [386]; $G=1.3 \times 10^2$ @ low V in TCB [389]

Table 4. continued

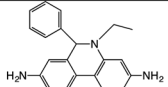
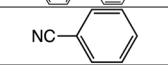
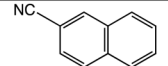
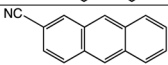
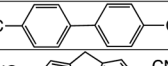
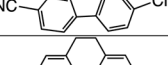
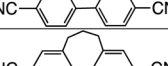
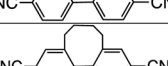
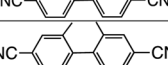
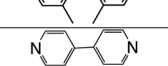

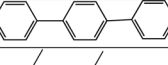
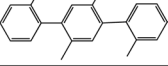
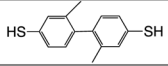
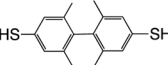
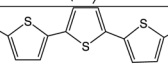
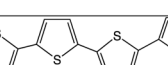

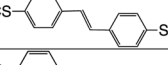
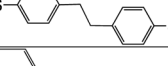
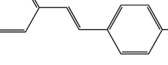
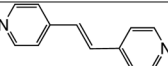
Method	Str.#	Structure	Results ( $G$ -, $\Phi_B$ -, $\beta$ -, $S$ -, $RF$ -) [Ref]
S	59		$G=1.06 \times 10^2$ @ 0.025 V in TCB [386]
P	60a		$G=2.0 \times 10^3$ & $\beta=0.45$ @ 0.3 V [369]
P	60b		$G=1.3 \times 10^3$ & $\beta=0.45$ @ 0.3 V [369]
P	60c		$G=2.5 \times 10^3$ & $\beta=0.45$ @ 0.3 V [369]
S	61		$[\phi=35.5^\circ]$ $G=3.64$ in TMB/THF [390]
S	62		$[\phi=1^\circ]$ $G=7.1$ in TMB/THF [390]
S	63		$[\phi=20.7^\circ]$ $G=5.1$ in TMB/THF [390]
S	64		$[\phi=44.8^\circ]$ $G=3.0$ in TMB/THF [390]
S	65		$[\phi=58.5^\circ]$ $G=1.3$ in TMB/THF [390]
S	66		$[\phi=89.3^\circ]$ $G<0.08$ in TMB/THF [390]
S	67a		$G=7.7 \times 10^2$ & $\beta=0.5$ @ 0.013 V in 0.1 M $\text{NaClO}_4(\text{aq})$ [89]; $G=7.7 \times 10^2$ @ low V in aq. $\text{NaClO}_4(\text{aq})$ & no gate effect [359]; $G=7.7$ & $RF=0.80$ @ 0.075 V [367]; $G=7.7 \times 10^2$ & $RF=0.8$ & $<30\%$ gating @ low V in 0.05 M $\text{NaClO}_4(\text{aq})$ [375]; $G=50$ & $S=-10$ (evap. film) [391]; $G=7.7 \times 10^2$ @ 0.075 V in vapor-dep. film; force monitored [392]; $G=46^{\text{HC}}$ & $G=12^{\text{LC}}$ @ 0.027 V in TCB [393]
S	67b		$G=5.0$ & $\beta=0.5$ @ 0.350 V in TCB [394]
M	68		$G=1.0 \times 10^2$ [395]
S	69		$[\phi=79.7^\circ]$ $G=1.0$ in TMB/THF [381]
S	70		$[\phi=89^\circ]$ $G=0.70$ in TMB/THF [381]
S	71a		$G=80$ @ 0.001 V [329]; $G=2.2$ & $RF=1.5$ @ low V & $V_g=0$ in $\phi\text{CH}_3$ [396];
S	71b		$G=5.8$ & $RF=1.5$ @ low V & $V_g=0$ in $\phi\text{CH}_3$ ; $G=1.5 \times 10^2$ @ $V_g=0.3$ V, increases @ $V_g=0.7$ V (oxidation; HOMO!) [396]
S	72		$G=1.0 \times 10^2$ & $RF=0.5$ @ 0.075 V in TCB [397]
S	73		$G=2.5$ & $RF=0.5$ @ 0.075 V in TCB [397]
S	74		$G=17$ @ low V in TCB [398]
S	75		$G=18$ & $S=-13$ (evap. film) [391]; $G=20$ & $\beta=0.5$ @ 0.350 V in TCB [394]
S	76		$G=0.50$ & $\beta=0.5$ @ 0.350 V in TCB [394]

Table 4. continued

Method	Str.#	Structure	Results ( $G$ -, $\Phi_B$ -, $\beta$ -, $S$ -, $RF$ -) [Ref]
S	77		$G=2.2$ @ low V in TCB [398]
S	78		$G=2.2$ @ low V in TCB [398]
S	79		$G=47$ @ low V & $S=+13$ (evap. film) [391]
S	80		[ $n=1$ ]: $G=93$ , [ $n=2$ ]: $G=48$ , [ $n=3$ ]: $G=29$ @ low V in TCB [398]
S	81		[ $n=1$ ]: $G=22$ , [ $n=2$ ]: $G=7.7$ , [ $n=3$ ]: $G=5.6$ @ low V in TCB [398]
S	82		[ $n=1$ ]: $G=1.6$ , [ $n=2$ ]: $G=2.0$ , [ $n=3$ ]: $G=1.3$ @ low V in TCB [398]
M	83a		$G=3.0 \times 10^3$ @ 0.5 V [399]
S	83a		$G=20$ @ 0.05 V in $\phi\text{CH}_3$ [380]
S	83b		$G=10$ @ 0.05 V in $\phi\text{CH}_3$ [380]; $G=13$ @ low V in $\text{CH}_3\text{CN} + \text{NaOH}$ [400]; $G=13$ [401]
S	84a		$G=42$ @ low V & $S=+10$ (evap. film) [391], $G=49^{\text{HC}}$ & $1.2^{\text{LC}}$ @ low V in TMB/THF [402]
M	84a		$G=49^{\text{HC}}$ & $1.2^{\text{LC}}$ @ low V [402]
S	84b		$G=25^{\text{HC}}$ & $1.0^{\text{LC}}$ @ low V [402]
S	85		$G=6$ @ low V in $\text{CH}_3\text{CN} + \text{NaOH}$ ; NDR @ 1.8 V [400]
S	86		[ $n=0$ ]: $G=3.7 \times 10^2$ ; [ $n=1$ ]: $G=2.5 \times 10^2$ ; [ $n=2$ ]: $G=1.9 \times 10^2$ , all @ 0.05 V in $\phi\text{CH}_3$ [380]
S	87a		$G=31^{\text{HC}}$ & $6^{\text{MC}}$ & $0.12^{\text{LC}}$ @ low V in TMB/THF [402]
M	87a		$G=39^{\text{HC}}$ & $0.12^{\text{LC}}$ @ low V [402]
S	87b		$G=13^{\text{HC}}$ & $2.4^{\text{MC}}$ & $\beta=0.31$ @ low V in TMB/ THF [402]
M	87b		$G=12^{\text{HC}}$ & $0.01^{\text{LC}}$ & $\beta=0.31$ @ low V [402]
S	87c		$G=3.1^{\text{HC}}$ & $\beta=0.31$ @ low V in TMB/THF [402]
S	88a		$G=1.2^{\text{HC}}$ & $\beta=0.17$ @ low V in TMB/THF [402]
M	88a		$G=1.5^{\text{HC}}$ @ low V [402]
S	88b		$G=0.77^{\text{HC}}$ , $\beta=0.17$ @ low V in TMB/THF [402]
M	88b		$G=1.2^{\text{HC}}$ @ low V [402]
S	88c		$G=0.31^{\text{HC}}$ , $\beta=0.17$ @ low V in TMB/THF [402]

Table 4. continued

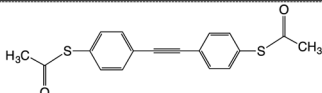

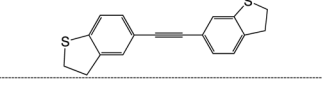
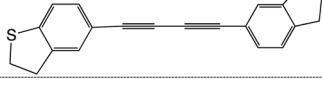

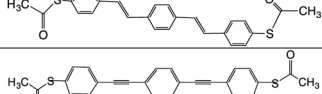
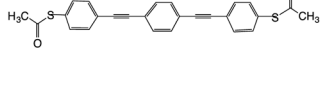
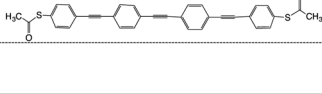
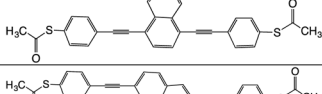
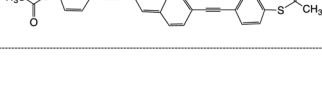
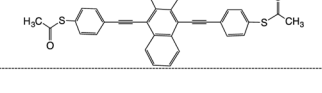
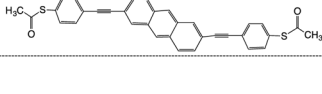
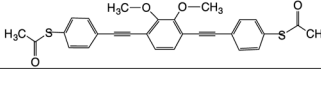
Method	Str.#	Structure	Results ( $G$ -, $\Phi_B$ -, $\beta$ -, $S$ -, $RF$ -) [Ref]
M	89a		$G=150^{HC}$ & $1.5^{LC}$ @ low V [402]; $G=117^{HC}$ & $1.67^{LC}$ @ 0.10 V [403]
S	89a		$G=120^{HC}$ & $2.1^{LC}$ , $\beta=0.32$ @ low V in TMB/THF [402]
S	89b		$G=56.1^{HC}$ & $1.73^{LC}$ & $\beta=0.32$ @ low V in TMB/THF [402]; $G=117^{HC}$ & $1.6^{LC}$ @ 0.10 V in (1:4)-(THF:TMB) [403]; for 89a, 89b, & 92: $\beta=0.37\pm 0.03$ [403]
M	89b		$G=61^{HC}$ @ low V [402]
S	90a		$G=250^{HC}$ , $0.61^{LC}$ , $\beta=0.29$ @ low V in TMB/THF [402]
M	90a		$G=250^{HC}$ , $0.98^{LC}$ @ low V [402]
S	90b		$G=63.0^{HC}$ , $0.234^{LC}$ , $\beta=0.29$ @ low V in TMB/THF [402]
M	90b		$G=200^{HC}$ , $0.39^{LC}$ @ low V [402]
S	90c		$G=15^{HC}$ , $\beta=0.29$ @ low V in TMB/THF [402]
M	90c		$G=39^{HC}$ , $0.08^{LC}$ @ low V [402]
M	91		$G=15$ @ 0.2 V [404]
M	92		$G=10$ @ 0.1 V; for 89a, 89b, & 92: $\beta=0.37\pm 0.03$ [403]; $G=22$ to $31$ @ low V & 300 K, $E_{HOMO}$ is 0.51 eV below $E_{Fermi}$ , $I\approx 0.0045$ eV [406]; $G=3.6$ & $\beta=1.11 \text{ \AA}^{-1}$ @ low V [407]
S	92		$G=9$ [404]; $G=13.9^{HC}$ & $0.76^{LC}$ @ 0.10 V in (1:4)-(THF:TMB); [for 89a, 89b, & 92]; $\beta=0.37\pm 0.03$ [403]; $G=6$ to $13$ [408]
M	93		$G=1.1^{HC}$ @ 0.10 V [403]
S	93		$G=1.22^{HC}$ @ 0.10 V in (1:4)-(THF:TMB) [403]
S	94		$G=20.8^{HC}$ & $2.0^{LC}$ @ 0.10 V in (1:4)-(THF:TMB) [403]
S	95		$G=4.12^{HC}$ @ 0.10 V in (1:4)-(THF:TMB) [403]
M	95		$G=6^{HC}$ & $0.04^{LC}$ @ 0.10 V [403]
M	96		$G=40$ to $46$ @ low V & 300 K, $E_{HOMO}$ is 0.37 eV below $E_{Fermi}$ , $I\approx 0.004$ eV [406],[405]
S	96		$G=36.8^{HC}$ & $1.65^{LC}$ @ 0.10 V in (1:4)-(THF:TMB) [403],[405]
M	97		$G=2.5^{HC}$ & $0.005^{LC}$ @ 0.10 V [403],[405]
S	97		$G=3.61^{HC}$ @ 0.10 V in (1:4)-(THF:TMB) [403]; $G=2.0\times 10^2$ @ low V [403]; [410]; $G=2.5$ [405],[409]
S	98		$G=3.1\times 10^2$ HC & $12^{MC}$ & $1.4^{LC}$ @ 0.1 V [411]

Table 4. continued

Method	Str.#	Structure	Results ( $G$ -, $\Phi_B$ -, $\beta$ -, $S$ -, $RF$ -) [Ref]
M	99		$G=11$ @ 0.2 V [404]
M	100		$G=11$ @ 0.2 V [404]
S	101		Large gate effect (nitro group gets reduced) in 0.1 M NaOH (aq.) & also in 0.1 M $\text{NH}_4\text{CH}_3\text{COONa}$ (aq.) [375]
S	102		$G=5 \times 10^{-3}$ or $G=7$ @ low V [403]; $G=8 \times 10^{-3}$ [409]
M	103		$G=4 \times 10^{-2}$ [403],[405],[410]
S	103		$G=30$ @ low V [403]; $G=2.5$ [409]; NDR [405],[410]
M	104		$G=77$ [412]
S	105		[5 double bonds]: $G=2.06 \pm 0.05$ @ 0.2 V in $\phi\text{CH}_3$ [413]
S	106		[7 double bonds]: $G=0.96 \pm 0.07$ @ 0.2 V in $\phi\text{CH}_3$ [413]
S	107		[9 double bonds]: $G=0.28 \pm 0.072$ @ 0.2 V in $\phi\text{CH}_3$ [413]
S	108		[11 double bonds]: $G=0.11 \pm 0.07$ @ 0.2 V in $\phi\text{CH}_3$ [413]; [n=5,7,9,11 double bonds]: for $n \rightarrow 0$ : $G=37 \pm 18$ & $\beta=0.22 \pm 0.04$ [413]
S	109		[n=0,1,2,3,4 meas.]: for $n \rightarrow 0$ $G=1.5 \times 10^2$ & $\beta=0.19$ @ low V in TCB [414]
M	110		$G=2$ & CS @ 0.1 V & 1.6 K [333]
S	111		[n=0,1,2,3,4 measured]; [n=4]: $G=6.2 \times 10^2$ & $\beta=0.19$ @ low V in TCB [414]
S	112		$G=0.9$ @ low V & $V_g=0$ in aq. 0.1 M $\text{NaClO}_4$ but $G=4 \times 10^2$ when $V_g=-0.7$ V vs. Ag/AgCl (reaches LUMO) [375]; $G=1.3$ @ 0.100 V & $V_{\text{gate}}=0$ V & $G$ is $T$ -activated in aq. $\text{NaClO}_4$ ( $\Delta E_{\text{activ}} \approx 0.35$ eV @ $V_g=0.2$ V: solvent reorg.) but $G$ is $T$ -indep. in $\phi\text{CH}_3$ ( $277 \leq T \leq 317$ ) [415]
S	113		$G=3.8$ @ low V & $V_g=0$ in aq. 0.1 M $\text{NaClO}_4$ ; $G$ increases until $V_g=-0.4$ V vs. Ag/AgCl; molecule desorbs @ $V_g=-0.5$ V [375]; $G=3.8$ (estim.) @ 0.100 V & $V_g=0$ V in aq. $\text{NaClO}_4$ [415]
S	114		$G=0.60$ @ 0.100 V & $V_g=0$ V & $G$ is $T$ -activated in aq. $\text{NaClO}_4$ ( $\Delta E_{\text{activ}} \approx 0.35$ eV at $V_g=0.2$ V: solvent reorg.) [415]

Table 4. continued

Method	Str.#	Structure	Results ( $G$ -, $\Phi_B$ -, $\beta$ -, $S$ -, $RF$ -) [Ref]
S	115		$G=8 \times 10^2$ @ low V in TCB [416]
S	116		$G=77$ @ low V in TCB [416]
S	117		[1.35:1.00 isomer mixture] $G=15$ @ low V in TCB [416]
S	118		$G=8 \times 10^3$ @ low V in TCB [416]
S	119		$G=8 \times 10^2$ @ low V in TCB [416]
S	120		$G=5 \times 10^3$ @ low V in TCB [416]
S	121		$G=75$ @ low V [387]
S	122		$G=256$ @ low V in TCB [389]
S	123		$G=2.7 \times 10^2$ @ low V in TCB [389]
S	124		$G=3.4 \times 10^2$ @ low V in TCB [389]
S	125		[ $n=1,2,3,4$ measured]: for $n \rightarrow 0$ $G=110$ & $\beta=0.1$ @ 0.1 V in hexadecane [417]
S	126		[ $n=1$ ]: $G=7.6 \times 10^{-1}$ ; [ $n=2$ ]: $G=9.22 \times 10^{-3}$ & $G=1.23 \times 10^{-2}$ ; [ $n=4$ ]: $G=3.6 \times 10^{-3}$ ; all @ 0.25 V in TMB [418]
S	127		$G=14$ @ low V in $\phi\text{CH}_3$ [419]



Table 4. continued

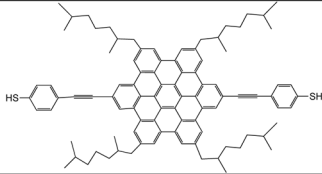
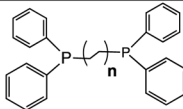

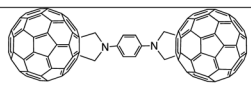
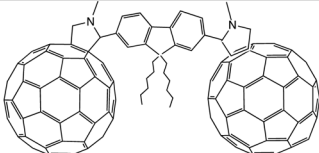
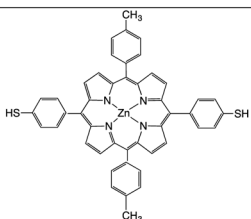
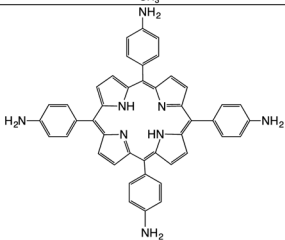
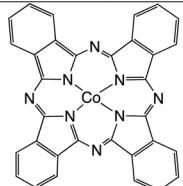
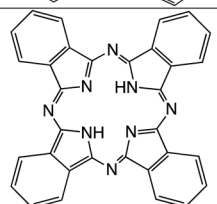
Method	Str.#	Structure	Results ( $G$ ?, $\Phi_B$ ?, $\beta$ ?, $S$ ?, $RF$ ?) [Ref]
S	128		$G=1.7$ @ low V in $\phi\text{CH}_3$ ; electrochem. gating in 1-butyl-3-methylimidazolium hexafluorophosphate solvent at V close to LUMO (max on/off ratios $\sim 50$ ) [419]
S	129		[ $n=2.5$ ]: $G=29$ & $S=1.1$ @ low V [391]; [ $n=1,2,3,4$ measured] for $n \rightarrow 0$ : $G=3.0 \times 10^3$ & $\beta=0.83$ @ low V in TCB [420]
S	16		[ $C_{60}$ ]: $G=500^{\text{HC}}$ to $20^{\text{HC}}$ @ low V in $C_{10}H_{22}$ (dep. on squeezing) [421]
Y	16		[ $C_{60}$ ]: on Cr using Fe/W nanotip @ -0.5 V & 5 K: TMR ratio $\equiv (G_{\text{up}}-G_{\text{dn}})/G_{\text{dn}} = 1.0 \pm 0.1$ [422]
M	130		$G=23$ @ low V [383]
S	131		$G=400^{\text{HC}}$ to $15^{\text{HC}}$ (dep. on squeezing!), $0.25^{\text{LC}}$ (indep. of squeezing) @ low V in TMB [421]
M	131		$G=120^{\text{HC}}$ & $0.77^{\text{LC}}$ @ 0.03 V [421]
M	132		[substituted ZnPc]: $G=1$ @ 0.5 V & 6 K [135]
M	133		[tetra(aminophenyl)porphyrin]: $G=1$ to 2 @ 0.001 to 0.4 V & 10 K [113]
Y	134		[CoPc]: STM of CoPc on Co island over Cu(111) using Co/W tip @ -0.1 V & 4.6 K: spin-dep. $G$ (1 to 2 nS) asymmetry [423]; STM of CoPc on Fe over W(110) using Cr/W nanotip: $G$ & image are spin-dep. @ -0.05 V & 6 K [424]
Y	135		[Phthalocyanine = $H_2Pc = C_{32}H_{18}N_8$ ]: STM on Co nanoislands over Cu(111) using Co/W nanotip @ 0.01 V & 4 K: $G_{\parallel} = 2.0 \times 10^4$ , $G_{\text{AP}} = 1.5 \times 10^4 \rightarrow (G_{\text{p}} - G_{\text{AP}})/G_{\text{AP}} = 0.61 \pm 0.09$ [425]

Table 4. continued

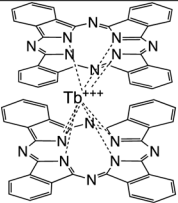
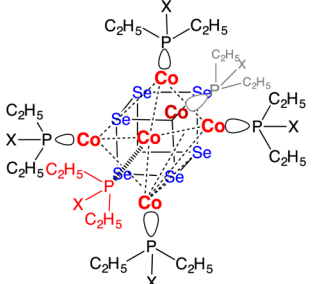
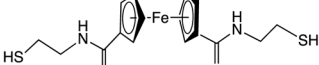
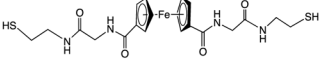
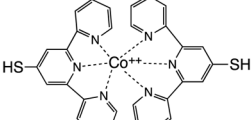
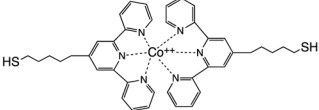
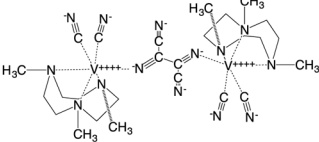
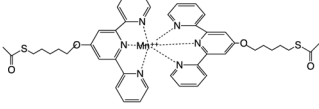
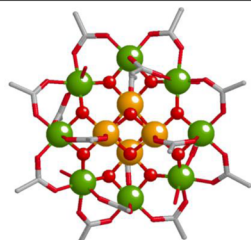
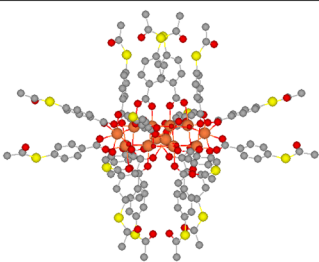
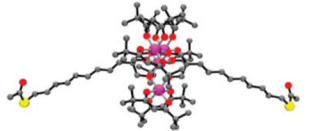
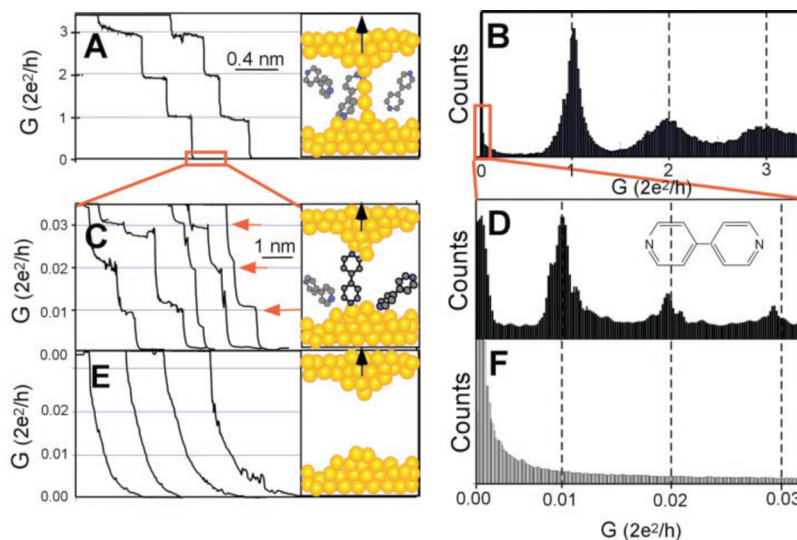
Method	Str.#	Structure	Results ( $G$ -, $\Phi_B$ -, $\beta$ -, $S$ -, $RF$ -) [Ref]
Y	136		[Tb <sup>III</sup> Pc <sub>2</sub> ]: STM of TbPc <sub>2</sub> ( $S=1/2$ on Pc ligands; $J=6$ overall) on Co nanoislands on Ir(111) using Fe/W nanotip (whose spin orientation is reset in field of $\pm 1$ T) @ 0.5 V & 6 K: spin-split HOMO & LUMO seen ( $\Delta E = 0.210$ eV) [426]
E	136		$G=189$ @ $H=-500$ Gauss to $G=191$ @ $H=+500$ Gauss: hysteresis due to Tb <sup>+++</sup> spin flips @ 0.1 K; Tb nuclear spin transitions (from equal populations @ $V_g=-0.1$ towards majority $I=+3/2$ @ -0.8 Volts) @ $V=0.0$ Volts & 0.08 K [427]
S	137		[Co <sub>6</sub> Se <sub>8</sub> [PX(C <sub>2</sub> H <sub>5</sub> ) <sub>2</sub> ] <sub>6</sub> , X= $\phi$ SCH <sub>3</sub> ]: $G=4 \times 10^2$ @ 0.75 V in TCB [428]; [Co <sub>6</sub> Se <sub>8</sub> [PX(C <sub>2</sub> H <sub>5</sub> ) <sub>2</sub> ] <sub>6</sub> , X= $\phi$ -CH-CH- $\phi$ SCH <sub>3</sub> ]: $G=0.8$ @ 0.75 V in TCB [428];
S	138		$G=23$ @ 0.1 V & gate bias=-0.1 V ( $G > 100$ for gate bias= 0.7 V) in 0.1 M HClO <sub>4</sub> [429]
S	139		$G \approx 7$ (noisy) @ 0.1 V & gate bias=-0.1 V ( $G > 30$ for gate bias= 0.5 V) in 0.1 M HClO <sub>4</sub> [429]
E	140a		$G=5 \times 10^4$ (Kondo peak) @ 1.5 K & $H=0$ ; Kondo peak $\rightarrow 0$ @ 18 K; Kondo peak @ 1.5 K & $H=0$ splits into 2 peaks as $H \rightarrow 10$ T [86]
E	140b		$G=5$ or 10 or 500 & CS @ low V & $V_g=0$ & $H=0$ ; CD (with $G=0$ Co <sup>++</sup> & Co <sup>+++</sup> regions) & $G$ maxima @ 0.1 K & $H=0$ for interdep. V & $V_g$ values (see Fig. 17); diamond shifts when $H \neq 0$ [86]
E	141		$G=5 \times 10^4$ or $G=4 \times 10^4$ & CD @ 0.3 K ( $V_2^+$ (spin-1/2) & $V_2^0$ (spin-0) regions) with $G$ maxima @ 0.1 K & $H=0$ for interdependent non-zero V & $V_g$ values; for $H \neq 0$ CD shifts & Kondo peak splits [318]
E	142		[Mn <sup>II</sup> (ter-pyr-O-(CH <sub>2</sub> ) <sub>6</sub> -SAc <sub>2</sub> )] [PF <sub>6</sub> ] <sub>2</sub> : CD @ 1.7 K; transition from high-spin $S=5/2$ ( $t_{2g}^3(e_g)^2$ ) ground-state to low-spin $S=1/2$ ( $t_{2g}^5(e_g)^0$ ) excited-state is induced @ 1.7 K by gate voltage $V_g \geq 0.9$ Volts (H-dep.) [430]
M	143		[Mn <sup>III</sup> <sub>8</sub> Mn <sup>IV</sup> <sub>4</sub> O <sub>12</sub> (OOCCH <sub>3</sub> ) <sub>16</sub> (H <sub>2</sub> O) <sub>4</sub> ] CB @ 0.3 K & $H=0$ ; $G=200$ maxima in CD are fncs of V & $V_g$ ; $H=0 \rightarrow 8$ T splits the Kondo maxima [431]

Table 4. continued

Method	Str.#	Structure	Results ( $G$ ?, $\Phi_B$ ?, $\beta$ ?, $S$ ?, $RF$ ?) [Ref]
E	144		[Mn <sup>III</sup> <sub>8</sub> Mn <sup>IV</sup> <sub>4</sub> O <sub>12</sub> (OOC- $\phi$ -S-CO-Me) <sub>16</sub> (H <sub>2</sub> O) <sub>4</sub> ]: CD, $\partial I/\partial V < 0$ (NDR), & regions of $G=0$ @ 3 K & 0.005 V & $V_g$ [432] [Mn <sup>III</sup> <sub>8</sub> Mn <sup>IV</sup> <sub>4</sub> O <sub>12</sub> (OOC-C <sub>15</sub> H <sub>30</sub> -S-CO-Me) <sub>16</sub> (H <sub>2</sub> O) <sub>4</sub> ]: CD @ 4 K & for certain $V \approx 0.005$ V & $V_g$ regions of maximum $G \approx 10$ , $\partial I/\partial V < 0$ , and $G=0$ due to forbidden spin ladder transitions [432]
M	145		{Fe <sup>III</sup> <sub>4</sub> [CH <sub>3</sub> CH(CH <sub>3</sub> ) <sub>2</sub> CO(CH <sub>2</sub> ) <sub>2</sub> COCH(CH <sub>3</sub> ) <sub>2</sub> CH <sub>3</sub> ] <sub>6</sub> [(CH <sub>2</sub> ) <sub>9</sub> SCO-CH <sub>3</sub> ] <sub>2</sub> }: $S=5$ SMM: $D=5.2 \times 10^{-5}$ eV, $E \approx 0$ ; spin states accessed @ 1.6 K by $V_g$ [433]
S	146	ds-[5'-(GC) <sub>4</sub> -3'-CH <sub>2</sub> CH <sub>2</sub> SH] DNA-like oligomer, a self-complementary B-form DNA H-bonded double strand; for bases G and C see top of Fig. 14	$G=1.0 \times 10^2$ @ low V in 0.1 M NaCl & 0.01 M phosphate buffer at pH7 [434]; no T-dep. between 378 K and 313 K & no electrochem. gating [435]
S	147	5'-CGCG(AT) <sub>m</sub> CGCG-3'-thiol DNA-like oligomer (a self-complementary B-form DNA H-bonded double strand); for bases G, C, A, and T see Fig. 14	[ $m=0$ ] $G=1.0 \times 10^2$ ; [ $m=1$ ] $G=5.8$ ; [ $m=2$ ] $G=0.3$ @ low V in 0.1 M NaCl & 0.01 M phosphate buffer at pH 7 [434]

<sup>a</sup>Methods: E = EBJ with Au electrodes; M = MBJ with Au electrodes; N = Au nanopore; P = SBJ with bulk Au electrode + Au nanoparticle atop a C-AFM tip; Q = electrodeposited Au nanogap; S = SBJ with bulk Au electrode + either scanned Au nanotip or scanned Au-tipped AFM probe; X = SAM (not unimolecular) studied with Ag<sup>TS</sup> electrode + EGaIn drop; Y = spin-polarized STM. <sup>b</sup> $\phi$  is the relevant intramolecular torsion angle.  $\Phi_B$  is the effective work function (eV) in eq 45. The listed  $G$  values are generally smaller than the Landauer–von Klitzing conductance quantum  $G_0 \equiv 77\,480.9$  nS of eq 14.  $\beta$  is the attenuation coefficient ( $\text{\AA}^{-1}$ ) of eq 53.  $S$  is the thermopower ( $\mu\text{V}/\text{K}$ ) of eq 64.  $RF$  is the bond rupture force (nN) for the Au-to-molecule bond (except when noted otherwise),  $V_g$  is a gate voltage, and  $H$  is the external magnetic field. Theoretical estimates of  $G$  were obtained for some of the molecules listed here.<sup>55,352</sup> CB = Coulomb blockade; CD = Coulomb diamond; and CS = Coulomb staircase. Superscripts HC, MC, and LC are for high-conductance, medium-conductance, and low-conductance peaks. Solvents: THF = tetrahydrofuran; TCB = 1,2,4-C<sub>6</sub>H<sub>3</sub>Cl<sub>3</sub>; TMB = 1,3,5-C<sub>6</sub>H<sub>3</sub>(CH<sub>3</sub>)<sub>3</sub>; and  $\phi\text{CH}_3$  = toluene.



**Figure 8.** Scanning break junction (SBJ).<sup>89</sup> (A, B) One, two, or three Au nanowires in parallel show histograms of conductances of multiples of the Landauer quantum  $G_0 = 2e^2/h$  (eq 59) when studied at room temperature in a modified STM. (C, D) Histograms for 4,4'-bipyridine (**67a**), dissolved in 0.1 M NaClO<sub>4</sub>, spanning the distance between the Au substrate and the Au NT show peaks at  $G$  values ca. 100 times smaller than  $G_0$ . (E, F) The pure solvent shows no peaks in conductance. Reprinted by permission from ref 89. Copyright 2003 American Association for the Advancement of Science.

off-resonance at the metal Fermi energy  $E = E_F$ , the thermopower  $S$  is given by

$$S = -(\pi^2 k_B^2 T / 3e) |\partial \ln P / \partial E|_{E=E_F} \quad (64)$$

#### 14. COULOMB BLOCKADE, COULOMB STAIRCASE, AND COULOMB DIAMONDS

The conductance of molecules can be affected by CBs. In a 3- $\mu\text{m}$ -long metallic single-walled carbon nanotube (SWCNT)

physisorbed and therefore weakly coupled to four Pt pads, measured in a four-probe geometry (which, because of weak and nonuniform coupling from nanotube to pads, becomes really a two-probe measurement), one sees CBs.<sup>90</sup> The two-electrode contact resistance is of the order of 0.5–1 M $\Omega$ . At  $\sim$ 5 mK, the *IV* measurements showed clear evidence of steps, which could be tuned on and off by applying different gate voltages to the Si/SiO<sub>2</sub> substrate below the Pt pads. The nanotube is assumed to have a small but finite capacitance *C*, and current is blocked until  $V_{\text{bias}} > e/2C$  is reached (with or without the help of an appropriate  $V_{\text{gate}}$ ); here  $k_{\text{B}}$  is Boltzmann's constant.<sup>90</sup>

This CB effect, already mentioned above, is seen in semiconducting quantum dots or in metallic islands if  $k_{\text{B}}T < e^2/2C$  (eq 8). A second condition for a CB is that the quantum dot or metallic island be weakly coupled to the electrodes. If the energy levels of the quantum dot of size *L* have separations  $\Delta$  typically described by a particle-in-a-box approximation, then

$$\Delta = \hbar^2/mL^2 \quad (65)$$

then the second condition for a CB becomes

$$k_{\text{B}}T < \Delta \quad (66)$$

A sphere of radius *R* has capacitance  $C = 4\pi\epsilon_0 R$ . Therefore, for a C<sub>60</sub> molecule,  $R = 0.4$  nm,  $C = 4.45 \times 10^{-20}$  F, and eq 65 sets  $T < 20\,900$  K. If the energy levels of C<sub>60</sub> are 0.5 eV apart, then eq 66 sets  $T < 4\,000$  K.

In metallic islands the energy level spacing  $\Delta$  is small ( $\Delta \ll k_{\text{B}}T$ ), while in semiconducting quantum dots this spacing exceeds thermal energies ( $k_{\text{B}}T < \Delta$ ). To repeat, both metallic islands and quantum dots can exhibit a CB if eq 66 holds. The take-home lesson is that even a metallic SWCNT, a quintessential conducting supermolecule, can behave as a quantum dot.<sup>330</sup>

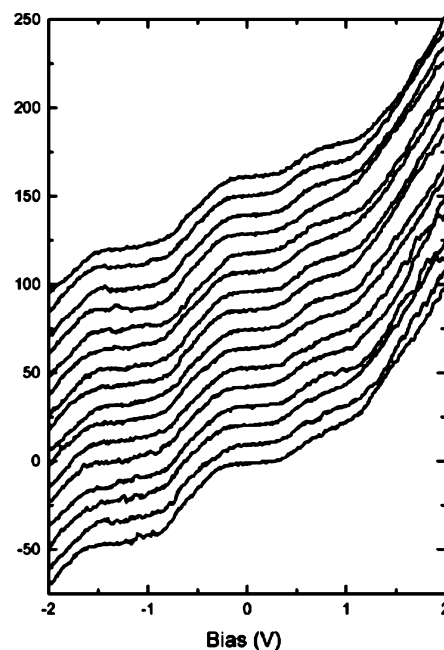
Coulomb staircase (CS: steps in the *IV* curve) have been measured for SWCNT (17) below 1 K,<sup>90</sup> for Au nanoparticles bonded to 36 at 300 K,<sup>331,332</sup> for 71a bonded to an MBJ at 300 K (Figure 9),<sup>329</sup> for the Co complex 140 at 1.5 K,<sup>86</sup> and for 47 at 1.7 K.<sup>333</sup>

For three samples of metallic SWCNT, the charging energy  $E_{\text{C}}$ , the quantum energy level separation  $\Delta$ , the sub-band mismatch  $\delta$ , the exchange energy *J*, and the excess Coulomb energy  $dU$  were measured at 0.3 K; for a sample of length  $L = 400$  nm,  $E_{\text{C}} = 4.3$  meV,  $\Delta = 9.0$  meV,  $\delta = 3.2$  meV,  $J = 0.4$  meV, and  $dU \approx 0$  were found.<sup>330</sup>

## 15. NEGATIVE DIFFERENTIAL RESISTANCE AND POTENTIAL POWER GAIN WITH TWO-PROBE METHODS

An all-organic computer has been discussed,<sup>69</sup> but the synthetic complexity of such a venture (making organic electronic components and also controlling all organic or polymeric interconnects at once) seems unrealistic at present. There may be a more urgent need to find electroactive molecules and devices with power gain.<sup>48,51</sup>

At the present time, only two-terminal unimolecular devices, such as resistors, insulators, or rectifiers, have been studied; all are interrogated by inorganic metal contacts (Au, Ti, Al, Mg, etc.). Two-terminal rectifier logic does not compete commercially with FET logic,<sup>334</sup> but electronic gain can be obtained by using either Esaki tunnel diodes<sup>97,98</sup> or organic NDR devices,<sup>96,335</sup> both two-terminal devices. This is because, in principle, the negative resistance of such devices, when added to an equal and opposite



**Figure 9.** Coulomb staircase (CS) at 300 K in  $\alpha,\alpha'$ -terthiophenedithiol (71a) in an MBJ: successive *IV* curves are shifted vertically for clarity. Reprinted by permission from ref 329. Copyright 1999 American Physical Society.

positive load resistance in the output circuit, could lead to a very large or infinite power gain. However, a technological effort to utilize organic NDR SAMs in the early 2000s failed because of bad reproducibility.

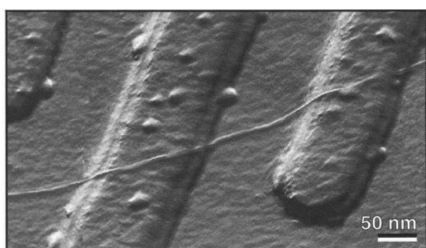
## 16. GATING IN FIELD-EFFECT TRANSISTORS AND IN MOLECULAR CONDUCTANCE

Many researchers have studied the effect of a centrally located electric field on the conductivity between two electrodes. Using the terminology of field-effect transistors (FETs), the two electrodes (nanoscopic or not) in ohmic contact with a molecule (or monolayer) can be called the source (S) and drain (D) electrodes, which are separated by a relatively thick insulator from an inorganic metal or semiconductor, which then functions as the gate (G) electrode; G exerts an electric field (but injects no charge) in the conductance pathway from S to D. LB monolayer FETs using conducting polymers were realized decades ago<sup>91</sup> and were made using thin-film sexithiophene,<sup>92,93</sup> the key to an FET is thinning the channel width of a semiconductor by using a gate electrode that is electrically insulated from the channel. One can even use shoe polish, if it is electrically semiconducting, as the working channel in an FET. At present one could use two-terminal break junctions (MBJ or EBJ) plus an STM tip as the third electrode; indeed, many FET applications of this type (molecular orbital gating) are known.<sup>336</sup> Electrochemical gating can also provide gain.<sup>337</sup>

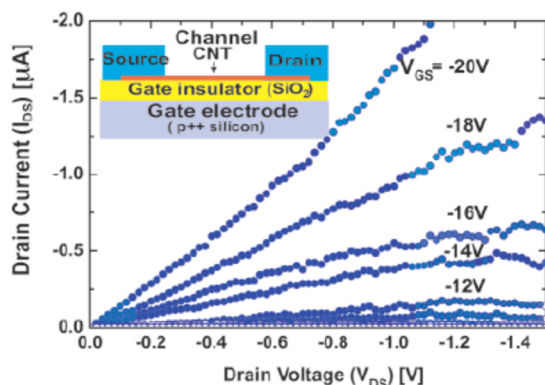
As mentioned above, FET behavior was observed by the group of Cees Dekker<sup>90</sup> by using an STM tip as the G electrode for a single-walled carbon nanotube (SWCNT) curled over parallel Au lines (S and D electrodes) (Figure 10); the power gain was  $< 1$ .<sup>90</sup>

Later improvements by Phaedon Avouris and co-workers (Figure 11) increased that gain.<sup>338</sup>

A three-capacitor model can describe the coupling of a molecule, or any nanoscopic object, to source, drain, and gate



**Figure 10.** AFM image of SWCNT curled over Au lines. Reprinted by permission from ref 90. Copyright 1997 Macmillan Publishing.



**Figure 11.** Output characteristics at 300 K for a CNT FET deposited over Si and contacted by Co (S and D) electrodes. Reprinted by permission from ref 338. Copyright 2002 American Chemical Society.

electrodes (Figure 12a) in the so-called weak-coupling limit (satisfied, e.g., by the SWCNT, which is attracted to the Pt electrodes only by relatively weak van der Waals forces).<sup>333</sup>

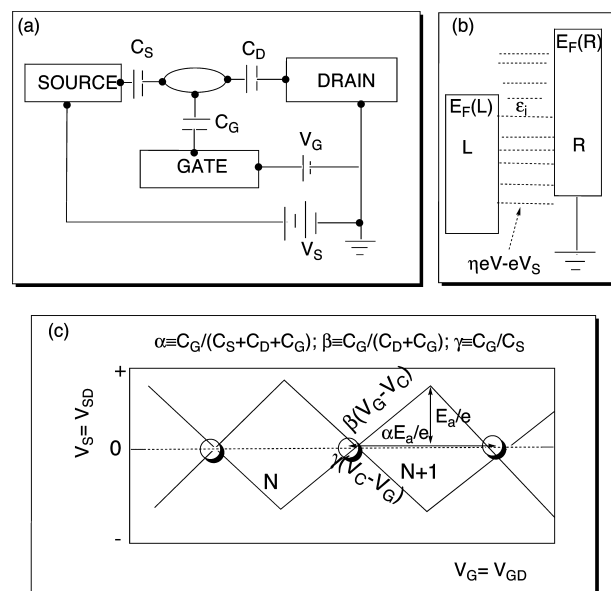
The conductance ( $dI/dV$ , color axis) in a  $V_S$  versus  $V_G$  plot (Figure 12c) can identify interesting conductance regimes in molecules and quantum dots studied by various BJ methods at 4.2 K.<sup>339</sup> In particular, certain enclosed quadrilaterals in these plots (Coulomb diamonds (CDs)) show no conductance at all in the CB regime (Figure 12c). An example of a CD will be shown later. The chemical potential  $\mu_{\text{QD}}$  of a quantum dot with energy levels  $\epsilon_i$  and bearing  $N$  electrons in an external potential  $V$  is given by

$$\mu_{\text{QD}} = (N - 1/2)e^2/C - eV + (1/2) \sum_{i=1}^{i=N} \epsilon_i \quad (67)$$

Keeping the chemical potential alternately equal to either  $V_G$  or  $V_D$  allows one to measure the quantities  $\alpha$ ,  $\beta$ , and  $\gamma$  defined in Figure 12c and therefore obtain the capacitances  $C_S$ ,  $C_G$ , and  $C_D$ .<sup>330</sup> Equations similar to eq 67 may link  $C_S$ ,  $C_G$ , and  $C_D$  to the interfacial energies between the molecule and metal electrodes. Until such equations are developed, it is difficult to calculate these capacitances a priori (i.e., theoretically), and therefore the knowledge of these capacitances a posteriori does not help yet in the design of future molecular devices. Unfortunately, most chemists are unfamiliar with capacitance models.<sup>66</sup>

## 17. SPINTRONICS

The nascent field of molecular spintronics<sup>340,341</sup> can be thought of as a refocusing of molecular electronics toward controlling not charge but spin states and spin–spin coupling for possible magnetic storage. Consider the macroscopic sandwich  $F_1|I|F_2$  with two outer ferromagnetic layers  $F_1$  and  $F_2$  and an inner insulating layer  $I$  with net spin: the magnetic coupling between  $F_1$



**Figure 12.** (a) Three-capacitor model for coupling between molecule, source (S), drain (D), and gate (G) electrodes. (b) Energy levels of quantum dot  $\epsilon_i$ ; the Fermi level of the left electrode (S) is shifted downward by a positive potential  $V_G$ , the Fermi level of the right electrode (D) remained at zero, and the energy level of the quantum dot shifted downward by  $\eta eV - eV_G$ , where  $\eta \equiv C_S/(C_S + C_D + C_G)$ . (c) CB or stability diagram of conductance (color axis) versus  $V_S$  and  $V_G$ : the irregular enclosed quadrilaterals (Coulomb diamonds (CDs)) are the areas for which no current can pass, because of capacitance effects. Current passes along the line segments between the quadrilaterals. At small bias, however, conductance is only seen within the small shaded circles. Adapted from refs 40, 330, and 339.

and  $F_2$  can be controlled (modulated) by the magnetic properties of the  $I$  layer, which behaves as a spin valve even when  $I$  is as thin as a monolayer.

Although practical magnetic devices have been historically inorganic materials, there was an early suggestion<sup>342</sup> that, under certain conditions, even organic crystals could show long-range ferromagnetic order (that is, a magnetization that vastly exceeds the sum of individual molecular paramagnets and has sufficient coercivity to preserve the large moment). This suggestion launched many other proposals as well as experimental searches for organic ferromagnetism, but only  $\alpha$ -nitronitroxide was proven to be ferromagnetic below a very low Curie critical temperature  $T_C = 1.1$  K.<sup>343</sup> Even when organometallic clusters have high spin and local ferromagnetic coupling within the cluster, they usually suffer from long-range antiferromagnetic coupling. There are a few exceptions. Long-range ferromagnetic behavior at 4 K was found in the metal–organic complex decamethylferricenium tetracyanoethenide, with onset at 4.8 K and a really square  $MH$  loop at 2 K ( $H$  is the external field and  $M$  is the magnetization).<sup>344</sup>

High-spin organometallic complexes (e.g.,  $\text{Mn}_{12}$  clusters) were pioneered by the groups of Roberta Sessoli, Dante Gatteschi, George Christou, David N. Hendrickson, Eugenio Coronado, and others: for instance,  $[\text{Mn}_{12}\text{O}_{12}(\text{OOC}-\text{Me})_{16}(\text{H}_2\text{O})_4] \cdot \text{MeCOOH} \cdot 3\text{H}_2\text{O}$  (**144**) has an  $S = 10$  ground state explained by eigenstates of a spin Hamiltonian:

$$H_{\text{spin}} = D(S^2 - 1/3S_z^2) + E(S_x^2 - S_y^2) + g_e \beta_e \mathbf{S} \cdot \mathbf{H}_0 \quad (68)$$

This spin Hamiltonian consists of a Zeeman term (the dot product between the external magnetic field  $\mathbf{H}_0$  and the overall electronic spin  $\mathbf{S}$ , with its Bohr magneton  $\beta_e$  and the gyromagnetic ratio  $g_e$ ) and of fine-structure splitting parameters  $D$  and  $E$  defined in a local diagonalized system ( $x, y, z$ ). For **144** the measured values were  $D = -0.6 \text{ cm}^{-1} = -7 \times 10^{-5} \text{ V}$  and  $E \approx 0$ ,<sup>345</sup> whence spin ladders of the transitions between the  $2S + 1$  eigenstates could be measured.<sup>345</sup> However, long-range intermolecular antiferromagnetic coupling prevails in the solid.<sup>345</sup> Another  $\text{Mn}_{12}$  salt, namely,  $\text{Mn}^{\text{II}}$ (hexafluoroacetylacetonate)<sub>2</sub>(2-isopropyl-4,4,5,5-tetramethylimidazoline-1-oxyl-3-oxide), with a nitroxide spin center in addition to the magnetism due to the  $\text{Mn}_{12}$  cluster, shows a long-distance ferromagnetic order thanks to ferrimagnetic chain components and high coercivity below 7.6 K.<sup>346</sup> These high-spin organometallic complexes have been called molecular magnets or single-molecule magnets (SMMs),<sup>347</sup> even though at 300 K they are unsuitable for your refrigerator door!

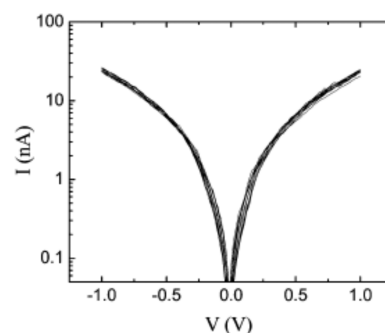
In the magnetics industry, a solenoid “writes” magnetic bits inductively on tape and hard or floppy disks, but, over time, reading the oriented magnetized bits became easier by measuring the changed electrical resistance of the magnetized bit, instead of its magnetic moment. Traditional ordinary magnetoresistance evidences only a small increase in electrical resistance in a magnetic field (e.g., 2% for permalloy at 0.1 T) and is too small an effect; the crucial discovery of giant magnetoresistance (GMR),<sup>348,349</sup> e.g., 50% in a 3-nm Fe/0.9-nm Cr bilayer at 4.2 K and 2 T, ushered in GMR at 300 K and GMR read heads. These GMR heads, used in magnetic hard disks today, read the increased local resistance of the magnetized bit, due to its oriented local magnetic field. More recently, tunneling through a thin MgO layer between two magnetic layers exhibits a tunneling magnetoresistance (TMR) predicted<sup>350</sup> and observed with resistance ratios over 200% at room temperature;<sup>351</sup> this quickly brought forth TMR heads in commerce.

## 18. CONDUCTIVITY OF MOLECULAR WIRES

Weiss and co-workers showed by STS that SAMs of aliphatic thiols chemisorbed on Au are  $\sim 10^3$  times less conductive than aromatic thiols.<sup>81,82</sup> Soon thereafter, Reed and co-workers showed that 1,4-benzenedithiol (**30a**) bonded to Au nanoelectrodes by MBJ had a device conductance of 75 nS at 1 V.<sup>85</sup> This result encouraged many physicists to study simple aliphatic or aromatic terminal bithiols by MBJ; all of these, however, were studied at applied voltages away from resonance with donor levels or affinity levels.<sup>40</sup>

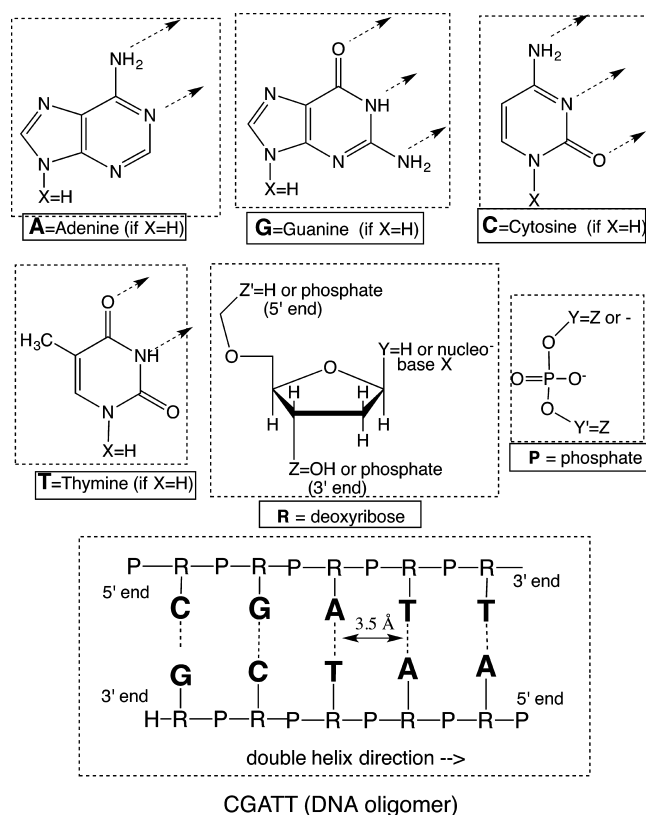
By studying the temperature dependence of the conductivity of alkanethiols of different chain lengths **27** (*n*-octanethiol, *n*-decanethiol, *n*-dodecanethiol, and *n*-hexadecanethiol), in nanopores between 77 and 300 K,<sup>321</sup> Reed and co-workers found that the symmetric  $IV$  curves could be fit to (i) the Simmons formula, eq 45, with  $\Phi_B = 1.39 \pm 0.01 \text{ eV}$  plus an additional factor  $\alpha = 0.65 \pm 0.01$  inserted into the two exponentials of eq 45 to modify the electronic mass  $m_e$  into an effective mass  $m^*$ , and (ii) the hopping model, eq 53, with  $\beta = 0.79 \pm 0.01 \text{ \AA}^{-1}$ .<sup>320,321</sup> The plot of  $\log_{10}I$  versus  $V$  for dodecanethiol **27c** (Figure 13) is remarkably independent of temperature.

While  $G_0$  has been measured and confirmed innumerable times for Au nanowires, the experimental maximum conductance of a Pt nanoelectrode is  $1.6G_0$ , rather than  $G_0$ , because surface Pt atoms have a more complicated set of atomic orbitals (the ground state of Au is  $[\text{Xe}]4f^{14}5d^{10}6s^1$ , with mostly 6s character, a peak at  $G_0$ , and only one conductance channel, while Pt is



**Figure 13.** Plot of  $\log_{10}I$  versus  $V$  for dodecanethiol (**27c**) studied in a nanopore between Au electrodes between  $T = 80\text{--}300 \text{ K}$ ; the data in 20 K steps are superimposed remarkably well. Reprinted by permission from ref 320. Copyright 2005 Institute of Physics.

$[\text{Xe}]4f^{14}5d^86s^2$ , with mixed 6s and 5d character, a major peak at  $1.6G_0$ , and three conductance channels).<sup>353</sup> When a single  $\text{H}_2$  molecule bridges the Pt–Pt gap, the first conductance peak shifts to  $G_0$ .<sup>353</sup>



**Figure 14.** Chemical components of the DNA double-helix, with H bond directions shown as arrows on each nucleobase, and (bottom) a depiction of the GCAT DNA oligomer **147**.

Tao’s SBJ work<sup>89</sup> was extended by the groups of Tao, Latha Venkataraman, Thomas Wandlowski, and others (Table 4). The conductance maxima were identified by histograms of observations versus conductance derived from thousands of repeated SBJ runs. For nanowires of Au atoms, the histograms clustered at integer multiples of the Landauer–von Klitzing conductance quantum  $G_0$  (presumably  $G_0$  for one,  $2G_0$  for two, and  $3G_0$  for three linear chains of Au atoms); the  $G$  values peaked at these points but had finite breadth, presumably whenever the

**Table 5. Conductances (nS) (HC = High, MC = Medium, and LC = Low) of  $\alpha,\omega$ -*n*-Alkanedithiols HS-(CH<sub>2</sub>)<sub>n</sub>-SH (19) and  $\alpha,\omega$ -*n*-Alkanediisothiocyanates SCN-(CH<sub>2</sub>)<sub>n</sub>-NCS (23) Measured in SBJ between Au, Pd, and Pt Electrodes at 300 K, and Fits to  $\Phi_B$  of Eq 45 and to  $\beta$  of Eq 53; From Refs 67 and 114**

<i>n</i> =	S-(CH <sub>2</sub> ) <sub>n</sub> -S...						SCN-(CH <sub>2</sub> ) <sub>n</sub> -NCS...						Au	
	Au			Pt			Au		Pd		Pt			
	HC	MC	LC	HC	MC		HC	MC	HC	MC	HC	MC	$\Phi_B$ /eV	$\beta/\text{\AA}^{-1}$
4				147 <sup>a</sup>	15 <sup>a</sup>		147 <sup>a</sup>	15 <sup>a</sup>	330 <sup>a</sup>	26 <sup>a</sup>	535 <sup>a</sup>	44 <sup>a</sup>	1.30 <sup>c</sup>	0.75 <sup>c</sup>
5		64 <sup>b</sup>	1.9 <sup>b</sup>											
6	93 <sup>a</sup>	17 <sup>a</sup>		194 <sup>a</sup>	30 <sup>a</sup>		15 <sup>a</sup>	1.5 <sup>a</sup>	46 <sup>a</sup>	4 <sup>a</sup>	55 <sup>a</sup>	5 <sup>a</sup>	1.34 <sup>d</sup>	0.81 <sup>d</sup>
	95 <sup>b</sup>	20 <sup>b</sup>	2.45 <sup>b</sup>											
8	20 <sup>a</sup>	4.6 <sup>a</sup>		37 <sup>a</sup>	6.6 <sup>a</sup>		2.6 <sup>a</sup>	0.33 <sup>a</sup>	5.1 <sup>a</sup>	0.46 <sup>a</sup>	7.7 <sup>a</sup>	0.58 <sup>a</sup>		
	21 <sup>b</sup>	4.4 <sup>b</sup>	0.89 <sup>b</sup>											
9	9.9 <sup>b</sup>	2.0 <sup>b</sup>	0.47 <sup>b</sup>											
10	1.7 <sup>a</sup>	0.33 <sup>a</sup>		3.3 <sup>a</sup>	0.60 <sup>a</sup>									
	1.68 <sup>b</sup>	0.45 <sup>b</sup>	0.22 <sup>b</sup>											

<sup>a</sup>Ref 114. <sup>b</sup>Refs 67 and 355. <sup>c</sup>For SCN-(CH<sub>2</sub>)<sub>4</sub>-NCS (ref 114). <sup>d</sup>For HS-(CH<sub>2</sub>)<sub>6</sub>-SH (ref 114).

Au atoms were not strictly in line with the atomically sharp Au tip. For molecules the clustering occurred at multiples of some fractions of  $G_0$ , with even greater line width, presumably because of several ways and orientations with which the molecule aligns with the nanoelectrodes.<sup>89</sup>

Even for very simple  $\alpha,\omega$ -alkanedithiols, up to three distinct conductance peaks have been seen (HC, MC, and LC) by several research teams (Table 5); careful density functional theory (DFT) calculations by Wandlowski and co-workers calculated that for 1,9-nonanedithiol (19e) the LC peak is due to a gauche conformation of the alkane, the MC peak is due to the all-trans atop-atop conformation (the thiolates are each bonded to only one Au atom), and the HC peak is due to the all-trans bridge-bridge conformation (the thiolates are each coordinated to two Au atoms).<sup>67</sup>

To repeat, a thiol R-S-H bonds to an Au surface by lifting up one Au atom out of the plane;<sup>253</sup> is thus MC the better result for the  $\alpha,\omega$ -alkanedithiols? Similarly, for 4,4'-bipyridine (67a) the cantilever deflection force measured in tandem with conductance measurements showed that two conductance maxima were related to variations in the force, i.e., to different van der Waals interactions between 67a and the Au electrodes.<sup>392</sup>

Warnings have been given about artifacts in SBJ measurements, especially when used in an electrochemical cell with water as a solvent;<sup>352</sup> the theoretical  $G$  values agree to within a factor of 3 with the measured values, except in the case of benzenedithiol (30a), where theory overestimates  $G$  by a factor of 50.<sup>352</sup> For 1,8-octanedithiol (19d) in toluene solution, a modified SBJ using a special logarithmic amplifier for the STM current detection yields (within the bias range 0.1–0.4 V) two conductances of  $13 \pm 4$  nS and  $3.25 \pm 1$  nS, presumably due to 2 different conformations or attachments of the molecule within the gap.<sup>352</sup>

Various improvements on MBJ and SBJ have been made. In SBJ, ac modulation (2 kHz) was added to the dc tip bias;<sup>358,362</sup> when a 1,8-octanedithiol (19d) molecule binds to Au, the ac component drops dramatically.<sup>358</sup> Another improvement<sup>328,391,415</sup> placed the substrate holder over a Peltier-effect heater;<sup>328,391,415</sup> this enabled a thermopower measurement, which yielded the sign of the current carrier.<sup>328,391</sup> Performing SBJ experiments in a micropotentiostat allows for electrochemical control of the scanned current.<sup>415</sup> A surface-enhanced Raman spectrum (SERS) was measured on a single 1,4-benzenedithiol (30a) molecule in an MBJ.<sup>376</sup> The “marriage”

of STM and inelastic electron tunneling spectroscopy (IETS) is discussed in section 29.

The measured conductances  $G$  correlate extremely well<sup>67</sup> with  $\cos^2 \phi$ , where  $\phi$  is the (measured or computed) dihedral twist or torsion angle for compounds 30b, 41–46, 69 and 70,<sup>381</sup> 32–35,<sup>386</sup> and 61–66;<sup>390</sup> high torsion angles decrease the conductance.

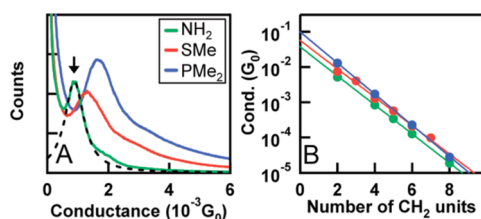
A persistent puzzle remained about the use of a (non-conducting) solvent in SBJ studies; none was used in MBJ studies. An effort was made to subtract the solvent from the histograms.<sup>436</sup> By switching to a conducting solvent and using an auxiliary electrode in an microelectrochemical cell, some gate control of the conductance in an SBJ could be attained.<sup>67</sup> However in aqueous solvents one must beware, and be aware, of ionic interferences and electrochemical side reactions.<sup>352</sup>

Molecule 85 exhibits NDR-like effects just before dielectric breakdown.<sup>400</sup> The shorter molecules 126 ( $n = 1$ ) and 126 ( $n = 2$ ) have temperature-independent SBJ conductances that suggest coherent tunneling (eq 16), between 275 and 325 K ( $n = 1$ ) and between 300 and 335 K ( $n = 2$ ), while the longer 126 ( $n = 3$ ) and 126 ( $n = 4$ ) have a pronounced temperature dependence, due to incoherent hopping conduction (eq 54).<sup>418</sup>

A recent experimental study on a single Zn porphyrin 134 chemisorbed to Au nanoelectrodes at 6 K could distinguish between the energy shift due to  $\Delta$  and the energy shift due to  $P_{el} + P_{ho}$ , and provided an estimate of the latter by image charge calculations.<sup>135</sup>

McCreery and co-workers have perfected a method of electrodepositing a compact layer of either diazonium salts or nitrodiazonium salts atop a heavily graphitized (0.5-nm roughness) pyrolyzed photoresist film atop Si, then electroreducing the aromatic layer, and covering all by a 30-nm Cu film; this dense array allows an immense number of IV cycles ( $1.5 \times 10^9$ ) without breakdown!<sup>437</sup> The exponentially decreasing conductance with increasing chain length yields a very reasonable  $\beta = 0.89/\text{CH}_2$  group or  $\beta = 0.75 \text{\AA}^{-1}$  (Figure 15).<sup>368</sup> Similar  $\beta$  values for various classes of molecular wires, measured by many groups, range from 1.1 to  $0.2 \text{\AA}^{-1}$ .<sup>79</sup> It is reassuring that measurements of transient absorption decay times in D–B–A molecules of varying lengths yield similar values.<sup>54</sup>

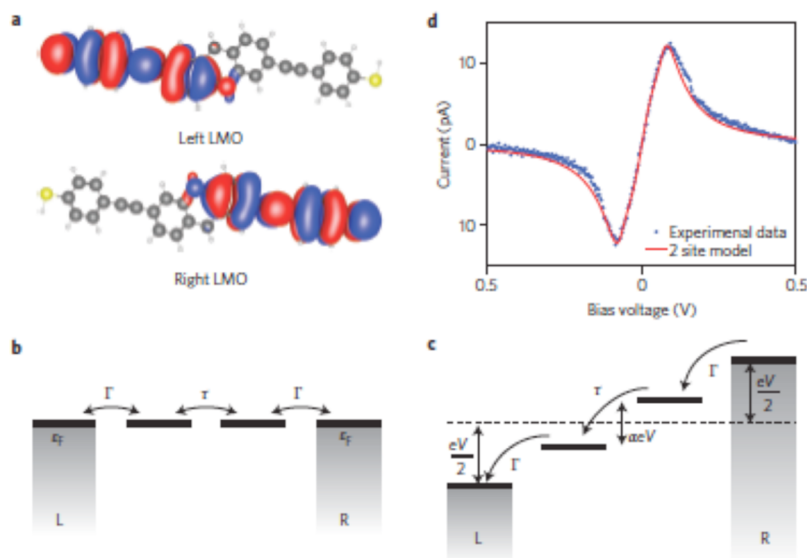
The group of Jan C. (“Kees”) Hummelen, collaborating with the groups of van der Zant, van der Molen, Wandlowski, and Chiechi, has studied the reduced conductance of cross-conjugated molecules 102 and 103, relative to normally



**Figure 15.** (A) Conductance histograms for  $\text{NH}_2-(\text{CH}_2)_4-\text{NH}_2$  **20** ( $n = 2$ , green),  $\text{PMe}_2-(\text{CH}_2)_4-\text{PMe}_2$  **21** ( $n = 2$ , blue), and  $\text{SMe}-(\text{CH}_2)_4-\text{SMe}$  **22** ( $n = 2$ , red). (B)  $\log_{10} G$  as a function of number of methylene groups in the molecules in  $\text{X}-(\text{CH}_2)_m-\text{X}$  for  $\text{X} = \text{NH}_2$  (green),  $\text{PH}_2$  (blue), and  $\text{SMe}$  (red). Reproduced by permission from ref 368. Copyright 2007 American Chemical Society.

conjugated molecules (**96**);<sup>403,406,408,409,412</sup> this decreased conductance is akin to the well-known principle in physical organic chemistry that there is reduced coupling for meta-disubstituted aromatic molecules (relative to para- or ortho-disubstituted ones). Also, when **102** is electrochemically reduced twice (from cross-conjugated anthraquinone to linearly conjugated anthrahydroquinone dianion), the conductivity should increase.<sup>438</sup> When thioacetates are used to make SAMs on Au substrates, it is important to add base to remove the acetyl groups and increase the order in the SAM.<sup>244</sup> Molecule **103** exhibits interrupted conjugation and also negative differential resistance (NDR) but no conductance maxima at 6 K; this NDR has been explained (Figure 16)<sup>410</sup> by considering a linear combination of the HOMO and HOMO-1 levels of **103** (generating a left localized MO (LMO), with amplitude maxima at the left half of **103**, and a right LMO with amplitudes localized on the right half). These energy levels are degenerate at zero applied bias but are split by a small bias  $V$  by an amount  $aeV$  by the Stark effect.<sup>410</sup>

By measuring the AFM rupture force (RF in Table 4) needed to break the binding of 1,8-octanedithiol (**19d**) to Au at 300 K (RF = 1.6 nN),<sup>361</sup> a value was found that was very similar to the values found for breaking a Au–Au bond (RF = 1.6 nN) at either room temperature<sup>361</sup> or at 4 K;<sup>441</sup> thus, it was decided that the bond broken in **19d** was a Au–Au bond rather than a Au–S bond.<sup>361,366</sup>



**Figure 16.** Explanation of the negative differential resistance (NDR) effect observed for molecule **103** in an MBJ at 6 K. The fit parameters are  $a = 0.74$ ,  $\Gamma = 10.2$  meV, and  $\tau = 24.1$  meV.<sup>410</sup> Reproduced by permission from ref 410. Copyright 2014 Macmillan Publishing Company.

One would like to know the enthalpy of adhesion (physisorption)  $\Delta H_{\text{ads}}$  of amines to Au; it must be smaller than that of chemisorption of thiols to Au. Indeed,  $\Delta H_{\text{ads}}$  was estimated by progressively heating the monolayers of **31a**, **47**, and **53** physisorbed on Au(111) and measuring the He atom specular reflectivity (which is at a maximum when the monolayer is totally desorbed);<sup>385</sup> half the monolayer was desorbed by at  $327 \pm 15$  K for **31a**,  $297 \pm 15$  K for **47**, and at  $415 \pm 15$  K for **53**. The Redhead formula gave  $\Delta H_{\text{ads}} = 1.0$  eV for **31a**, 1.2 eV for **47**, and 0.9 eV for **53**; these values are twice the calculated values but are close to the experimental estimates for the chemisorption of thiols of Au.<sup>385</sup>

From time-dependent MBJ measurements of **31a** versus **41**, the Au– $\text{NH}_2$  bond was estimated to be 5 orders of magnitude less stable than the Au–S bond.<sup>382</sup> By extrapolating to zero length (zero repeat units  $n$ ) the measured conductances  $G$  of oligomers, one can get an estimated contact resistance  $R_C \equiv \lim_{n \rightarrow 0} G^{-1}$  for various molecular terminal group(s). For oligoynes the trend of  $R_C$  is 1,4-benzenedithiol (smallest resistance)  $< \text{SH} < \text{NH}_2 < \text{pyridine} < \text{NO}_2 \approx$  dihydrobenzo[*b*]-thiophene  $\ll \text{CN}$ ; for oligophenyleneethynylenes the trend is  $\text{C} < \text{SH} < \text{pyridine}$ .<sup>79</sup>

Emphasis has been placed on measurements of only the dc electrical resistance  $R$  or its temperature or thickness dependence, but the capacitance  $C$  of monolayers (or single molecules) should not be neglected. By measuring the complex impedance  $Z$  as a function of frequency,<sup>102,372</sup> one can extract  $R$  and  $C$  data from an equivalent circuit model. For sandwiches with an area of  $2.82 \times 10^3 \mu\text{m}^2$  of alkanethiolates **27d**–**27g**, parallel equivalent circuit values  $R = 1$ – $400 \Omega \text{ cm}^2$  and  $C = 1$ – $3 \mu\text{F cm}^{-2}$  were extracted (whence the circuit time constant  $\tau \equiv RC$  is between 1 and 1 200  $\mu\text{s}$ ).<sup>372</sup>

In recent MBJ studies,<sup>135</sup> as the nominal gap between the Au nanoelectrodes was mechanically reduced to less than the molecular length, the bithiol molecules still bridged the electrodes, but the molecules had probably started to “ride and slide” atop at least one electrode (the Au–thiolate cluster could migrate between Au sites). Sterically shielded thiols could prevent such riding motion.



When designing efficient unimolecular devices, we seek medium coupling to the electrodes, and we may be able to assess the capacitances linking these devices to the electrodes if at 4 K CBs can be found for them (i.e., if the coupling is not too strong). Measurements of single molecules in SBJs, expanded beyond mere conductance to mechanical forces, absorption/emission of light, thermopower, and spintronics effects, have been reviewed recently.<sup>78</sup>

The exact geometry of the molecule chemisorbed onto a metal surface is difficult to determine,<sup>66</sup> but valuable insight is now available in very difficult experiments combining STM and single-molecule Raman spectroscopy,<sup>439</sup> or simultaneous STM and inelastic tunneling spectroscopy (IETS),<sup>440</sup> discussed later. Some insight is also available by monitoring in the same experiment the AFM cantilever force and the single-molecule SBJ conductance;<sup>361,392</sup> as may be expected, the through-molecule conductance and the mechanical force felt by the AFM cantilever tip share a similar dependence on the distance between the tip and the substrate.<sup>441–444</sup>

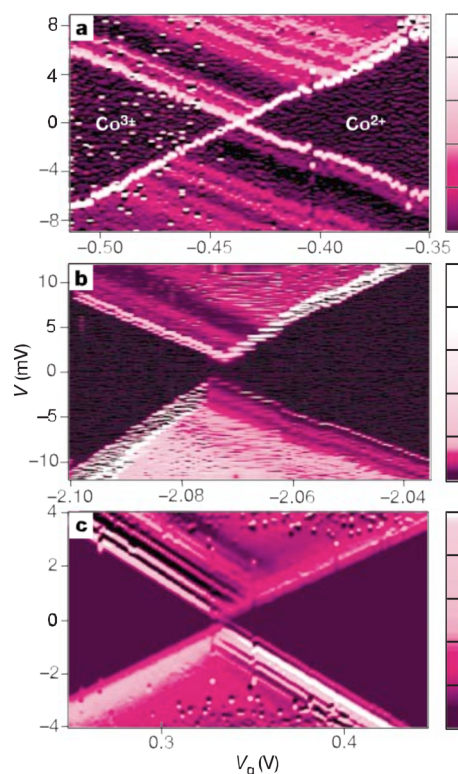
Resonance Raman emissions, enhanced by Au nanoparticles or by the tunneling process, have been detected for *p*-mercaptoaniline in an EMBJ<sup>439</sup> at 1490 and 1498  $\text{cm}^{-1}$  or fishing-mode STM (SBJ) plus tip-enhanced Raman spectroscopy.<sup>445</sup> When a molecule is on a metal surface, light emission is strongly quenched by surface plasmon-polaritons within the metal,<sup>446</sup> so molecule-specific emission features are hard to detect.<sup>447</sup> Inserting a thin insulator did help: a ca. 5-Å-thick  $\text{Al}_2\text{O}_3$  layer was grown atop NiAl(110), then a ca. 2-Å-thick layer of Zn(II)etioporphyrin I was sublimed above it, and the sandwich was probed by STM at ultrahigh vacuum using a Ag (or a W) tip. Fluorescence emission under bias (rather than inelastic tunneling emission) was detected with vibrational subpeak separations of  $40 \pm 2$  meV.<sup>448</sup> The spectroscopy in molecular junctions was reviewed recently.<sup>64</sup>

The thermopower values  $S$  were positive (hole conduction) for molecules **24a–24c**, **39** ( $n = 1–4$ ),<sup>328</sup> and **79** and **84a**.<sup>381</sup>  $S$  was negative (electron conduction through LUMOs?) for **67a** and **75**;  $S$  was almost zero for **122**.<sup>391</sup> From the energetics shown in Table 2, the  $S < 0$  results for **67a** and **75** in Table 4 seem counterintuitive. The temperature dependence of the conductance of  $\alpha,\omega$ -dithiols **19b**, **19c**, **19d**, and **19e** in the range  $293 \leq T \leq 353$  K was ascribed to a redistribution of the contributing conformers.<sup>356</sup>

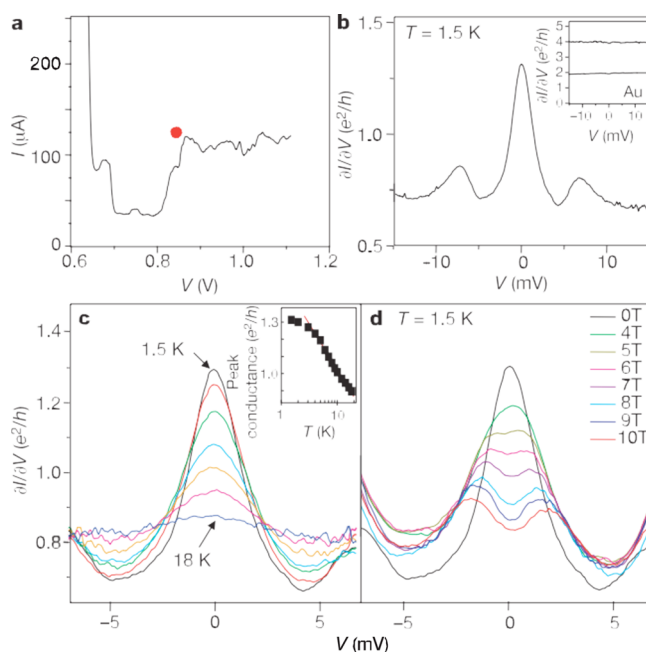
We next review relevant unimolecular spintronics results. In the first EBJ study at cryogenic temperatures,<sup>86</sup> not only was a CB observed in Co complexes **140a** and **140b**, bonded to 2 Au electrodes (source and drain, with a bias  $V$  across them) and subjected to an electric field by applying a potential  $V_g$  to the gate, but also there were CDs in the conductance as a function of  $V$  and  $V_g$  (Figure 17);<sup>86</sup> the high-conductance ridges correspond to the oxidation from  $\text{Co}^{2+}$  (right) to  $\text{Co}^{3+}$  (left). The Kondo effect for **140a** is shown in Figure 18.<sup>86</sup>

Similar results have also been seen for the divanadium complex **141**,<sup>318</sup> for **142**,<sup>430</sup> and for the SMMs **143**,<sup>431</sup> **144**,<sup>432</sup> and **145**.<sup>432</sup> In the  $S = 5$   $\text{Fe}_4$  cluster SMM **145**, the spin states were accessed (but not changed) at 1.6 K by using a gate voltage  $V_g$ .<sup>433</sup>

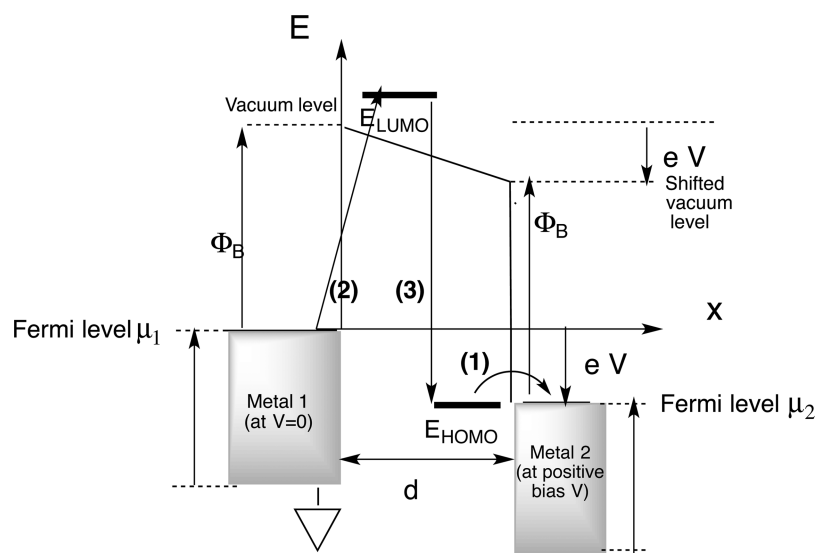
In the SMM **142** consisting of an organometallic Mn(II) complex with an  $S = 5/2$  ground state, the magnetic fine-structure and Zeeman splittings could be followed at 1.7 K by inelastic tunneling processes in the CB region. A gate voltage  $V_g = 0.9$  V (at magnetic field  $H = 0$ , increasing linearly with magnetic field) could excite  $\text{Mn}^{2+}$  from its high-spin  $S = 5/2$  ground state



**Figure 17.** For three samples of **140b**, color plots of differential conductance  $dI/dV$  at 0.1 K and at zero applied magnetic field as a function of the bias voltage  $V$  between source and drain and of the gate voltage  $V_g$ . The white ridges correspond to maximum conductance: (a) 5 nS, (b) 10 nS, and (c) 550 nS.<sup>86</sup> Reproduced by permission from ref 86. Copyright 2002 Macmillan Publishing Company.



**Figure 18.** Kondo peak for the Co complex **140a** at either 1.5 K (a) and (b) or as a function of temperature (1.5–18 K) in zero applied magnetic field (c), or at 1.5 K as a function of magnetic field (0–10 T) (d). As the field increases, the peak splits in two.<sup>86</sup> Reproduced by permission from ref 86. Copyright 2002 Macmillan Publishing Company.



**Figure 19.** At a positive bias  $V$  applied to metal electrode 2, in step (1), resonant tunneling of an electron (transmission factor  $T = 1$ ) occurs from  $E_{\text{HOMO}}$  to the Fermi level  $\mu_2$  of metal electrode 2 (which were put into mutual resonance by the applied voltage  $V$ ). This is followed by nonresonant tunneling (2), (3) of a second electron from Fermi level  $\mu_1$  of metal electrode 1 through a barrier of height  $E_{\text{LUMO}}$  to refill  $E_{\text{HOMO}}$ .

to a low-spin  $S = 1/2$  excited state by (somehow) increasing the partial charges on the ligands without reducing  $\text{Mn}^{2+}$ .<sup>430</sup>

Giant magnetoresistance was measured by STM for a single phthalocyanine molecule  $\text{H}_2\text{Pc}$  135 on ferromagnetic Co nanoislands on a Cu(111) substrate probed by parallel or antiparallel orientations of the magnetization of a Co-coated W nanotip at 4 K;<sup>425</sup>  $G_{\parallel} = 2.0 \times 10^4$  and  $G_{\text{AP}} = 1.5 \times 10^4$  yields a GMR ratio  $= (G_{\text{P}} - G_{\text{AP}})/G_{\text{AP}} = 0.61 \pm 0.09$  and a tunneling magnetoresistance ratio  $G_{\text{P}}/G_{\text{AP}} = 140\%$  at  $-0.35$  V bias.<sup>425</sup> These single-molecule spintronics results have expanded our understanding of molecular conductance. The conductances of DNA oligomers 146 and 147 are discussed in section 31.

## 19. TRANSITION VOLTAGE SPECTROSCOPY

A study on chemisorbed monolayers of alkanethiols on Au, plotting  $\ln_e(|I|V^{-2})$  versus  $V^{-1}$ , found a roughly V-shaped curve, with a good fit to the abbreviated Simmons equation (eq 46) at low  $V$  and a good fit to Fowler–Nordheim tunneling (eq 44) above a transition voltage  $V_{\text{tr}}$ .<sup>301</sup> Using alternate tunneling equations by Stratton<sup>296</sup> and Hartman<sup>449</sup> that are simpler than eq 45, an approximate theoretical value for  $V_{\text{tr}}$  was suggested:<sup>302</sup>

$$V_{\text{tr}} = (2^{3/2} \hbar / e m_e^{1/2} d) (\mu - E_{\text{HOMO}})^{1/2} \quad (69)$$

Other estimates are  $V_{\text{tr}} = 1.15 (\mu - E_{\text{HOMO}})^{450}$  or, very simply,<sup>336</sup>

$$V_{\text{tr}} = \mu - E_{\text{HOMO}} \quad (70)$$

The name “TV spectroscopy”,<sup>302,451</sup> or a more modest appellation,<sup>452</sup> was given for measuring this transition from a trapezoidal barrier at low  $V$  (Simmons tunneling, eq 45) to a triangular barrier at high  $V$  (Fowler–Nordheim tunneling, eq 44). However, an unsymmetrical V-shaped plot of  $\ln_e(|I|/V^2)$  versus  $1/V$ , with a local minimum at  $V_{\text{tr}}$ , bespeaks of some transition between normal tunneling (linear, not necessarily Simmons-like) to some superlinear tunneling (not necessarily a Fowler–Nordheim-like cold-emission mechanism);<sup>302</sup> the position (and/or distortion) and coupling of molecular orbitals (filled or empty) to the adjacent metal electrodes (Figure 1) must become a component of a more complete theory.<sup>302</sup>

Several experimental values for  $V_{\text{tr}}$  have been found: (i)  $V_{\text{tr}} \approx 0.62\text{--}0.95$  V at 300 K in the series phenylthiol, naphthylthiol, anthrylthiol, biphenylthiol, to terphenylthiol;<sup>301</sup> (ii)  $V_{\text{tr}} \approx 1.7$  V for a molecular wire of 2-[4-(2-mercaptoethyl)phenyl]-ethanethiol mixed with a  $10^{-6}$  mole fraction pentane-1-thiol at 260 K;<sup>452</sup> (iii)  $V_{\text{tr}} \approx 1.2$  V for several alkanethiols between 9 and 24 Å in length at 300 K;<sup>453</sup> (iv)  $V_{\text{tr}} = 1.95$  V for 1,8-octanedithiol<sup>336</sup> and  $V_{\text{tr}} = 1.14$  V for 1,4-benzenedithiol.<sup>336</sup> The merits of  $V_{\text{m}}$  have been discussed intensely<sup>454–457</sup> and will be revisited later.<sup>458</sup>

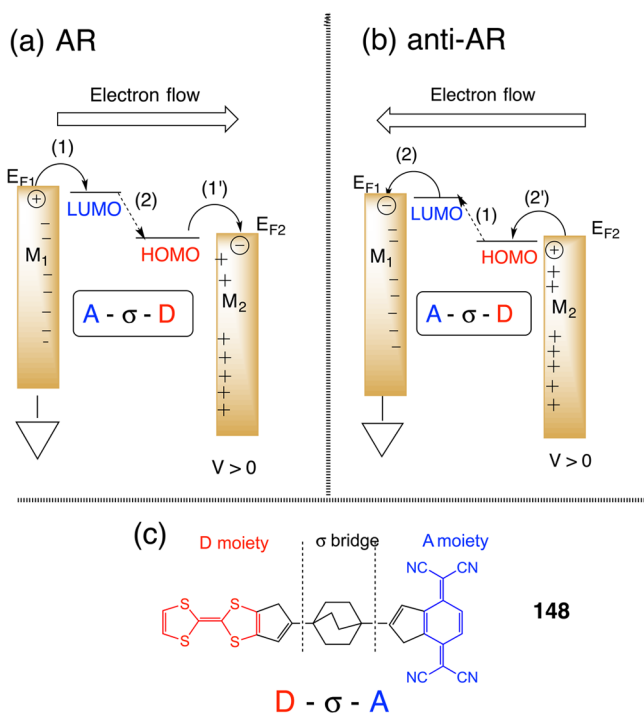
In Figure 5 the molecular orbitals of molecules in the gap are not shown. Physicists usually assume a linear drop of the applied electric field (or bias voltage) across the molecule or molecular monolayer. More likely, the voltage drop may be more complicated if electrons are pulled temporarily into (or from) an available molecular orbital. Once the electron exits the molecule or monolayer and enters the second electrode, the matching of chemical potentials (=partial molar Gibbs free energies) between the two metal electrodes requires that the full voltage drop be accounted for. Future theory and experiments should be planned to differentiate between tunneling through molecules with accessible energy levels and an insulator with a very high-lying conduction band (e.g., diamond-like carbon).<sup>302</sup> Some thought has been devoted to specifically discussing  $\epsilon_{\text{HOMO}}$  and  $\epsilon_{\text{LUMO}}$  for the molecule in the gap.<sup>302,306,307,450</sup>

We may also discuss these energy levels within an organic monolayer between metal electrodes, in a picture like Figure 19. In complicated molecules the largest HOMO (or LUMO) amplitudes may be larger for atoms that are physically closer to one electrode than the other; this can be described by an asymmetry parameter  $p$  ( $0 \leq p \leq 1$ ) as in eq 50,<sup>306,459</sup> partially localized with its center of gravity, and larger amplitudes closer to one of the metals, e.g.,  $M_2$  (i.e., pinning of the molecular orbital to the Fermi level of  $M_2$ ).

## 20. ASYMMETRIES IN $I/V$ CURVES: RECTIFICATION

The  $I/V$  curves described above are symmetric with respect to bias (whatever is in the first quadrant is reproduced in the third quadrant). The first proposal for asymmetric  $I/V$  curves was

AR proposal for a molecular rectifier (Figure 20):<sup>13</sup> the ground state has low polarity ( $D^0-\sigma-A^0$ ) with the HOMO localized



**Figure 20.** (a) The Aviram–Ratner proposal or Ansatz<sup>13</sup> for unimolecular rectification posits a single D-σ-A molecule, where D is a strong electron donor (easily oxidized), A is a strong electron acceptor (easily reduced), and σ is a covalent bridge between them. The first steps for a low-polarity  $D^0-\sigma-A^0$  are (1) an electron moving from the left electrode M<sub>1</sub> to the molecular LUMO and (1') an electron moving from the molecular HOMO to the right electrode M<sub>2</sub>; this is followed by (2) an internal relaxation of the resultant zwitterion  $D^+-\sigma-A^-$  to the ground-state  $D^0-\sigma-A^0$ . The overall direction of preferred electron flow would be from left to right (AR mechanism). (b) The opposite mechanism, which starts (1) with field-induced internal autoionization  $D^0-\sigma-A^0$  to the excited state  $D^+-\sigma-A^-$ , followed by electron transfers (2) and (2') to the two electrodes; the overall preferred electron flow would be from right to left (anti-AR mechanism). If the ground state is a high-polarity zwitterion, then the arguments must be reversed. (c) Molecule 148 proposed by Aviram and Ratner.

mainly on the donor moiety D and the LUMO wave function amplitudes mainly localized on the A moiety. The first easily accessible electronic excited state is the high-polarity zwitterion  $D^+-\sigma-A^-$ .<sup>13</sup> The electronic excited state of opposite polarity  $D^--\sigma-A^+$  is not accessible; it lies several eV above  $D^+-\sigma-A^-$  and may not even be chemically stable.<sup>13</sup>

There are by now two possible mechanisms, shown as AR and anti-AR in Figure 20. For both mechanisms, under sufficient positive bias V metal M<sub>1</sub> is grounded and LUMO is in resonance with Fermi level E<sub>F1</sub>, while HOMO is in resonance with Fermi level E<sub>F2</sub>.<sup>13</sup>

In the AR mechanism, the first step (1, 1') moves an electron from the HOMO to M<sub>1</sub> and from M<sub>2</sub> to the LUMO (against the applied potential); in the second step (2) the excited zwitterionic state  $D^+-\sigma-A^-$  decays to the less polar ground state  $D^0-\sigma-A^0$ . Small minus signs (small plus signs) were added on the inside surface of the left (right) electrode; a circled positive charge and a circled negative charge show that the electron flow from the left

electrode to the right electrode pushes an electron against the overall charges on the electrodes.

In the anti-AR mechanism, thanks to the applied electric field, in the first step (1) the molecule is excited from  $D^0-\sigma-A^0$  to  $D^+-\sigma-A^-$ ; in the second step (2, 2') the electron is moved from the LUMO to M<sub>2</sub> and from M<sub>1</sub> to HOMO. The circled positive negative charges in Figure 20 show that the electron flow from the right electrode to the left electrode pushes the electron to where negative charges are already present.

In the AR mechanism (which could be depicted as  $\leftarrow D^-A \leftarrow$ ) the electron for V > 0 moves from M<sub>1</sub> to M<sub>2</sub> (against the bias). In the anti-AR mechanism (which could be depicted as  $\rightarrow D^-A \rightarrow$ ) the electron moves from M<sub>2</sub> to M<sub>1</sub> (i.e., along the bias). Figure 20c shows the model rectifier molecule 148 proposed by AR;<sup>13</sup> it was never synthesized.

As shown below, the experimental evidence overwhelmingly favors the anti-AR interpretation. A Marcus theory analysis<sup>460</sup> and another theoretical study<sup>461</sup> consider only the anti-AR mechanism. New thoughts about how asymmetric conduction through a molecule can occur have been presented.<sup>462</sup>

When a weak electron donor and a weak electron acceptor were used, calculations predicted and experiment confirmed poor asymmetry, i.e., weak rectification (no surprise!).<sup>463</sup> This suggests the obvious for the future: more electroactive donors and acceptors.

## 21. RECTIFIER OR DIODE: WHAT IS IN A NAME?

Terminology can be baffling. The early 1900s saw the development of vacuum tube diodes, then triodes, tetrodes, pentodes, etc. Inorganic crystal rectifiers (or point-contact rectifiers or crystal detectors), e.g., metal wire on PbS crystal, had been introduced in 1874; they were crucial in the development of Marconi crystal radio in the early 1900s.<sup>464</sup> When inorganic pn junction rectifiers (n-doped Ge + P-doped Si, or later n-doped Si and p-doped Si) were developed in the 1940s, the term rectifier was reserved for these new solid-state devices and the older crystal point-contact rectifiers. However, the term diode has also been applied to solid-state devices: Zener avalanche diode and Esaki tunnel diode. Operationally, rectification was extended to mean both solid-state and vacuum-tube devices, in that they all rectified alternating-current signals into some form of direct current. For clarity, we should promise to reserve diodes for vacuum-tube devices and rectifiers for all the others.

In a solid-state pn junction rectifier, the applied voltage for which electron flow (or hole flow) is larger, or enhanced, is called forward bias; the direction of much less current flow is called reverse bias. p-Doped (n-doped) regions in inorganic semiconductors (Ge, Si, GaAs) are electron-poor (electron-rich); therefore, within a pn junction rectifier the direction of enhanced positive current (thanks to Benjamin Franklin's unfortunate choice of sign) or of hole flow is from p to n (the direction of enhanced electron flow is from n to p). In organic rectifiers (unimolecular or not), we avoid the term "diode", and we should always specify the sign of the voltage applied and concentrate deliberately on the direction of favored electron flow; the term "forward bias" should be restricted to when V > 0, regardless of what is going on.

Table 6. List of All Unimolecular Rectifiers (Structures 149–202) (Single-Molecule or Ordered Monolayer)<sup>a</sup>

Left Electrode (deposition method = LB, LS, or SAM)	Str.	Molecule(s): oriented so that its left end is physisorbed (LB or LS) or chemisorbed (SAM) to the left electrode. D=electron donor ( $\approx$ "n-junction"); A=electron acceptor ( $\approx$ "p-junction")	Right electrode (NT = nanotip; NP = nanoparticle)	Rectification ratio $RR$ (Eq. 71) @ stated $V$ @ temperature (f=fades on recycling; p=persistent), and direction of favored electron flow at stated $V$ ; rectifier type=(A, S, or U); IVT= intervalence transfer band max. / nm; [Ref]
Bulk Ag (LB)	149		Mg/Ag pad	$RR=2$ @ 0.7 V & 300 K; $\rightarrow D-A \rightarrow$ ; type=U+A [99]; $RR=7.5$ @ 0.6 V & 300 K (7 Z-type monolayers); $\rightarrow D-A \rightarrow$ [100]
Bulk Al (LB)	149		Al pad	$RR=26$ @ 1.5 V & 300 K (f); $\rightarrow D-A \rightarrow$ ; type=U+A [101],[102]; $RR=20$ @ 1 V; $\rightarrow D-A \rightarrow$ [103]; $RR=2$ to 27 @ 2.2 V & 300 K (f); $\rightarrow D-A \rightarrow$ ; type=U+A; IVT=750 [104],[105],[480]
Bulk Au (LB)	149		Au NT (STS)	$RR=11$ @ 1 V (f); $\rightarrow D-A \rightarrow$ ; type=U+A [481]
Bulk Au (LB)	149		Au pad	$RR=4$ @ 15 V & 8 K (10 Z-type monolayers) $\leftarrow D \leftarrow \leftarrow$ [119]
Bulk Au (LB)	150		Au pad	$RR=3-64$ @ 1.5 V (f); $\rightarrow D-A \rightarrow$ ; type=U+A; IVT=530 [482]
Bulk Au (SAM)	151		Au NT (STS)	[C <sub>3</sub> ] $RR=30$ @ 1 V & 300 K (p); $\rightarrow D-A \rightarrow$ ; type=U+A [481],[483]
Bulk Au (SAM)	152		Au NT (STS)	[C <sub>10</sub> ] $RR=11$ @ 1 V & 300 K (p); $\rightarrow D-A \rightarrow$ ; type=U+A; [481],[483],[484]
Bulk Au (LS $\rightarrow$ SAM)	153		Au pad	[C <sub>11</sub> ] $RR=2-7$ @ 1.5 V & 300 K (p); $\rightarrow D-A \rightarrow$ ; type=U+A; IVT=740 [483],[485]
Bulk Au (LS $\rightarrow$ SAM)	154		Au pad	[C <sub>14</sub> ] $RR=2-7$ @ 1.5 V & 300 K (p); type=U+A; $\rightarrow D-A \rightarrow$ ; IVT=740 [483],[486]
Bulk Au (LS $\rightarrow$ SAM)	155		Au pad	[C <sub>16</sub> ] $RR=2$ @ 2 V and 60 @ 12 V (p); type=U+A; $\rightarrow D-A \rightarrow$ ; IVT=740 [483],[486]
Bulk Au (SAM)	155		Au NT (STS)	[C <sub>16</sub> ] $RR=11$ @ 1 V (p); type=U+A; $\rightarrow D-A \rightarrow$ [481],[483]
Bulk Au (SAM)	156		Au NT + decanethiol	$RR=11$ @ 1 V; $\rightarrow D-A \rightarrow$ [487]
Bulk Au (LB)	157		Pt/Ir NT	$RR=20$ to 25 @ 1 V; $\rightarrow D-A \rightarrow$ ; type=U+A [488]
Bulk Au (LB)	158		Pt/Ir NT (STS)	$RR=10$ to 25 @ 1 V; $\leftarrow D-A \leftarrow \leftarrow$ ; type=U+A [488]
Bulk Au (SAM)	159		Pt/Ir NT (STS)	No rectification [489]
Bulk Au (SAM)	160		Pt/Ir NT (STS)	$RR=12$ @ 1 V; $\rightarrow D-A \rightarrow$ ; type=U+A [489]
Bulk Au (SAM)	161		Pt/Ir NT (STS)	$RR=100$ to 200 @ 1 V; $\rightarrow A-D \rightarrow$ ; type=U+A [490]
Bulk Au (SAM)	162		Pt/Ir NT (STS)	$RR=400$ to 450 @ 1 V; $\rightarrow A-D \rightarrow$ ; type=U+A [490]
Bulk Au (SAM)	163		Pt/Ir NT (STS)	$RR=14 \pm 1$ @ 1 V; $\leftarrow D-A \leftarrow \leftarrow$ ; type=U+A [490]
Bulk Au (SAM)	164		Pt/Ir NT (STS)	$RR=10 \pm 1$ @ 1 V; $\leftarrow D-A \leftarrow \leftarrow$ ; type=U+A [490]

Table 6. continued

Left Electrode (deposition method= LB, LS, or SAM)	Str.	Molecule(s): oriented so that its left end is physisorbed (LB or LS) or chemisorbed (SAM) to the left electrode. D=electron donor ( $\approx$ "n-junction"); A=electron acceptor ( $\approx$ "p-junction")	Right electrode (NT=nanotip; NP=nano-particle)	Rectification ratio $RR$ (Eq. 71) @ stated $V$ @ temperature (f=fades on recycling; p=persistent), and direction of favored electron flow at stated $V$ ; rectifier type=(A, S, or U); IVT= intervalence transfer band max. / nm; [Ref]
Bulk Au (SAM)	165		Pt/Ir NT (STS)	$RR=30 \pm 1$ @ 1 V; $\leftarrow$ D-A $\leftarrow$ ; type=U+A [490]
Bulk Au (SAM)	166		Pt/Ir NT (STS)	$RR=15$ to $70$ @ 1 V; $\leftarrow$ D-A $\leftarrow$ ; type=U+A [478]
Bulk Au (SAM)	167		Pt/Ir NT (STS)	$RR=3,000$ @ 1 V; $\leftarrow$ D-A $\leftarrow$ ; type=U+A [478]
Bulk Au (SAM)	168		Pt/Ir NT (STS)	$RR=700$ to $900$ @ 1 V; $\leftarrow$ D-A $\leftarrow$ ; type=U+A [478]
Bulk Au (SAM)	169		Pt/Ir or Au NT (STS)	$RR=50$ @ 1 V $\rightarrow$ A-D $\rightarrow$ [491]
Bulk Au (LB)	170		Au pad	$RR=8-60$ @ 1.5 V (f); $\leftarrow$ A-D $\leftarrow$ ; type=U; IVT=490 [492]
Bulk Au (LB)	171		Au pad	$RR=2$ @ 1.3 V (f); $\rightarrow$ D-A $\rightarrow$ ; type=U; IVT=720 [109]
Bulk Au (LS)	172		Au pad	$RR=11$ @ 4.4 V (p); $\rightarrow$ D-A $\rightarrow$ ; type=U [493]
Bulk Au (LB)	173		Au pad	$RR=2-5$ @ 2 V (f); $\rightarrow$ D-A $\rightarrow$ ; type=U+A [494]
Bulk Au (LB)	174		Au pad	$RR=14-28$ @ 1 V (p); $\rightarrow$ D-A $\rightarrow$ ; type=U+A; IVT=595 [494]
Bulk Au (LB)	175		Au pad	$RR=3$ @ 1 V (f); $\rightarrow$ D-A $\rightarrow$ ; type=U+A [495]
Bulk Au (LS)	176		Au pad	$RR=6-60$ @ 1.5 V (p); $\rightarrow$ D-A $\rightarrow$ below 2 V; type=U; but $RR=1/(2$ to $150)$ @ 5.5 V (p); $\leftarrow$ D-A $\leftarrow$ ; type=U [459]
Bulk Au (LB $\rightarrow$ SAM)	177		Au pad	$RR=20.5 \pm 3.5$ @ 1.5 V (p); $\leftarrow$ D-A $\leftarrow$ type=U+A; but $RR=(1/14.0) \pm (1/1.16)$ @ 2 V (p); $\rightarrow$ D-A $\rightarrow$ ; type=U+A [458]
Bulk Au + thio-glycolic acid M	178		Pt/Ir NT (STS)	$RR=18$ @ 1 V; $\leftarrow$ D-A $\leftarrow$ ; type=U+A; [496]
Bulk Au (SAM)	179		Au NP+ Pt/Ir NT (STS)	$RR=1/(2$ to $7)$ @ 1.5 V; $\leftarrow$ D-A $\leftarrow$ ; type=U [497]
Bulk Au (SAM)	180		Au NP (SAM)+ Pt/Ir NT	$RR=3$ to $7$ @ 1.5 V; $\leftarrow$ D-A $\leftarrow$ ; type=U [497]

Table 6. continued

Left Electrode (deposition method = LB, LS, or SAM)	Str.	Molecule(s): oriented so that its left end is physisorbed (LB or LS) or chemisorbed (SAM) to the left electrode. D=electron donor ( $\approx$ "n-junction"); A=electron acceptor ( $\approx$ "p-junction")	Right electrode (NT = nanotip; NP = nanoparticle)	Rectification ratio $RR$ (Eq. 71) @ stated $V$ @ temperature ( $f$ = fades on recycling; $p$ = persistent), and direction of favored electron flow at stated $V$ ; rectifier type = (A, S, or U); $IVT$ = intervalence transfer band max. / nm; [Ref]
Au MBJ (SAM)	181		Au MBJ (SAM)	$RR=1.4$ to $10$ @ $1.5$ V & $30$ K; (rectification maybe $\leftarrow A-A' \leftarrow$ ) [498]
Bulk Au (SAM)	182		Au NP (SAM) + Pt/Ir NT (STS)	$RR=5$ @ $1.5$ V & $300$ K; $\rightarrow D-A \rightarrow$ [499]
Bulk Au (SAM)	183		Pt/Ir NT (STS)	$RR=100$ @ $1$ V; $\leftarrow D-A \leftarrow$ ; type = U+A [500]
Bulk Ag (SAM)	184		Hg drop (SAM)	$RR=9 \pm 2$ @ $1$ V; $\rightarrow A \rightarrow$ ; type = A [466]
Bulk Si	185		Bulk Al	$RR=4.8 \pm 3.3$ @ $1$ V; $\leftarrow \leftarrow D \leftarrow$ ; type = A [501]
Bulk Si	186		Bulk Al	$RR=13.3 \pm 13$ @ $1$ V; $\leftarrow \leftarrow D \leftarrow$ ; type = A [501]
Bulk Si	187		Bulk Al	$RR=8.1 \pm 2.9$ @ $1$ V; $\leftarrow \leftarrow D \leftarrow$ ; type = A; [501]
Bulk Si	188		Bulk Al	$RR=9.4 \pm 3.8$ @ $1$ V; $\leftarrow \leftarrow D \leftarrow$ ; type = A [501]
Bulk Si	189		Bulk Al	$RR=4.7 \pm 2.9$ @ $1$ V; type = A [501]
Bulk Si	190		Bulk Al	$RR=6.7 \pm 2$ @ $1$ V; $\leftarrow \leftarrow D \leftarrow$ ; type = A [501]
Bulk Si	191		Bulk Al	$RR=3.6 \pm 1.4$ @ $1$ V; $\leftarrow \leftarrow D \leftarrow$ ; type = A [501]
Bulk Si	192		Bulk Al	$RR=4.6 \pm 2$ @ $1$ V; $\leftarrow \leftarrow D \leftarrow$ ; type = A [501]
Ag <sup>TS</sup>	193		EGaIn drop	$RR=10^2 \pm 3$ @ $1$ V; $\leftarrow \leftarrow D \leftarrow$ ; type = A [122],[123]
Ag <sup>TS</sup>	194		EGaIn drop	$RR=1 \pm 2$ @ $1$ V; no rectification [122],[123]
Ag <sup>TS</sup>	195		EGaIn drop	$RR=2 \pm 2$ @ $1$ V; no rectification [122],[123]
Ag <sup>TS</sup>	196		EGaIn drop	$RR=5 \times 10^2 \pm 4$ @ $1$ V; $\leftarrow \leftarrow D \leftarrow$ ; type = A [122],[123]
Ag <sup>TS</sup>	197		EGaIn drop	$RR=1 \pm 2$ @ $1$ V; no rectification; [122],[123]
Bulk Au	97		EGaIn drop	$RR=1.5$ @ $0.4$ V; rectifier? [502]
Bulk Au	102		EGaIn drop	$RR=2.3$ @ $0.4$ V; rectifier? [502]
Bulk Au	103		EGaIn drop	$RR=2.5$ @ $0.4$ V; rectifier? [502]

Table 6. continued

Left Electrode (deposition method= LB, LS, or SAM)	Str.	Molecule(s): oriented so that its left end is physisorbed (LB or LS) or chemisorbed (SAM) to the left electrode. D=electron donor ( $\approx$ "n-junction"); A=electron acceptor ( $\approx$ "p-junction")	Right electrode (NT=nanotip; NP=nano-particle)	Rectification ratio $RR$ (Eq. 71) @ stated $V$ @ temperature ( $f$ =fades on recycling; $p$ =persistent), and direction of favored electron flow at stated $V$ ; rectifier type=(A, S, or U); $IVT$ = intervalence transfer band max. / nm; [Ref]
Bulk Au	198		Au NP+ AFM tip	$RR=1.2$ @ 1 V; almost no rectif. $\rightarrow D-A \rightarrow$ ; type=U [503]
Bulk Au	199		Au pad	$RR=2.95$ to $36/7$ @ 4 V & 300 K $Fe^{+++} \rightarrow Fe^{++}$ ; type=A [504]
Bulk Au	200		Au NT STS	$RR=3.5$ @ 2 V & 300 K; $Ru^{++} \rightarrow Ru^{+++}$ ; type=A [505]
Bulk Au (LB)	201		Au pad	$RR=90-150$ ; $\langle RR \rangle = 116$ @ 3 V & 300 K; $\leftarrow D-A \leftarrow$ [506]
Bulk Au	202		Au-coat. AFM tip	$[m=2, n=1]$ ; $RR=30$ @ 1.0 V & 300 K; $\leftarrow D-A \leftarrow$ ; other $m, n$ & were studied [507]

<sup>a</sup>The molecules that form SAMs are depicted with their structure before chemisorption; after covalent attachment to Au, thiols  $-R-H$  and thioacetates  $-R-S-C(O)-CH_3$  become thiolates  $-R-$ , while after chemisorption to Si, the trichlorosilanes  $-RSiCl_3$  become siloxanes  $-RSi(O)-$ . Arrows  $\rightarrow$  show the direction of favored electron flow (if this traverses a longer aliphatic chain, a double arrow  $\rightarrow\rightarrow$  is shown). The rectification mechanisms (A, S, and U) are given, when known.

## 22. THREE MECHANISMS FOR RECTIFICATION BY MOLECULES

There are three distinct mechanisms for asymmetrical conduction (rectification) in metallomonolayer/metal or metal/molecule/metal sandwiches:<sup>10,306</sup>

(1) Schottky barriers (interface dipoles): We shall call molecules that rectify by this process as "S" (for Schottky)<sup>129,130</sup> rectifiers.<sup>10,306</sup>

(2) Asymmetric placement of the chromophore (i.e., the part of the molecule whose molecular orbital must be accessed during conduction) within the metallomonolayer/metal sandwich, e.g., because of the presence of a long alkyl tail:<sup>10,47,306,401,465</sup> We shall call molecules that rectify by this process as "A" (for asymmetric) rectifiers.<sup>10,11</sup> This second process was recently confirmed experimentally<sup>466</sup> and was alluded to in earlier work.<sup>467</sup>

(3) When the current exploits electron transfers between molecular orbitals, whose significant probability amplitudes are asymmetrically placed within the chromophore: This third process we think of as true unimolecular rectification, and we shall call this process "U" (for unimolecular) rectification.<sup>10,11,306</sup> These U rectifiers are what we endeavor to achieve.

There are also two modes of interaction between electrodes and molecules:

(1) Interaction with only one energy level (donor level or HOMO, affinity level or LUMO).<sup>10,306,307</sup>

(2) Interaction with both levels (donor and affinity level, or HOMO and LUMO) as in the AR Ansatz.<sup>10,11,13</sup>

It can be difficult to determine experimentally whether rectification is enhanced by interactions with one or two energy levels.

Placing an ordered array of organic molecules between two inorganic metal electrodes (using covalent tethers to electrodes for self-assembly, using alkyl tails to stabilize LB or LS monolayer formation, or measuring individual molecules covalently bridging two STM tips) may mean that the resulting monolayer may behave as an A or S rectifier, as well as a U rectifier. This is why true unimolecular rectification (U type only) is so rare.<sup>47</sup>

In assessing rectification, one measures the rectification ratio (RR), defined as the current at a positive bias  $V$  divided by the absolute value of the current at the corresponding negative bias  $-V$ :

$$RR(V) \equiv -I(V)/I(-V) \quad (71)$$

For inorganic bulk systems, RR can be very large. Ge point-contact rectifiers used as microwave detectors had RR of the order of  $10^6$  at 1 V by 1945.<sup>468</sup> A medium-sized doped Si rectifier has  $RR = 2.5 \times 10^6$  and  $I = 60$  A at 1 V and 298 K.<sup>469</sup> Very large RR values (of the order of  $10^6$ ) are seen in inorganic Schottky barrier rectifiers<sup>131,470</sup> (the claim<sup>56</sup> that for inorganic junction rectifiers RR hovers between 50 and 100 was incorrect). In fact, organic rectifiers have rather small RRs, in comparison to the inorganic ones. Huge apparent RR values were seen in organic monolayers when Au stalactites or stalagmites (whiskers of Au atoms) were driven by electromigration partially through the

monolayers without shorting them; the return current is ohmic.<sup>109,110</sup> These are deceptive artifacts due to well-known metal whiskers! It has been suggested that the relatively low RR values in the known organic systems make them unsuitable for practical applications.<sup>471</sup>

For inorganic diodes based on doped Si or Ge, the Ebers–Moll equation for the current  $J$  is applicable:<sup>472</sup>

$$J = J_0 [\exp(eV/k_B T) - 1] \quad (72)$$

(and  $J = 0$  at  $V = 0$ ). Equation 72 resembles several equations discussed earlier but has not entered explicitly into discussions of organic rectification.

In both inorganic semiconductor regions meeting at the rectifying junction, there is also the temperature-dependent equilibrium constant  $K(T)$  linking the net concentration of free electrons  $[n]$  and the concentration of free holes  $[p]$ ,

$$[n][p] = K(T) \quad (73)$$

with separate Arrhenius factors influencing the population of electrons and holes. For organic semiconductors eq 72 is valid but eq 73 is not applicable.

### 23. UNIMOLECULAR RECTIFICATION BY ONE LEVEL: SCHOTTKY BARRIER RECTIFIERS (S)

Rectification in LB monolayers and single molecules (interrogated by scanned probe methods) has been seen since 1990. Daniel J. Sandman, J. R. Sambles, and co-workers found a Schottky barrier LB monolayer and multilayer rectifier.<sup>116,117</sup>

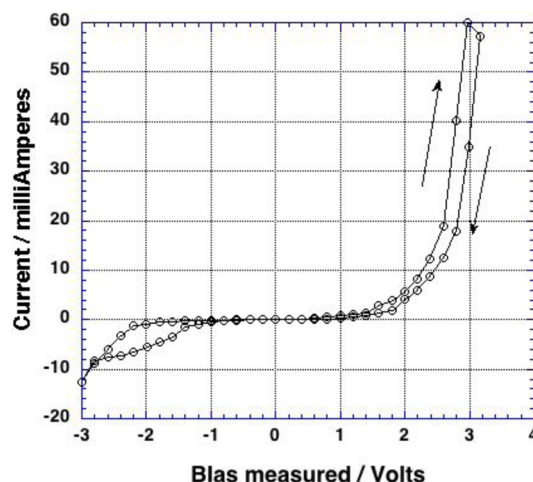
A SAM rectifier with a colossal rectification ratio ( $1.5 \times 10^5$  at 2.3 V) was claimed;<sup>473</sup> however, the Ti electrode is known to penetrate and react chemically even with alkanethiol SAMs.<sup>115</sup> Therefore, this is most likely a Schottky barrier rectifier.<sup>474</sup> Such Schottky barrier rectification was also seen elsewhere.<sup>116,117,475,476</sup> Schottky barrier rectification in an alkanethiol SAM, due to surface oxidation of the Ti electrode, has been measured.<sup>477</sup> A TCNQ alkanethiolate chemisorbed onto Ag was interrogated by an Hg electrode:<sup>466</sup> as discussed later, this may also be an S rectifier.<sup>478</sup>

Very recently a radically different mechanism for rectification by a single molecule was advanced:<sup>479</sup> by assuming large but unequal polarizations and Fermi-level pinning at both molecule/metal interfaces,<sup>148,149</sup> due to different chemisorptive attachments, this proposal jettisons the U idea of an electroactive molecule in the gap. The molecule would have two oligoenes, separated by a short saturated sigma bond; this would be a pure S rectifier.<sup>479</sup>

### 24. UNIMOLECULAR RECTIFICATION (U BY ONE OR TWO LEVELS)

The big leap forward was rectification observed by J. R. Sambles, Geoffrey J. Ashwell, and co-workers in an LB multilayer and also an LB monolayer of a zwitterionic  $D^+-\pi-A^-$  molecule **149** (Table 6) in 1990 and 1993.<sup>99,100</sup> This result was replicated, but using the same metal on both sides of the  $D^+-\pi-A^-$  LB monolayer: Al,<sup>101–103</sup> then cold Au.<sup>104,105</sup> Table 6 summarizes all rectifier results. Figure 21 shows an asymmetric  $IV$  curve (rectification) for molecule **149** between Au electrodes.<sup>105</sup>

The first confirmed rectifier (**149**) has a zwitterionic ground state  $D^+-\pi-A^-$  (confirmed by spectroscopic measurements), made possible by an internal dihedral angle (ca.  $30^\circ$ ) between the quinolinium plane and the 3CNQ plane, presumably caused by steric hindrance; the electronic excited state  $D^0-\pi-A^0$  is of much



**Figure 21.** Rectification in an LB monolayer of **149** between Au electrodes. Reprinted by permission from ref 105. Copyright 2001 American Chemical Society.

lower polarity. The zwitterionic ground state for **149** was seen in LB films but also in solutions<sup>508</sup> and in related crystal structures.<sup>509,510</sup> In AR language,<sup>13</sup> the positively charged quinolinium ring in **149** would be the electron acceptor A and the negatively charged 3CNQ ring would be the electron donor moiety D.

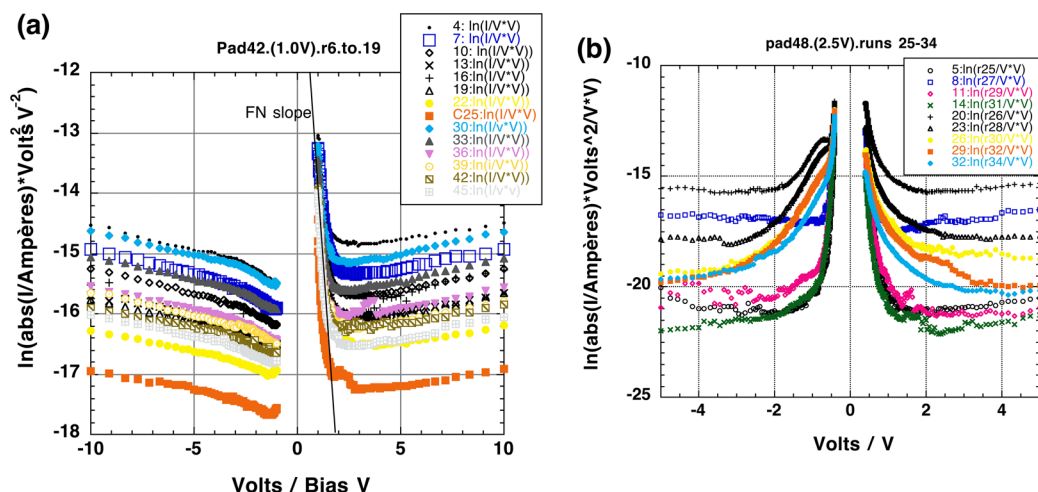
Several theoretical calculations for molecules similar to **149** had indicated the possibility of a quinonoid ground state  $D^0-\pi-A^0$  (and zwitterionic excited state  $D^+-\pi-A^-$ ).<sup>511–513</sup> The low-polarity ground-state  $D^0-\pi-A^0$  was indeed found experimentally for compounds **151–155**;<sup>483</sup> its direction of rectification was opposite from that of compounds **149** and **150**!<sup>483</sup> It was opined that the zwitterionic ground-state  $D^+-\pi-A^-$  for **149** and **150** was aided by intermolecular charge-transfer interactions.<sup>483</sup> Surprisingly, the length of the alkyl chain ( $C_mH_{2m}$ ) had little effect on the rectification.<sup>483</sup> To obviate the A rectifier effect, a dodecanethiol was bonded to the NT so that the alkyl chains on both sides of **156** are of equal length; not much change was seen.<sup>483</sup> References 485 and 486 support the ground-state  $D^0-\pi-A^0$ .

For most molecules listed in Table 6, RR decreases to 1 (i.e., no more rectification) upon repeated measurements for the same sandwich (cycling); the weak LB or LS physisorption and low packing density within the monolayer enable molecular motion induced by the large electric fields used (2 V across 2 nm is 1 GV  $m^{-1}$ ).<sup>101</sup> If however, the LB or LS film is particularly rigid (molecules **172** and **176**) or if the SAM formation stabilizes the orientation of the molecule between the electrodes (**151–155** and **177**), then RR does not decay.<sup>109,459,486</sup> Attention was given to reproducibility and statistics for the reported measurements.<sup>102,105,459</sup>

Of course, detecting an enhanced electron current in  $IV$  curves (Table 6) is not a direct proof of the involvement of 2 molecular energy levels, rather than 1, in the U process. For **176**, however, a reversed rectification direction seems to indicate a transition from resonance with 1 level to resonance with 2 levels.<sup>459</sup> The same Janus effect is also seen for **177**.<sup>458</sup>

The measurement of inelastic tunneling spectra at 4.2 K for a monolayer of **176** finds an elastic signal that is direct evidence of orbital-mediated tunneling (see below).<sup>459</sup> This strongly suggests that the elastic signal has gone through the molecule, in resonance with a molecular energy level, i.e., this was the long-





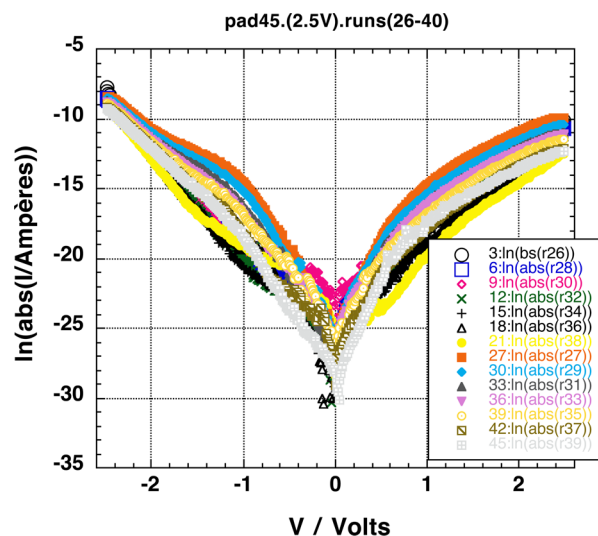
**Figure 22.** Fowler–Nordheim plot ( $\log_{10}II^{-2}$ ) versus  $V^{-1}$  for 177 at 300 K. (a) Scan range  $\pm 1$  V: a clear transition voltage  $V_{tr}$  is seen;  $V_{tr} = 0.54$  V for  $V > 0$  and  $-0.47$  V for  $V < 0$ . (b) Scan range  $\pm 2.5$  V: a transition voltage is not clear. Reprinted by permission from ref 458. Copyright 2014 Royal Society of Chemistry.

sought proof of through-bond tunneling rather than through-space tunneling<sup>514</sup> in the monolayer of 176 at 4.2 K.<sup>459</sup>

The unwelcome gradual decreases in the electrical conductivity and in the RR of an LB monolayer of 149 (from an initial value  $RR = 27^{37,39}$  to almost  $RR = 1.0$  upon repeated cycling) led to combining the LB and SAM techniques, by measuring thioacetyl variants of 149, which could bind strongly to Au electrodes.<sup>486</sup> These variants were synthesized with the aim of preparing molecules that can (i) form good Pockels–Langmuir monolayers at the air–water interface and then (ii) bind covalently to an Au substrate after either LB or LS transfer. The good ordering, afforded by the LB technique, should combine with a sturdy chemical bond to the Au substrate (SAM formation) after LB transfer. 153 gave disappointing results: the Pockels–Langmuir film collapsed at relatively low surface pressures, compared to 149, and yielded disordered LB monolayers, with competition between strong physisorption by the dicyanomethanide end of the molecule and Au-to-thiolate chemisorption. The monolayer rectified in either direction, depending on where in the LB monolayer, i.e., on which molecule (right-side up or upside down), the STM tip was probing. Longer-chain methyl thioester variants 154 and 155 did much better: rectification was observed in standard  $IV$  measurements.<sup>486</sup>

Several groups developed SAMs of new molecules chemisorbed onto Au and saw rectification by STS.<sup>478,489,496–498,515,516</sup> The surprising, unexpected, and unexplained result was that an ionic lawn of gegenions<sup>167</sup> increased rectification ratios to as much as 3 000.<sup>478</sup> A sequential chemical synthesis protocol atop a bulk Au substrate was developed for long asymmetric compounds similar to 202 (which is 7-nm long but rectifies nicely).<sup>507</sup>

Much has been said about transition voltage spectroscopy in molecular wires (see earlier). For rectifier 177,  $V_{tr}$  can be identified for scan ranges not exceeding 1 V (Figure 22a) but not for larger scan ranges (Figure 22b).<sup>458</sup> As can be seen from plots of  $\log_{10}I$  versus  $V$  for 177 (Figure 23), the current nonlinearities for rectifiers are complex, and even more complex when the direction of rectification changes.<sup>458</sup>



**Figure 23.** Plot of  $\ln_e|I|$  vs  $V$  for a monolayer of 177 between Au electrodes at 300 K (14 repeated scans in the range  $\pm 2.5$  V: below 2 V, 177 has larger currents at positive bias; beyond that, the currents are larger at negative bias). There are several changes in the slope! Reprinted by permission from ref 458. Copyright 2014 Royal Society of Chemistry.

## 25. RECTIFICATION IN MACROSCOPIC FILMS AND LANGMUIR–BLODGETT MULTILAYERS

Rectification in macroscopic films<sup>517–519</sup> and in LB multilayers<sup>520–524</sup> has been observed since the 1960s and has been reviewed before.<sup>11,524</sup> The initial report of unimolecular rectification was for multilayers (and also one monolayer) of 149;<sup>99</sup> Ashwell et al. confirmed that Z-type 30-layer films of 149 rectify between Au electrodes.<sup>480</sup> Of course, the currents are 3 orders of magnitude smaller than those reported for the monolayer.<sup>39</sup> Various other LB multilayers have been found to be rectifiers;<sup>525–529</sup> dipole reversal was also observed.<sup>530</sup>

## 26. A AND S RECTIFICATION BY RESONANCE WITH ONLY ONE MOLECULAR ENERGY LEVEL

Using STM, Melvin Pomerantz and co-workers showed rectification by a porphyrin covalently bonded to a carboxylated

highly oriented pyrolytic graphite surface.<sup>531</sup> Jürgen Rabe and co-workers measured by STM an unsymmetrical tunneling current through an alkylated hexabenzocoronene, deposited on graphite; the current is unsymmetrical probably because this molecule is asymmetrically placed between the electrodes.<sup>532</sup> An unsymmetrical STS current was also seen in an oligo(phenylethynyl)-benzenethiol.<sup>533</sup> By STM, rectification was found for an amine-terminated monolayer touching a carboxyl-terminated silane, possibly by proton migration from the carboxylic end to the adjacent amine.<sup>534</sup>

Whitesides, Rampi, Ratner, and co-workers studied a SAM of the thiodetylTCNQ of **184** chemisorbed onto Ag touching a SAM of varying amounts of alkanethiols of **184** ( $C_{16}H_{33}SH$  shown in **184**) chemisorbed onto Hg. When the two SAMs were put into mechanical contact, rectification was seen ( $RR = 9 \pm 2$  at 1 V). The relative ratio of the alkanethiol to the thioalkylTCNQ and the alkyl chain length of the alkanethiol ( $C_{14}H_{29}SH$ ,  $C_{16}H_{33}SH$ , and  $C_{18}H_{37}SH$ ) were modified, with reasonable changes of RR.<sup>466</sup> Because the alkyl chains are of different length, the **183** system could be classified as an A rectifier.<sup>306</sup> However, if perfect interdigitation between the two SAMs occurred, then **184** may be an S rectifier.<sup>466</sup>

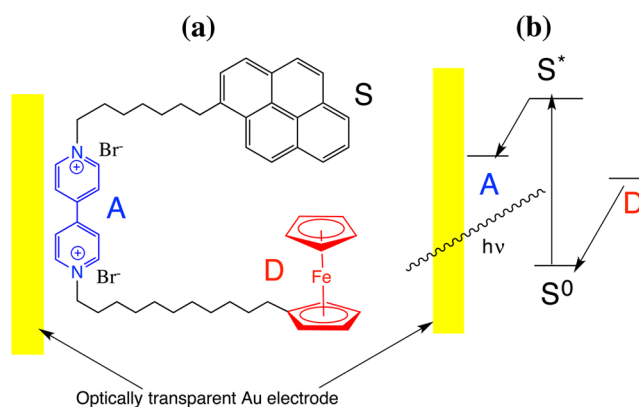
Vuillaume and co-workers studied asymmetric conduction of chemisorbed SAMs **185–192** between Si and Al electrodes.<sup>501</sup> Whitesides and co-workers studied SAMs **193–197** chemisorbed (separately) onto template-stripped (very flat) Ag electrodes  $Ag^{TS535}$  contacted by a macroscopic GaIn eutectic drop (EGaIn, with its varying covering of  $Ga_2O_3$ ), and they emphasize their detailed statistical analyses.<sup>122,123</sup> Several articles from that group encourage the use of EGaIn<sup>536</sup> and describe the rheology of oxide-covered EGaIn droplets.<sup>537</sup> Using microchannels in polymers allowed measurements of  $Ag^{TS}|SAMI|Ga_2O_3|GaIn$  sandwiches between 100 and 293 K.<sup>123</sup> A theory paper about rectification was also published.<sup>462</sup> An odd–even effect in currents was seen when the SAMs were alkanethiols in  $Ag^{TS}|HS-C_{n-1}H_{2n-2}CH_3$  ( $n = 9–19$ ) $|Ga_2O_3|GaIn$  sandwiches.<sup>538</sup> The transport mechanism seems to be by direct tunneling at low  $V$  (with contributions from hopping) and by Fowler–Nordheim for  $|V| \geq 1.3–2$  V.<sup>124</sup> A half-wave rectifier at 50 Hz was also demonstrated.<sup>124</sup> It was emphasized that the conductivity is dominated by the SAM and not the  $Ga_2O_3|GaIn$ .<sup>125</sup> Clearly, asymmetric placement of the ferrocene unit with the gap assures an A mechanism for rectification.

## 27. MONOLAYER PHOTODIODE AND ELECTROCHEMICAL RECTIFICATION

Masamichi Fujihira and co-workers produced the first electrochemical LB photodiode (Figure 24);<sup>539</sup> this work was repeated and extended.<sup>540–546</sup> Electrochemical rectification, measured by standard solution electrochemistry methods at a monolayer-modified electrode, has been reported by several groups.<sup>547–557</sup>

## 28. RECTIFICATION TO HELP ARTIFICIAL PHOTOSYNTHESIS

In the decades-long quest of practical single molecules for artificial photosynthesis, a big stumbling block has been that, while the forward electron transfer rate  $k_+$  through very complicated molecules is often large, the back electron transfer or recombination rate  $k_-$  has also been appreciable, and technologically useful large ratios ( $k_+/k_-$ ) have proven elusive. Using permanent molecular dipoles<sup>558</sup> or even electrets (assemblages of dipoles)<sup>559</sup> to enhance ( $k_+/k_-$ ) (dipole-



**Figure 24.** First electrochemical LB monolayer photodiode on semitransparent Au, from ref 539.

mediated rectification) has become an active thrust (the ratios are measured by transient absorption spectroscopy of the relevant molecules in solution).

## 29. INELASTIC ELECTRON TUNNELING SPECTROSCOPY ORBITAL-MEDIATED TUNNELING AND STM

Inelastic electron tunneling spectroscopy (IETS) was a lucky offshoot of an effort to detect the possible phase loss of Cooper pairs as they transit from a superconductor (Pb) at 4.2 K through a thin insulator (polymethylmethacrylate was chosen) to a normal metal (Al): steps in the  $IV$  curve were detected, which, when differentiated twice ( $d^2I/dV^2$ ), showed peaks at the vibrational energies of C–H and C–C and C–O bonds!<sup>560–562</sup> IETS allows the measurement of vibrational energy absorptions at very low temperatures: both infrared and Raman transitions are observed, since electron–electron scattering is involved, and electromagnetic radiation selection rules (i.e.,  $\mu_{trans} \cdot E \neq 0$ ) do not apply here. IETS has been reviewed often.<sup>68,563–567</sup> The IETS phenomenon is shown in Figure 25; its detection is described in Figure 26.<sup>568</sup>

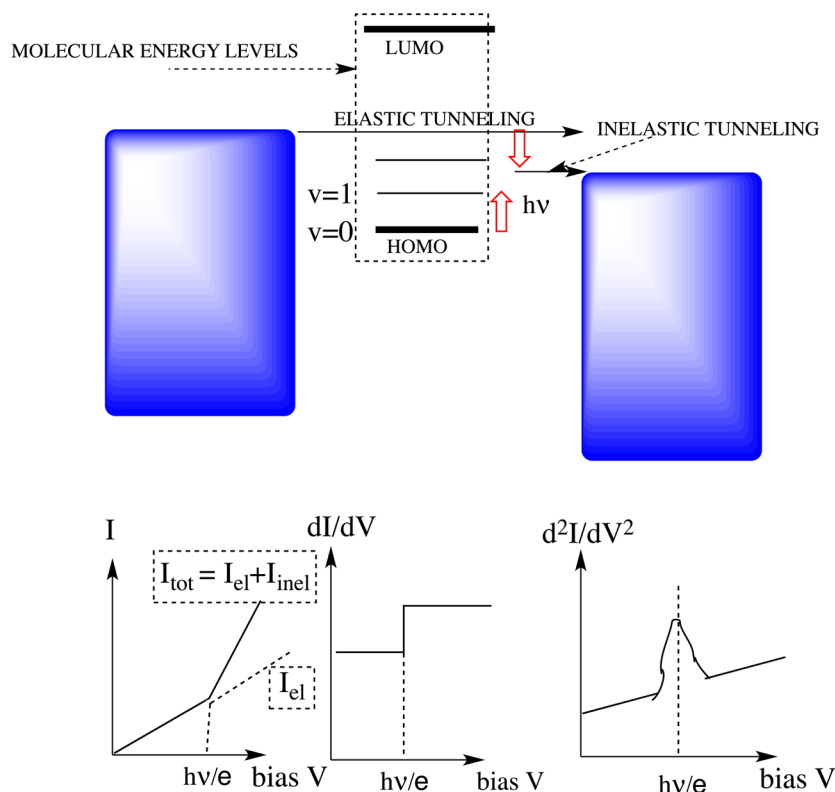
The  $d^2I/dV^2$  peaks broaden dramatically with increasing temperature and cannot be detected at room temperature. Indeed, the IETS vibrational peaks have an overall line width  $W_{fwhm}$  (full width at half-maximum, in  $cm^{-1}$  units):<sup>68,96,459</sup>

$$W_{FWHM} = [(W_{NLW})^2 + (2.29T)^2 + (7.07V_{ACmod})^2]^{1/2} \quad (74)$$

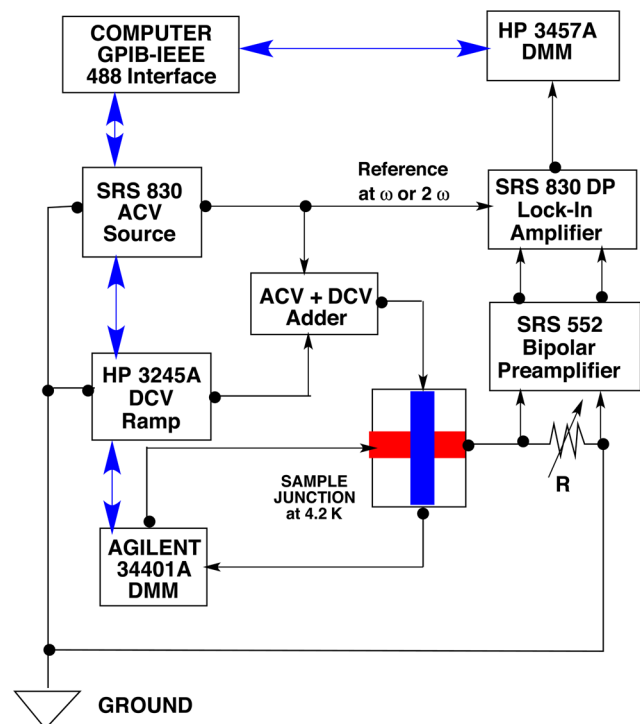
where  $W_{NLW}$  is the natural vibration line-width (typically  $\Gamma_{NLW} = 0.001$  V =  $8.066$   $cm^{-1}$ ),  $T$  is the absolute temperature, and  $V_{ACmod}$  is the applied AC modulation voltage (volts). Thus, for  $T = 4.2$  K and  $V_{ACmod} = 0.004$  V, one gets  $W_{fwhm} = 55.5$   $cm^{-1}$ ,<sup>459</sup> which is broader than an IR line width; above 77 K the vibrational IETS signal is difficult to detect. IETS is very sensitive to electronic noise and needs careful vibration isolation. For typical materials the ratio inelastic current/elastic current is thought to be  $\sim 0.02–0.05$ . Overtone bands and combination bands are not seen very often in IETS.<sup>68</sup> The IETS instrumentation uses second harmonic detection (see bottom of Figure 26).

Reed and co-workers detected IETS for alkanethiols bonded to Au in a nanopore (Figure 27).<sup>50,319,320</sup> The spectra were later computed theoretically using density functional theory and the Landauer formalism.<sup>569,570</sup>

Most initial IETS work concentrated to biases below 0.5 V. By extending the range to 2 V, Kerry W. Kipps and co-worker found



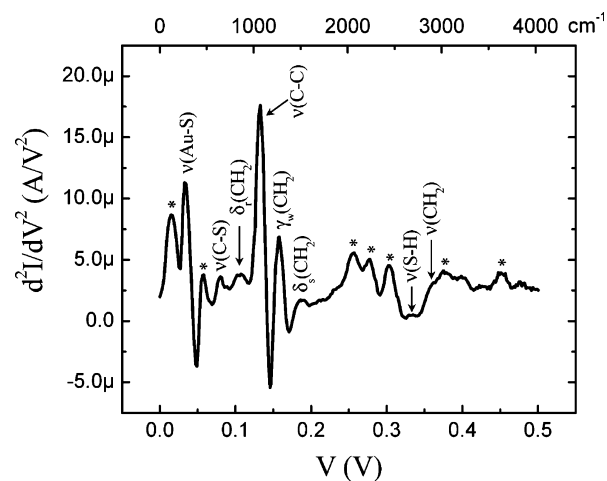
**Figure 25.** Schematic energy diagram for elastic and inelastic processes (the molecular HOMO is excited from  $\nu = 0$  to  $\nu = 1$  by borrowing the vibrational energy  $h\nu$  from the tunneling electron).



Second harmonic detection:

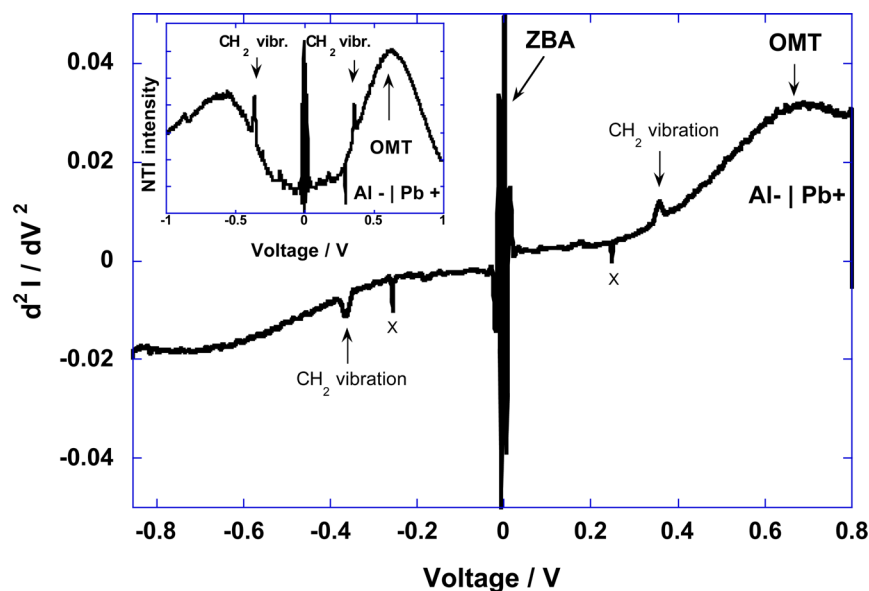
$$I(V) = I(V_{DC} + V_{AC} \cos(\omega t + \theta)) = \{\text{Taylor series}\} = \\ = I(V_{DC}) + [dI(V_{DC})/dV] V_{AC} [\cos(\omega t + \theta)] + \\ + (1/8) [d^2I(V_{DC})/dV^2] V_{AC}^2 [1 + \cos(2\omega t + \theta)]$$

**Figure 26.** IETS circuit and second harmonic detection, reproduced with permission from ref 568. Copyright 2006 Andrei Honciuc.

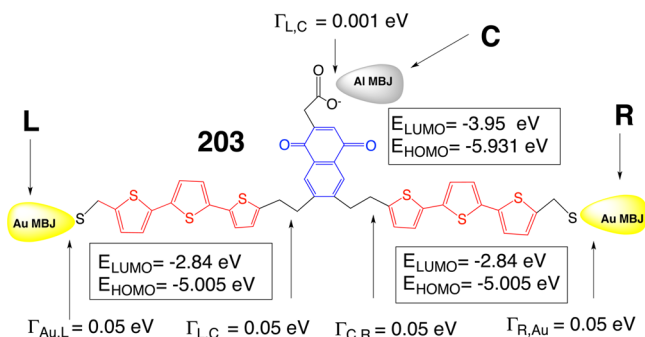


**Figure 27.** IET spectrum of SAM of 1,8-octanedithiol **19d** in a nanopore measured at 4.2 K at  $2\omega$  using an AC modulation  $\omega = 503$  Hz. The peaks marked \* are probably due to  $\text{Si}_3\text{N}_4$ . Reproduced by permission from ref 319. Copyright 2004 American Chemical Society.

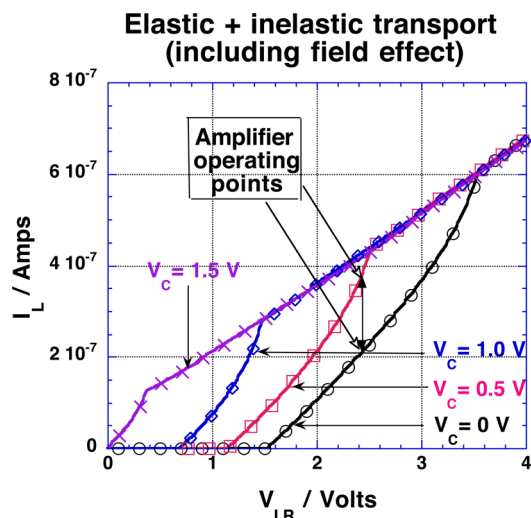
that resonance with an available electronic energy level leads to elastic orbital-mediated tunneling (OMT), which is typically detected in a  $dI/dV$  plot.<sup>68,153,571,572</sup> Metzger and co-worker detected such OMT in an LB monolayer of **177** at 4.2 K at the same potential as the onset of rectification;<sup>459</sup> this strongly suggests that the elastic signal has gone through the molecule, in resonance with a molecular energy level, i.e., this was most likely the long-sought proof of through-bond tunneling rather than through-space tunneling<sup>514</sup> in the monolayer of **177** at 4.2 K (Figure 28).<sup>459</sup> The peaks in Figure 28 clustered around  $V = 0$  are vibrational peaks of the oxides in the electrodes; the “X” peaks are



**Figure 28.** IETS + OMT peaks for an LB monolayer of 177 measured between Pb and Al electrodes at 4.2 K. Reprinted by permission from ref 459. Copyright 2007 American Chemical Society.



**Figure 29.** Proposed unimolecular amplifier 203, from ref 597.



**Figure 30.** Computed  $IV$  curves for proposed unimolecular amplifier 203 show displaced  $IV$  curves as a function of the voltage  $V_C$  on the center Al electrode C; the computed power gain is 3.08. Reprinted by permission from ref 597. Copyright 2013 Royal Society of Chemistry.

one-bin artifacts, and the prominent molecular IETS peak is the  $\text{CH}_2$  vibration (with opposite phases at positive and negative

bias). The broad feature marked OMT (very small at negative bias) occurs at the same bias as the measured enhanced rectification current measured separately.<sup>459</sup>

Wilson Ho has combined IETS with STM.<sup>440,448,573–580</sup> The work started with IET spectra plus the STM visualization of  $\text{C}_2\text{H}_2$  and  $\text{C}_2\text{D}_2$  adsorbed at 8 K on  $\text{Cu}(100)$ <sup>440</sup> and on  $\text{Cu}(001)$ ,<sup>575</sup> then  $\text{CO}$ ,  $\text{C}_6\text{H}_6$ , and pyrrolidine,<sup>576</sup> and motions and even chemical reactions on the  $\text{Cu}(001)$  or  $\text{Pt}(111)$  surfaces at 8 K.<sup>576</sup> A reaction of  $\text{H}_2\text{S}$  with  $\text{C}_2$  on  $\text{Cu}(001)$  produces CCH and SH radicals, confirmed by IETS.<sup>575</sup> When individual Cu phthalocyanine ( $\text{CuPc}$ ) and magnesium porphyrin are deposited (pancake-down) atop a thin  $\text{Al}_2\text{O}_3$  film grown carefully on a NiAl surface, then interesting IET spectra and STM images are seen at 15 K. They involve different vibrational transitions, accessed at different biases, for the neutral molecule and for its excited monocation.<sup>577,581</sup> The metal-to-molecule in-plane interaction between short chains of 2–3 Au atoms moved by the STM tip onto two sides of a single  $\text{CuPc}$  molecule pancake-down on NiAl(110) allows for exploring the differential conductances within  $\text{CuPc}$  as a function of added Au atoms.<sup>579</sup> Carefully growing a 0.5-nm-thick  $\text{Al}_2\text{O}_3$  layer atop a NiAl(110) surface decoupled a  $\text{CuPc}$  molecule placed atop the  $\text{Al}_2\text{O}_3$  from the surface plasmons of NiAl; thus, the electroluminescence (without vibronic features, from the monocation) of Zn(II) etioporphyrin as a function of applied bias could be measured at 13 K, for a bias between 0.5 and 1 V between an Ag nanotip and the NiAl subsurface. The emission range was between 600 and 880 nm (1.40–2.0 V) but was possible for only two out of six STM-resolved conformations of the molecule.<sup>448</sup> For naphthalocyanine on 0.5-nm-thick  $\text{Al}_2\text{O}_3$  on NiAl(110) at 11 K, submolecular vibrational spectra could be measured by STM.<sup>578</sup> For Mg porphyrin adsorbed on 0.5-nm-thick  $\text{Al}_2\text{O}_3$  on NiAl(110) at 10 K, differential conductance and the light emission with vibration substructure (0.046 eV) were measured, with a quantum yield below 0.0014 photons per electron.<sup>580</sup>

For a potentially practical reason the issue of electroluminescence and fluorescence from single molecules is of great interest. At present, Si devices can only decay from an

excited state by phonon emission (this can cause melting of Si devices at the 10–15 nm design rule limit), while molecules can also decay by photon emission. Catastrophic heating could be avoided if the fluorescence and electroluminescence of molecules could become a large component of their relaxation from an excited state. This can be measured by the quantum efficiency  $QE = (\text{photons out}/\text{electrons in})$ . The results thus far are not very encouraging. Placing molecules onto bulk metal surfaces quenches their fluorescence because of surface plasmons in the metal, but if the metal is a very sharp tip (as in STM), then fluorescence is not quenched but greatly enhanced. Carefully collected light emission (but not quantified) during an STM scan was used as a photon map of the substrate surface.<sup>582</sup> For an  $\text{Al}_2\text{O}_3$  film IETS was accompanied by light emission ( $QE \approx 10^{-5}$ ).<sup>583</sup> For  $\text{C}_{60}$ , enhanced photoemission due to tip-induced plasmons in STM was reported.<sup>584</sup> For Cu-tetra-[3,5-di-*tert*-butylphenyl]porphyrin sublimed onto a Cu(110) surface (submonolayer coverage) and probed by an ITO-coated optically transparent STM tip,  $QE \approx 3 \times 10^{-6}$  was reported.<sup>585</sup> For *meso*-tetrakis(3,5-di-*tert*-butylphenyl)porphyrin molecules placed on Au(100) and interrogated by a W nanotip, light emission  $QE \approx 10^{-5}$  was found.<sup>586</sup> For *meso*-tetrakis-(3,5-di-*tert*-butylphenyl)porphyrin on Ag using a Pt/Ir nanotip, a larger STM-excited luminescence with  $QE \approx 10^{-5}$  was obtained.<sup>587</sup>

### 30. UNIMOLECULAR AMPLIFIER

Despite their elegant name, the single-electron transistor,<sup>87</sup> the single-atom transistor,<sup>86</sup> and the single-molecule transistor<sup>588</sup> are not transistors with power gain; they are CB devices. Therefore, we must seriously consider three-terminal devices with power gain. Can we do it with electrical contacts to a single molecule? Bringing 3 or 4 nanoelectrodes to within a molecular length (2 nm) remains a worthwhile experimental challenge.<sup>589</sup> Theoreticians have long discussed three-terminal devices.<sup>590–596</sup> Some proposals suggested the molecular equivalent of a bipolar junction transistor or a vacuum-tube triode.<sup>48,51</sup>

A theoretical model for how a single molecule (e.g., **203**) can have power gain as a unimolecular amplifier has been published.<sup>597</sup> It is not an FET but rather the molecular analogue of a bipolar junction transistor or a vacuum-tube triode: the Al control electrode C covalently bonded to a molecule controls the electron flow from the Au electrode L to the Au electrode R (Figure 29). The calculated *IV* curve (Figure 30) shows power gain.<sup>597</sup>

### 31. DNA CONDUCTIVITY, COMPLEMENTARITY, AND ORIGAMI

A claim by Jacqueline K. Barton<sup>598</sup> that DNA should be a highly conducting compound (low-band gap semiconductor or even metal, a double helix  $\pi$ -way) elicited huge interest but disagreed with the proven principles for organic metals and superconductors;<sup>3</sup> the ionization potentials and electron affinities of the 4 DNA bases (adenine, guanine, cytosine, and thymine; see Figure 14) definitely rule out a high-conductivity  $\pi$ -way. DNA is a sodium salt whose ionic semiconductivity masks any  $\pi$ -way effects. Alas, one experiment even claimed that DNA was a superconductor!<sup>599</sup> More orthodox studies of oligonucleotides of various degrees of folding and complexity<sup>600</sup> have become a vital area, which is not, however, germane to this review.

A molecular wire study of double-stranded and end-thiolated DNA oligomers **146** and **147** by SBJ techniques showed that these molecular wires were semiconductors;<sup>434</sup> a possible

interference by sodium ion conductance was ruled out.<sup>434</sup> The conductance is dominated by holes, probably by a mechanism between superexchange and incoherent hopping.<sup>601</sup>

The AT-GC complementarity has been used to detect dramatic changes in fluorescence. When a fluorophore-tagged single strand meets with its complementary single strand, then fluorescence quenching occurs; this can be detected at the single-molecule level.<sup>602</sup> A second scientific area,<sup>603,604</sup> using base-pair complementarity, is DNA origami:<sup>605</sup> short single strands can couple with their complement, thus enabling the synthesis of topologically creative structures (e.g., Holliday junctions<sup>606</sup> and Borromean loops<sup>607</sup>), which can be characterized, mainly by AFM.

### 32. CONCLUSION

UME has benefitted greatly from the worldwide interest in nanoscience and nanotechnology, as well as from generous funding from governmental agencies worldwide. However, it has been neglected by industry or commerce as not yet mature: what the military industry in the United States calls a killer application has not yet emerged. Is UME a child, a grown-up, or still a teenager? We have learned a lot already; there is still wonderful science to be done.

### AUTHOR INFORMATION

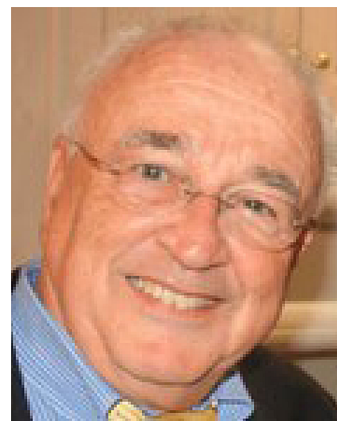
#### Corresponding Author

\*Tel.: 1-205-348-5952. Fax: 1-205-348-9104. E-mail: rmetzger@ua.edu.

#### Notes

The authors declare no competing financial interest.

#### Biography



Robert Melville Metzger was born in Yokohama, Japan, of Hungarian diplomat parents in 1940, moved to Paris, France, in 1946, to Merano, Italy, in 1947, and then to Los Angeles, CA, in 1959. He speaks, reads, and writes in five languages. After earning degrees in chemistry at UCLA (B.S., 1962, research with Willard F. Libby) and Caltech (Ph.D., 1968, research with Harden M. McConnell) and postdocs at Stanford (with Paul G. Simpson and Michel Boudart), he taught Italian at Stanford (1970–71) and chemistry at the Universities of Mississippi (1971–86) and Alabama (1986–present). He was Coulter Professor at Mississippi and is Professor of Chemistry and Materials Science at Alabama. He has published 222 papers and 1 patent and edited 3 books, 4 symposium proceedings volumes, and 1 graduate-level textbook (*A Physical Chemist's Toolbox*, Wiley, 2012). He graduated 14 Ph.D.'s and 1 M.S., directed the research of 15 undergraduates, and gave talks or was on foreign sabbaticals in 30 countries. He studied the Madelung energies

for organic donor–acceptor crystals (but could not stabilize the partially ionic ground state of organic metals). By combustion calorimetry he determined that TTF TCNQ is thermodynamically stable and built a semimicro rotating-bomb combustion calorimeter for organic compounds. He solved crystal structures (including P-3CNQ), studied triplet excitons in TCNQ salts with Heimo J. Keller and the conditions for conductivity in inorganic transition metal oxides with Jerry B. Torrance, and worked briefly on cuprate superconductors. With William D. Doyle he worked on  $\alpha'$ -Fe<sub>16</sub>N<sub>2</sub> and on magnetic nanowires in hexagonally ordered anodized alumina nanopores. With Michael P. Cava and M. V. Lakshikantham he worked on new organic donors and semiconductors. Metzger spent the last 25 years on organic rectifiers.

## ACKNOWLEDGMENTS

This work was supported in part by the United States National Science Foundation (Grant 08-48206) and by the Deutsche Forschungsgemeinschaft (Mercator Professorship 2011–2012 at the Dresden University of Technology). Many discussions and hard work over the last three decades by co-workers and collaborators past and present (and deceased) are acknowledged with deep gratitude and fond remembrance: Profs. Geoffrey J. Ashwell, Michael Patrick Cava (1926–2010), Gianaurelio Cuniberti, Norman E. Heimer, Andrei Honciuc, Tsuyoshi Kawai, Daniell L. Mattern, Charles Anthony Panetta (1932–2012), Ian Robert Peterson (1945–2005), Mark A. Ratner, Mark A. Reed, Gunzi Saito, John Roy Sambles, Walter J. Shumate, Charles W. Spangler, Dominique Vuillaume, Tao Xu, and Herre S. J. van der Zant; Drs. Ari Aviram, Jeffrey W. Baldwin, Bo Chen, Archana Jaiswal, M. V. Lakshikantham (1931–2006), Daijiro Nozaki, Akihiko Otsuka, Dmitry Ryndyk, Hiromi Sakurai, Hiroaki Tachibana, Cormac Toher, and Xiang-Li Wu; and my current students, Marcus S. Johnson and Chad L. Horton.

## REFERENCES

- (1) Metzger, R. M. Prospects for Truly Unimolecular Devices. *NATO ASI Ser.* **1991**, B248, 659–666.
- (2) Tour, J. M.; Kozaki, M.; Seminario, J. M. Molecular Scale Electronics: A Synthetic/Computational Approach to Digital Computing. *J. Am. Chem. Soc.* **1998**, *120*, 8486–8493.
- (3) Metzger, R. M. Semiconductors to Superconductors: Organic Lower-Dimensional Systems. *Encycl. Appl. Phys.* **1996**, *17*, 215–239.
- (4) Shirakawa, H.; Louis, E. J.; MacDiarmid, A. G.; Chiang, C. K.; Heeger, A. J. Synthesis of Electrically Conducting Organic Polymers: Halogen Derivatives of Polyacetylene, (CH)<sub>x</sub>. *J. Chem. Soc., Chem. Commun.* **1977**, 578–580.
- (5) Bäessler, H.; Köhler, A. Charge Transport in Organic Semiconductors. *Springer Top. Curr. Chem.* **2012**, *312*, 1–66.
- (6) Tang, C. W.; VanSlyke, S. A. Organic Electroluminescent Diodes. *Appl. Phys. Lett.* **1987**, *51*, 913–915.
- (7) Burroughes, J. H.; Bradley, D. D. C.; Brown, A. R.; Marks, R. N.; MacKay, K.; Friend, R. H.; Burns, P. L.; Holmes, A. B. Light-Emitting Diodes Based on Conjugated Polymers. *Nature* **1990**, *347*, 539–541.
- (8) Kamtekar, K. T.; Monkman, A. P.; Bryce, M. R. Recent Advances in White Organic Light-Emitting Materials and Devices (WOLEDs). *Adv. Mater.* **2010**, *22*, 572–582.
- (9) Schlenker, C. W.; Thompson, M. E. Current Challenges in Organic Photovoltaic Solar Energy Conversion. *Springer Top. Curr. Chem.* **2012**, *312*, 175–212.
- (10) Metzger, R. M. Unimolecular Electrical Rectifiers. *Chem. Rev.* **2003**, *103*, 3803–3834.
- (11) Metzger, R. M.; Mattern, D. L. Unimolecular Electronic Devices. *Springer Top. Curr. Chem.* **2012**, *313*, 39–84.
- (12) Feynman, R. P. There Is Plenty of Room at the Bottom. *Caltech Eng. Sci.* **1960**, *23* (5), 22–36. Also in *Miniaturization*; Gilbert, H. D., Ed.; Reinhold: New York, 1961; p 282.
- (13) Aviram, A.; Ratner, M. A. Molecular Rectifiers. *Chem. Phys. Lett.* **1974**, *29*, 277–283.
- (14) Carter, F. L., Ed. *Molecular Electronic Devices*; Dekker: New York, 1982.
- (15) Carter, F. L., Ed. *Molecular Electronic Devices II*; Dekker: New York, 1987.
- (16) Carter, F. L.; Siatkowski, R. E.; Wohltjen, H., Eds. *Molecular Electronic Devices*; Proc. 3rd Intl. Symp.; North-Holland: Amsterdam, 1988.
- (17) Aviram, A., Ed. *Molecular Electronics—Science and Technology*; New York Engineering Foundation: New York, 1989.
- (18) Aviram, A. Molecular Electronics—Science and Technology. *Ann. Inst. Phys. Conf. Proc.* **1992**, 262.
- (19) Aviram, A.; Ratner, M. A. Molecular Electronics—Science and Technology. *Ann. N. Y. Acad. Sci.* **1998**, 852.
- (20) Aviram, A.; Ratner, M.; Mujica, V. Molecular Electronics II. *Ann. N. Y. Acad. Sci.* **2002**, 960.
- (21) Reimers, J. R.; Picconatto, C. A.; Ellenbogen, J. C.; Shashidhar, R. Molecular Electronics III. *Ann. N. Y. Acad. Sci.* **2003**, 1006.
- (22) Taube, H. Electron Transfer between Metal Complexes—A Retrospective View. *Angew. Chem., Int. Ed.* **1984**, *23*, 329–394.
- (23) Libby, W. F. Theory of Electron Exchange Reactions in Aqueous Solution. *J. Phys. Chem.* **1952**, *56*, 863–868.
- (24) Marcus, R. A. On the Theory of Oxidation–Reduction Reactions Involving Electron Transfer. I. *J. Chem. Phys.* **1956**, *24*, 966–978.
- (25) Hush, N. S. Adiabatic Theory of Outer Sphere Electron-Transfer Reactions in Solution. *Trans. Faraday Soc.* **1961**, *57*, 557–580.
- (26) McConnell, H. M. Intramolecular Charge Transfer in Aromatic Free Radicals. *J. Chem. Phys.* **1961**, *35*, 508–515.
- (27) Ratner, M. A.; Jortner, J. Molecular Electronics: Some Directions. In *Molecular Electronics: A Chemistry for the 21st Century*; Jortner, J., Ratner, M., Eds.; Blackwell Science: Oxford, UK, 1997; pp 5–72.
- (28) Blodgett, K. B. Films Built by Depositing Successive Monomolecular Layers on a Solid Surface. *J. Am. Chem. Soc.* **1935**, *57*, 1007–1022.
- (29) Blodgett, K. B.; Langmuir, I. Built-Up Films of Barium Stearate and Optical Properties. *Phys. Rev.* **1937**, *51*, 964–982.
- (30) Bigelow, W. C.; Pickett, D. L.; Zisman, W. A. Oleophobic Monolayers. I. Films Adsorbed from Solution in Nonpolar Liquids. *J. Colloid Sci.* **1946**, *1*, 513–538.
- (31) Sagiv, J. Organized Monolayers by Adsorption. I. Formation and Structure of Oleophobic Mixed Monolayers on Solid Surfaces. *J. Am. Chem. Soc.* **1980**, *102*, 92–98.
- (32) Bain, C. D.; Troughton, E. B.; Tao, Y. T.; Evail, J.; Whitesides, G. M.; Nuzzo, R. G. Formation of Monolayer Films by the Spontaneous Assembly of Organic Thiols from Solution onto Gold. *J. Am. Chem. Soc.* **1989**, *111*, 321–335.
- (33) Moore, G. E. Cramming More Components onto Integrated Circuits. *Electronics* **1965**, *38*, 114–117.
- (34) *International Technology Roadmap for Semiconductors*, 2012 Metrology Road Map.
- (35) Metzger, R. M.; Day, P.; Papavassiliou, G. C., Eds. *Lower-Dimensional Systems and Molecular Electronics*; NATO ASI Series B248; Plenum Press: New York, 1990.
- (36) Ashwell, G. J., Ed. *Molecular Electronics*; Wiley: New York, 1992.
- (37) Tour, J. M. *Molecular Electronics: Commercial Insights, Chemistry, Devices, Architectures, and Programming*; World Scientific: Singapore, 2003).
- (38) Reed, M. A.; Lee, T., Eds. *Molecular Nanoelectronics*; American Scientific Publishers: Stevenson Ranch, CA, 2003.
- (39) Cuniberti, G.; Fagas, G.; Richter, K., Eds. *Introducing Molecular Electronics*; Springer Lecture Notes Physics; Springer: Berlin, 2005; p 680.
- (40) Cuevas, J. C.; Scheer, E. *Molecular Electronics: An Introduction to Theory and Experiment*; World Scientific: Singapore, 2010.
- (41) Lyshevski, S. E., Ed. *Nano and Molecular Electronics Handbook*; CRC Press: Boca Raton, FL, 2007.

- (42) Metzger, R. M., Ed. *Unimolecular and Supramolecular Electronics I and II: Chemistry and Physics Meet at the Metal–Molecule Interface*; Springer Top. Curr. Chem.; Springer: Berlin, 2012; pp 312–313
- (43) Ulman, A. Formation and Structure of Self-Assembled Monolayers. *Chem. Rev.* **1996**, *96*, 1533–1554.
- (44) Reed, M. A.; Zhou, C.; Deshpande, M. R.; Muller, C. J.; Burgin, T. P.; Jones, L.; Tour, J. M. The Electrical Measurement of Molecular Junctions. *Ann. N. Y. Acad. Sci.* **1998**, *852*, 133–144.
- (45) Tour, J. M. Molecular Electronics. Synthesis and Testing of Components. *Acc. Chem. Res.* **2000**, *33*, 791–804.
- (46) Nitzan, A. Electron Transmission Through Molecules and Molecular Interfaces. *Annu. Rev. Phys. Chem.* **2001**, *52*, 681–750.
- (47) Mujica, V.; Ratner, M. A.; Nitzan, A. Molecular Rectification: Why Is It So Rare? *Chem. Phys.* **2002**, *281*, 147–150.
- (48) Metzger, R. M. Unimolecular Rectifiers and Proposed Unimolecular Amplifier. *Ann. N. Y. Acad. Sci.* **2003**, *1006*, 252–276.
- (49) Chen, J.; Lee, T.; Su, J.; Wang, W.; Reed, M. A.; Rawlett, A. M.; Kozaki, M.; Yao, Y.; Jagessar, R. C.; Dirk, S. M.; Price, D. W.; Tour, J. M.; Grubisha, D. S.; Bennett, D. W. Molecular Electronic Devices. In *Molecular Nanoelectronics*; Reed, M. A., Lee, T., Eds.; American Scientific Publishers: Valencia, CA, 2003; Chapter 3, pp 39–114.
- (50) Wang, W.; Lee, T.; Reed, M. A. Elastic and Inelastic Electron Tunneling in Alkane Self-Assembled Monolayers. *J. Phys. Chem. B* **2004**, *108*, 18398–18407.
- (51) Metzger, R. M. Three Unimolecular Rectifiers and a Proposed Unimolecular Amplifier. In *Organic Conductors, Superconductors and Magnets: From Synthesis to Molecular Electronics*; NATO ASI Ser. II; Ouahab, L., Yagubskii, E., Eds.; Kluwer: Dordrecht, The Netherlands, 2004; pp 269–293.
- (52) Jortner, J.; Nitzan, A.; Ratner, M. A. Foundations of Molecular Electronics—Charge Transport in Molecular Conduction Junctions. In *Introducing Molecular Electronics*; Lecture Notes in Physics; Cuniberti, G., Richter, K., Fagas, G., Eds.; Springer: Berlin/Heidelberg, 2005; Vol. 680, pp 13–54.
- (53) Tao, N. J. Electron Transport in Molecular Junctions. *Nat. Nanotechnol.* **2006**, *1*, 173–181.
- (54) Newton, M. D.; Smalley, J. F. Interfacial Bridge-Mediated Electron Transfer: Mechanistic Analysis Based on Electrochemical Kinetics and Theoretical Modelling. *Phys. Chem. Chem. Phys.* **2007**, *9*, 555–572.
- (55) Lindsay, S. M.; Ratner, M. A. Molecular Transport Junctions: Clearing Mists. *Adv. Mater.* **2007**, *19*, 23–31.
- (56) Metzger, R. M. Unimolecular Electronics: Results and Prospects. In *Nano and Molecular Electronics Handbook*; Lyshevski, S. E., Ed.; CRC Press, Taylor and Francis Group: Boca Raton, FL, 2007; pp 3-1–3-25.
- (57) Bumm, L. A. Measuring Molecular Junctions: What is the Standard? *ACS Nano* **2008**, *2*, 403–408.
- (58) Metzger, R. M. Unimolecular Electronics. *J. Mater. Chem.* **2008**, *18*, 4364–4396.
- (59) Woodruff, D. P. The Interface Structure of *n*-Alkylthiolate Self-Assembled Monolayers on Coinage Metal Surfaces. *Phys. Chem. Chem. Phys.* **2008**, *10*, 7211–7221.
- (60) Han, B.; Li, Z.; Li, C.; Pobelov, I.; Su, G.; Aguilar-Sanchez, R.; Wandlowski, T. From Self-Assembly to Charge Transport with Single Molecules—An Electrochemical Approach. In *Templates in Chemistry III*; Springer Top. Curr. Chem.; Broekmann, P., Dötz, K.-H., Schalley, C., Eds.; Springer: Berlin/Heidelberg, 2009; Vol. 287, pp 181–255.
- (61) Chen, F.; Tao, N. J. Electron Transport in Single Molecules: From Benzene to Graphene. *Acc. Chem. Res.* **2009**, *42*, 429–438.
- (62) Nichols, R. J.; Haiss, W.; Higgins, S. J.; Leary, E.; Martin, S.; Bethell, D. The Experimental Determination of the Conductance of Single Molecules. *Phys. Chem. Chem. Phys.* **2010**, *12*, 2801–2815.
- (63) Karthäuser, S. Control of Molecule-Based Transport for Future Molecular Devices. *J. Phys.: Condens. Matter* **2011**, *23*, 013001.
- (64) Shamai, T.; Seltzer, Y. Spectroscopy of Molecular Junctions. *Chem. Soc. Rev.* **2011**, *40*, 2293–2305.
- (65) Srisombat, L.; Jamison, A. C.; Lee, T. R. Stability: A Key Issue for Self-Assembled Monolayers on Gold as Thin-Film Coatings and Nanoparticle Protectant. *Colloids Surf., A* **2011**, *390*, 1–19.
- (66) Solomon, G.; Herrmann, C.; Ratner, M. A. Molecular Electronic Junctions Transport: Some Pathways and Some Ideas. *Springer Top. Curr. Chem.* **2012**, *313*, 1–38.
- (67) Li, C.; Mishchenko, A.; Wandlowski, T. Charge Transport in Single Molecular Junctions at the Solid/Liquid Interface. *Springer Top. Curr. Chem.* **2012**, *313*, 121–188.
- (68) Higgs, K. W. Tunneling Spectroscopy of Organic Monolayers and Single Molecules. *Springer Top. Curr. Chem.* **2012**, *313*, 189–216.
- (69) Renaud, N.; Hliwa, M.; Joachim, C. Single Molecule Logical Devices. *Springer Top. Curr. Chem.* **2012**, *313*, 217–268.
- (70) Tsutsui, M.; Taniguchi, T. Single Molecule Electronics and Devices. *Sensors* **2012**, *12*, 7259–7298.
- (71) Lörtscher, E. Wiring Molecules into Circuits. *Nat. Nanotechnol.* **2013**, *8*, 381–384.
- (72) Ratner, M. A. Brief History of Molecular Electronics. *Nat. Nanotechnol.* **2013**, *8*, 378–381.
- (73) McCreery, R. L.; Yan, H.; Bergren, A. J. A Critical Perspective on Molecular Electronic Junctions: There Is Plenty of Room in the Middle. *Phys. Chem. Chem. Phys.* **2013**, *15*, 1065–1081.
- (74) Mirjani, F.; Thijssen, J. M.; Whitesides, G. M.; Ratner, M. Charge Transport across Insulating Self-Assembled Monolayers: Non-Equilibrium Approaches and Modeling to Relate Current and Molecular Structure. *ACS Nano* **2014**, *8*, 12428–12436.
- (75) Chen, S.; Zhao, Z.; Liu, H. Charge Transport at the Metal–Organic Interface. *Annu. Rev. Phys. Chem.* **2013**, *64*, 221–245.
- (76) Yan, H.; Bergren, A. J.; McCreery, R.; Della Rocca, M. L.; Martin, P.; Lafarge, P.; Lacroix, J. C. Activationless Charge Transport across 4.5 to 22 nm in Molecular Electronic Junctions. *Proc. Natl. Acad. Sci. U. S. A.* **2013**, *110*, 5326–5330.
- (77) Jia, C.; Guo, X. Molecule–Electrode Interfaces in Molecular Electronic Devices. *Chem. Soc. Rev.* **2013**, *42*, 5642–5660.
- (78) Aradhya, S. V.; Venkataraman, L. Single-Molecule Junctions Beyond Electronic Transport. *Nat. Nanotechnol.* **2013**, *8*, 399–410.
- (79) Kaliginedi, V.; Rudnev, A. V.; Moreno-García, P.; Baghernejad, M.; Huang, C.; Hong, W.; Wandlowski, T. Promising Anchoring Groups for Single-Molecule Conductance Measurements. *Phys. Chem. Chem. Phys.* **2014**, *16*, 23529–23539.
- (80) van der Molen, S. J.; Naaman, R.; Scheer, E.; Neaton, J. B.; Nitzan, A.; Natelson, D.; Tao, N. J.; van der Zant, H.; Major, M.; Ruben, M.; Reed, M.; Calame, M. Visions for a Molecular Future. *Nat. Nanotechnol.* **2013**, *8*, 385–389.
- (81) Bumm, L. A.; Arnold, J. J.; Cygan, M. T.; Dunbar, T. D.; Burgin, T. P.; Jones, L.; Allara, D. L.; Tour, J. M.; Weiss, P. S. Are Single Molecular Wires Conducting? *Science* **1996**, *271*, 1705–1707.
- (82) Moore, A. M.; Mantooth, B. A.; Donhauser, Z. J.; Yao, Y.; Tour, J. M.; Weiss, P. S. Real Time Measurements of Conductance Switching and Motion of Single Oligo(phenylene ethynylene) Molecules. *J. Am. Chem. Soc.* **2007**, *129*, 10352–10353.
- (83) Moreland, J.; Ekin, J. W. Electron Tunneling Experiments Using Nb–Sn “Break” Junctions. *J. Appl. Phys.* **1985**, *58*, 3888–3895.
- (84) Krans, J. M.; van Ruitenbeek, J. M.; de Jongh, L. J. Atomic Structure and Quantized Conductance in Metal Point Contacts. *Physica* **1996**, *B218*, 228–233.
- (85) Reed, M. A.; Zhou, C.; Muller, C. J.; Burgin, T. P.; Tour, J. M. Conductance of a Molecular Junction. *Science* **1997**, *278*, 252–254.
- (86) Park, J.; Pasupathy, A. N.; Goldsmith, J. I.; Chang, C.; Yaish, Y.; Petta, J. R.; Rinkoski, M.; Sethna, J. P.; Abruña, H. D.; McEuen, P. L.; Ralph, D. C. Coulomb Blockade and the Kondo Effect in Single Atom Transistors. *Nature* **2002**, *417*, 722–725.
- (87) Averin, D. V.; Likharev, K. K. Coulomb Blockade of Single-Electron Tunneling and Coherent Oscillations in Small Tunnel Junctions. *J. Low-Temp. Phys.* **1986**, *62*, 345–373.
- (88) Page 424 in ref 40.
- (89) Xu, B.; Tao, N. J. Measurement of Single-Molecule Resistance by Repeated Formation of Molecular Junctions. *Science* **2003**, *301*, 1221–1223.
- (90) Tans, S. J.; Devoret, M. H.; Dai, H.; Thess, A.; Smalley, R. E.; Geerligs, L. J.; Dekker, C. Individual Single-Wall Carbon Nanotubes as Quantum Wires. *Nature* **1997**, *386*, 474–477.

- (91) Paloheimo, J.; Kuivalainen, P.; Stubb, H.; Vuorimaa, E.; Yli-Lahti, P. Molecular Field-Effect Transistors Using Conducting Polymer Langmuir–Blodgett Films. *Appl. Phys. Lett.* **1990**, *56*, 1157–1159.
- (92) Garnier, F.; Horowitz, G.; Peng, X.; Fichou, D. An All-Organic “Soft” Thin Film Transistor with Very High Carrier Mobility. *Adv. Mater.* **1990**, *2*, 592–594.
- (93) Jones, E. T. T.; Chyan, O. M.; Wrighton, M. S. Preparation and Characterization of Molecule-Based Transistors with a 50-nm Source-Drain Separation with Use of Shadow Deposition Techniques: Toward Faster, More Sensitive Molecule-Based Devices. *J. Am. Chem. Soc.* **1987**, *109*, 5526–5528.
- (94) Collier, C. P.; Mattersteig, G.; Wong, E. W.; Beverly, K.; Sampaio, J.; Raymo, F. M.; Stoddart, J. F.; Heath, J. R. A [2]Catenane Based Solid-State Electronically Reconfigurable Switch. *Science* **2000**, *289*, 1172–1175.
- (95) Green, J. E.; Choi, J. W.; Boukai, A.; Bunimovich, Y.; Johnston-Halperin, E.; DeIonno, E.; Luo, Y.; Sheriff, B. A.; Xu, K.; Shin, Y. S.; Tseng, H.-R.; Stoddart, J. F.; Heath, J. R. A 160-Kilobit Molecular Electronic Memory Patterned at  $10^{11}$  Bits Per Square Centimetre. *Nature* **2007**, *445*, 414–417.
- (96) Chen, J.; Reed, M. A.; Rawlett, A. M.; Tour, J. M. Large On-Off Ratios and Negative Differential Resistance in a Molecular Electronic Device. *Science* **1999**, *286*, 1550–1552.
- (97) Esaki, L. New Phenomenon in Narrow Germanium p-n Junctions. *Phys. Rev.* **1958**, *109*, 603–604.
- (98) Esaki, L. Long Journey into Tunneling. *Rev. Mod. Phys.* **1974**, *46*, 237–244.
- (99) Ashwell, G. J.; Sambles, J. R.; Martin, A. S.; Parker, W. G.; Szablewski, M. Rectifying Characteristics of MgI(C<sub>16</sub>H<sub>33</sub>–Q3CNQ LB Film)/Pt Structures. *J. Chem. Soc., Chem. Commun.* **1990**, 1374–1376.
- (100) Martin, A. S.; Sambles, J. R.; Ashwell, G. J. Molecular Rectifier. *Phys. Rev. Lett.* **1993**, *70*, 218–221.
- (101) Metzger, R. M.; Chen, B.; Höpfner, U.; Lakshmikantham, M. V.; Vuillaume, D.; Kawai, T.; Wu, X.; Tachibana, H.; Hughes, T. V.; Sakurai, H.; Baldwin, J. W.; Hosch, C.; Cava, M. P.; Brehmer, L.; Ashwell, G. J. Unimolecular Electrical Rectification in Hexadecylquinolinium Tricyanoquinodimethanide. *J. Am. Chem. Soc.* **1997**, *119*, 10455–10466.
- (102) Vuillaume, D.; Chen, B.; Metzger, R. M. Electron Transfer through a Monolayer of Hexadecylquinolinium Tricyanoquinodimethanide. *Langmuir* **1999**, *15*, 4011–4017.
- (103) Chen, B.; Metzger, R. M. Rectification between 370 and 105 K in Hexadecylquinolinium Tricyanoquinodimethanide. *J. Phys. Chem. B* **1999**, *103*, 4447–4451.
- (104) Xu, T.; Peterson, I. R.; Lakshmikantham, M. V.; Metzger, R. M. Rectification by a Monolayer of Hexadecylquinolinium Tricyanoquinodimethanide between Gold Electrodes. *Angew. Chem., Int. Ed.* **2001**, *40*, 1749–1752.
- (105) Metzger, R. M.; Xu, T.; Peterson, I. R. Electrical Rectification by a Monolayer of Hexadecylquinolinium Tricyanoquinodimethanide Measured between Macroscopic Gold Electrodes. *J. Phys. Chem. B* **2001**, *105*, 7280–7290.
- (106) Novoselov, K. S.; Geim, A. K.; Morozov, S. V.; Jiang, D.; Zhang, Y.; Dubonos, S. V.; Grigorieva, I. V.; Firsov, A. A. Electric Field Effect in Atomically Thin Carbon Films. *Science* **2004**, *306*, 666–669.
- (107) Hegner, M.; Wagner, P.; Semenza, G. Ultralarge Atomically Flat Template-Stripped Au Surfaces for Scanning Probe Microscopy. *Surf. Sci.* **1993**, *291*, 39–46.
- (108) Wagner, P.; Hegner, M.; Güntherodt, H.-J.; Semenza, G. Formation and *In Situ* Modification of Monolayers Chemisorbed on Ultraflat Template-Stripped Gold Surfaces. *Langmuir* **1995**, *11*, 3867–3875.
- (109) Metzger, R. M.; Baldwin, J. W.; Shumate, W. J.; Peterson, I. R.; Mani, P.; Mankey, G. J.; Morris, T.; Szulczewski, G.; Bosi, S.; Prato, M.; Comito, A.; Rubin, Y. Large Current Asymmetries and Potential Device Properties of a Langmuir–Blodgett Monolayer of Dimethylanilinoazafullerene Sandwiched between Gold Electrodes. *J. Phys. Chem. B* **2003**, *107*, 1021–1027.
- (110) Stewart, D. R.; Ohlberg, D. A. A.; Beck, P. A.; Chen, Y.; Williams, R. S.; Jeppesen, J. O.; Nielsen, K. A.; Stoddart, J. F. Molecule-Independent Electrical Switching in Pt/Organic Monolayer/Ti Devices. *Nano Lett.* **2004**, *4*, 133–136.
- (111) Haick, H.; Ghabboun, J.; Cahen, D. Pd versus Au as Evaporated Metal Contacts to Molecules. *Appl. Phys. Lett.* **2005**, *86*, 042113.
- (112) Prins, F.; Hayashi, T.; de Vos van Steenwijk, B. J. A.; Gao, B.; Osorio, E. A.; Muraki, K.; van der Zant, H. S. J. Room-Temperature Stability of Pt Nanogaps Formed by Self-Breaking. *Appl. Phys. Lett.* **2009**, *94*, 123108.
- (113) Prins, F.; Shaikh, A. J.; van Esch, J. H.; Eelkema, R.; van der Zant, H. S. J. Platinum-Nanogaps for Single-Molecule Electronics: Room-Temperature Stability. *Phys. Chem. Chem. Phys.* **2011**, *13*, 14297–14301.
- (114) Ko, C.-K.; Huang, M.-J.; Fu, M.-D.; Chen, C.-H. Superior Contact for Single-Molecule Conductance: Electronic Coupling of Thiolate and Isothiocyanate on Pt, Pd, and Au. *J. Am. Chem. Soc.* **2010**, *132*, 756–764.
- (115) Walker, A. V.; Tighe, T. B.; Cabarcos, O. M.; Reinard, M. D.; Haynie, B. C.; Uppili, S.; Winograd, N.; Allara, D. L. The Dynamics of Noble Metal Atom Penetration through Methoxy-Terminated Alkanethiolate Monolayers. *J. Am. Chem. Soc.* **2004**, *126*, 3954–3963.
- (116) Geddes, N. J.; Sambles, J. R.; Jarvis, D. J.; Parker, W. G.; Sandman, D. J. Fabrication and Investigation of Asymmetric Current–Voltage Characteristics of a Metal/Langmuir–Blodgett Monolayer/Metal Structure. *Appl. Phys. Lett.* **1990**, *56*, 1916–1918.
- (117) Geddes, N. J.; Sambles, J. R.; Jarvis, D. J.; Parker, W. G.; Sandman, D. J. The Electrical Properties of Metal-Sandwiched Langmuir–Blodgett Multilayers and Monolayers of a Redox-Active Organic Molecular Compound. *J. Appl. Phys.* **1992**, *71*, 756–768.
- (118) Okazaki, N.; Sambles, J. R. A New Fabrication Technique and Current–Voltage Properties of a Au/LB/Au Structure. In *Extended Abstracts of the International Symposium on Organic Molecular Electronics*, Nagoya, Japan, 2000; pp 66–67.
- (119) Okazaki, N.; Sambles, J. R.; Jory, M. J.; Ashwell, G. J. Molecular Rectification at 8 K in an Au/C<sub>16</sub>H<sub>33</sub>Q–3CNQ LB film/Au Structure. *Appl. Phys. Lett.* **2002**, *81*, 2300–2302.
- (120) Holmlin, R. E.; Haag, R.; Chabynyc, M. L.; Ismagilov, R. F.; Cohen, A. E.; Rampi, M. A.; Whitesides, G. M. Electron Transport through Thin Organic Films in Metal–Insulator–Metal Junctions Based on Self-Assembled Monolayers. *J. Am. Chem. Soc.* **2001**, *123*, 5075–5085.
- (121) Sayed, S. Y.; Fereiro, J. A.; Yan, H.; McCreery, R. L.; Bergren, A. J. Charge Transport in Molecular Electronic Junctions: Compression of the Molecular Tunnel Barrier in the Strong-Coupling Regime. *Proc. Natl. Acad. Sci. U.S.A.* **2012**, *109*, 11498–11503.
- (122) Nijhuis, C. A.; Reus, W. F.; Whitesides, G. M. Molecular Rectification in Metal–SAM–Metal Oxide–Metal Junctions. *J. Am. Chem. Soc.* **2009**, *131*, 17814–17827.
- (123) Nijhuis, C.; Reus, W. F.; Barber, J. R.; Dickey, M. D.; Whitesides, G. M. Charge Transport and Rectification in Arrays of SAM-Based Tunneling Junctions. *Nano Lett.* **2010**, *10*, 3611–3619.
- (124) Nijhuis, C.; Reus, W. F.; Siegel, A. C.; Whitesides, G. M. A Molecular Half-Wave Rectifier. *J. Am. Chem. Soc.* **2011**, *133*, 15397–15411.
- (125) Reus, W. F.; Thuo, M. M.; Shapiro, N. D.; Nijhuis, C. A.; Whitesides, G. M. The SAM, Not the Electrodes, Dominates Charge Transport in Metal–Monolayer//Ga<sub>2</sub>O<sub>3</sub>/Gallium–Indium Eutectic Junctions. *ACS Nano* **2012**, *6*, 4806–4822.
- (126) Weis, O. Direct Contact Superpolishing of Sapphire. *Appl. Opt.* **1992**, *31*, 4355–4362.
- (127) Cahen, D.; Kahn, A. Electron Energetics at Surfaces and Interfaces: Concepts and Experiments. *Adv. Mater.* **2004**, *15*, 271–277.
- (128) Mott, N. F. Note on the Contact between a Metal and an Insulator or Semiconductor. *Math. Proc. Cambridge Phil. Soc.* **1938**, *34*, 568–572.
- (129) Schottky, W. Halbleitertheorie der Sperrschicht. *Naturwissenschaften* **1938**, *26*, 843–843.
- (130) Schottky, W. Zur Halbleitertheorie der Sperrschicht- und Spitzengleichrichter. *Z. Phys.* **1939**, *113*, 367–414.
- (131) Tung, R. T. Recent Advances in Schottky Barrier Concepts. *Mater. Sci. Eng.* **2001**, *R35*, 1–138.



- (132) Langmuir, I. The Effect of Space Charge and Initial Velocities on the Potential Distribution and Thermionic Current between Parallel Plane Electrodes. *Phys. Rev.* **1923**, *21*, 419–435.
- (133) Ishii, H.; Sugiyama, K.; Ito, E.; Seki, K. Energy Level Alignment and Interfacial Electronic Structures at Organic/Metal and Organic/Organic Interfaces. *Adv. Mater.* **1999**, *11*, 605–624.
- (134) Topham, B. J.; Kumar, M.; Soos, Z. G. Profiles of Work Function Shifts and Collective Charge Transfer in Submonolayer Metal–Organic Films. *Adv. Funct. Mater.* **2011**, *21*, 1931–1940.
- (135) Perrin, M. L.; Verzijl, C. J. O.; Martin, C. A.; Shaikh, A. J.; Eelkema, R.; van Esch, J. H.; van Ruitenbeek, J. M.; Thijssen, J. M.; van der Zant, H. S. J.; Dulić, D. Large Tunable Image-Charge Effects in Single-Molecule Junctions. *Nat. Nanotechnol.* **2013**, *8*, 282–287.
- (136) Alloway, D. M.; Hofmann, M.; Smith, D. L.; Gruhn, N. E.; Graham, A. L.; Colorado, R., Jr.; Wysocki, V. H.; Lee, T. R.; Lee, P. A.; Armstrong, N. R. Interface Dipoles Arising from Self-Assembled Monolayers on Gold: UV-Photoemission Studies of Alkanethiols and Partially Fluorinated Alkanethiols. *J. Phys. Chem. B* **2003**, *107*, 11690–11699.
- (137) Rusu, P. C.; Brocks, G. Surface Dipoles and Work Functions of Alkylthiolates and Fluorinated Alkylthiolates on Au(111). *J. Phys. Chem. B* **2006**, *110*, 22628–22634.
- (138) Howell, S.; Kuila, D.; Kasibhatla, B.; Kubiak, C. P.; Janes, D.; Reifengerger, R. Molecular Electrostatics of Conjugated Self-Assembled Monolayers on Au(111) Using Electrostatic Force Microscopy. *Langmuir* **2002**, *18*, 5120–5125.
- (139) de Boer, B.; Hadipour, A.; Mandoc, M. M.; van Woudenberg, T.; Blom, P. W. M. Tuning of Metal Work Functions with Self-Assembled Monolayers. *Adv. Mater.* **2005**, *17*, 621–625.
- (140) de la Llave, E.; Clarenc, R.; Schiffrin, D. J.; Williams, F. J. Organization of Alkane Amines on a Gold Surface: Structure, Surface Dipole, and Electron Transfer. *J. Phys. Chem. C* **2014**, *118*, 468–475.
- (141) Rusu, P. C.; Brocks, G. Work Functions of Self-Assembled Monolayers on Metal Surfaces by First-Principles Calculations. *Phys. Rev. B* **2006**, *74*, 073414.
- (142) Lyons, L. E. Ionized States of Molecular Crystals. *Aust. J. Chem.* **1957**, *10*, 365–367.
- (143) Hill, I. G.; Mäkinen, A. J.; Kafafi, Z. H. Distinguishing Between Interface Dipoles and Band Bending at Metal/tris-(8-Hydroxyquinoline) Aluminum Interfaces. *Appl. Phys. Lett.* **2000**, *77*, 1825–1827.
- (144) Hill, I. G.; Mäkinen, A. J.; Kafafi, Z. H. Initial Stages of Metal/Organic Semiconductor Interface Formation. *J. Appl. Phys.* **2000**, *88*, 889–895.
- (145) Xue, Y.; Datta, S.; Ratner, M. A. Charge Transfer and “Band Lineup” in Molecular Electronic Devices: A Chemical and Numerical Interpretation. *J. Chem. Phys.* **2001**, *115*, 4292–4299.
- (146) Seki, K.; Ishii, H. Photoemission Studies of Functional Organic Materials and Their Interfaces. *J. Electron Spectrosc. Relat. Phenom.* **1998**, *88–91*, 821–830.
- (147) Hwang, J.; Wan, A.; Kahn, A. Energetics of Metal–Organic Interfaces: New Experiments and Assessment of the Field. *Mater. Sci. Eng.* **2009**, *R64*, 1–31.
- (148) Van Dyck, C.; Geskin, V.; Cornil, J. Fermi-Level Pinning and Orbital Polarization Effects in Molecular Junctions: The Role of Metal-Induced Gap States. *Adv. Funct. Mater.* **2014**, *24*, 6154–6165.
- (149) Tung, R. T. Chemical Bonding and Fermi Level Pinning at Metal–Semiconductor Interfaces. *Phys. Rev. Lett.* **2000**, *84*, 6078–6081.
- (150) Metzger, R. M. The Quest for D– $\sigma$ –A Unimolecular Rectifiers and Related Topics in Molecular Electronics. In *Molecular and Biomolecular Electronics*; ACS Adv. Chem. Series; Birge, R. R., Ed.; American Chemical Society: Washington, DC, **1994**; Vol. 240, pp 81–129.
- (151) Ruoff, R. S.; Kadish, K. M.; Boudas, P.; Chen, E. C. M. The Relationship between the Electron Affinities and Half-Wave Reduction Potentials of Fullerenes, Aromatic Hydrocarbons, and Metal Complexes. *J. Phys. Chem.* **1995**, *99*, 8843–8850.
- (152) Trasatti, S. The Absolute Electrode Potential: An Explanatory Note (Recommendations 1986). *Pure Appl. Chem.* **1986**, *58*, 955–966.
- (153) Mazur, U.; Hipps, K. W. Orbital-Mediated Tunneling, Inelastic Electron Tunneling, and Electrochemical Potentials for Metal Phthalocyanine Thin Films. *J. Phys. Chem. B* **1999**, *103*, 9721–9727.
- (154) Richardson, D. E. Thermochemical Interpretation of Electrode Potentials for Transition-Metal Complexes. *Inorg. Chem.* **1990**, *29*, 3213–3217.
- (155) Huber, E. E., Jr. The Effect of Mercury Contamination on the Work Function of Gold. *Appl. Phys. Lett.* **1966**, *8*, 169–171.
- (156) Gray, D. E., Ed. *American Institute of Physics Handbook*, Second ed.; McGraw-Hill: New York, NY, 1963.
- (157) Fomenko, V. S. In *Handbook of Thermionic Properties*; Samsanov, G. V., Ed.; Plenum Press Data Div.: New York, NY, 1966.
- (158) Ashcroft, N. W.; Mermin, N. D. *Solid State Physics*; Saunders: Philadelphia, PA, 1976.
- (159) Anderson, P. A. Work Function of Gold. *Phys. Rev.* **1959**, *115*, 553–554.
- (160) Michaelson, H. B. The Work Function of the Elements and Its Periodicity. *J. Appl. Phys.* **1977**, *48*, 4729–4733.
- (161) Skriver, H. L.; Rosengard, R. M. Surface Energy and Work Functions of Elemental Metals. *Phys. Rev.* **1992**, *B46*, 7157–7168.
- (162) Hansson, G. V.; Flodstrom, S. A. Photoemission Study of the Bulk and Surface Electronic Structure of Single Crystals of Gold. *Phys. Rev. B* **1978**, *18*, 1572–1585.
- (163) Wacks, M. E.; Dibeler, V. H. Electron Impact Studies of Aromatic Hydrocarbons. I. Benzene, Naphthalene, Anthracene, and Phenanthrene. *J. Chem. Phys.* **1959**, *31*, 1557–1562.
- (164) Sato, N.; Seki, K.; Inokuchi, H. Polarization Energies of Organic Solids Determined by Ultraviolet Photoelectron Spectroscopy. *J. Chem. Soc., Faraday Trans. II* **1981**, *77*, 1621–1633.
- (165) Sato, N.; Inokuchi, H.; Silinsh, E. A. Reevaluation of Electronic Polarization Energies in Organic Molecular Crystals. *Chem. Phys.* **1987**, *115*, 269–277.
- (166) Jordan, K. D.; Burrow, K. B. Studies of the Temporary Anion States of Unsaturated Hydrocarbons by Electron Transmission Spectroscopy. *Acc. Chem. Res.* **1978**, *11*, 341–348.
- (167) Dudde, R.; Reihl, B.; Otto, A.  $\pi^*$  and  $\sigma^*$  Molecular Orbitals of Condensed Films of Chlorobenzenes and Hexafluorobenzene Observed by Inverse Photoemission. *J. Chem. Phys.* **1990**, *92*, 3930–3934.
- (168) Pysh, E. S.; Yang, N. C. Polarographic Oxidation Potentials of Aromatic Compounds. *J. Am. Chem. Soc.* **1963**, *85*, 2125–2130.
- (169) Clar, E.; Robertson, J. M.; Schloegl, R.; Schmidt, W. Photoelectron Spectra of Polynuclear Aromatics. 6. Applications to Structural Elucidation: “Circumanthracene”. *J. Am. Chem. Soc.* **1981**, *103*, 1320–1328.
- (170) Wentworth, W. E.; Becker, R. S. Potential Method for the Determination of Electron Affinities of Molecules: Application to Some Aromatic Hydrocarbons. *J. Am. Chem. Soc.* **1962**, *84*, 4263–4266.
- (171) Peover, M. E.; White, B. S. The Electro-Oxidation of Polycyclic Aromatic Hydrocarbons in Acetonitrile Studied by Cyclic Voltammetry. *J. Electroanal. Chem.* **1967**, *13*, 93–99.
- (172) Ando, N.; Kobuko, S.; Mitsui, M.; Nakajima, A. Photoelectron Spectroscopy of Pyrene Cluster Anions (Pyrene)<sub>n</sub> (n=1–20). *Chem. Phys. Lett.* **2004**, *389*, 279–283.
- (173) Scheidt, J.; Weinkauff, R. Photodetachment Photoelectron Spectroscopy of Perylene and Cs<sub>2</sub>: Two Extreme Cases. *Chem. Phys. Lett.* **1997**, *274*, 18–22.
- (174) Crocker, L.; Wang, T. B.; Kebarle, P. Electron Affinities of Some Polycyclic Aromatic Hydrocarbons, Obtained from Electron-Transfer Equilibria. *J. Am. Chem. Soc.* **1993**, *115*, 7818–7822.
- (175) Berkowitz, J. Photoelectron Spectroscopy of Phthalocyanine Vapors. *J. Chem. Phys.* **1979**, *70*, 2819–2828.
- (176) Pope, M. Surface Ionization Energies of Organic Compounds: Phthalocyanines. *J. Chem. Phys.* **1962**, *36*, 2810–2811.
- (177) Clack, D. W.; Hush, N. S.; Woolsey, I. S. Reduction Potentials of Some Metal Phthalocyanines. *Inorg. Chim. Acta* **1976**, *19*, 129–132.
- (178) Chen, W.; Huang, H.; Chen, S.; Huang, Y. L.; Gao, X. Y.; Wee, A. T. S. Molecular Orientation-Dependent Ionization Potential of Organic Thin Films. *Chem. Mater.* **2008**, *20*, 7017–7021.

- (179) Djurovich, P. I.; Mayo, E. I.; Forrest, S. R.; Thompson, M. E. Measurement of the Lowest Unoccupied Molecular Orbital Energies of Molecular Organic Semiconductors. *Org. Electronics* **2009**, *10*, 515–520.
- (180) Zahn, D. R. T.; Gavril, G. N.; Gorgoi, M. The Transport Gap of Organic Semiconductors Studied Using the Combination of Direct and Inverse Photoemission. *Chem. Phys.* **2006**, *325*, 99–112.
- (181) Gao, W.; Kahn, A. Electronic Structure and Current Injection in Zinc Phthalocyanine Doped with Tetrafluorotetracyanoquinodimethane: Interface Versus Bulk Effect. *Org. Electron.* **2002**, *3*, 53–63.
- (182) Nakato, Y.; Ozaki, M.; Egawa, A.; Tsubomura, H. Organic Amino Compounds with Very Low Ionization Potentials. *Chem. Phys. Lett.* **1971**, *9*, 615–616.
- (183) Laidlaw, R. K.; Miura, Y.; Grant, J. L.; Cooray, L.; Clark, M.; Kispert, L. D.; Metzger, R. M. Hydrogen Bonding and Cation Radical Formation of Methyl 4-(*N,N*-Dimethylamino)phenyl Carbamate, DMAPCMe. *J. Chem. Phys.* **1987**, *87*, 4967–4971.
- (184) Ballard, R. E.; Jones, J.; Read, D.; Inchley, A.; Cranmer, M. He(I) Photoelectron Studies of Liquids and Gases. *Chem. Phys. Lett.* **1987**, *137*, 125–129.
- (185) Lichtenberger, D. L.; Johnston, R. L.; Hinkelmann, K.; Suzuki, T.; Wudl, F. Relative Electron Donor Strengths of Tetrathiafulvalene Derivatives: Effects of Chemical Substitutions and the Molecular Environment from a Combined Photoelectron and Electrochemical Study. *J. Am. Chem. Soc.* **1990**, *112*, 3302–3307.
- (186) Chen, W.; Cava, M. P.; Takassi, M. A.; Metzger, R. M. Synthesis of Bis-(2,5-dimethylpyrrolo-(3,4-*d*))-tetrathiafulvalene, an Annulated TTF Derivative with Good Electron Donor Properties. *J. Am. Chem. Soc.* **1988**, *110*, 7903–7904.
- (187) Heinis, T.; Chowdhury, S.; Scott, S. L.; Kebarle, P. Electron Affinities of Benzo-, Naphtho-, and Anthraquinones Determined from Gas-Phase Equilibria Measurements. *J. Am. Chem. Soc.* **1988**, *110*, 400–407.
- (188) Kebarle, P.; Chowdhury, S. Electron Affinities and Electron-Transfer Reactions. *Chem. Rev.* **1987**, *87*, 513–534.
- (189) Eggins, B. R. Interpretation of Electrochemical Reduction and Oxidation Waves of Quinone–Hydroquinone System in Acetonitrile. *J. Chem. Soc. D: Chem. Commun.* **1969**, 1267–1268.
- (190) Terenin, A.; Vilesov, F. Photoionization and Photodissociation of Aromatic Molecules by Vacuum Ultraviolet Radiation. In *Advances in Photochemistry*; Noyes, W. A., Hammond, G. S., Pitts, J. N., Eds.; Interscience: New York, NY, 1964; Vol. 2, pp 385–421.
- (191) Ahsraf, M.; Headridge, J. B. Voltammetric Oxidation of Anthraquinones in Acetonitrile and Nitromethane. *Talanta* **1969**, *16*, 1439–1431.
- (192) Jeftić, L.; Manning, G. A Survey on the Electrochemical Reduction of Quinones. *J. Electroanal. Chem.* **1970**, *26*, 195–200.
- (193) Peover, M. E. A Polarographic Investigation into the Redox Behaviour of Quinones: The Roles of Electron Affinity and Solvent. *J. Chem. Soc.* **1962**, 4540–4549.
- (194) Acker, D. S.; Hertler, W. R. Substituted Quinodimethans. I. Preparation and Chemistry of 7,7,8,8-Tetracyanoquinodimethane. *J. Am. Chem. Soc.* **1962**, *84*, 3370–3374.
- (195) Herman, F.; Batra, I. P. Electronic Structure of the Tetracyanoquinodimethane (TCNQ) Molecule. *Phys. Rev. Lett.* **1974**, *33*, 94–97.
- (196) Jin, C.; Haufler, R. E.; Hettich, R. L.; Barshick, C. M.; Compton, R. N.; Puretzky, A. A.; Dem'yanenko, A. V.; Tuinman, A. A. Synthesis and Characterization of Molybdenum Carbide Clusters Mo<sub>*n*</sub>C<sub>*4n*</sub> (*n* = 1 to 4). *Science* **1994**, *263*, 68–71.
- (197) Romaner, L.; Heimel, G.; Brédas, J.-L.; Gerlach, A.; Schreiber, F.; Johnson, R. L.; Zegehegen, J.; Duhm, S.; Koch, N.; Joer, E. Impact of Bidirectional Charge Transfer and Molecular Distortions on the Electronic Structure of a Metal–Organic Interface. *Phys. Rev. Lett.* **2007**, *99*, 256801.
- (198) Wheland, R. C.; Gillson, J. L. Synthesis of Electrically Conductive Organic Solids. *J. Am. Chem. Soc.* **1976**, *98*, 3916–3925.
- (199) Wang, L. S.; Conceição, J.; Jin, C.; Smalley, R. E. Threshold Photodetachment of C<sub>60</sub><sup>-</sup>. *Chem. Phys. Lett.* **1991**, *182*, 5–11.
- (200) Wang, B.; Zhao, J.; Cui, C.; Wang, M.; Wang, Z.; He, Q. Electrochemical Synthesis, Characterization and Electrochromic Properties of a Copolymer Based on 1,4-Bis(2-Thienyl)Naphthalene and Pyrene. *Opt. Mater.* **2013**, *34*, 1095–1101.
- (201) Salbeck, J.; Kunkely, H.; Langhals, H.; Saalfrank, R. W.; Daub, J. The Electron-Transfer Behavior of Fluorescent Dyes Perylenebisdicarboximides and Dioxaindenoindenedione Studied by Cyclic Voltammetry and UV-Visible Spectroelectrochemistry. *Chimia* **1989**, *43*, 6–9.
- (202) Zanello, P.; Cinquantini, A.; Mangani, S.; Opromolla, G.; Pardi, L.; Janiak, C.; Rausch, M. D. The Redox Behaviour of Ferrocene Derivatives. VI. Benzylferrocenes. The Crystal Structure of Deca-benzylferrocenium Tetrafluoroborate. *J. Organomet. Chem.* **1994**, *471*, 171–177.
- (203) Slattery, D. K.; Linkous, C. A.; Gruhn, N. Photocatalytic Water-Splitting Using Organic Pigments as Semiconductors. *Polym. Prepr.* **2000**, *41*, 866–867.
- (204) Rajagopal, A.; Wu, C. L.; Kahn, A. Energy Level Offset at Organic Semiconductor Heterojunctions. *J. Appl. Phys.* **1998**, *83*, 2649–2655.
- (205) Anderson, J. D.; McDonald, E. M.; Lee, P. A.; Anderson, M. L.; Ritchie, E. L.; Hall, H. K.; Hopkins, T.; Mash, E. A.; Wang, J.; Padias, A.; Thayumanavan, S.; Barlow, S.; Marder, S. R.; Jabbour, G. E.; Shaheen, S.; Kippelen, B.; Peyghambarian, N.; Wightman, R. M.; Armstrong, N. R. Electrochemistry and Electrogenerated Chemiluminescence Processes of the Components of Aluminum Quinolate/Triarylamine, and Related Organic Light-Emitting Diodes. *J. Am. Chem. Soc.* **1998**, *120*, 9646–9655.
- (206) Akaike, K.; Kanai, K.; Yoshida, H.; Tsutsumi, J.; Nishi, T.; Sato, N.; Ouchi, Y.; Seki, K. Ultraviolet Photoelectron Spectroscopy and Inverse Photoemission Spectroscopy of [6,6]-Phenyl-C<sub>61</sub>-Butyric Acid Methyl Ester in Gas and Solid Phases. *J. Appl. Phys.* **2008**, *104*, 023710.
- (207) de Vries, J.; Steger, H.; Kamke, B.; Menzel, C.; Weisser, B.; Kamke, W.; Hertel, I. V. Single-Photon Ionization of C<sub>60</sub>- and C<sub>70</sub>-Fullerene with Synchrotron Radiation: Determination of the Ionization Potential of C<sub>60</sub>. *Chem. Phys. Lett.* **1992**, *188*, 159–162.
- (208) Sato, N.; Saito, Y.; Shinohara, H. Threshold Ionization Energy of C<sub>60</sub> in the Solid State. *Chem. Phys.* **1992**, *162*, 433–438.
- (209) Allemand, P.-M.; Koch, A.; Wudl, F.; Rubin, Y.; Diederich, F.; Alvarez, M. M.; Anz, S. J.; Whetten, R. L. Two Different Fullerenes Have the Same Cyclic Voltammetry. *J. Am. Chem. Soc.* **1991**, *113*, 1050–1051.
- (210) Suzuki, S.; Bower, C.; Watanabe, Y.; Zhou, O. Work Functions and Valence Band States of Pristine and Cs-Intercalated Single-Walled Carbon Nanotube Bundles. *Appl. Phys. Lett.* **2000**, *76*, 4007–4009.
- (211) Song, S. M.; Park, J. K.; Sul, O. J.; Cho, B. J. Determination of Work Function of Graphene under a Metal Electrode and Its Role in Contact Resistance. *Nano Lett.* **2012**, *12*, 3887–3892.
- (212) Dweydari, A. W.; Mee, C. H. B. Work Function Measurements on (100) and (110) Surfaces of Silver. *Phys. Status Solidi A* **1975**, *27*, 223–230.
- (213) Anderson, P. A. The Work Function of Copper. *Phys. Rev.* **1949**, *76*, 388–390.
- (214) Suhrmann, R.; Wedler, G. Neuere Messungen der Elektronen-Austrittspotentiale von ungeordneten und geordneten Metallfilmen. *Z. Angew. Phys.* **1962**, *14*, 70–74.
- (215) Curioni, A.; Boero, M.; Andreoni, W. Alq<sub>3</sub>: Ab Initio Calculations of Its Structural and Electronic Properties in Neutral and Charged States. *Chem. Phys. Lett.* **1998**, *294*, 263–271.
- (216) Langmuir, I.; Schaefer, V. F. Activities of Urease and Pepsin Monolayers. *J. Am. Chem. Soc.* **1938**, *60*, 1351–1360.
- (217) Scaini, D.; Castronuovo, M.; Casalis, L.; Scoles, G. Electron Transfer Mediating Properties of Hydrocarbons as a Function of Chain Length: A Differential Scanning Conductive Tip Atomic Force Microscopy Investigation. *ACS Nano* **2008**, *2*, 507–515.
- (218) Chen, W.; Qi, D.-C.; Huang, H.; Gao, X.; Wee, A. T. S. Organic–Organic Heterojunction Interfaces: Effect of Molecular Orientation. *Adv. Funct. Mater.* **2011**, *21*, 410–424.
- (219) Love, J. C.; Estroff, L. A.; Kriebel, J. K.; Nuzzo, R. G.; Whitesides, G. M. Self-Assembled Monolayers of Thiolates on Metals as a Form of Nanotechnology. *Chem. Rev.* **2005**, *105*, 1103–1169.

- (220) Frey, S.; Shaporenko, A.; Zharnikov, M.; Harder, P.; Allara, D. L. Self-Assembled Monolayers of Nitrile-Functionalized Alkanethiols on Gold and Silver Substrates. *J. Phys. Chem. B* **2003**, *107*, 7716–7725.
- (221) Taylor, C. E.; Schwartz, D. K. Octadecanoic Acid Self-Assembled Monolayer Growth at Sapphire Surfaces. *Langmuir* **2003**, *19*, 2665–2672.
- (222) Chen, F.; Huang, Z.; Tao, N. Forming Single Molecular Junctions Between ITO Electrodes. *Appl. Phys. Lett.* **2007**, *91*, 162106.
- (223) Linford, M. R.; Chidsey, C. E. D. Alkyl Monolayers Covalently Bonded to Silicon Surfaces. *J. Am. Chem. Soc.* **1993**, *115*, 12631–12632.
- (224) Niederhauser, T. L.; Lua, Y.-Y.; Jaing, G.; Davis, S. D.; Matheson, R.; Hess, D. A.; Mowat, I. A.; Linford, M. R. Arrays of Chemomechanically Patterned Patches of Homogeneous and Mixed Monolayers of 1-Alkenes and Alcohols on Single Silicon Surfaces. *Angew. Chem., Int. Ed.* **2002**, *41*, 2353–2354.
- (225) Buriak, J. M.; Allen, M. J. Lewis Acid Mediated Functionalation of Porous Silicon with Substituted Alkenes and Alkynes. *J. Am. Chem. Soc.* **1998**, *120*, 1339–1340.
- (226) Himmel, H. J.; Kaschke, M.; Harder, P.; Wöll, C. Adsorption of Organic Monolayers on Pyrite (FeS<sub>2</sub>) (100). *Thin Solid Films* **1996**, *284–285*, 275–280.
- (227) Venkataraman, L.; Klare, J. E.; Tam, I. W.; Nuckolls, C.; Hybertsen, M. S.; Steigerwald, M. L. Single-Molecule Circuits with Well-Defined Molecular Conductance. *Nano Lett.* **2006**, *6*, 458–462.
- (228) Hickman, J. J.; Laibinis, P. E.; Auerbach, D. I.; Zou, C.; Garner, T. J.; Whitesides, G. M.; Wrighton, M. S. Toward Orthogonal Self-Assembly of Redox-Active Molecules on Platinum and Gold: Selective Reaction of Disulfide with Gold and Isocyanide with Platinum. *Langmuir* **1992**, *8*, 357–359.
- (229) Yan, H.; Bergren, A. J.; McCreery, R. L. All-Carbon Molecular Tunnel Junctions. *J. Am. Chem. Soc.* **2011**, *133*, 19168–19177.
- (230) Stewart, M. P.; Maya, F.; Kosynkin, D. V.; Dirk, S. M.; Stapleton, J. J.; McGuinness, C. L.; Allara, D. L.; Tour, J. M. Direct Covalent Grafting of Conjugated Molecules onto Si, GaAs, and Pd Surfaces from Aryldiazonium Salts. *J. Am. Chem. Soc.* **2004**, *126*, 370–378.
- (231) Zharnikov, M.; Küller, A.; Shaporenko, A.; Schmidt, E.; Eck, W. Aromatic Self-Assembled Monolayers on Hydrogenated Silicon. *Langmuir* **2003**, *19*, 4682–4687.
- (232) Joy, V. T.; Mandler, D. Surface Functionalization of H-Terminated Silicon Surfaces with Alcohols Using Iodoform As an In Situ Iodinating Agent. *Chem. Phys. Chem.* **2002**, *3*, 973–975.
- (233) Pellerite, M. J.; Dunbar, T. D.; Boardman, K. D.; Wood, E. J. Effects of Fluorination on Self-Assembled Monolayer Formation from Alkanephosphonic Acids on Aluminum: Kinetics and Structure. *J. Phys. Chem. B* **2003**, *107*, 11726–11736.
- (234) Neves, B. R. A.; Salmo, M. E.; Russell, P. E.; Troughton, E. B., Jr. Spread Coating of OPA on Mica: From Multilayers to Self-Assembled Monolayers. *Langmuir* **2001**, *17*, 8193–8198.
- (235) Helmy, R.; Fadeev, A. Y. Self-Assembled Monolayers Supported on TiO<sub>2</sub>: Comparison of C<sub>18</sub>H<sub>37</sub>SiX<sub>3</sub> (X = H, Cl, OCH<sub>3</sub>), C<sub>18</sub>H<sub>37</sub>Si(CH<sub>3</sub>)<sub>2</sub>Cl, and C<sub>18</sub>H<sub>37</sub>PO(OH)<sub>2</sub>. *Langmuir* **2002**, *18*, 8924–8928.
- (236) Pawsey, S.; Yach, K.; Reven, L. Self-Assembly of Carboxyalkylphosphonic Acids on Metal Oxide Powders. *Langmuir* **2002**, *18*, 5205–5212.
- (237) Yim, C. T.; Pawsey, S.; Morin, F. G.; Reven, L. Dynamics of Octadecylphosphonate Monolayers Self-Assembled on Zirconium Oxide: A Deuterium NMR Study. *J. Phys. Chem. B* **2002**, *106*, 1728–1733.
- (238) Hähner, G.; Hofer, R.; Klingenfuss, I. Order and Orientation in Self-Assembled Long Chain Alkanephosphate Monolayers Adsorbed on Metal Oxide Surfaces. *Langmuir* **2001**, *17*, 7047–7052.
- (239) Zwahlen, M.; Tosatti, S.; Textor, M.; Hähner, G. Orientation in Methyl- and Hydroxyl-Terminated Self-Assembled Alkanephosphate Monolayers on Titanium Oxide Surfaces Investigated with Soft X-ray Absorption. *Langmuir* **2002**, *18*, 3957–3962.
- (240) Laibinis, P. E.; Whitesides, G. M.; Allara, D. L.; Tapoo, Y. T.; Farikh, A. N.; Nuzzo, R. G. Comparison of the Structures and Wetting Properties of Self-Assembled Monolayers of *n*-Alkanethiols on the Coinage Metal Surfaces, Copper, Silver, Gold. *J. Am. Chem. Soc.* **1991**, *113*, 7152–7167.
- (241) Magnussen, O. M.; Ocko, B. M.; Deutsch, M.; Regan, M. J.; Pershan, P. S.; Abernathy, D.; Grübel, G.; Legrand, J.-F. Self-Assembly of Organic Films on a Liquid Metal. *Nature* **1996**, *384*, 250–252.
- (242) Mekhalif, Z.; Laffineur, F.; Couturier, N.; Delhalle, J. Elaboration of Self-Assembled Monolayers of *n*-Alkanethiols on Nickel Polycrystalline Substrates: Time, Concentration, and Solvent Effects. *Langmuir* **2003**, *19*, 637–645.
- (243) Tour, J. M.; Jones, L., II; Pearson, D. L.; Lamba, J. J. S.; Burgin, T. P.; Whitesides, G. M.; Allara, D. L.; Parikh, A. N.; Atre, S. Self-Assembled Monolayers and Multilayers of Conjugated Thiols,  $\alpha,\omega$ -Dithiols, and Thioacetyl-Containing Adsorbates. Understanding Attachments between Potential Molecular Wires and Gold Surfaces. *J. Am. Chem. Soc.* **1995**, *117*, 9529–9534.
- (244) Valkenier, H.; Huisman, E. H.; van Hal, P. A.; de Leeuw, D. M.; Chiechi, R. C.; Hummelen, J. C. Formation of High-Quality Self-Assembled Monolayers of Conjugated Dithiols on Gold: Base Matters. *J. Am. Chem. Soc.* **2011**, *133*, 4930–4939.
- (245) Troughton, E. B.; Bain, C. D.; Whitesides, G. M.; Nuzzo, R. G.; Allara, D. L.; Porter, M. D. Monolayer Films Prepared by the Spontaneous Self-Assembly of Symmetrical and Unsymmetrical Dialkyl Sulfides from Solution onto Gold Substrates: Structure, Properties, and Reactivity of Constituent Functional Groups. *Langmuir* **1988**, *4*, 365–385.
- (246) Han, S. W.; Lee, S. J.; Kim, K. Self-Assembled Monolayers of Aromatic Thiol and Selenol on Silver: Comparative Study of Adsorptivity and Stability. *Langmuir* **2001**, *17*, 6981–6987.
- (247) Han, S. W.; Kim, K. Self-Assembled Monolayers of Organoselenium Compounds on Gold: Surface-Enhanced Raman Scattering Study. *J. Colloid Interface Sci.* **2001**, *240*, 492–497.
- (248) Fadeev, A. Y.; Helmy, R.; Marcinko, S. Self-Assembled Monolayers of Organosilicon Hydrides Supported on Titanium, Zirconium, and Hafnium Dioxides. *Langmuir* **2002**, *18*, 7521–7529.
- (249) Koide, Y.; Such, M. W.; Basu, R.; Evmenenko, G.; Cui, J.; Dutta, P.; Hersam, M. C.; Marks, T. J. Hot Microcontact Printing for Patterning ITO Surfaces. Methodology, Morphology, Microstructure, and OLED Charge Injection Barrier Imaging. *Langmuir* **2003**, *19*, 86–93.
- (250) Scholz, F.; Kaletova, E.; Stensrud, E. S.; Ford, W. E.; Kohutova, A.; Mucha, M.; Stibor, I.; Michl, J.; von Wrochem, F. Formation of *n*-Alkyl Monolayers by Organomercury Deposition on Gold. *J. Phys. Chem. Lett.* **2013**, *4*, 2624–2629.
- (251) Khobragade, D.; Stensrud, E. S.; Mucha, M.; Smith, J. R.; Pohl, R.; Stibor, I.; Michl, J. Preparation of Covalent Long-Chain Trialkylstannyl and Trialkylsilyl Salts and an Examination of their Adsorption on Gold. *Langmuir* **2010**, *26*, 8483–8490.
- (252) Cheng, Z.-L.; Skouta, R.; Vazquez, H.; Widawsky, J. R.; Schneebeil, S.; Chen, W.; Hybertsen, M. S.; Breslow, R.; Venkataraman, L. In Situ Formation of Highly Conducting Au–C Contacts for Single-Molecule Junctions. *Nat. Nanotechnol.* **2011**, *6*, 353–357.
- (253) Yu, M.; Bovet, N.; Satterly, C. J.; Bengió, S.; Lovelock, K. R. J.; Milligan, K.; Jones, R. G.; Woodruff, D. P.; Dhanak, V. True Nature of an Archetypical Self-Assembly System: Mobile Au-Thiolate Species on Au(111). *Phys. Rev. Lett.* **2006**, *97*, 166102.
- (254) Porter, M. D.; Bright, T. B.; Allara, D. L.; Chidsey, C. E. D. Spontaneously Organized Molecular Assemblies. 4. Structural Characterization of *n*-Alkyl Thiol Monolayers on Gold by Optical Ellipsometry, Infrared Spectroscopy, and Electrochemistry. *J. Am. Chem. Soc.* **1987**, *109*, 3559–3569.
- (255) Tarlow, M. J.; Newman, J. G. Static Secondary Ion Mass Spectrometry of Self-Assembled Alkanethiol Monolayers on Gold. *Langmuir* **1992**, *8*, 1398–1405.
- (256) Tarazona-Vazquez, F.; Balbuena, P. B. Complexation of the Lowest Generation poly(Amidoamine)-NH<sub>2</sub> Dendrimers with Metal Ions, Metal Atoms, and Cu(II) Hydrates: An Ab Initio Study. *J. Phys. Chem. B* **2004**, *108*, 15992–16001.

- (257) Lavrich, D. J.; Wetterer, S. M.; Bernasek, S. L.; Scoles, G. Physisorption and Chemisorption of Alkanethiols and Alkyl Sulfides on Au(111). *J. Phys. Chem. B* **1998**, *102*, 3456–3465.
- (258) Wetterer, S. M.; Lavrich, D. J.; Cummings, T.; Scoles, G.; Bernasek, S. Energetics and Kinetics of the Physisorption of Hydrocarbons on Au(111). *J. Phys. Chem. B* **1998**, *102*, 9266–9275.
- (259) Carniti, P.; Gervasini, A.; Bennici, S. Experimental and Modelization Approach in the Study of Acid-Site Energy Distribution by Base Desorption. Part I: Modified Silica Surfaces. *J. Phys. Chem. B* **2005**, *109*, 1528–1536.
- (260) Marcus, R. A. Electron Transfer Reactions in Chemistry: Theory and Experiment (Nobel Lecture). *Angew. Chem., Int. Ed.* **1993**, *32*, 1111–1121.
- (261) Calcaterra, L. T.; Closs, G. L.; Miller, J. R. Fast Intramolecular Electron Transfer in Radical Ions over Long Distances Across Rigid Saturated Hydrocarbon Spacers. *J. Am. Chem. Soc.* **1983**, *105*, 670–671.
- (262) Miller, J. R.; Calcaterra, L. T.; Closs, G. L. Intramolecular Long-Distance Electron Transfer in Radical Anions. The Effects of Free Energy and Solvent on the Reaction Rates. *J. Am. Chem. Soc.* **1984**, *106*, 3047–3049.
- (263) Ohm, G. S. *Die Galvanische Kette, Mathematisch Bearbeitet*; T. H. Riemann: Berlin, 1827.
- (264) Maxwell, J. C. *A Treatise on Electricity and Magnetism*; Oxford, Clarendon Press: Oxford, U.K., 1873, and Dover: New York, 1954; Vol. 1.
- (265) Sharvin, Yu. V. A Possible Method for Studying Fermi Surfaces. *Zh. Eksp. Teor. Fiz.* **1965**, *48*, 984; *Sov. Phys. JETP* **1965**, *21*, 655.
- (266) Landauer, R. Spatial Variation of Currents and Fields Due to Localized Scatterers in Metallic Conduction. *IBM J. Res. Dev.* **1957**, *1*, 223–231.
- (267) Landauer, R. Spatial Variation of Currents and Fields Due to Localized Scatterers in Metallic Conduction. *IBM J. Res. Dev.* **1988**, *32*, 306–316.
- (268) Büttiker, M.; Imry, Y.; Landauer, R.; Pinhas, S. Generalized Many-Channel Conductance Formula with Application to Small Rings. *Phys. Rev. B* **1985**, *31*, 6207–6215.
- (269) Keldysh, L. V. Diagram Technique for Non-Equilibrium Processes. *Zh. Eksp. Teor. Fiz.* **1964**, *47*, 1515–1517; *Sov. Phys. JETP* **1965**, *20*, 1018.
- (270) Kondo, J. Resistance Minimum in Dilute Magnetic Alloys. *Prog. Theor. Phys.* **1964**, *32*, 37–49.
- (271) Haldane, F. D. M. Scaling Theory of the Asymmetric Anderson Model. *Phys. Rev. Lett.* **1978**, *40*, 416–419.
- (272) Goldhaber-Gordon, D.; Shtrikman, S.; Mahalu, D.; Abusch-Magder, D.; Meirav, U.; Kastner, M. A. Kondo Effect in a Single-Electron Transistor. *Nature* **1998**, *391*, 156–159.
- (273) van der Wiel, W. G.; De Franceschi, S.; Fujisawa, T.; Elzerman, J. M.; Tarucha, S.; Kouwenhoven, L. P. The Kondo Effect in the Unitary Limit. *Science* **2000**, *289*, 2105–2108.
- (274) Reed, M. A.; Randall, J. N.; Aggarwal, R. J.; Matyi, R. J.; Moore, T. M.; Wetsel, A. E. Observation of Discrete Electronic States in a Zero-Dimensional Semiconductor Nanostructure. *Phys. Rev. Lett.* **1988**, *60*, 535–537.
- (275) Fulton, T. A.; Dolan, G. J. Observation of Single-Electron Charging Effects in Small Tunnel Junctions. *Phys. Rev. Lett.* **1987**, *59*, 109–112.
- (276) Kastner, M. A. The Single-Electron Transistor. *Rev. Mod. Phys.* **1992**, *64*, 849–858.
- (277) Klein, D. L.; Roth, R.; Lim, A. K. L.; Alivisatos, A. P.; McEuen, P. L. A Single-Electron Transistor Made from a Cadmium Selenide Nanocrystal. *Nature* **1997**, *389*, 699–701.
- (278) Ritz, W. Über eine neue Methode zur Lösung gewisser Variationsprobleme der mathematischen Physik. *Z. Reine Angew. Math.* **1909**, *135*, 1–61.
- (279) Stallinga, P. Electronic Transport in Organic Materials: Comparison of Band Theory with Percolation/(Variable Range) Hopping Theory. *Adv. Mater.* **2011**, *23*, 3356–3362.
- (280) Simmons, J. G. Generalized Formula for the Electric Tunnel Effect between Similar Electrodes Separated by a Thin Insulating Film. *J. Appl. Phys.* **1963**, *34*, 1793–1803.
- (281) Fowler, R. H.; Nordheim, L. Electron Emission in Intense Electric Fields. *Proc. R. Soc. London* **1928**, *118*, 173–181.
- (282) Simmons, J. G. Electric Tunnel Effect between Dissimilar Electrodes Separated by a Thin Insulating Film. *J. Appl. Phys.* **1963**, *34*, 2581–2590.
- (283) Richardson, O. W. On the Negative Radiation from Hot Platinum. *Proc. Cambridge Philos. Soc.* **1901**, *11*, 286–295.
- (284) Richardson, O. W. Some Applications of the Electron Theory of Matter. *Philos. Mag.* **1912**, *23*, 594–627.
- (285) Bethe, H. Theory of the Boundary Layer of Crystal Rectifiers. *MIT Radiat. Lab. Rep.* **1942**, #43–12.
- (286) Frenkel, J. On Pre-Breakdown Phenomena in Insulators and Electronic Semiconductors. *Tech. Phys. USSR* **1938**, *5*, 685–695.
- (287) Frenkel, J. On the Theory of Electric Breakdown of Dielectrics and Electronic Semiconductors. *Phys. Rev.* **1938**, *54*, 647–648.
- (288) Mark, P.; Helfrich, W. Space-Charge-Limited Currents in Organic Crystals. *J. Appl. Phys.* **1962**, *33*, 205–215.
- (289) Levine, I. N. *Quantum Chemistry*; Allyn & Bacon: Boston, MA, 1970; Vol. I.
- (290) Landau, L. D.; Lifschitz, E. M. *Quantum Mechanics Non-Relativistic Theory*; Sykes, J. B., Bell, J. S., translators; Pergamon Press Ltd.: London, 1958.
- (291) Gundlach, K. H.; Simmons, J. G. Range of Validity of the WKB Tunnel Probability, and Comparison of Experimental Data and Theory. *Thin Solid Films* **1969**, *4*, 61–79.
- (292) Schottky, W. Über Kalte und Warme Elektronenentladungen. *Z. Phys.* **1923**, *14*, 63–106.
- (293) Nordheim, L. W. The Effect of the Image Force on the Emission and Reflection of Electrons by Metals. *Proc. R. Soc. London* **1928**, *A121*, 626–639.
- (294) Good, R. H., Jr.; Müller, E. W. In *Handbuch der Physik*; Springer-Verlag: Berlin, 1956; Vol. 21, pp 176–231.
- (295) Price, P. J.; Radcliffe, J. M. Esaki Tunneling. *IBM J. Res. Dev.* **1959**, *3*, 364–371.
- (296) Stratton, R. Volt–Current Characteristics for Tunneling through Insulating Films. *J. Phys. Chem. Solids* **1962**, *23*, 1177–1190.
- (297) Duke, C. B. *Tunneling in Solids*; Academic Press: New York, 1969.
- (298) Tsu, R.; Esaki, L. Tunneling through a Finite Superlattice. *Appl. Phys. Lett.* **1973**, *22*, 562–564.
- (299) Gehring, A. Doctoral Dissertation, Technical University of Vienna, Austria, Nov. 2003.
- (300) Simmons, J. G. Conduction in Thin Dielectric Films. *J. Phys. D* **1971**, *4*, 613–657.
- (301) Beebe, J. M.; Kim, B.; Gadzuk, J. W.; Frisbie, C. D.; Kushmerick, J. G. Transition from Direct Tunneling to Field Emission in Metal–Molecule–Metal Junctions. *Phys. Rev. Lett.* **2006**, *97*, 026801.
- (302) Huisman, E. H.; Guédon, C. M.; van Wees, B. J.; van der Molen, S. J. Interpretation of Transition Voltage Spectroscopy. *Nano Lett.* **2009**, *11*, 3909–3913.
- (303) Newns, D. M. Self-Consistent Model of Hydrogen Chemisorption. *Phys. Rev.* **1969**, *178*, 1123–1135.
- (304) Anderson, P. W. Localized Magnetic States in Metals. *Phys. Rev.* **1961**, *124*, 41–43.
- (305) Bâldea, I. Ambipolar Transition Voltage Spectroscopy: Analytical Results and Experimental Agreement. *Phys. Rev. B* **2012**, *85*, 035442.
- (306) Peterson, I. R.; Vuillaume, D.; Metzger, R. M. Analytical Model for Molecular-Scale Charge Transport. *J. Phys. Chem. A* **2001**, *105*, 4702–4707.
- (307) Hall, L. E.; Reimers, J. R.; Hush, N. S.; Silverbrook, K. Formalism, Analytical Model, and A Priori-Green’s Function-Based Calculations on the Current–Voltage Characteristics of Molecular Wires. *J. Chem. Phys.* **2000**, *112*, 1510–1521.

- (308) Mujica, V.; Kemp, M.; Roitberg, A.; Ratner, M. Current–Voltage Characteristics of Molecular Wires: Eigenvalue Staircase, Coulomb Blockade, and Rectification. *J. Chem. Phys.* **1996**, *104*, 7296–7305.
- (309) Kramers, H. A. L'interaction entre les Atomes Magnétogènes dans un Cristal Paramagnétique. *Physica* **1934**, *1*, 182–192.
- (310) Anderson, P. W. Antiferromagnetism. Theory of Superexchange Interaction. *Phys. Rev.* **1950**, *79*, 350–356.
- (311) Goodenough, J. B. Theory of the Role of Covalence in the Perovskite-Type Manganites [La, M(II)]MnO<sub>3</sub>. *Phys. Rev.* **1955**, *100*, 564–573.
- (312) Goodenough, J. B. An Interpretation of the Magnetic Properties of the Perovskite-Type Mixed Crystals La<sub>1-x</sub>Sr<sub>x</sub>CoO<sub>3-x</sub>. *J. Phys. Chem. Solids* **1958**, *6*, 287–297.
- (313) Kanamori, J. Superexchange Interaction and Symmetry Properties of Electron Orbitals. *J. Phys. Chem. Solids* **1959**, *10*, 87–98.
- (314) Li, X.-Q.; Zhang, H.; Yan, Y. A Superexchange-Mediated Sequential Hopping Theory for Charge Transfer in DNA. *J. Phys. Chem. A* **2001**, *105*, 9563–9567.
- (315) Datta, S. Electrical Resistance: An Atomistic View. *Nanotechnology* **2004**, *15*, S433–S461.
- (316) von Klitzing, K. The Quantized Hall Effect. *Rev. Mod. Phys.* **1986**, *58*, 519–531.
- (317) Heimel, G.; Duhm, S.; Salzmann, I.; Gerlach, A.; Strozecka, A.; Niederhausen, J.; Bürker, C.; Hosokai, T.; Fernandez-Torrente, I.; Schulze, G.; Winkler, S.; Wilke, A.; Schlesinger, R.; Frisch, J.; Bröker, B.; Vollmer, A.; Detlefs, B.; Pflaum, J.; Kera, S.; Franke, K. J.; Ueno, N.; Pascual, J. I.; Schreiber, F.; Koch, N. Charged and Metallic Molecular Monolayers through Surface-Induced Aromatic Stabilization. *Nat. Chem.* **2013**, *5*, 187–194.
- (318) Liang, W.; Shores, M. P.; Bockrath, M.; Long, J. R.; Park, H. Kondo Resonance in a Single-Molecule Transistor. *Nature* **2002**, *417*, 725–729.
- (319) Wang, W.; Lee, T.; Kretzschmar, I.; Reed, M. A. Inelastic Electron Tunneling Spectroscopy of an Alkanedithiol Self-Assembled Monolayer. *Nano Lett.* **2004**, *4*, 643–646.
- (320) Wang, W.; Lee, T.; Reed, M. A. Electron Tunneling in Self-Assembled Monolayers. *Rep. Prog. Phys.* **2005**, *68*, 523–544.
- (321) Wang, W.; Lee, T.; Reed, M. A. Mechanism of Electron Conduction in Self-Assembled Alkanedithiol Monolayer Devices. *Phys. Rev. B* **2003**, *68*, 035416.
- (322) Kushmerick, J. G.; Holt, D. B.; Yang, J. C.; Naciri, J.; Moore, M. H.; Shashidhar, R. Metal–Molecule Contacts and Charge Transport across Monomolecular Layers: Measurement and Theory. *Phys. Rev. Lett.* **2002**, *89*, 086802.
- (323) Kushmerick, J. G.; Holt, D. B.; Pollack, S. K.; Ratner, M. A.; Yang, J. C.; Schull, T. L.; Naciri, J.; Moore, M. H.; Shashidhar, R. Effect of Bond-Length Alternation in Molecular Wires. *J. Am. Chem. Soc.* **2002**, *124*, 10654–10655.
- (324) Tian, J.-H.; Yang, Y.; Liu, B.; Schöllhorn, B.; Wu, D.-Y.; Maisonhaute, E.; Muns, A. S.; Chen, Y.; Amatore, C.; Tao, N. J.; Tian, Z.-Q. Fabrication and Characterization of Adjustable Nanogaps Between Gold Electrodes on Chip for Electrical Measurement of Single Molecules. *Nanotechnology* **2010**, *21*, 274012.
- (325) Cui, X. D.; Primak, A.; Zarate, X.; Tomfohr, J.; Sankey, O. F.; Moore, A. L.; Moore, T. A.; Gust, D.; Harris, G.; Lindsay, S. M. Reproducible Measurement of Single-Molecule Conductivity. *Science* **2001**, *294*, 571–574.
- (326) Ludolph, B.; van Ruitenbeek, J. Thermopower of Atomic-Size Metallic Contacts. *Phys. Rev. B* **1999**, *59*, 12290–12293.
- (327) Reddy, P.; Jang, S. Y.; Segalman, Y.; Majumdar, A. Thermoelectricity in Molecular Junctions. *Science* **2007**, *315*, 1568–1571.
- (328) Widawsky, J. R.; Chen, W.; Vazquez, H.; Kim, T.; Breslow, R.; Hybertsen, M. S.; Venkataraman, L. Length-Dependent Thermopower of Highly Conducting Au–C Bonded Single Molecule Junctions. *Nano Lett.* **2013**, *13*, 2889–2894.
- (329) Kergueris, C.; Bourgoign, J.-P.; Palacin, S.; Esteve, D.; Urbina, C.; Magoga, M.; Joachim, C. Electron Transport Through a Metal–Molecule–Metal Junction. *Phys. Rev. B* **1999**, *59*, 12505–12513.
- (330) Sapmaz, S.; Jarillo-Herrero, P.; Kong, J.; Dekker, C.; Kouwenhoven, L. P.; van der Zant, H. S. J. Electronic Excitation Spectrum of Metallic Carbon Nanotubes. *Phys. Rev. B* **2005**, *71*, 153402.
- (331) Andres, R. P.; Bein, T.; Dorogi, M.; Feng, S.; Henderson, J. I.; Kubiak, C. P.; Mahoney, W.; Osifchin, R. G.; Reifenberger, R. “Coulomb Staircase” at Room Temperature in a Self-Assembled Molecular Nanostructure. *Science* **1996**, *272*, 1323–1328.
- (332) Dorogi, M.; Gomez, J.; Osifchin, R.; Andres, R. P.; Reifenberger, R. Room-Temperature Coulomb Blockade from a Self-Assembled Molecular Nanostructure. *Phys. Rev. B* **1995**, *52*, 9071–9077.
- (333) Osorio, E. A.; Bjørnholm, T.; Lehn, J.-M.; Ruben, M.; van der Zant, H. S. J. Single-Molecule Transport in Three-Terminal Devices. *J. Phys.: Condens. Matter* **2008**, *20*, 374121.
- (334) Ellenbogen, J. C.; Love, J. C. Architectures for Molecular Electronic Computers: I. Logic Structures and an Adder Designed from Molecular Electronic Diodes. *Proc. IEEE* **2000**, *88*, 386–426.
- (335) Chen, J.; Wang, W.; Reed, M. A.; Rawlett, A. M.; Price, D. W.; Tour, J. M. Room-Temperature Negative Differential Resistance in Nanoscale Molecular Junctions. *Appl. Phys. Lett.* **2000**, *77*, 1224–1226.
- (336) Song, H.; Kim, Y.; Jang, Y. H.; Jeong, H.; Reed, M. A.; Lee, T. Observation of Molecular Orbital Gating. *Nature* **2009**, *462*, 1039–1043.
- (337) Pobelov, I. V.; Li, Z.; Wandlowski, T. Electrolyte Gating in Redox-Active Tunneling Junctions—An Electrochemical STM Approach. *J. Am. Chem. Soc.* **2008**, *130*, 16045–16054.
- (338) Avouris, P. Molecular Electronics with Carbon Nanotubes. *Acc. Chem. Res.* **2002**, *35*, 1026–1034.
- (339) Thijssen, J. M.; van der Zant, H. S. J. Charge Transport and Single-Electron Effects in Nanoscale Systems. *Phys. Status Solidi* **2008**, *B245*, 1455–1470.
- (340) Sanvito, S. Molecular Spintronics. *Chem. Soc. Rev.* **2011**, *40*, 3336–3355.
- (341) Szulczewski, G. Spin-Polarized Electron Tunneling and Magnetoresistance in Molecular Junctions. *Springer Top. Curr. Chem.* **2012**, *311*, 275–302.
- (342) McConnell, H. M. Comments about “Organic Ferromagnetism”. *Proc. Robert A. Welch Found. Conf. Chem. Res.* **1967**, *11*, 144–150.
- (343) Awaga, K.; Inabe, T.; Nagashima, U.; Maruyama, Y. Two-Dimensional Network of the Ferromagnetic Organic Radical, 2-(4-Nitrophenyl)-4,4,5,5-Tetramethyl-4,5-Dihydro-1H-Imidazol-1-Oxyl 3-N-Oxide. *J. Chem. Soc., Chem. Commun.* **1989**, 1617–1618.
- (344) Chittipeddi, S.; Cromack, K. R.; Miller, J. S.; Epstein, A. J. Crossover from 1-D to 3-D Ferromagnetism in Molecular Decamethylferrocenium Tetracyano-ethenide (DMeFc) (TCNE). *Phys. Rev. Lett.* **1987**, *58*, 2695–2698.
- (345) Sessoli, R.; Tsai, H. L.; Schake, A. R.; Wang, S.; Vincent, J. B.; Foltz, K.; Gatteschi, D.; Christou, G.; Hendrickson, D. N. High-Spin Molecules: [Mn<sub>12</sub>O<sub>12</sub>(O<sub>2</sub>CR)<sub>16</sub>(H<sub>2</sub>O)<sub>4</sub>]. *J. Am. Chem. Soc.* **1993**, *115*, 1804–1816.
- (346) Caneschi, A.; Gatteschi, D.; Sessoli, R.; Rey, P. Toward Molecular Magnets: The Metal–Radical Approach. *Acc. Chem. Res.* **1989**, *22*, 392–398.
- (347) Bogani, L.; Wernsdorfer, W. Molecular Spintronics Using Single-Molecule Magnets. *Nat. Mater.* **2008**, *7*, 179–186.
- (348) Grünberg, P.; Schreiber, R.; Pang, Y.; Brodsky, M. B.; Sowers, H. Layered Magnetic Structures: Evidence for Antiferromagnetic Coupling of Fe Layers across Cr Interlayers. *Phys. Rev. Lett.* **1986**, *57*, 2442–2445.
- (349) Baibich, M. N.; Broto, J. M.; Fert, A.; Dau, F. N. V.; Petroff, F.; Etienne, P.; Creuzet, G.; Friederich, A.; Chazelas, J. Giant Magnetoresistance of (001)Fe/(001)Cr Magnetic Superlattices. *Phys. Rev. Lett.* **1988**, *61*, 2472–2475.
- (350) Butler, W. H.; Zhang, X. G.; Schulthess, T. C.; MacLaren, J. M. Spin-Dependent Tunneling Conductance of Fe|MgO|Fe Sandwiches. *Phys. Rev. B* **2001**, *63*, 054416.
- (351) Parkin, S. S. P.; Kaiser, C.; Panchula, A.; Rice, P. M.; Hughes, B.; Samant, M.; Yang, S. H. Giant Tunneling Magnetoresistance at Room Temperature with MgO (100) Tunnel Barriers. *Nat. Mater.* **2004**, *3*, 862–867.

- (352) He, J.; Sankey, O.; Lee, M.; Tao, N.; Li, X.; Lindsay, S. Measuring Single Molecule Conductance with Break Junctions. *Faraday Disc.* **2006**, *131*, 145–154.
- (353) Smit, R. H. M.; Noat, Y.; Untledt, C.; Lang, N. D.; van Hemert, M. C.; van Ruitenbeek, J. M. Measurement of the Conductance of a Hydrogen Molecule. *Nature* **2002**, *419*, 906–908.
- (354) Hihath, J.; Arroyo, C. R.; Rubio-Bollinger, G.; Tao, N.; Agrait, N. Study of Electron–Phonon Interactions in a Single Molecule Covalently Connected to Two Electrodes. *Nano Lett.* **2008**, *8*, 1673–1678.
- (355) Li, C.; Pobelov, I.; Wandlowski, T.; Bagrets, B.; Arnold, A.; Evers, F. Charge Transport in Single Au–Alkanedithiol–Au Junctions: Coordination Geometries and Conformational Degrees of Freedom. *J. Am. Chem. Soc.* **2008**, *130*, 318–326.
- (356) Haiss, W.; van Zalinge, H.; Bethell, D.; Ulstrup, J.; Schiffrin, D. J.; Nichols, R. J. Thermal Gating of the Single-Molecule Conductance of Alkanedithiols. *Faraday Disc.* **2006**, *131*, 253–264.
- (357) Ulrich, J.; Esrail, D.; Pontius, W.; Venkataraman, L.; Millar, D.; Doerrer, L. H. Variability of Conductance in Molecular Junctions. *J. Phys. Chem. Lett. B* **2006**, *110*, 2462–2466.
- (358) Xia, J. L.; Diez-Perez, I.; Tao, N. J. Electron Transport in Single Molecules Measured by a Distance-Modulation Assisted Break Junction Method. *Nano Lett.* **2008**, *8*, 1960–1964.
- (359) Li, X. L.; He, H. X.; Xu, B. Q.; Xiao, X. Y.; Nagahara, L. A.; Amlani, I.; Tsui, R.; Tao, N. J. Measurement of Electron Transport Properties of Molecular Junctions Fabricated by Electrochemical and Mechanical Methods. *Surf. Sci.* **2004**, *573*, 1–10.
- (360) Chen, F.; Li, X.; Hihath, J.; Huang, Z.; Tao, N. Effect of Anchoring Groups on Single-Molecule Conductance: Comparative Study of Thiol-, Amine-, and Carboxylic-Acid-Terminated Molecules. *J. Am. Chem. Soc.* **2006**, *128*, 15874–15881.
- (361) Huang, Z.; Xu, B.; Chen, Y.; Di Ventra, M.; Tao, N. Measurement of Current-Induced Local Heating in a Single Molecule Junction. *Nano Lett.* **2006**, *6*, 1240–1244.
- (362) Xu, B. Modulating the Conductance of a Au–Octanedithiol–Au Molecular Junction. *Small* **2007**, *3*, 2061–2065.
- (363) Li, X.; He, J.; Hihath, J.; Xu, B.; Lindsay, S. M.; Tao, N. Conductance of Single Alkanedithiols: Conduction Mechanism and Effect of Molecule–Electrode Contacts. *J. Am. Chem. Soc.* **2006**, *128*, 2135–2141.
- (364) Hihath, J.; Bruot, C.; Tao, N. Electron–Phonon Interactions in Single Octanedithiol Molecular Junctions. *ACS Nano* **2010**, *4*, 3823.
- (365) Tao, N. Measurement and Control of Single Molecule Conductance. *J. Mater. Chem.* **2005**, *5*, 3260–3263.
- (366) Huang, Z.; Chen, F.; Bennett, P. A.; Tao, N. Single Molecule Junctions Formed via Au–Thiol Contact: Stability and Breakdown Mechanism. *J. Am. Chem. Soc.* **2007**, *129*, 13225–13231.
- (367) Frei, F.; Aradhya, S. V.; Koentopp, M.; Hybertsen, M. S.; Venkataraman, L. Mechanics and Chemistry: Single-Molecule Bond-Rupture Forces Correlate with Molecular Backbone Structure. *Nano Lett.* **2011**, *11*, 1518–1523.
- (368) Park, Y. S.; Whalley, A. C.; Kamenetska, M.; Steigerwald, M. L.; Hybertsen, M. S.; Nuckolls, C.; Venkataraman, L. Contact Chemistry and Single-Molecule Conductance: A Comparison of Phosphines, Methyl Sulfides, Amines. *J. Am. Chem. Soc.* **2007**, *129*, 15768–15769.
- (369) Kim, B.; Beebe, J. M.; Jun, Y.; Zhu, X.-Y.; Frisbie, C. D. Correlation between HOMO Alignment and Contact Resistance in Molecular Junctions: Aromatic Thiols versus Aromatic Isocyanides. *J. Am. Chem. Soc.* **2006**, *128*, 4970–4971.
- (370) Ahn, S.; Aradhya, S. V.; Klausen, R. S.; Capozzi, B.; Roy, X.; Steigerwald, M. L.; Nuckolls, C.; Venkataraman, L. Electronic Transport and Mechanical Stability of Carboxyl Linked Single-Molecule Junctions. *Phys. Chem. Chem. Phys.* **2012**, *14*, 13841–13845.
- (371) Frei, M.; Aradhya, S. V.; Hybertsen, M. S.; Venkataraman, L. Linker-Dependent Bond Rupture Force Measurements in Single-Molecule Junctions. *J. Am. Chem. Soc.* **2012**, *134*, 4003–4006.
- (372) Sangeeth, C. S. S.; Wan, A.; Nijhuis, C. A. Equivalent Circuits of a Self-Assembled Monolayer-Based Tunnel Junction Determined by Impedance Spectroscopy. *J. Am. Chem. Soc.* **2014**, *136*, 11134–11144.
- (373) Xiao, X.; Xu, B.; Tao, N. Conductance Titration of Single Peptide Molecules. *J. Am. Chem. Soc.* **2004**, *126*, 5370–5371.
- (374) Yang, W. R.; Jones, M. W.; Li, X.; Eggers, P. K.; Tao, N.; Gooding, J. J.; Paddon-Row, M. N. Conductance of Single Rigid Norbornylogous Bridges. *J. Phys. Chem. C* **2008**, *112*, 9072–9080.
- (375) Li, X.; Xu, B.; Xiao, X.; Yang, X.; Zang, L.; Tao, N. Controlling Charge Transport in Single Molecules Using Electrochemical Gate. *Faraday Disc.* **2006**, *131*, 111–120.
- (376) Tian, J.; Liu, B.; Li, X.; Yang, Z.-L.; Ren, B.; Wu, S.-T.; Tao, N.; Tian, Z.-Q. Study of Molecular Junctions with Combined Surface-Enhanced Raman and Mechanically Controllable Break Junction Method. *J. Am. Chem. Soc.* **2006**, *128*, 14748–14749.
- (377) Tsutsui, M.; Teramae, Y.; Kurokawa, S.; Sakai, A. High-Conductance States of Single Benzenedithiol Molecules. *Appl. Phys. Lett.* **2006**, *89*, 163111.
- (378) Ghosh, S.; Halimun, H.; Mahapatro, A. K.; Choi, J.; Lodha, L.; Janes, D. Device Structure for Electronic Transport through Individual Molecules Using Nanoelectrodes. *Appl. Phys. Lett.* **2005**, *87*, 233509.
- (379) Xiao, X.; Xu, B.; Tao, N. J. Measurement of Single Molecule Conductance: Benzenedithiol and Benzenedimethanethiol. *Nano Lett.* **2004**, *4*, 267–271.
- (380) Xing, Y.; Park, T.-H.; Venkatramani, R.; Keinan, S.; Beratan, D. N.; Therien, M. J.; Borguet, E. Optimizing Single-Molecule Conductivity of Conjugated Organic Oligomers with Carbodithioate Linkers. *J. Am. Chem. Soc.* **2010**, *132*, 7946–7956.
- (381) Vonlanthen, D.; Mishchenko, A.; Elbing, M.; Neuburger, M.; Wandlowski, T.; Mayor, M. Chemically Controlled Conductivity: Torsion-Angle Dependence in a Single-Molecule Biphenyldithiol Junction. *Angew. Chem., Int. Ed.* **2009**, *48*, 8886–8890.
- (382) Tsutsui, M.; Taniguchi, T.; Kawai, T. Quantitative Evaluation of Metal–Molecule Contact Stability at the Single-Molecule Level. *J. Am. Chem. Soc.* **2009**, *131*, 10552–10556.
- (383) Martin, C. A.; Ding, D.; Sørensen, J. K.; Bjørnholm, T.; van Ruitenbeek, J. M.; van der Zant, H. S. J. Fullerene-Based Anchoring Groups for Molecular Electronics. *J. Am. Chem. Soc.* **2008**, *130*, 13198–13199.
- (384) Venkataraman, L.; Park, Y. S.; Whalley, A. C.; Nuckolls, C.; Hybertsen, M. S.; Steigerwald, M. L. Electronics and Chemistry: Varying Single Molecule Junction Conductance with Chemical Substituent. *Nano Lett.* **2007**, *7*, 502–506.
- (385) Dell’Angela, M.; Kladnik, G.; Cossaro, A.; Verdini, A.; Kamenetska, M.; Tamblyn, I.; Quek, S. Y.; Neaton, J. B.; Cvetko, D.; Morgante, A.; Venkataraman, L. Relating Energy Level Alignment and Amine-Linked Single Molecule Junction Conductance. *Nano Lett.* **2010**, *10*, 2470–2474.
- (386) Venkataraman, L.; Klare, J. E.; Nuckolls, C.; Hybertsen, M. S.; Steigerwald, M. L. Dependence of Single-Molecule Junction Conductance on Molecular Conformation. *Nature* **2006**, *442*, 904–907.
- (387) Vázquez, H.; Skouta, R.; Schneebeil, S.; Kamenetska, M.; Breslow, R.; Venkataraman, L.; Hybertsen, M. S. Probing the Conductance Superposition Law in Single Molecule Circuits with Parallel Paths. *Nat. Nanotechnol.* **2012**, *7*, 663–667.
- (388) Chen, W.; Widawsky, J. R.; Vázquez, H.; Schneebeil, S. T.; Hybertsen, M. S.; Breslow, R.; Venkataraman, L. Highly Conducting Pi-Conjugated Molecular Junctions Covalently Bonded to Gold Electrode. *J. Am. Chem. Soc.* **2011**, *133*, 17160–17163.
- (389) Schneebeil, S.; Kamenetska, M.; Foss, F.; Vázquez, H.; Skouta, R.; Hybertsen, M.; Venkataraman, L.; Breslow, R. The Electrical Properties of Biphenylenes. *Org. Lett.* **2010**, *12*, 4114–4117.
- (390) Mishchenko, A.; Zotti, L. A.; Vonlanthen, D.; Bürkle, M.; Pauly, F.; Cuevas, J. C.; Mayor, M.; Wandlowski, T. Single-Molecule Junctions Based on Nitrile-Terminated Biphenyls: A Promising New Anchoring Group. *J. Am. Chem. Soc.* **2011**, *133*, 184–187.
- (391) Widawsky, J. R.; Darancet, P.; Neaton, J. B.; Venkataraman, L. Simultaneous Determination of Conductance and Thermopower of Single Molecule Junctions. *Nano Lett.* **2012**, *12*, 354–358.
- (392) Aradhya, S. V.; Frei, M.; Hybertsen, M. S.; Venkataraman, L. van der Waals Interactions in Metal–Organic Interfaces at the Single-Molecule Level. *Nat. Mater.* **2012**, *11*, 872–876.

- (393) Quek, S. Y.; Kamenetska, M.; Steigerwald, M. L.; Choi, H. J.; Louie, S. G.; Hybertsen, M. S.; Neaton, J.; Venkataraman, L. Mechanically-Controlled Binary Conductance Switching of a Single-Molecule Junction. *Nat. Nanotechnol.* **2009**, *4*, 230–234.
- (394) Kamenetska, M.; Quek, S. Y.; Whalley, A. C.; Steigerwald, M. L.; Choi, H. J.; Louie, S. G.; Nuckolls, C.; Hybertsen, M. S.; Neaton, J. B.; Venkataraman, L. Conductance and Geometry of Pyridine-Linked Single-Molecule Junctions. *J. Am. Chem. Soc.* **2010**, *132*, 6817–6821.
- (395) Lörtscher, E.; Weber, H. B.; Riel, H. Statistical Approach to Investigating Transport through Single Molecule. *Phys. Rev. Lett.* **2007**, *98*, 176807.
- (396) Xu, B. Q.; Li, X. L.; Xiao, X. Y.; Sakaguchi, H.; Tao, N. J. Electromechanical and Conductance Switching Properties of Single Oligothiophene Molecules. *Nano Lett.* **2005**, *5*, 1491–1495.
- (397) Aradhya, S. V.; Meisner, J. S.; Krikorian, M.; Ahn, S.; Parameswaran, R.; Steigerwald, M. L.; Nuckolls, C.; Venkataraman, L. Dissecting Contact Mechanics from Quantum Interference in Single-Molecule Junctions of Stilbene Derivatives. *Nano Lett.* **2012**, *12*, 1643–1647.
- (398) Meisner, J. S.; Ahn, S.; Aradhya, S. V.; Krikorian, M.; Parameswaran, R.; Steigerwald, M. L.; Venkataraman, L.; Nuckolls, C. The Importance of Direct Metal- $\pi$  Coupling in Electronic Transport Through Conjugated Single-Molecule Junctions. *J. Am. Chem. Soc.* **2012**, *134*, 20440–20445.
- (399) Zotti, L. A.; Kirchner, T.; Cuevas, J.-C.; Pauly, F.; Huhn, T.; Scheer, E.; Erbe, A. Revealing the Role of Anchoring Groups in the Electrical Conduction Through Single-Molecule Junctions. *Small* **2010**, *6*, 1529–1535.
- (400) Xiao, X. Y.; Nagahara, L. A.; Rawlett, A.; Tao, N. J. Electrochemical Gate-Controlled Conductance of Single Oligo-(phenylene ethynylene)s. *J. Am. Chem. Soc.* **2005**, *127*, 9235–9240.
- (401) Kornilovich, P. E.; Bratkovsky, A. M.; Williams, R. S. Current Rectification by Molecules with Asymmetric Tunneling Barriers. *Phys. Rev. B* **2002**, *66*, 165436.
- (402) Moreno-García, P.; Gulcur, M.; Manrique, D. Z.; Pope, T.; Hong, W.; Kaliginedi, V.; Huang, C.; Batsanov, A. S.; Bryce, M. R.; Lambert, C.; Wandlowski, T. Single-Molecule Conductance of Functionalized Oligoynes: Length Dependence and Junction Evolution. *J. Am. Chem. Soc.* **2013**, *135*, 12228–12240.
- (403) Kaliginedi, V.; Moreno-García, P.; Valkenier, H.; Hong, W.; García-Suárez, V. M.; Buitner, P.; Otten, J. L. H.; Hummelen, J. C.; Lambert, C. J.; Wandlowski, T. Correlations between Molecular Structure and Single-Junction Conductance: A Case Study with Oligo(phenylene-ethynylene)-Type Wires. *J. Am. Chem. Soc.* **2012**, *134*, 5262–5275.
- (404) Huber, R.; González, M. T.; Wu, S.; Langer, M.; Grunder, G.; Horhoiu, V.; Mayor, M.; Bryce, M. R.; Wang, C.; Jitchati, R.; Schönenberger, C.; Calame, M. Electrical Conductance of Conjugated Oligomers at the Single-Molecule Level. *J. Am. Chem. Soc.* **2008**, *130*, 1080–1084.
- (405) Valkenier, H.; Guédon, C. M.; Markussen, T.; Thygesen, K. S.; van der Molen, S. J.; Hummelen, J. C. Cross-Conjugation and Quantum Interference: A General Correlation? *Phys. Chem. Chem. Phys.* **2014**, *16*, 653–662.
- (406) Frisenda, R.; Perrin, M. L.; Valkenier, H.; Hummelen, J. C.; van der Zant, H. S. J. Statistical Analysis of Single-Molecule Breaking Traces. *Phys. Status Solidi B* **2013**, *250*, 2431–2436.
- (407) Liu, K.; Wang, X.; Wang, F. Probing Charge Transport of Ruthenium-Complex-Based Molecular Wires at the Single-Molecule Level. *ACS Nano* **2008**, *2*, 2315–2323.
- (408) Guédon, C. M.; Valkenier, H.; Markussen, T.; Thygesen, K. S.; Hummelen, J. C.; van der Molen, S. J. Observation of Quantum Interference in Molecular Charge Transport. *Nat. Nanotechnol.* **2012**, *7*, 305–309.
- (409) Hong, W.; Valkenier, H.; Mészáros, G.; Manrique, D. Z.; Mishchenko, A.; Putz, A.; Moreno-García, P.; Lambert, C. J.; Hummelen, J. C.; Wandlowski, T. An MCBJ Case Study: The Influence of  $\pi$ -Conjugation on the Single-Molecule Conductance at a Solid/Liquid Interface. *Beilstein J. Nanotechnol.* **2011**, *2*, 699–713.
- (410) Perrin, M. L.; Frisenda, R.; Koole, M.; Seldenthuis, J. S.; Ceils Gil, J. A.; Valkenier, H.; Hummelen, J. C.; Renaud, N.; Grozema, F. C.; Thijssen, J. M.; Dulić, D.; van der Zant, H. S. J. Large Negative Differential Conductance in Single-Molecule Break Junctions. *Nat. Nanotechnol.* **2014**, *9*, 830–834.
- (411) Weibel, N.; Błaszczak, A.; von Hänisch, C.; Mayor, M.; Pobelov, I.; Wandlowski, T.; Chen, F.; Tao, N. Redox-Active Catechol-Functionalized Molecular Rods: Suitable Protection Groups and Single-Molecule Transport Investigations. *Eur. J. Org. Chem.* **2008**, *1*, 136–149.
- (412) Parker, C. R.; Wei, Z.; Arroyo, C. R.; Jennum, K.; Li, T.; Santella, M.; Bovet, N.; Zhao, G.; Hu, W.; van der Zant, H. S. J.; Vanin, M.; Solomon, G. C.; Larsen, B. W.; Nørgaard, K.; Nielsen, M. B. A New Class of Extended Tetrathiafulvalene Cruciform Molecules for Molecular Electronics with Dithiafulvene-4,5-Dithiolate Anchoring Groups. *Adv. Mater.* **2013**, *25*, 405.
- (413) He, J.; Chen, F.; Li, J.; Sankey, O. F.; Terazono, Y.; Herrero, C.; Gust, D.; Moore, T. A.; Moore, A. L.; Lindsay, S. M. Electronic Decay Constant of Carotenoid Polyenes from Single-Molecule Measurements. *J. Am. Chem. Soc.* **2005**, *127*, 1384–1385.
- (414) Meisner, J. S.; Kamenetska, M.; Krikorian, M.; Steigerwald, M. L.; Venkataraman, L.; Nuckolls, C. A Single-Molecule Potentiometer. *Nano Lett.* **2011**, *11*, 1575–1579.
- (415) Li, X.; Hihath, J.; Chen, F.; Masuda, T.; Zang, L.; Tao, N. Thermally Activated Electron Transport in Single Redox Molecules. *J. Am. Chem. Soc.* **2007**, *129*, 11535–11542.
- (416) Schneebeli, S.; Kamenetska, M.; Cheng, Z.; Skouta, R.; Friesner, R. A.; Venkataraman, L.; Breslow, R. Single-Molecule Conductance through Multiple  $\pi$ - $\pi$  Stacked Benzene Rings Determined with Direct Electrode-to-Benzene Ring Connections. *J. Am. Chem. Soc.* **2011**, *133*, 2136–2139.
- (417) Yamada, R.; Kunazawa, H.; Notoushi, T.; Tanaka, S.; Tada, H. Electrical Conduction of Oligothiophene Molecular Wires. *Nano Lett.* **2008**, *8*, 1237–1240.
- (418) Hines, T.; Diez-Perez, I.; Hihath, J.; Liu, H. M.; Wang, Z.-S.; Zhao, J. W.; Zhou, G.; Müllen, K.; Tao, N. J. Transition from Tunneling to Hopping in Single Molecular Junctions by Measuring Length and Temperature Dependence. *J. Am. Chem. Soc.* **2010**, *132*, 11658–11664.
- (419) Diez-Perez, I.; Li, Z.; Hihath, J.; Li, J.; Zhang, C.; Yang, X.; Zang, L.; Dai, Y.; Feng, X.; Müllen, K.; Tao, N. J. Gate-Controlled Electron Transport in Coronenes: Bottom-Up Approach Towards Graphene Transistors. *Nat. Commun.* **2010**, *1*, 31.
- (420) Parameswaran, R.; Widawsky, J. R.; Vazquez, H.; Park, Y. S.; Boardman, B. M.; Nuckolls, C.; Steigerwald, M. L.; Hybertsen, M. S.; Venkataraman, L. Reliable Formation of Single Molecule Junctions with Air-Stable Diphenylphosphine Linkers. *J. Phys. Chem. Lett.* **2010**, *1*, 2114–2119.
- (421) Moreno-García, P.; La Rosa, A.; Koliwoška, V.; Bermejo, D.; Hong, W.; Yoshida, K.; Baghernejad, M.; Filippone, S.; Broekmann, P.; Wandlowski, T.; Martín, N. Charge Transport in  $C_{60}$ -Based Dumbbell-type Molecules: Mechanically Induced Switching between Two Distinct Conductance States. *J. Am. Chem. Soc.* **2015**, *137*, 2318–2327.
- (422) Kawahara, S. L.; Lagoute, J.; Repain, V.; Chacon, C.; Girard, Y.; Rousset, S.; Smogunov, A.; Barreteau, C. Large Magnetoresistance through a Single Molecule Due to a Spin-Split Hybridized Orbital. *Nano Lett.* **2012**, *12*, 4558–4563.
- (423) Iacovita, C.; Rastei, M. V.; Heinrich, B. W.; Brumme, T.; Kortus, J.; Limot, L.; Bucher, J. P. Visualizing the Spin of Individual Cobalt-Phthalocyanine Molecules. *Phys. Rev. Lett.* **2008**, *101*, 116602.
- (424) Brede, J.; Atodiresei, N.; Kuck, S.; Lazic, P.; Caciuc, V.; Morikawa, Y.; Hoffmann, G.; Blügel, S.; Wiesendanger, R. Spin- and Energy-Dependent Tunneling through a Single Molecule with Intramolecular Spatial Resolution. *Phys. Rev. Lett.* **2010**, *105*, 047204.
- (425) Schmaus, S.; Bagrets, A.; Nahas, Y.; Yamada, T. K.; Bork, A.; Bowen, M.; Beaurepaire, E.; Evers, F.; Wulfhekel, W. Giant Magnetoresistance through a Single Molecule. *Nat. Nanotechnol.* **2011**, *6*, 185–189.
- (426) Schwöbel, J.; Fu, Y.; Brede, J.; Dilullo, A.; Hoffmann, G.; Klyatskaya, S.; Ruben, M.; Wiesendanger, R. Real-Space Observation of

Spin-Split Molecular Orbitals of Adsorbed Single-Molecule Magnets. *Nat. Commun.* **2012**, *3*, 953.

(427) Vincent, R.; Klyatskaya, S.; Ruben, M.; Wernsdorfer, W.; Balestro, F. Electronic Read-Out of a Single Nuclear Spin Using Molecular Spin Transistor. *Nature* **2012**, *488*, 357–360.

(428) Roy, X.; Schenck, C. L.; Ahn, S.; Lalancette, R. A.; Venkataraman, L.; Nuckolls, C.; Steigerwald, M. L. Quantum Soldering of Individual Quantum Dots. *Angew. Chem., Int. Ed.* **2012**, *51*, 12473–12476.

(429) Xiao, X.; Brune, D.; He, J.; Lindsay, S.; Gorman, C. B.; Tao, N. Redox-Gated Electron Transport in Electrically Wired Ferrocene Molecules. *Chem. Phys.* **2006**, *326*, 138–143.

(430) Osorio, E. A.; Moth-Poulsen, K.; van der Zant, H. S. J.; Paaske, J.; Hedegård, P.; Flensburg, K.; Bendix, J.; Bjørnholm, T. Electrical Manipulation of Spin States in Single Electrostatically Gated Transition-Metal Complex. *Nano Lett.* **2010**, *10*, 105–110.

(431) Jo, M.-H.; Grose, J. E.; Baheti, K.; Deshmukh, M. M.; Sokol, J. J.; Rumberger, E. M.; Hendrickson, D. N.; Long, J. R.; Park, H.; Ralph, D. C. Signatures of Molecular Magnetism in Single-Molecule Transport Spectroscopy. *Nano Lett.* **2006**, *6*, 2014–2020.

(432) Heersche, H. B.; de Groot, Z.; Folk, J. A.; van der Zant, H. S. J.; Romeike, C.; Wegewijs, M. R.; Zobbi, L.; Barreca, D.; Tondello, E.; Cornia, A. Electron Transport through Single Mn<sub>12</sub> Molecular Magnets. *Phys. Rev. Lett.* **2006**, *96*, 206801.

(433) Zyazin, A. S.; van der Berg, J. W. G.; Osorio, E. A.; van der Zant, H. S. J.; Konstantinidis, N. P.; Leijnse, M.; Wegewijs, M. R.; May, F.; Hofstetter, W.; Danieli, C.; Cornia, A. Electric-Field-Controlled Magnetic Anisotropy in a Single Molecule. *Nano Lett.* **2010**, *10*, 3307–3311.

(434) Xu, B.; Zhang, P.; Li, X.; Tao, N. Direct Conductance Measurement of Single DNA Molecules in Aqueous Solution. *Nano Lett.* **2004**, *4*, 1105–1108.

(435) Hihath, J.; Chen, F.; Zhang, P.; Tao, N. Thermal and Electrochemical Gate Effects on DNA Conductance. *J. Phys.: Condens. Matter* **2007**, *19*, 215202.

(436) Hybertsen, M. S.; Venkataraman, L.; Klare, J. E.; Whalley, A. C.; Steigerwald, M. L.; Nuckolls, C. Amine-Linked Single-Molecule Circuits: Systematic Trends across Molecular Families. *J. Phys.: Condens. Matter* **2008**, *20*, 374115.

(437) Bergren, A. J.; McCreery, R. L.; Stoyanov, S. R.; Gusarov, S.; Kovalenko, A. Electronic Characteristics and Charge Transport Mechanisms for Large-Area Aromatic Molecular Junctions. *J. Phys. Chem. C* **2010**, *114*, 15806–15815.

(438) van Dijk, E. H.; Myles, D. J. T.; van der Veen, M. H.; Hummelen, J. C. Synthesis and Properties of an Anthraquinone-Based Redox Switch for Molecular Electronics. *Org. Lett.* **2006**, *8*, 2333–2336.

(439) Ward, D. R.; Halas, N. J.; Cizek, J. W.; Tour, J. M.; Wu, Y.; Nordlander, P.; Natelson, D. Simultaneous Measurement of Electronic Conduction and Raman Response in Molecular Junctions. *Nano Lett.* **2008**, *8*, 919–924.

(440) Stipe, B. C.; Rezaei, M. A.; Ho, W. Single-Molecule Vibrational Spectroscopy and Microscopy. *Science* **1998**, *280*, 1732–1735.

(441) Rubio, G.; Agraït, N.; Vieira, S. Atomic-Sized Metallic Contacts: Mechanical Properties and Electronic Transport. *Phys. Rev. Lett.* **1996**, *76*, 2302–2305.

(442) Xu, B. Q.; Xiao, X.; Tao, N. J. Measurement of Single-Molecule Electromechanical Properties. *J. Am. Chem. Soc.* **2003**, *125*, 16164–16165.

(443) Ternes, M.; González, C.; Lutz, C. P.; Hapala, P.; Giessibl, F. J.; Jelínek, P.; Heinrich, A. J. Interplay of Conductance, Force, and Structural Change in Metallic Point Contacts. *Phys. Rev. Lett.* **2011**, *106*, 016802.

(444) Wagner, C.; Fournier, N.; Tautz, F. S.; Temirov, R. Measurement of the Binding Energies of the Organic-Metal Perylene-Teracarboxylic-Dianhydride/Au(111) Bonds by Molecular Manipulation Using an Atomic Force Microscope. *Phys. Rev. Lett.* **2012**, *109*, 076102.

(445) Liu, Z.; Ding, S.-Y.; Chen, Z.-B.; Wang, X.; Tian, J.-H.; Anema, J. R.; Zhou, X.-S.; Wu, D.-Y.; Mao, B.-W.; Xu, X.; Ren, B.; Tian, Z.-Q.

Revealing the Molecular Structure of Single-Molecule Junctions in Different Conductance States by Fishing-Mode Tip-Enhanced Raman Spectroscopy. *Nat. Commun.* **2011**, *2*, 305–311.

(446) Barnes, W. L. Topical Review: Fluorescence Near Interfaces: The Role of Photonic Mode Density. *J. Mod. Opt.* **1998**, *45*, 661–689.

(447) Hoffmann, G.; Libiouille, L.; Berndt, R. Tunneling-Induced Luminescence from Adsorbed Organic Molecules with Submolecular Lateral Resolution. *Phys. Rev. B* **2002**, *65*, 212107.

(448) Qiu, X. H.; Nazin, G. V.; Ho, W. Vibrationally Resolved Fluorescence Excited with Submolecular Precision. *Science* **2003**, *299*, 542–546.

(449) Hartman, T. E. Tunneling through Asymmetric Barriers. *J. Appl. Phys.* **1964**, *35*, 3283–3294.

(450) Bâldea, I. Revealing Molecular Orbital Gating by Transition Voltage Spectroscopy. *Chem. Phys.* **2010**, *377*, 15–20.

(451) Aradai, M.; Tsukuda, M. Theoretical Calculations of Electron Transport in Molecular Junctions: Inflection Behavior in Fowler-Nordheim Plot and Its Origin. *Phys. Rev. B* **2010**, *81*, 235114.

(452) Pakoulev, A. V.; Burtman, V. Temperature-Dependent Barrier Crossover Regime in Tunneling Single-Molecule Devices Based on the Matrix of Isolated Molecules. *J. Phys. Chem. C* **2009**, *113*, 21413–21421.

(453) Beebe, J. M.; Kim, B.; Frisbie, C. D.; Kushmerick, J. G. Measuring Relative Barrier Heights in Molecular Electronic Junctions with Transition Voltage Spectroscopy. *ACS Nano* **2008**, *2*, 827–832.

(454) Mirjani, F.; Thijssen, J. M.; van der Molen, S. J. Advantages and Limitations of Transition Voltage Spectroscopy: A Theoretical Analysis. *Phys. Rev. B* **2011**, *84*, 115402.

(455) Trouwborst, M. L.; Martin, C. A.; Smit, R. H. M.; Guédon, C. M.; Baart, T. A.; van der Molen, S. J.; van Ruitenbeek, J. M. Transition Voltage Spectroscopy and the Nature of Vacuum Tunneling. *Nano Lett.* **2011**, *11*, 614–617.

(456) Bâldea, I. Transition Voltage Spectroscopy: Artefacts of the Simmons Approach. *J. Phys. Chem. Solids* **2012**, *73*, 1151–1153.

(457) Vilan, A.; Cahen, D.; Kraiser, E. Rethinking Transition Voltage Spectroscopy within a Generic Taylor Expansion View. *ACS Nano* **2013**, *7*, 695–706.

(458) Johnson, M. S.; Kota, R.; Mattern, D. L.; Hill, C. M.; Vasiliu, M.; Dixon, D. A.; Metzger, R. M. A Two-Faced “Janus” Unimolecular Rectifier Exhibits Rectification Reversal. *J. Mater. Chem. C* **2014**, *2*, 9892–9902.

(459) Honciuc, A.; Metzger, R. M.; Gong, A.; Spangler, C. W. Elastic and Inelastic Electron Tunneling Spectroscopy of a New Rectifying Monolayer. *J. Am. Chem. Soc.* **2007**, *129*, 8310–8319.

(460) Sutin, N.; Bruntschwig, B. S.; Creutz, C. Using the Marcus Inverted Region for Rectification in Donor–Bridge–Acceptor Assemblies. *J. Phys. Chem. B* **2003**, *107*, 10687–10690.

(461) Pan, J. B.; Zhang, Z. H.; Deng, X. Q.; Qiu, M.; Guo, C. The Transport Properties of D– $\sigma$ –A Molecules: A Strikingly Opposite Rectification Direction. *Appl. Phys. Lett.* **2011**, *98*, 013503.

(462) Nijhuis, C. A.; Reus, W. F.; Whitesides, G. M. Mechanism of Rectification in Tunneling Junctions Based on Molecules with Asymmetric Potential Drops. *J. Am. Chem. Soc.* **2010**, *132*, 18386–18401.

(463) Stokbro, K.; Taylor, J.; Brandbyge, M. Do Aviram–Ratner Diodes Rectify? *J. Am. Chem. Soc.* **2003**, *125*, 3674–3675.

(464) Braun, F. Über die Stromleitung durch Schwefelmetalle. *Ann. Phys. Chem.* **1874**, *153*, 556–563.

(465) Liu, R.; Ke, S.-H.; Yang, W.; Baranger, H. U. Organometallic Molecular Rectifiers. *J. Chem. Phys.* **2006**, *124*, 024718.

(466) Chabinyč, M. L.; Chen, X.; Holmlin, R. E.; Jacobs, H.; Skulason, H.; Frisbie, C. D.; Mujica, V.; Ratner, M. A.; Rampi, M. A.; Whitesides, G. M. Molecular Rectification in a Metal–Insulator–Metal Junction Based on Self-Assembled Monolayers. *J. Am. Chem. Soc.* **2002**, *124*, 11730–11736.

(467) Roth, S.; Blumentritt, S.; Burghard, M.; Fischer, C. M.; Philipp, G.; Müller-Schwannecke, C. Charge Transport in LB Microsandwiches. *Synth. Met.* **1997**, *86*, 2415–2418.

(468) Scaff, J. H.; Ohl, R. S. Development of Silicon Crystal Rectifiers for Microwave Radar Receivers. *Bell Syst. Tech. J.* **1947**, *26*, 1–30.



- (469) Prince, M. B. Diffused p-n Junction Silicon Rectifiers. *Bell. Syst. Tech. J.* **1956**, *36*, 661–684.
- (470) Gulians, E. A.; Ji, C.; Song, Y. J.; Anderson, W. A. A 0.5- $\mu\text{m}$ -Thick Polycrystalline Schottky Diode with Rectification Ratio of  $10^6$ . *Appl. Phys. Lett.* **2002**, *80*, 1474–1476.
- (471) Stadler, R.; Geskin, V.; Cornil, J. A Theoretical View of Unimolecular Rectification. *J. Phys.: Condens. Matter* **2008**, *20*, 374105.
- (472) Ebers, J. J.; Moll, J. L. Large-Signal Behavior of Junction Transistors. *Proc. IRE* **1954**, *42*, 1761–1772.
- (473) Chang, S.-C.; Li, Z.; Lau, C. N.; Larade, B.; Williams, R. S. Investigation of a Model Molecular-Electronic Rectifier with an Evaporated Ti-Metal Top Contact. *Appl. Phys. Lett.* **2003**, *83*, 3198–3200.
- (474) Ashwell, G. J.; Stokes, R. J. Do Alkyl Tunneling Barriers Contribute to Molecular Rectification? *J. Mater. Chem.* **2004**, *14*, 1228–1230.
- (475) Sandman, D. J.; Geddes, N. J.; Sambles, J. R.; Parker, W. G. United States Patent 5,057,878, Oct. 15, 1991.
- (476) Sandman, D. J.; Geddes, N. J.; Sambles, J. R.; Parker, W. G. MIM Device and Fabrication Method. United States Patent 5,152,805, Oct. 6, 1992.
- (477) Zhou, C.; Deshpande, M. R.; Reed, M. A.; Jones, L., II; Tour, J. M. Nanoscale Metal/Self-Assembled Monolayer/Metal Heterostructures. *Appl. Phys. Lett.* **1997**, *71*, 611–613.
- (478) Ashwell, G. J.; Urasinska, B.; Tyrrell, W. D. Molecules that Mimic Schottky Diodes. *Phys. Chem. Chem. Phys.* **2006**, *8*, 3314–3319.
- (479) Van Dyck, C.; Ratner, M. Molecular Rectifiers: A New Design Based on Asymmetric Anchoring Moieties. *Nano Lett.* **2015**, *15*, 1577–1584.
- (480) Ashwell, G. J.; Paxton, G. A. N. Multifunctional Properties of Z- $\beta$ -(N-Hexadecyl-quinolinium)- $\alpha$ -cyano-4-styryldicyanomethanide: A Molecular Rectifier, Optically Non-Linear Dye, and Ammonia Sensor. *Aust. J. Chem.* **2002**, *55*, 199–204.
- (481) Ashwell, G. J.; Chwialkowska, A.; High, L. R. H. Au-S-C<sub>n</sub>H<sub>2n</sub>-Q3CNQ: Self-Assembled Monolayers for Molecular Rectification. *J. Mater. Chem.* **2004**, *14*, 2389–2394.
- (482) Honciuc, A.; Otsuka, A.; Wang, Y.-H.; McElwee, S. K.; Woski, S. A.; Saito, G.; Metzger, R. M. Polarization of Charge-Transfer Bands and Rectification in Hexadecylquinolinium 7,7,8-Tricyanoquinodimethanide and Its Tetrafluoro Analog. *J. Phys. Chem. B* **2006**, *110*, 15085–15094.
- (483) Girlando, A.; Sissa, C.; Terenziani, F.; Painelli, A.; Chwialkowska, A.; Ashwell, G. J. In Situ Spectroscopic Characterization of Rectifying Molecular Monolayers Self-Assembled on Gold. *Chem. Phys. Chem.* **2007**, *8*, 2195–2201.
- (484) Ashwell, G. J.; Hamilton, R.; High, L. R. H. Molecular Rectification: Asymmetric Current–Voltage Curves from Self-Assembled Monolayers of a Donor–(Bridge)–Acceptor Dye. *J. Mater. Chem.* **2003**, *13*, 1501–1503.
- (485) Jaiswal, A.; Amaresh, R. R.; Lakshikantham, M. V.; Honciuc, A.; Cava, M. P.; Metzger, R. M. Electrical Rectification in a Monolayer of Zwitterions Assembled by Either Physisorption or Chemisorption. *Langmuir* **2003**, *19*, 9043–9050.
- (486) Jaiswal, A.; Rajagopal, D.; LakshmiKantham, M. V.; Cava, M. P.; Metzger, R. M. Unimolecular Rectification and Other Properties of CH<sub>3</sub>C(O)S–C<sub>14</sub>H<sub>28</sub>Q<sup>+</sup>–3CNQ<sup>–</sup> and CH<sub>3</sub>C(O)S–C<sub>16</sub>H<sub>32</sub>Q<sup>+</sup>–3CNQ<sup>–</sup> Organized by Self-Assembly, Langmuir–Blodgett, and Langmuir–Schaefer Techniques. *Phys. Chem. Chem. Phys.* **2007**, *9*, 4007–4017.
- (487) Ashwell, G. J.; Tyrrell, W. D.; Whittam, A. J. Molecular Rectification: Self-Assembled Monolayers of a Donor–( $\pi$ -Bridge)–Acceptor Chromophore Connected via a Truncated Au–S–(CH<sub>2</sub>)<sub>3</sub> Bridge. *J. Mater. Chem.* **2003**, *13*, 2855–2857.
- (488) Ashwell, G. J.; Robinson, B. J.; Amiri, M. A.; Locatelli, D.; Quici, S.; Roberto, D. Dipole Reversal in Langmuir–Blodgett Films of an Optically Nonlinear Dye and its Effect on the Polarity for Molecular Rectification. *J. Mater. Chem.* **2005**, *15*, 4203–4205.
- (489) Ashwell, G. J.; Chwialkowska, A.; High, L. R. H. Rectifying Au–S–C<sub>n</sub>H<sub>2n</sub>–P3CNQ Derivatives. *J. Mater. Chem.* **2004**, *14*, 2848–2851.
- (490) Ashwell, G. J.; Chwialkowska, A. Controlled Alignment of Molecular Diodes via Ionic Assembly of Cationic Donor–( $\pi$ -Bridge)–Acceptor Molecules on Anionic Surfaces. *Chem. Commun.* **2006**, 1404–1406.
- (491) Ashwell, G. J.; Mohib, A. Improved Molecular Rectification from Self-Assembled Monolayers of a Sterically Hindered Dye. *J. Am. Chem. Soc.* **2005**, *127*, 16238–16244.
- (492) Baldwin, J. W.; Amaresh, R. R.; Peterson, I. R.; Shumate, W. J.; Cava, M. P.; Amiri, M. A.; Hamilton, R.; Ashwell, G. J.; Metzger, R. M. Rectification and Nonlinear Optical Properties of a Langmuir–Blodgett Monolayer of a Pyridinium Dye. *J. Phys. Chem. B* **2002**, *106*, 12158–12164.
- (493) Honciuc, A.; Jaiswal, A.; Gong, A.; Ashworth, K.; Spangler, C. W.; Peterson, I. R.; Dalton, L. R.; Metzger, R. M. Current Rectification in a Langmuir–Schaefer Monolayer of Fullerene-bis-[4-diphenylamino-4''-(N-ethyl-N-2''-ethyl)amino-1,4-diphenyl-1,3-butadiene] Malonate between Au Electrodes. *J. Phys. Chem. B* **2005**, *109*, 857–871.
- (494) Shumate, W. J.; Mattern, D. L.; Jaiswal, A.; Burgess, J.; Dixon, D. A.; White, T. R.; Honciuc, A.; Metzger, R. M. Spectroscopic and Rectification Studies of Three Donor–Sigma–Acceptor Compounds, Consisting of a One-Electron Donor (Pyrene or Ferrocene), a One-Electron Acceptor (Perylenebisimide), and a C19 Swallowtail. *J. Phys. Chem. B* **2006**, *110*, 11146–11159.
- (495) Shumate, W. J. Ph.D. Dissertation, University of Alabama, Tuscaloosa, AL, 2005.
- (496) Ng, M.-K.; Yu, L. Synthesis of Amphiphilic Conjugated Diblock Oligomers as Molecular Diodes. *Angew. Chem., Int. Ed.* **2002**, *41*, 3598–3601.
- (497) Jiang, P.; Morales, G. M.; You, W.; Yu, L. P. Synthesis of Diode Molecules and Their Sequential Assembly to Control Electron Transport. *Angew. Chem., Int. Ed.* **2004**, *43*, 4471–4475.
- (498) Elbing, M.; Ochs, R.; Keontopp, M.; Fischer, M.; von Hänisch, C.; Weigend, F.; Evers, F.; Weber, H. B.; Mayor, M. A Single-Molecule Diode. *Proc. Natl. Acad. Sci. U.S.A.* **2005**, *102*, 8815–8820.
- (499) Morales, G. M.; Jiang, J.; Yuan, S.; Lee, Y.; Sanchez, A.; You, W.; Yu, L. Inversion of the Rectifying Effect in Diblock Molecular Diodes by Protonation. *J. Am. Chem. Soc.* **2005**, *127*, 10456–10457.
- (500) Ashwell, G. J.; Ewington, J.; Robinson, B. J. Organic Rectifying Junctions Fabricated by Ionic Coupling. *Chem. Commun.* **2006**, 618–620.
- (501) Lenfant, S.; Guerin, D.; Van, F. T.; Chevrot, C.; Palacin, S.; Bourgoin, J.-P.; Bouloussa, O.; Rondelez, F.; Delerue, C.; Vuillaume, D. Electron Transport through Rectifying Self-Assembled Monolayer Diodes on Silicon: Fermi-Level Pinning at the Molecule–Metal Interface. *J. Phys. Chem. B* **2006**, *110*, 13947–13958.
- (502) Fracasso, D.; Valkenier, H.; Hummelen, J. C.; Solomon, G. C.; Chiechi, R. C. Evidence for Quantum Interference in SAMs of Arylethynylene Thiolates in Tunneling Junctions with Eutectic Ga–In (EGaIn) Top-Contacts. *J. Am. Chem. Soc.* **2011**, *133*, 9556–9563.
- (503) Yee, S. K.; Sun, J.; Darancet, P.; Tilley, T. D.; Majumdar, A.; Neaton, J. B.; Segalman, R. A. Inverse Rectification in Donor–Acceptor Molecular Heterojunctions. *ACS Nano* **2011**, *5*, 9256–9263.
- (504) Wickramasinghe, L. D.; Perera, M. M.; Li, L.; Mao, G.; Zhou, Z.; Verani, C. N. Rectification in Nanoscale Devices Based on an Asymmetric Five-Coordinate Iron(III) Phenolate Complex. *Angew. Chem., Int. Ed.* **2013**, *52*, 13346–13350.
- (505) Lee, Y.; Yuan, S.; Sanchez, A.; Yu, L. Charge Transport Mediated by d-Orbitals in Transition Metal Complexes. *Chem. Commun.* **2008**, 247–249.
- (506) Gayathri, S. S.; Patnaik, A. Electrical Rectification from a Fullerene[60]-Dyad Based Metal–Organic–Metal Junction. *Chem. Commun.* **2006**, 1977–1979.
- (507) Luo, L.; Balhorn, L.; Vlaisavljevich, B.; Ma, D.; Gagliardi, L.; Frisbie, C. D. Hopping Transport and Rectifying Behavior in Long Donor–Acceptor Molecular Wires. *J. Phys. Chem. C* **2014**, *118*, 26485–26497.
- (508) Baldwin, J. W.; Chen, B.; Street, S. C.; Konovalov, V. V.; Sakurai, H.; Hughes, T. V.; Simpson, C. S.; LakshmiKantham, M. V.; Cava, M. P.; Kispert, L. D.; Metzger, R. M. Spectroscopic Studies of Hexadecylqui-

nolinium Tricyanoquinodimethanide. *J. Phys. Chem. B* **1999**, *103*, 4269–4277.

(509) Metzger, R. M.; Heimer, N. E.; Ashwell, G. J. Crystal and Molecular Structure and Properties of Picolytricyanoquinodimethan, the Zwitterionic Donor– $\pi$ –Acceptor Adduct between  $\text{Li}^+\text{TCNQ}^-$  and 1,2-Dimethylpyridinium Iodide. *Mol. Cryst. Liq. Cryst.* **1984**, *107*, 133–149.

(510) Bell, N. A.; Crouch, D. J.; Simmonds, D. J.; Goeta, A. E.; Gelbrich, T.; Hursthouse, M. B. Structural and Solvatochromic Studies of a Series of Tricyanoquinodimethane-Based Zwitterions. *J. Mater. Chem.* **2002**, *12*, 1274–1279.

(511) Krzeminski, C.; Delerue, C.; Allan, G.; Vuillaume, D.; Metzger, R. M. Theory of Rectification in a Molecular Monolayer. *Phys. Rev. B* **2001**, *64*, 085405.

(512) Broo, A.; Zerner, M. C. Electronic Structure of Donor–Spacer–Acceptor Molecules of Potential Interest for Molecular Electronics. IV Geometry and Device Properties of P3CNQ and Q3CNQ. *Chem. Phys.* **1995**, *196*, 423–436.

(513) Pickholz, M.; dos Santos, M. C. AM1/CI Study of a Molecular Rectifier. *J. Mol. Struct.: THEOCHEM* **1998**, *432*, 89–96.

(514) Hoffmann, R. Interaction of Orbitals Through Space and Through Bonds. *Acc. Chem. Res.* **1971**, *4*, 1–9.

(515) Ashwell, G. J.; Berry, M. Hybrid SAM/LB Device Structures: Manipulation of the Molecular Orientation for Nanoscale Electronic Applications. *J. Mater. Chem.* **2004**, *14*, 108–110.

(516) Ashwell, G. J.; Tyrrell, W. D.; Whittam, A. J. Molecular Rectification: Self-Assembled Monolayers in Which Donor–( $\pi$ -Bridge)–Acceptor Moieties Are Centrally Located and Symmetrically Coupled to Both Gold Electrodes. *J. Am. Chem. Soc.* **2004**, *126*, 7102–7110.

(517) Meinhard, J. E. Organic Rectifying Junction. *J. Appl. Phys.* **1964**, *35*, 3059–3060.

(518) Pietro, W. J. Rectifying Junctions Based on Metallophthalocyanine Thin Films. *Adv. Mater.* **1994**, *6*, 239–242.

(519) Hamm, S.; Wachtel, H. Rectifying Organic Junctions of Molecular Assemblies Based on Perylene Ion Salts. *J. Chem. Phys.* **1995**, *103*, 10689–10695.

(520) Polymeropoulos, E. E.; Möbius, D.; Kuhn, H. Monolayer Assemblies with Functional Units of Sensitizing and Conducting Molecular Components: Photovoltage, Dark Conduction, and Photoconduction in Systems with Aluminium and Barium Electrodes. *Thin Solid Films* **1980**, *68*, 173–190.

(521) Sugi, M.; Sakai, K.; Saito, M.; Kawabata, Y.; Iizima, S. Photoelectric Effects in Heterojunction Langmuir–Blodgett Film Diodes. *Thin Solid Films* **1985**, *132*, 69–76.

(522) Fischer, C. M.; Burghard, M.; Roth, S.; v. Klitzing, K. Organic Quantum Wells: Molecular Rectification and Single-Electron Tunneling. *Europhys. Lett.* **1994**, *28*, 129–134.

(523) Schmelzer, M.; Burghard, M.; Fischer, C. M.; Roth, S.; Göpel, W. With Organized Metal/Organic Film/Metal Heterostructures Towards Molecular Electronic Devices. *Synth. Met.* **1995**, *71*, 2087–2088.

(524) Fischer, C. M.; Burghard, M.; Roth, S. Dark Conductivity and Photoconductivity of Asymmetric Gold/(Langmuir–Blodgett Film)/Gold Tunnel Junctions. *Synth. Met.* **1996**, *76*, 237–240.

(525) Brady, A. C.; Hodder, B.; Martin, A. S.; Sambles, J. R.; Ewels, C. P.; Jones, R.; Briddon, P. R.; Musa, A. M.; Panetta, C. A.; Mattern, D. L. Molecular Rectification with MID $\sigma$ A LB Film/M Junctions. *J. Mater. Chem.* **1999**, *9*, 2271–2275.

(526) Ashwell, G. J.; Gandolfo, D. S. Molecular Rectification Using a Gold/(LB Film)/Gold Structure. *J. Mater. Chem.* **2001**, *11*, 246–248.

(527) Ashwell, G. J.; Gandolfo, D. S.; Hamilton, R. Molecular Rectification: Characterization of a Dye Sandwiched between Gold Electrodes. *J. Mater. Chem.* **2002**, *12*, 416–420.

(528) Zhou, S.; Liu, Y.; Qui, W.; Xu, Y.; Huang, X.; Li, Y.; Jiang, L.; Zhu, D. Synthetic Molecular Rectifier of a Langmuir–Blodgett Film Based on a Novel Asymmetrically Substituted Dicyano-tri-*tert*-butylphthalocyanine. *Adv. Funct. Mater.* **2002**, *12*, 65–60.

(529) Cingolani, R.; Rinaldi, R.; Maruccio, G.; Biasco, A. Nanotechnology Approaches to Self-Organized Bio-Molecular Devices. *Physica E* **2002**, *13*, 1229–1235.

(530) Ashwell, G. J.; Gandolfo, D. S. Molecular Rectification: Dipole Reversal in a Cationic Donor–( $\pi$  Bridge)–Acceptor Dye. *J. Mater. Chem.* **2002**, *12*, 411–415.

(531) Pomerantz, M.; Aviram, A.; McCorkle, R. A.; Li, L.; Schrott, A. G. Rectification of STM Current to Graphite Covered with Phthalocyanine Molecules. *Science* **1992**, *255*, 1115–1118.

(532) Stabel, A.; Herwig, P.; Müllen, K.; Rabe, J. P. Diodelike Current–Voltage Curves for a Single Molecule–Tunneling Spectroscopy with Submolecular Resolution of an Alkylated, *peri*-Condensed Hexabenzocoronene. *Angew. Chem., Int. Ed.* **1995**, *34*, 1609–1611.

(533) Dhirani, A.; Lin, P.-H.; Guyot-Sionnest, P.; Zehner, R. W.; Sita, L. R. Self-Assembled Molecular Rectifiers. *J. Chem. Phys.* **1997**, *106*, 5249–5243.

(534) Langer, J. J.; Martynski, M. Nano-Scale Protonic Rectifier: A Preliminary Report. *Synth. Met.* **1999**, *102*, 1160–1161.

(535) Weiss, E. A.; Chiechi, R. C.; Kaufman, G. K.; Kriebel, J. K.; Li, Z.; Duati, M.; Rampi, M. A.; Whitesides, G. M. Influence of Defects on the Electrical Characteristics of Mercury–Drop Junctions: Self-Assembled Monolayers of *n*-Alkanethiolates on Rough and Smooth Silver. *J. Am. Chem. Soc.* **2007**, *129*, 4336–4349.

(536) Chiechi, R. C.; Weiss, E. A.; Dickey, M. D.; Whitesides, G. M. Gallium–Indium (EGaIn): A Moldable Liquid Metal for Electrical Characterization of Self-Assembled Monolayers. *Angew. Chem., Int. Ed.* **2008**, *47*, 142–144.

(537) Dickey, M. D.; Chiechi, R. C.; Larsen, R. J.; Weiss, E. A.; Weitz, D. A.; Whitesides, G. M. Eutectic Gallium–Indium (EGaIn): A Liquid Metal Alloy for the Formation of Stable Structures in Microchannels at Room Temperature. *Adv. Funct. Mater.* **2008**, *18*, 1097–1104.

(538) Thuo, M. M.; Reus, W. F.; Nijhuis, C. A.; Barber, J. R.; Kim, C.; Schulz, M. D.; Whitesides, G. M. Odd–Even Effects in Charge Transport across Self-Assembled Monolayers. *J. Am. Chem. Soc.* **2011**, *133*, 2962–2975.

(539) Fujihira, M.; Nishiyama, K.; Yamada, H. Photoelectrochemical Responses of Optically Transient Electrodes Modified with Langmuir–Blodgett Films Consisting of Surfactant Derivatives of Electron Donor, Acceptor and Sensitizer Molecules. *Thin Solid Films* **1986**, *132*, 77–82.

(540) Choi, J.-W.; Jung, G.-Y.; Oh, S. Y.; Lee, W. H.; Shin, D. M. Photoinduced Electron Transfer in a MIM Device Composed of TCNQ–Pyrene–Ferrocene LB Films. *Thin Solid Films* **1996**, *284*–285, 876–878.

(541) Choi, J.-W.; Kim, M. J.; Chung, S. W.; Oh, S. Y.; Lee, W. H.; Shin, D. M. Molecular Photodiode Consisting of Flavin–Viologen Hetero-Langmuir–Blodgett Films. *Mol. Cryst. Liq. Cryst.* **1996**, *280*, 367–372.

(542) Choi, J.-W.; Kim, M. J.; Chung, S. W.; Oh, S. Y.; Shin, D. M.; Lee, W. H. Molecular Photodiode Consisting of Flavin–Viologen–TCNQ LB Multilayers. *Mol. Cryst. Liq. Cryst.* **1997**, *294*, 217–220.

(543) Choi, J.-W.; Chung, W. S.; Oh, S. Y.; Lee, W. H.; Shin, D. M. Photoinduced Electron Transfer in a MIM Device Composed of Ferrocene–Flavin–Viologen–TCNQ Molecular Heterojunctions. *Thin Solid Films* **1998**, *327*–329, 671–675.

(544) Choi, J.-W.; Nam, Y.-S.; Lee, W.-H.; Kim, D.; Fujihira, M. Rectified Photocurrent of the Protein-Based Bio-Photodiode. *Appl. Phys. Lett.* **2001**, *79*, 1570–1572.

(545) Choi, J.-W.; Nam, Y.-S.; Park, S.-J.; Lee, W.-H.; Kim, D.; Fujihira, M. Rectified Photocurrent of Molecular Photodiode Consisting of Cytochrome *c*/GPF Hetero Thin Films. *Biosens. Bioelectron.* **2001**, *16*, 819–825.

(546) Choi, J.-W.; Nam, Y.-S.; Kong, B.-S.; Lee, W. H.; Park, K. M.; Fujihira, M. Bioelectronic Device Consisting of Cytochrome *c*/poly-L-Aspartic Acid Adsorbed Hetero-Langmuir–Blodgett Films. *J. Biotechnol.* **2002**, *94*, 225–233.

(547) Sato, Y.; Itoigawa, H.; Uosaki, K. Unidirectional Electron Transfer at Self-Assembled Monolayers of 11-Ferrocenyl-1-Undecanethiol on Gold. *Bull. Chem. Soc. Jpn.* **1993**, *66*, 1032–1037.

- (548) Alleman, K. S.; Weber, K.; Creager, S. E. Electrochemical Rectification at a Monolayer-Modified Electrode. *J. Phys. Chem.* **1996**, *100*, 17050–17058.
- (549) Abruña, H. D.; Denisevich, P.; Umaña, M.; Meyer, T. J.; Murray, R. W. Rectifying Interfaces Using Two-Layer Films of Electrochemically Polymerized Vinylpyridine and Vinylbipyridine Complexes of Ruthenium and Iron on Electrodes. *J. Am. Chem. Soc.* **1981**, *103*, 1–5.
- (550) Denisevich, P.; Willman, K. W.; Murray, R. W. Unidirectional Current Flow and Charge State Trapping at Redox Polymer Interfaces on Bilayer Electrodes: Principles, Experimental Demonstration, and Theory. *J. Am. Chem. Soc.* **1981**, *103*, 4727–4737.
- (551) Pickup, P. G.; Kutner, W.; Leidner, C. R.; Murray, R. W. Redox Conduction in Single and Bilayer Films of Redox Polymer. *J. Am. Chem. Soc.* **1984**, *106*, 1991–1998.
- (552) Chidsey, C. E. D.; Murray, R. W. Electroactive Polymers and Macromolecular Electronics. *Science* **1986**, *231*, 25–31.
- (553) Smith, D. K.; Lane, G. A.; Wrighton, M. S. pH Dependence of the Electrochemical Behavior of Surfaces Modified with a Polymer Derived from a Monomer Consisting of Two Viologen Subunits Linked by a Quinone: Evidence for Rectification by Synthetic Molecular Materials. *J. Am. Chem. Soc.* **1986**, *108*, 3522–3525.
- (554) Smith, D. K.; Tender, L. M.; Lane, G. A.; Licht, S.; Wrighton, M. S. Chemically Induced Release of Charge from a Rectifying Polymer Based on Viologen and Quinone Subunits. *J. Am. Chem. Soc.* **1989**, *111*, 1099–1105.
- (555) Palmore, G. T. R.; Smith, D. K.; Wrighton, M. S. pH-Dependent Rectification in Redox Polymers: Characterization of Electrode-Confined Siloxane Polymers Containing Naphthoquinone and Benzylviologen Subunits. *J. Phys. Chem. B* **1997**, *101*, 2437–2450.
- (556) Oh, S.-K.; Baker, L. A.; Crooks, R. M. Electrochemical Rectification Using Mixed Monolayers of Redox-Active Ferrocenyl Dendrimers and *n*-Alkanethiols. *Langmuir* **2002**, *18*, 6981–6987.
- (557) Berchmans, S.; Ramalechume, C.; Lakshmi, V.; Yegnaraman, V. Diode-Like Electron Transfer in Mixed Monolayer Assembly. *J. Mater. Chem.* **2002**, *12*, 2538–2542.
- (558) Galoppini, E.; Fox, M. A. Effect of the Electric Field Generated by the Helix Dipole on Photoinduced Intramolecular Electron Transfer in Dichromophoric  $\alpha$ -Helical Peptides. *J. Am. Chem. Soc.* **1996**, *118*, 2299–2300.
- (559) Bao, D.; Upadhyayula, S.; Larsen, J. M.; Xia, B.; Georgieva, B.; Nuñez, V.; Espinoza, E. M.; Hartman, J. D.; Wurch, M.; Chang, A.; Lin, T.; Larkin, J.; Vasquez, K.; Beran, G. J. O.; Vullev, V. I. Dipole-Mediated Rectification of Intramolecular Photoinduced Charge Separation and Charge Recombination. *J. Am. Chem. Soc.* **2014**, *136*, 12966–12973.
- (560) Lambe, J.; Jaklevic, R. C. Molecular Vibration Spectra by Inelastic Electron Tunneling. *Phys. Rev.* **1968**, *165*, 821–832.
- (561) Jaklevic, R. C.; Lambe, J. Experimental Study of Quantum Size Effects in Thin Metal Films by Electron Tunneling. *Phys. Rev. B* **1975**, *12*, 4146–4160.
- (562) Jaklevic, R. C.; Lambe, J.; Kirtley, J.; Hansma, P. K. Structure at 0.8 eV in Metal–Insulator–Metal Tunneling Junctions. *Phys. Rev. B* **1977**, *15*, 4103–4104.
- (563) Hansma, P. K. Inelastic Electron Tunneling. *Phys. Rep.* **1977**, *30*, 145–206.
- (564) Hansma, P. K.; Kirtley, J. Recent Advances in Inelastic Electron Tunneling Spectroscopy. *Acc. Chem. Res.* **1978**, *11*, 440–445.
- (565) Gauvin, S.; Leblanc, R. M. Inelastic Electron Tunneling Spectrometer for Complete Calibrated Measurements of Any Two or Four Terminal Junctions. *Rev. Sci. Instrum.* **1992**, *63*, 149–156.
- (566) Wang, Y.; Mallik, R. R.; Henriksen, P. N. Easily Realized Inelastic Electron Tunneling Spectrometer. *Rev. Sci. Instrum.* **1993**, *64*, 890–895.
- (567) Hippy, K. W.; Mazur, U. Inelastic Electron Tunneling: An Alternative Molecular Spectroscopy. *J. Phys. Chem.* **1993**, *97*, 7803–7814.
- (568) Honciuc, A. Ph.D. Dissertation, University of Alabama, Tuscaloosa, AL, 2006.
- (569) Galperin, M.; Nitzan, A.; Ratner, M. A.; Stewart, D. R. Molecular Transport Junctions: Asymmetry in Inelastic Tunneling Processes. *J. Phys. Chem. B* **2005**, *109*, 8519–8522.
- (570) Solomon, G. C.; Gagliardi, A.; Pecchia, A.; Frauenheim, T.; Di Carlo, A.; Reimers, J. R.; Hush, N. S. Understanding the Inelastic Electron-Tunneling Spectra of Alkanedithiols on Gold. *J. Chem. Phys.* **2006**, *124*, 094704.
- (571) Hippy, K. W.; Mazur, U.  $^4A_2 \rightarrow ^4T_2$  and  $^4T_2 \rightarrow ^4T_1$  Electronic Transitions in Cobalt (III) Tetrachloride. An FT-IR and Inelastic Electron Tunneling Spectroscopy Study. *J. Am. Chem. Soc.* **1987**, *109*, 3861–3865.
- (572) Mazur, U.; Hippy, K. W. Resonant Tunneling Bands and Electrochemical Reduction Potentials. *J. Phys. Chem.* **1995**, *99*, 6684–6688.
- (573) Stipe, B. C.; Rezaei, M. A.; Ho, W. A Variable-Temperature Scanning Tunneling Microscope Capable of Single-Molecule Vibrational Spectroscopy. *Rev. Sci. Instrum.* **1999**, *70*, 137–143.
- (574) Lauhon, L. J.; Ho, W. Direct Observation of the Quantum Tunneling of Single Hydrogen Atoms with a Scanning Tunneling Microscope. *Phys. Rev. Lett.* **2000**, *85*, 4566–4569.
- (575) Lauhon, L. J.; Ho, W. Effects of Temperature and Other Experimental Variables on Single Molecule Vibrational Spectroscopy with the Scanning Tunneling Microscope. *Rev. Sci. Instrum.* **2001**, *72*, 216–223.
- (576) Ho, W. Single-Molecule Chemistry. *J. Chem. Phys.* **2002**, *117*, 11033–11061.
- (577) Nazin, G. V.; Wu, S. W.; Ho, W. Tunneling Rates in Electron Transport Through Double-Barrier Molecular Junctions in a Scanning Tunneling Microscope. *Proc. Natl. Acad. Sci. U.S.A.* **2005**, *102*, 8832–8837.
- (578) Ogawa, N.; Mikaelian, G.; Ho, W. Spatial Variations in Submolecular Vibronic Spectroscopy on a Thin Insulating Film. *Phys. Rev. Lett.* **2007**, *98*, 166103.
- (579) Nazin, G. V.; Qiu, X. H.; Ho, W. Visualization and Spectroscopy of a Metal–Molecule–Metal Bridge. *Science* **2003**, *302*, 77–81.
- (580) Wu, S. W.; Nazin, G. V.; Ho, W. Intramolecular Photon Emission from a Single Molecule in a Scanning Tunneling Microscope. *Phys. Rev. B* **2008**, *77*, 205430.
- (581) Qiu, X. H.; Nazin, G. V.; Ho, W. Vibronic States in Single Molecule Electron Transport. *Phys. Rev. Lett.* **2004**, *92*, 206102.
- (582) Berndt, R.; Gimzewski, J. K. Photon-Emission in Scanning-Tunneling-Microscopy—Interpretation of Photon Maps of Metallic Systems. *Phys. Rev. B* **1993**, *48*, 4746–4754.
- (583) Lambe, J.; McCarthy, S. L. Light Emission from Inelastic Electron Tunneling. *Phys. Rev. Lett.* **1976**, *37*, 923–925.
- (584) Berndt, R.; Gaisch, R.; Gimzewski, J. K.; Reihl, B.; Schlittler, R. R.; Schneider, W. D.; Tschudy, M. Photon Emission at Molecular Resolution Induced by a Scanning Tunneling Microscope. *Science* **1993**, *262*, 1425–1427.
- (585) Fujita, D.; Ohgi, T.; Deng, W.-L.; Ishige, K.; Okamoto, T.; Yokoyama, S.; Kamikado, T.; Mashiko, S. Photon Emission Induced by Tunneling Electrons from a Cu(100) Surface Covered with Porphyrin Molecules. *Surf. Sci.* **2001**, *493*, 702–707.
- (586) Dong, Z.-C.; Guo, X.-L.; Trifonov, A. S.; Dorozhkin, P. S.; Miki, K.; Kimura, K.; Yokoyama, S.; Mashiko, S. Vibrationally Resolved Fluorescence from Organic Molecules near Metal Surfaces in a Scanning Tunneling Microscope. *Phys. Rev. Lett.* **2004**, *92*, 086801.
- (587) Liu, H. W.; Nishitani, R.; Han, T. Z.; Ie, Y.; Aso, Y.; Iwasaki, H. STM Fluorescence of Porphyrin Enhanced by a Strong Plasmonic Field and its Nanoscale Confinement in an STM Cavity. *Phys. Rev. B* **2009**, *79*, 125415.
- (588) Keane, Z. K.; Cizek, J. W.; Tour, J. M.; Natelson, D. Three-Terminal Devices to Examine Single-Molecule Conductance Switching. *Nano Lett.* **2006**, *6*, 1518–1521.
- (589) Tour, J. M.; Rawlett, A. M.; Kozaki, M.; Yao, Y.; Jagessar, R. C.; Dirk, S. M.; Price, D. W.; Reed, M. A.; Zhou, C.-W.; Chen, J.; Wang, W.; Campbell, I. Synthesis and Preliminary Testing of Molecular Wires and Devices. *Chem.—Eur. J.* **2001**, *7*, 5118–5134.
- (590) Wilson, E. G. Principles of a Three-Dimensional Molecular Electronic Memory. *Electron. Lett.* **1983**, *19*, 237–238.

(591) Abe, K.; Fujita, S.; Lee, T. H. Novel Nonvolatile Logic Circuits with Three-Dimensionally Stacked Nanoscale Memory Device. *NSTI Nanotech* **2005**, *3*, 203–205.

(592) del Valle, M.; Tejedor, C.; Cuniberti, G. Defective Transport Properties of Three-Terminal Carbon Nanotube Junctions. *Phys. Rev. B* **2005**, *71*, 125306.

(593) Reis, M. A. L.; Saraiva-Souza, A.; Del Nero, J. Capacitive Effects in a Three-Terminal Organic Nano-Device. *J. Comput. Theor. Nanosci.* **2008**, *6*, 1–5.

(594) Lang, N. D.; Solomon, P. M. Gating of a Three-Leg Molecule. *ACS Nano* **2009**, *3*, 1437–1440.

(595) Saha, K. K.; Nikolic, B. K.; Meunier, V.; Lu, W.; Bernholc, J. Quantum-Interference-Controlled Three-Terminal Molecular Transistors Based on a Single Ring-Shaped-Molecule Connected to Graphene Nanoribbon Electrodes. *Phys. Rev. Lett.* **2010**, *105*, 236803.

(596) Kumar, M. J.; Nadda, K. Bipolar Charge Plasma Transistor: A Novel Three-Terminal Device. *IEEE Trans. Electron Devices* **2012**, *59*, 962–967.

(597) Toher, C.; Nozaki, D.; Cuniberti, G.; Metzger, R. M. Unimolecular Amplifier: Principles of a Three-Terminal Device with Power Gain. *RSC Nanoscale* **2013**, *5*, 6975–6984.

(598) Holmlin, R. E.; Dandliker, P. J.; Barton, J. K. *Angew. Chem., Int. Ed.* **1997**, *36*, 2714.

(599) Kasumov, A. Y.; Kociak, M.; Gueron, S.; Reulet, B.; Volkov, V. T.; Klinov, D. V.; Bouchiat, H. Proximity-Induced Superconductivity in DNA. *Science* **2001**, *291*, 280–282.

(600) Genereux, J. C.; Barton, J. K. Mechanisms for DNA Charge Transport. *Chem. Rev.* **2010**, *110*, 1642–1662.

(601) Renaud, N.; Berlin, Y. A.; Lewis, F. D.; Ratner, M. A. Between Superexchange and Hopping: An Intermediate Charge-Transfer Mechanism in Poly(A)-Poly(T) DNA Hairpins. *J. Am. Chem. Soc.* **2013**, *135*, 3953–3963.

(602) Koenig, P.; Reines, S. A.; Cantor, C. R. Pyrene Derivatives as Fluorescent Probes of Conformation Near the 3' Termini of Polyribonucleotides. *Biopolymers* **1977**, *16*, 2231–2242.

(603) Seeman, N. C. Nucleic Acid Junctions and Lattices. *J. Theor. Biol.* **1982**, *99*, 237–247.

(604) Seeman, N. C. DNA Components for Molecular Architecture. *Acc. Chem. Res.* **1997**, *30*, 357–363.

(605) Gu, H.; Chao, J.; Xiao, S.-J.; Seeman, N. C. A Proximity-Based Programmable DNA Nanoscale Assembly Line. *Nature* **2010**, *465*, 202–205.

(606) Sha, R.; Liu, F.; Seeman, N. C. Atomic Force Measurement of the Interdomain Angle in Symmetric Holliday Junctions. *Biochemistry* **2002**, *41*, 5950–5955.

(607) Mao, C.; Sun, W.; Seeman, N. C. Designed Two-Dimensional DNA Holliday Junction Arrays Visualized by Atomic Force Microscopy. *J. Am. Chem. Soc.* **1999**, *121*, 5437–5443.